Dissertation zur Erlangung des Doktorgrades
der Fakultät für Chemie und Pharmazie
der Ludwigs-Maximilians-Universität München

Temperature-Induced Unfolding, Aggregation, and Interaction of Therapeutic Monoclonal Antibodies

Tim Andreas Menzen

aus

Neuwied

2014

ERKLÄRUNG

Diese Dissertation wurde im Sinne von §7 der Promotionsordnung vom 28. November 2011 von Herrn Prof. Dr. Wolfgang Frieß betreut.

EIDESSTATTLICHE VERSICHERUNG

Diese Dissertation wurde eigenständig und ohne unerlaubte Hilfe erarbeitet.

München, 27. Juni 2014

_____

Tim Menzen

Dissertation eingereicht am:	30.06.2014
1. Gutachter:	Prof. Dr. Wolfgang Frieß
2. Gutachter:	Prof. Dr. Gerhard Winter
Mündliche Prüfung am:	19.09.2014

Acknowledgements

Most of all, I want to express my deepest gratitude to my supervisor Prof. Dr. Wolfgang Frieß. I highly appreciate his valuable advice, guidance, and the fruitful and inspiring discussions. I am deeply grateful for numerous opportunities to express myself and develop in most interesting scientific projects and collaborations. On both personal and professional level, interaction with him was always most exciting. Many thanks for the good time, at university and during the outstanding team activities with him and his family.

I highly appreciate the co-reference of Prof. Dr. Gerhard Winter. I want to thank him as chair of Pharmaceutical Technology and Biopharmaceutics for the excellent work conditions, and for the numerous extraordinary social events like the skiing and hiking trips, which I have always enjoyed very much.

Prof. Dr. Angelika Vollmar, chair of Pharmaceutical Biology at the Department of Pharmacy, is gratefully acknowledged for providing the RT7300 RT-PCR for our protein melting experiments.

I would like to thank Prof. Dr. Petra Schwille for the opportunity to perform FCS/FCCS experiments at the Biotechnology Center of the Technische Universität Dresden, Germany. Especially, I want to thank Dr. Jörg Mütze for his scientific advice and support on the measurements and data analysis during my visits in Dresden.

I highly appreciate the collaboration with Prof. Dr. Christoph Haisch at the Institute of Hydrochemistry of the Technische Universität München, Germany. I hold his scientific input and contribution in high regard. I want to thank him for the outstanding chance to work with lasers and optics. Thanks to the leader of the chair Prof. Dr. Reinhard Niessner and his entire research group, who made me feel most comfortable in their labs. Special thanks to Christoph Berger for giving me a kick-start in LabVIEW® programing and GPIB communication.

I want to thank Wyatt Technologies Europe and especially Dr. Dierk Roessner and Dr. Roger Scherrers for their generous support with the DLS measurements. I really enjoyed my stay at their European headquarters in Dernbach, Germany.

Coriolis Pharma in Martinsried, Germany is kindly acknowledged for the opportunity to use the attenuated SYPRO® Orange filter module for the qTower 2.2 RT-PCR.

I would like to thank all the students also involved in this thesis for their excellent work: Franziska Wurst (Master practical course section A), Aureliè Launay from the University of Angers, France (Erasmus program), Vanessa Welk (Master advanced practical course section A), Hannah Chen from the Emory University of Atlanta, USA (DAAD RISE program), Ritu Mann-Nüttel (Bachelor thesis), and last but not least Corinna Dürr (Master thesis). The DAAD and Erasmus are acknowledged for providing such excellent programs, which offer great experiences for all participants.

I want to thank all my present and former colleagues at the institute and especially my “iLab” colleague Philipp Matthias for the great atmosphere and their friendships. Finally, I want to thank my family for their ongoing confidence and encouragement.

Table of contents

1 Introduction

1.1 Therapeutic monoclonal antibodies

For over a decade, monoclonal antibodies (mAbs) dominate the market of recombinant therapeutic proteins.[1] About half of the sales of biological products, also known as biologics, in the year 2012 were achieved by therapeutic antibodies.[2] Furthermore, the top 6 biologics with blockbuster status were all antibody-related products,[2] with adalimumab, etanercept, and infliximab directed against tumor necrosis factor (TNF), rituximab targeting CD20, trastuzumab binding to human epidermal growth factor 2 (HER2), and bevacizumab aiming at vascular endothelial growth factor (VEGF). The sales numbers underline the impressive impact of mAbs in the treatment of autoimmune and inflammatory diseases,[3] as well as cancer.[4,5] Furthermore, many new products are in clinical trials and expect approval by the authorities with a high rate of success.[6,7]

Antibodies are globular proteins of the family of immunoglobulins (Ig). From the five structurally similar classes of Igs (A, D, E, G, M), IgG is the most abundant in serum. The IgG function is related to the different domains of the antibody. The antigen-binding site is located at the tips of each Fab fragment (fragment antigen binding), whereas the Fc fragment (fragment crystallizable) mediates various receptor functions. The fragments were historically obtained and investigated by enzymatic cleavage with papain.[8] Two Fab fragments and one Fc are connected via a highly flexible hinge region to form the overall Y-shape of the antibody. Breaking it down to the primary structure, the mAb molecule is symmetrical, consisting of two pairs of identical amino acids chains of characteristic length and features.[9] The longer one (heavy chain, H) consist of three domains with highly conserved, constant structure (CH1, CH2, CH3) and one domain which shows a high variability between mAbs with different specificity (VH). The shorter chain (light chain, L) similarly consists of a constant (CL) and a variable domain (VL). The variable and one constant region of heavy and light chain (VH+VL, CH1+CL) are connected via a disulfide bond and noncovalent interactions to form the stable Fab fragment. The remaining constant regions of the heavy chain (CH2, CH3) form the Fc fragment. The two halves of the

full mAb molecule, each consisting of a heavy and a light chain, are linked with two disulfide bonds at the hinge region and noncovalent interactions of CH2 and CH3, which involve protein-protein interactions as well as interactions between glycans that are attached to the CH2 domain of each heavy chain. The molecular weights of light and heavy chain are about 25 and 50 kDa, leading to about 50 kDa of each Fab and Fc fragment, and consequently approximately 150 kDa of the full mAb molecule.

The high specificity against antigenic epitopes and high adaptability of mAbs are realized by three hypervariable regions in VH and VL that form the complementarity-determining region (CDR) of the Fab fragment. A monoclonal antibody is directed against only one target epitope via a specific CDR. Using the tools of molecular biology, recombinant mAb molecules are created with tailored primary sequence to capture therapeutic targets. The drawback of immunogenic reactions of the patient against the first mAbs from mice,[10] was subsequently minimized by chimeric,[11] humanized,[12] and fully human mAbs.[13-15]

Moreover, the mAb structure was subject to various modifications and variations over the recent years. Tuning the Fc-receptor interactions might not only affect the clearance but also the efficiency. Furthermore, bispecific variants were investigated for advanced targeting. Full mAb molecules benefit from a long plasma half-live due to their molecular size and specific Fc mediated recycling. In contrast fragments of Fab down to single-chain variable fragments (scFv), minibodies, heavy chain antibodies, and single domain antibodies are examples for strategies to improve tissue penetration and distribution. Excellent reviews are available in literature about the second and next generation mAbs described in this paragraph.[16,17] Last but not least, the success of mAbs is related to the advances of modern biotechnology that allow the production, purification and formulation of therapeutic proteins in large scale to meet the requirements of typically high doses in therapy.[18]

1.2 The challenge of protein instabilities

Safety and efficacy of therapeutic protein products are particularly challenging due to multiple instability reactions of the protein molecules. Protein instabilities are often divided into chemical and physical instabilities,[19-21] whereas the latter are either of colloidal or conformational type. Chemical reactions such as oxidation, reduction, hydrolysis, and other covalent changes directly alter the primary structure of the

protein. In contrast, primary structure is maintained in case of physical instabilities but the higher order structure, the microscopic and/or the macroscopic appearance of the protein is affected. Both physical stability and instability are mediated by short (hard sphere, van der Waals, hydrophobic, H-bonds, etc.) and long-range (electrostatic) interactions. These are responsible for the proteins' secondary and tertiary structure,[22] but also govern the behavior of protein molecules in solution.[23,24] Colloidal instabilities from attractive protein-protein interactions lead to clustering of protein molecules known as protein aggregation. Protein aggregation renders a large and inhomogeneous group of instability products. Aggregation pathways, kinetics, and driving factors are complex, leading to usually an inhomogeneous aggregate population of varying size and morphology.[25] Correspondingly protein aggregates can range from dimers to multimers, from native like associates to denatured precipitates, from ordered fibrils to amorphous structures, and from reversible clusters to stable particles.[25,26] These categories are helpful to describe the characteristics of protein instabilities, but should not be considered as unique and independent. Chemical instabilities can lead to structural changes and also reduced activity when the CDR,[27-29] or the Fc-receptor binding sites are affected.[30-34] Furthermore, structural changes can lead to aggregation, e.g., via exposed hydrophobic surfaces,[35,36] but can also facilitate chemical reactions.[37] Especially, inherent characteristics of the protein itself affect the quality and quantity of protein stability and instability, e.g., post-translational glycosylation,[38] or structural hotspots for aggregation.[39] Furthermore, heat, extreme pH, agitation, drying, freeze/thaw, adsorption/desorption, and other stress factors are major drivers of these protein instabilities.[22,25]

1.3 The role of temperature in the context of protein stability

Although organisms are known which can endure conditions of extreme temperature, like hyperthermophiles or psychrophiles, most organisms are mesophilic, i.e., their enzymes are active at temperatures between 25 and 50 °C.[40] The highest thermodynamic stability, which is the largest free energy difference between the unfolded and folded state of the protein, is typically observed at physiological temperatures or slightly below.[41,42] Moreover, the thermal stability reflected by the protein melting temperature (T_m), certainly above physiological temperatures, indicates the resistance against thermal unfolding. A high thermal stability is commonly beneficial for therapeutic proteins to maintain the active native state *in*

vivo, *ex vivo*, and upon storage. The T_m value, which is affected by the environment of the protein, is therefore very important during research and development (R&D). Therefore, the role of temperature in the context of thermodynamic and thermal stability, and upon storage is introduced in the following.

1.3.1 Thermodynamic protein stability

Thermodynamic stability is defined as the free energy change upon unfolding ΔG_{unf} which is the difference in free energy of the unfolded and the folded state of the protein. Thus, thermodynamic stability arises from the native as well as the unfolded structure of the protein. A common expression of ΔG_{unf} is the Gibbs-Helmholtz equation

$$\Delta G_{unf} = \Delta H_{ref} - T\Delta S_{ref} + \Delta C_p \left[T - T_{ref} - T \ln\left(\frac{T}{T_{ref}}\right)\right] \quad (1\text{-}1)$$

with the change in enthalpy and entropy of unfolding ΔH_{ref} and ΔS_{ref} at an arbitrary reference temperature T_{ref}, respectively. ΔCp is the change in heat capacity of the protein. The thermodynamic protein stability curve obtained from the Gibbs-Helmholtz equation has two intersections at which ΔG_{unf} is zero that are referred to as the cold denaturation temperature (T_{cd}) and the melting temperature (T_m).[43]

1.3.2 Protein thermal stability

In the simple case of a reversible two-step unfolding process, the protein molecule is either in the native or the unfolded state at a given temperature. The reaction is characterized by the equilibrium constant that describes the ratio of native and unfolded molecules. The temperature at equality between both states, that means when half of the protein is unfolded, is the T_m value and ΔG_{unf} is zero. Consequently, the T_m value is an indicator of protein thermal stability. A higher T_m value means that fewer molecules populate the unfolded state at a given temperature. Thus, a higher T_m value is beneficial for therapeutic protein drugs as a high T_m value sustains the active, native conformation at physiological temperatures. Furthermore, it reduces the probability for conformational alteration potentially accompanied by chemical and colloidal instabilities.

To obtain a higher intrinsic thermal stability, three different thermodynamic ways were proposed,[44] that is a higher ΔH (larger stability curve), a reduced ΔC_p (broader

stability curve), and a lower ΔS (right shift of the stability curve). Structural differences were studied on proteins from various thermophile organisms that have higher thermodynamic stability.[41,45] The most common ways to increase the T_m value were a higher $\Delta G_{unf,}$ a lower ΔCp, or both in combination.[45] Figure 1-1 presents the thermodynamic protein stability curve of a mAb which was investigated by Lazar et al. using intrinsic fluorescence changes upon guanidine hydrochloride (GnHCl) denaturation.[46] The obtained ΔG_{unf} values at various temperatures were used to calculate ΔH, ΔS, and ΔC_p via the Gibbs-Helmholtz equation.[46] The highest thermodynamic stability of the mAb was observed at 18 °C (Figure 1-1). Most mesophilic proteins have a maximum ΔG_{unf} value at ambient temperatures or at least below body temperature.[41,42] The derived thermal stability with a T_m value of 60 °C is in the range of a typical therapeutic mAb.

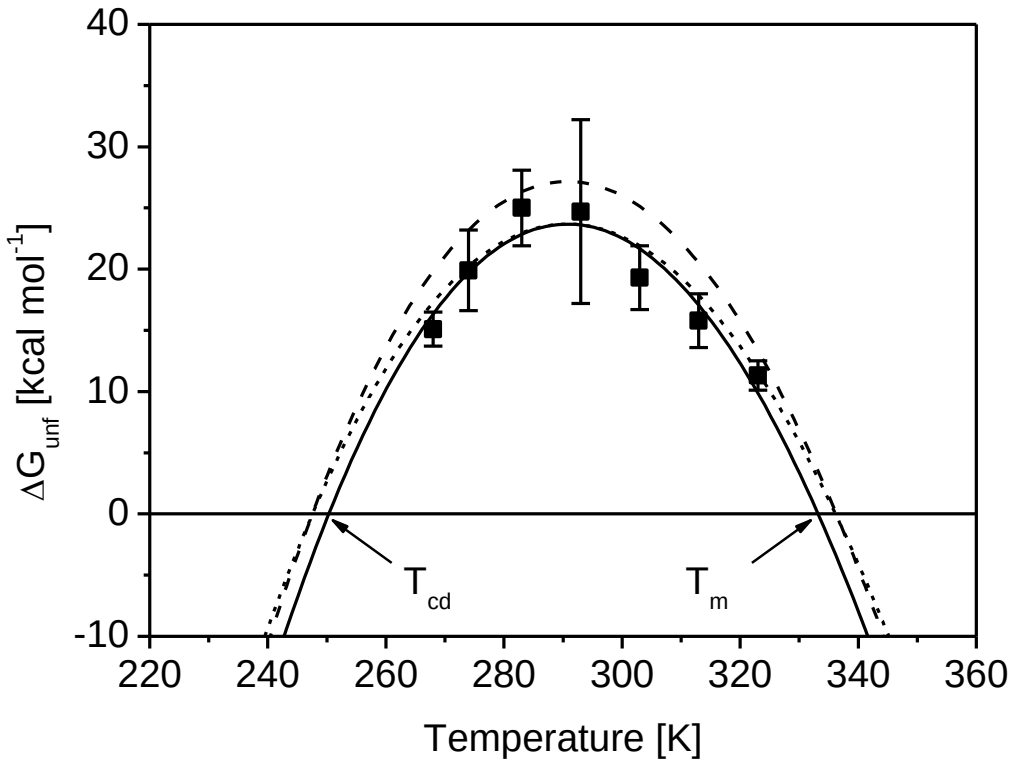

Figure 1-1. Protein stability curve of mAb1 reported by Lazar et al.[46] The black line resembles the fitted Gibbs-Helmholtz equation (eq. (1-1)) to the obtained ΔG_{unf} values at various temperatures obtained from GnHCl denaturation.[46] The highest thermodynamic stability is observed at 291 K (ΔS = 0) with ΔH_{291K} of 26.6 kcal mol^{-1}, and ΔCp of 8 kcal mol^{-1} K^{-1}. The data was used to calculate the stability curves of hypothetical variants with the same maximum ΔG_{unf} but either ΔCp of 7 kcal mol^{-1} K^{-1} (dotted line) or ΔH of 30.1 kcal mol^{-1} (dashed line). In both cases a higher T_m value (and lower T_{cd}) of 3 K was obtained.

Intrinsic stabilization of the protein could be obtained from structural modifications, as ΔH can be increased by introducing more stabilizing interactions (H-bonds, salt bridges, etc.) and ΔCp is correlated to the accessible (hydrophobic) surface area which is exposed to the solvent upon unfolding.[45] A more densely packed structure or structural elements which are maintained in the unfolded state reduce Cp.[45] In both cases, a higher T_m value is obtained. Using the data from Lazar et al.,[46] a T_m increase of 3 °C was obtained from the Gibbs-Helmholtz equation when ΔH was exemplarily increased by 3.5 kcal mol^{-1} and ΔC_p was decreased by 1 kcal mol^{-1} K^{-1}, respectively (Figure 1-1). Furthermore, extrinsic factors, which are maintained by the protein formulation, affect the thermal stability. Therefore, it is important to investigate the thermal stability of the protein during formulation development of therapeutic drugs.

For thermal stability analysis, typically differential scanning calorimetry (DSC) is used to obtain T_m values of proteins in solution. DSC also reveals the thermodynamic properties ΔH and ΔCp that can be used to calculate the thermodynamic stability via the Gibbs-Helmholtz equation but only in cases of reversible two-state unfolding reactions, which are typically not observed for large and complex multi-domain proteins such as mAbs. Typically, noncooperative unfolding of unique domains and protein aggregation is observed. Therefore, the thermodynamic information is confined to the “apparent” T_m value. Finally, it has to be noted that a high thermodynamic stability (high ΔG_{unf}) does not necessarily mean a high thermal stability (high T_m) and vice versa.

1.3.3 Protein stability upon storage

Storage stability over a certain time period is essential for a therapeutic product to provide appropriate shelf-life. The time dependence of instability processes is a challenge for drug product development. Commonly accelerated storage stability studies at elevated temperature are utilized as kinetics are assumed to increase with temperature according to Arrhenius law. In this case, a higher temperature raises the probability of a molecule to pass the activation energy barrier, leading to an increased rate constant and thus faster (instability) reaction. The complexity and quantity of the physicochemical protein instabilities often lead to nonlinear relationships between parental material and degradation products.[47,48]

If the accelerated storage temperature is above the onset of unfolding of the protein, also different processes can occur due to the altered structure and the results might not agree with storage data at lower temperatures. Therefore, the results from thermal stability analysis should be considered for the interpretation of storage stability data. Moreover, the T_m value is routinely analyzed in order to predict storage stability. If for example irreversible aggregation occurs after unfolding of a certain mAb domain, then a higher T_m value of this domain probably reduces the aggregate formation, because the likeliness of unfolded molecules at temperatures below T_m is decreased. This is true for all instability pathways that start from nonnative protein structure.

In conclusion, a higher T_m value is beneficial and can enhance storage stability, but is predictive only in cases where degradation is linked to unfolded protein structure. Therefore, thermal stability screenings and accelerated stability studies can rationalize the development process and can support the investigation of degradation pathways, but real-time storage stability data is essential for filing a new product to the authorities to prove safety and efficacy.

1.4 Formulation development of proteins

The protein formulation can be described as the environment of the protein to maintain its function and to be finally administered to the patient. The size, charge, and physicochemical properties of multi-domain proteins such as mAbs primarily limit the routes of administration to intravenous or subcutaneous with a small number of exceptions. Although freeze- or spray-dried products are convenient to increase the shelf-life, the protein is finally administered in solution. Therefore, protein activity and stability in aqueous solution are essential for its therapeutic use. Special requirements due to parenteral administration like physiological tonicity or pH need to be considered. Moreover, subcutaneous injection may require high protein concentrations to administer the therapeutic dose in a small volume.[49] In such high-concentrated mAb solutions enhanced protein-protein interactions, self-association, and high viscosity present additional challenges.[49-51] Additionally, during production (filtration, pumping, filling), shipping, storage, handling, and administration, the protein is exposed to various stresses. This involves unfavorable sheer forces, light exposure, and surface interactions. Thus, the protein formulation needs to be

optimized towards maintaining the active, native conformation of the protein, reducing unfavorable attractive and supporting repulsive protein-protein interactions, and protecting the protein from stress.

Some common rules for formulation development have been established and extensively reviewed.[19,22,52] The pH value of the solution defines the net charge of the protein. The colloidal stability is typically low at neutral net charge of the protein and increases at pH values where repulsive electrostatic forces occur. But extreme pH values induce unfolding by intramolecular repulsion and chemical degradation. To maintain the pH, organic and inorganic buffers are used. The choice of the substance is primarily related to the desired pH value of the solution for high buffer capacity. Specific stabilizing or destabilizing effects of different buffer substances at the same pH value can occur from direct interactions, ionic strength, or solvent effects. Salts modify the tonicity and ionic strength of the solution, and have shielding effects on charges. Furthermore, ions have specific effects on the protein solubility and stability described by the Hofmeister series. Typically, sugars, sugar alcohols, and polyols are used for tonicity adjustments. They can also nonspecifically enhance the stability of the protein by preferential exclusion of the excipient from the protein surface and thus preferential hydration of the protein. To reduce adsorption to surfaces and protein instabilities induced by interfacial stress, surfactants are added routinely.

1.5 High-throughput screenings for protein stability

The vast instability reactions of proteins (see chapter 1.2) demand a comprehensive physical and chemical characterization of the protein during R&D of therapeutic proteins. Even more, proteins are intentionally stressed to provoke protein instabilities in order to rank candidates and to identify instability mechanisms of most concern. Especially at an early development stage, the availability of purified drug substance is limited and furthermore, the cost of goods of the protein material is very high. It is essential for any assay that the amount of sample consumed by the analysis is as low as possible or that the sample might even be recyclable for further analysis. Over the recent years, many analytical techniques were adapted to multi-well plate formats and automated sampling to allow small sample volumes and high-throughput screenings (HTS).[53,54]

For analysis of protein aggregation, high performance size exclusion chromatography (HP-SEC) and dynamic light scattering (DLS) are prominent examples for good automation and well plate format analysis techniques in the small aggregate size range. Larger particles that scatter visible light and lead to turbidity of the solution are conveniently detected by assessing the transmission also on small scale an in well plate format. Furthermore, smart real-time image analysis and improved microfluidic systems are going to establish flow imaging techniques as HTS in the near future.[55]

In contrast, the high-throughput analysis of chemical instabilities is challenging and complex mass spectrometry (MS) investigations are time consuming. In some cases, for example for the detection of oxidized species, straight liquid chromatography techniques are described.[56,57]

Light absorption (circular dichroism, second derivative UV spectra) and both intrinsic and extrinsic fluorescence spectroscopy are routinely used to detect changes in secondary or tertiary structure arising from the spectral properties of mainly the aromatic residues of the protein. Optical spectrometers are available in both multi-well plate and automated sampling formats. But vibrational (Fourier transform infrared, near infrared, and Raman) spectroscopy is challenging for HTS for technical reasons.[54]

Automatized DSC with liquid sampling technologies is available from various manufacturers. The DSC technique is suffering from comparably high sample amounts and long analysis times due to single measurements and extensive cleaning procedures. In contrast, differential scanning fluorimetry (DSF) indirectly monitors protein unfolding of samples in parallel by means of an extrinsic fluorescent dye and a multi-well plate format.[58] Thus, DSF is a powerful and promising technique for high-throughput thermal analysis of therapeutic proteins.[59-61]

1.6 References

1. Pavlou AK, Belsey MJ 2005. The therapeutic antibodies market to 2008. Eur J Pharm Biopharm 59(3):389-396.

2. La Merie. 2013. Blockbuster Biologics 2012, R&D Pipeline News. Stuttgart: La Merie Publishing. Accessed 03/03/2014, at: http://www.pipelinereview.com/free-downloads/Blockbuster_Biologics_2012_RDPN_Special_May_2013.pdf.

3. Chan AC, Carter PJ 2010. Therapeutic antibodies for autoimmunity and inflammation. Nat Rev Immunol 10(5):301-316.

4. Scott AM, Wolchok JD, Old LJ 2012. Antibody therapy of cancer. Nat Rev Cancer 12(4):278-287.

5. Weiner LM, Surana R, Wang S 2010. Monoclonal antibodies: versatile platforms for cancer immunotherapy. Nat Rev Immunol 10(5):317-327.

6. Reichert JM, Wenger JB 2008. Development trends for new cancer therapeutics and vaccines. Drug Discov Today 13(1–2):30-37.

7. Reichert JM 2012. Marketed therapeutic antibodies compendium. mAbs 4(3):413-415.

8. Porter RR 1959. The hydrolysis of rabbit y-globulin and antibodies with crystalline papain. Biochem J 73:119-126.

9. Edelman GM, Cunningham BA, Gall WE, Gottlieb PD, Rutishauser U, Waxdal MJ 1969. The Covalent Structure of an Entire γG Immunoglobulin Molecule. Proceedings of the National Academy of Sciences 63(1):78-85.

10. Köhler G, Milstein C 1975. Continuous cultures of fused cells secreting antibody of predefined specificity. Nature 256(5517):495-497.

11. Morrison SL, Johnson MJ, Herzenberg LA, Oi VT 1984. Chimeric human antibody molecules: mouse antigen-binding domains with human constant region domains. Proceedings of the National Academy of Sciences 81(21):6851-6855.

12. Jones PT, Dear PH, Foote J, Neuberger MS, Winter G 1986. Replacing the complementarity-determining regions in a human antibody with those from a mouse. Nature 321(6069):522-525.

13. Lonberg N, Taylor LD, Harding FA, Trounstine M, Higgins KM, Schramm SR, Kuo CC, Mashayekh R, Wymore K, McCabe JG, et al. 1994. Antigen-specific human antibodies from mice comprising four distinct genetic modifications. Nature 368(6474):856-859.

14. McCafferty J, Griffiths AD, Winter G, Chiswell DJ 1990. Phage antibodies: filamentous phage displaying antibody variable domains. Nature 348(6301):552-554.

15. Green LL, Hardy MC, Maynard-Currie CE, Tsuda H, Louie DM, Mendez MJ, Abderrahim H, Noguchi M, Smith DH, Zeng Y, David NE, Sasai H, Garza D, Brenner DG, Hales JF, McGuinness RP, Capon DJ, Klapholz S, Jakobovits A 1994. Antigen-specific human monoclonal antibodies from mice engineered with human Ig heavy and light chain YACs. Nat Genet 7(1):13-21.

16. Chames P, Van Regenmortel M, Weiss E, Baty D 2009. Therapeutic antibodies: successes, limitations and hopes for the future. Br J Pharmacol 157(2):220-233.

17. Beck A, Wurch T, Bailly C, Corvaia N 2010. Strategies and challenges for the next generation of therapeutic antibodies. Nat Rev Immunol 10(5):345-352.

18. Jones SD, Castillo FJ, Levine HL 2007. Advances in the Development of Therapeutic Monoclonal Antibodies. BioPharm International 10:96-114.

19. Manning M, Chou D, Murphy B, Payne R, Katayama D 2010. Stability of Protein Pharmaceuticals: An Update. Pharm Res 27(4):544-575.

20. Manning M, Patel K, Borchardt R 1989. Stability of Protein Pharmaceuticals. Pharm Res 6(11):903-918.

21. Wang W 2005. Protein aggregation and its inhibition in biopharmaceutics. Int J Pharm 289(1-2):1-30.

22. Wang W 1999. Instability, stabilization, and formulation of liquid protein pharmaceuticals. Int J Pharm 185(2):129-188.

23. Arzenšek D, Kuzman D, Podgornik R 2012. Colloidal interactions between monoclonal antibodies in aqueous solutions. J Colloid Interface Sci 384(1):207-216.

24. Rosenbaum DF, Zukoski CF 1996. Protein interactions and crystallization. J Cryst Growth 169(4):752-758.

25. Mahler H-C, Friess W, Grauschopf U, Kiese S 2009. Protein aggregation: Pathways, induction factors and analysis. J Pharm Sci 98(9):2909-2934.

26. Narhi LO, Schmit J, Bechtold-Peters K, Sharma D 2012. Classification of protein aggregates. J Pharm Sci 101(2):493-498.

27. Haberger M, Bomans K, Diepold K, Hook M, Gassner J, Schlothauer T, Zwick A, Spick C, Kepert JF, Hienz B, Wiedmann M, Beck H, Metzger P, Mølhøj M, Knoblich C, Grauschopf U, Reusch D, Bulau P 2014. Assessment of chemical modifications of sites in the CDRs of recombinant antibodies: Susceptibility vs. functionality of critical quality attributes. mAbs 6(2):327-339.

28. Rehder DS, Chelius D, McAuley A, Dillon TM, Xiao G, Crouse-Zeineddini J, Vardanyan L, Perico N, Mukku V, Brems DN, Matsumura M, Bondarenko PV 2008. Isomerization of a Single Aspartyl Residue of Anti-Epidermal Growth Factor Receptor Immunoglobulin γ2 Antibody Highlights the Role Avidity Plays in Antibody Activity. Biochemistry (Mosc) 47(8):2518-2530.

29. Harris RJ, Kabakoff B, Macchi FD, Shen FJ, Kwong M, Andya JD, Shire SJ, Bjork N, Totpal K, Chen AB 2001. Identification of multiple sources of charge heterogeneity in a recombinant antibody. Journal of Chromatography B: Biomedical Sciences and Applications 752(2):233-245.

30. Bertolotti-Ciarlet A, Wang W, Lownes R, Pristatsky P, Fang Y, McKelvey T, Li Y, Li Y, Drummond J, Prueksaritanont T, Vlasak J 2009. Impact of methionine oxidation on the binding of human IgG1 to FcRn and Fcγ receptors. Mol Immunol 46(8–9):1878-1882.

31. Wang W, Vlasak J, Li Y, Pristatsky P, Fang Y, Pittman T, Roman J, Wang Y, Prueksaritanont T, Ionescu R 2011. Impact of methionine oxidation in human IgG1 Fc on serum half-life of monoclonal antibodies. Mol Immunol 48(6–7):860-866.

32. Pan H, Chen K, Chu L, Kinderman F, Apostol I, Huang G 2009. Methionine oxidation in human IgG2 Fc decreases binding affinities to protein A and FcRn. Protein Sci 18(2):424-433.

33. Loew C, Knoblich C, Fichtl J, Alt N, Diepold K, Bulau P, Goldbach P, Adler M, Mahler H-C, Grauschopf U 2012. Analytical protein A chromatography as a quantitative tool for the screening of methionine oxidation in monoclonal antibodies. J Pharm Sci 101(11):4248-4257.

34. Schlothauer T, Rueger P, Stracke JO, Hertenberger H, Fingas F, Kling L, Emrich T, Drabner G, Seeber S, Auer J, Koch S, Papadimitriou A 2013. Analytical FcRn affinity chromatography for functional characterization of monoclonal antibodies. mAbs 5(4):576-586.

35. Vermeer AWP, Norde W 2000. The Thermal Stability of Immunoglobulin: Unfolding and Aggregation of a Multi-Domain Protein. Biophys J 78(1):394-404.

36. Kumar V, Dixit N, Zhou L, Fraunhofer W 2011. Impact of short range hydrophobic interactions and long range electrostatic forces on the aggregation kinetics of a monoclonal antibody and a dual-variable domain immunoglobulin at low and high concentrations. Int J Pharm 421(1):82-93.

37. Sinha S, Zhang L, Duan S, Williams TD, Vlasak J, Ionescu R, Topp EM 2009. Effect of protein structure on deamidation rate in the Fc fragment of an IgG1 monoclonal antibody. Protein Sci 18(8):1573-1584.

38. Latypov RF, Hogan S, Lau H, Gadgil H, Liu D 2012. Elucidation of Acid-induced Unfolding and Aggregation of Human Immunoglobulin IgG1 and IgG2 Fc. J Biol Chem 287(2):1381-1396.

39. Perchiacca JM, Bhattacharya M, Tessier PM 2011. Mutational analysis of domain antibodies reveals aggregation hotspots within and near the complementarity determining regions. Proteins: Struct, Funct, Bioinf 79(9):2637-2647.

40. Vieille C, Zeikus GJ 2001. Hyperthermophilic Enzymes: Sources, Uses, and Molecular Mechanisms for Thermostability. Microbiol Mol Biol Rev 65(1):1-43.

41. Jaenicke R 1991. Protein stability and molecular adaptation to extreme conditons. Eur J Biochem 202(3):715-728.

42. Kumar S, Tsai C-J, Nussinov R 2001. Thermodynamic Differences among Homologous Thermophilic and Mesophilic Proteins. Biochemistry (Mosc) 40(47):14152-14165.

43. Becktel WJ, Schellmann JA 1987. Protein Stability Curves. Biopolymers 26:1859-1877.

44. Nojima H, Ikai A, Oshima T, Noda H 1977. Reversible thermal unfolding of thermostable phosphoglycerate kinase. Thermostability associated with mean zero enthalpy change. J Mol Biol 116(3):429-442.

45. Razvi A, Scholtz JM 2006. Lessons in stability from thermophilic proteins. Protein Sci 15(7):1569-1578.

46. Lazar KL, Patapoff TW, Sharma VK 2010. Cold denaturation of monoclonal antibodies. mAbs 2(1):42-52.

47. Sreedhara A, Cordoba A, Zhu Q, Kwong J, Liu J 2012. Characterization of the Isomerization Products of Aspartate Residues at Two Different Sites in a Monoclonal Antibody. Pharm Res 29(1):187-197.

48. Brummitt RK, Nesta DP, Roberts CJ 2011. Predicting accelerated aggregation rates for monoclonal antibody formulations, and challenges for low-temperature predictions. J Pharm Sci 100(10):4234-4243.

49. Liu J, Nguyen MDH, Andya JD, Shire SJ 2005. Reversible self-association increases the viscosity of a concentrated monoclonal antibody in aqueous solution. J Pharm Sci 94(9):1928-1940.

50. Harn N, Allan C, Oliver C, Middaugh CR 2007. Highly concentrated monoclonal antibody solutions: Direct analysis of physical structure and thermal stability. J Pharm Sci 96(3):532-546.

51. Kanai S, Liu J, Patapoff TW, Shire SJ 2008. Reversible self-association of a concentrated monoclonal antibody solution mediated by Fab–Fab interaction that impacts solution viscosity. J Pharm Sci 97(10):4219-4227.

52. Chi EY, Krishnan S, Randolph TW, Carpenter JF 2003. Physical Stability of Proteins in Aqueous Solution: Mechanism and Driving Forces in Nonnative Protein Aggregation. Pharm Res 20(9):1325-1336.

53. Samra HS, He F 2012. Advancements in High Throughput Biophysical Technologies: Applications for Characterization and Screening during Early Formulation Development of Monoclonal Antibodies. Mol Pharm 9(4):696-707.

54. He F, Razinkov VI, Middaugh CR, Becker GW. 2013. High-Throughput Biophysical Approaches to Therapeutic Protein Development. In Narhi LO, editor Biophysics for Therapeutic Protein Development, ed., New York: Springer.

55. Goda K, Ayazi A, Gossett DR, Sadasivam J, Lonappan CK, Sollier E, Fard AM, Hur SC, Adam J, Murray C, Wang C, Brackbill N, Di Carlo D, Jalali B 2012. High-throughput single-microparticle imaging flow analyzer. Proceedings of the National Academy of Sciences 109(29):11630-11635.

56. Teshima G, Li M-X, Danishmand R, Obi C, To R, Huang C, Kung J, Lahidji V, Freeberg J, Thorner L, Tomic M 2011. Separation of oxidized variants of a monoclonal antibody by anion-exchange. J Chromatogr A 1218(15):2091-2097.

57. Yang J, Wang S, Liu J, Raghani A 2007. Determination of tryptophan oxidation of monoclonal antibody by reversed phase high performance liquid chromatography. J Chromatogr A 1156(1–2):174-182.

58. Pantoliano MW, Petrella EC, Kwasnoski JD, Lobanov VS, Myslik J, Graf E, Carver T, Asel E, Springer BA, Lane P, Salemme FR 2001. High-Density Miniaturized Thermal Shift Assays as a General Strategy for Drug Discovery. J Biomol Screen 6(6):429-440.

59. He F, Hogan S, Latypov RF, Narhi LO, Razinkov VI 2010. High throughput thermostability screening of monoclonal antibody formulations. J Pharm Sci 99(4):1707-1720.

60. Goldberg DS, Bishop SM, Shah AU, Sathish HA 2011. Formulation development of therapeutic monoclonal antibodies using high-throughput fluorescence and static light scattering techniques: Role of conformational and colloidal stability. J Pharm Sci 100(4):1306-1315.

61. Li Y, Mach H, Blue JT 2011. High throughput formulation screening for global aggregation behaviors of three monoclonal antibodies. J Pharm Sci 100(6):2120-2135.

2 Aim and outline of the thesis

The work in this thesis aimed at the analysis of protein unfolding, interaction, and aggregation of therapeutic mAbs upon heating. The objectives focused on the determination and interpretation of T_m with respect to formulation development. Furthermore, the results from temperature-ramped interaction parameter investigations, and the application of novel and unique techniques to study protein aggregation are presented with a focus on a deeper understanding of the thermal stability of mAbs and mAb domains.

As a first objective, the DSF method is introduced and optimized in chapter 3 with respect of the requirements of protein formulation development. This includes hardware considerations, sample preparation, experimental parameters, and finally data analysis and automatized data handling. A robust DSF method is established using two different RT-PCR machines.

In chapter 4, both intrinsic and extrinsic factors affecting the thermal stability of mAb samples are investigated by DSF and DSC. The influence of deglycosylation on the thermal stability is investigated on two mAbs which differ in an additional glycosylation site in the Fab region. Furthermore, the stabilizing or destabilizing effects of selected buffers, excipients like the basic amino acids arginine and histidine, and pH are studied. Finally, the correlation of DSF and DSC is evaluated and discussed.

SYPRO® Orange is very popular for DSF experiments as it is very sensitive to protein unfolding based on interaction with hydrophobic patches which become exposed upon heating. However, surfactants present in the formulation also interact with SYPRO® Orange, disturbing the unfolding signal of the protein. The DSF method is challenged in chapter 5 with mAb samples containing surfactants and scenarios which typically occur during formulation development. Limitations and opportunities like the application of a rotor dye like DCVJ, which shows promising results due to less interaction with the surfactant micelles, are presented.

The observation in previous chapters that mAb aggregation is linked to the unfolding of certain domains raises the question of the driving forces of protein aggregation upon heating. Temperature-ramped DLS measurements are performed to determine the interaction parameter k_D, related to the second osmotic virial coefficient that indicates net attraction or net repulsion of the protein molecules. Moreover, DLS and turbidity measurements additionally monitor particle formation upon heating. Thus, the experiments presented in chapter 6 link the investigations of thermal unfolding, aggregation, and interaction mAb molecules.

The objective of chapter 7 is the investigation of aggregate growth via fluorescence correlation spectroscopy (FCS) and fluorescence cross-correlation spectroscopy (FCCS). Using mAb aggregates formed by heat stress, the adsorption of native and stressed mAb monomers to the existing aggregates is studied with fluorescently labeled mAb molecules. The interesting techniques allow the challenging analysis of heterogeneous species containing both monomers and aggregates.

A completely new and orthogonal technique for the detection of protein aggregates is studied in chapter 8. A laser-induced breakdown detection (LIBD) setup is used to sense the formation of mAb aggregates upon thermal unfolding. Therefore, an optical setup using a strong laser is coupled with a temperature-controlled cuvette and the breakdown events caused by plasma formation of protein particles is monitored. The LIBD results are compared to previously performed temperature-ramped studies.

Finally, a summary of the results is given. It highlights the benefits and drawbacks of the used analytical techniques and concludes the thesis.

3 Differential scanning fluorimetry (DSF) for the high-throughput analysis of protein melting

3.1 Introduction

In living organisms, proteins are typically in the native state which is folded to a certain conformation that facilitates the function of the protein. The enthalpy minimum is gained from stabilizing protein-protein and protein-solvent interactions against the unfavorable increase in entropy of the system. This leads to the fact that proteins typically form a hydrophobic core consisting of nonpolar and uncharged amino acids, whereas hydrophilic residues are exposed to the aqueous solvent. DSF is based on the environmental sensitivity of a fluorescent dye such as ANS, Bis-ANS, and SYPRO® Orange. These probes are quenched in water and show high quantum yields in solvents with low dielectric constant.[1] Upon thermal unfolding, the protein structure is lost and the hydrophobic residues and patches are exposed to the solvent, facilitating interaction with the probe.[2] Monitoring the fluorescence intensity as a function of the temperature shows a prominent fluorescence increase upon unfolding. The obtained fluorescence melting transitions are subsequently analyzed to obtain the apparent melting temperature (T_m) of the protein. This principle was introduced 2001 by Pantoliano and coworkers for the high-throughput screening (HTS) of small molecule binders to proteins.[3] In this case, a low-molecular weight ligand will stabilize the native state and will lead to a higher thermal stability, and the positive T_m shift is used for hit identification. This thermal shift assay was spread after Lo et al. described the application of RT-PCR machines for DSF in 2004.[4] In contrast to the custom setup built by Pantoliano et al.,[3] which was registered as ThermoFluor® in the United States,[5] the use of marketed RT-PCR allowed the application of DSF in common laboratories.[4,6] Following up these publications, DSF evolved into an essential screening tool for fragment-based drug discovery (FBDD),[7-9] with numerous recent publications in this scientific area.[10-18]

In a similar way as ligands binding to the native protein, other extrinsic factors like the buffer species, pH, ionic strength, and excipients affect the thermal stability of proteins. Stabilizing conditions lead to an increased T_m value, whereas destabilizing

conditions reduce T_m of the protein. In 2006 Ericsson et al. studied the T_m values of *Escherichia coli* proteins with the aim to find high thermal stabilities which promote crystallizability.[19] DSF was applied by Mezzasalma et al. to increase the yield during production and purification of two proteins by finding stabilizing and avoiding destabilizing solution conditions.[20] Crowther and coworkers investigated the effect of various buffers on the DSF melting curves and T_m value of recombinant proteins from *Plasmodium* parasites.[21] A design of experiment (DOE) approach was chosen by Ablinger et al. to optimize the formulation of granulocyte colony stimulating factor (G-CSF).[22] Moreover, DSF was used by several authors for formulation development of therapeutic mAbs. A high-throughput thermal stability screening of four different mAb molecules was performed by He et al. in 2010.[23] The conformational and colloidal stability of four different mAbs was investigated by Goldberg et al. later in the same year by DSF and temperature-ramped SLS experiments.[24] In 2011, Li and coworker also studied colloidal and thermal stabilities of three mAb using several high-throughput techniques (turbidity, fluorescence, DSF, DLS, and flow cytometry).[25] King et al. investigated the predictability of thermal stability based on the DSF results of 77 mAbs.[26]

This chapter gives a comprehensive discussion on DSF method development. It considers the aspects of data analysis of the experimental data to obtain the outcome parameters T_m and $T_{m,onset}$. Furthermore, experimental parameters significantly influencing the results, such as fluorescent dye and protein concentration, are discussed. Although SYPRO® Orange is the most common fluorescent dye used for DSF, other popular dyes are reported. The hardware requirements necessary for DSF are discussed on the example of two RT-PCR machines. Finally, investigations on the validity of the obtained T_m values are presented. The DSF method evaluated in this chapter is applied for the analysis of various investigations presented in the chapters 4 through 6.

3.2 Materials and methods

3.2.1 mAb model protein

A therapeutic IgG1 model monoclonal antibody (“MAb”) produced in CHO cells with ε_{280nm} of 1.49 ml g^{-1} cm^{-1} was used.

3.2.2 Differential scanning fluorimetry (DSF)

The DSF method is introduced and developed in this chapter. Every step from, hardware requirements and setup, to sample preparation, experimental parameter influencing the outcome, and finally, the data analysis are comprehensively discussed. All experiments, if not stated otherwise, were performed on a RT7300 RT-PCR machine (Applied Biosystems, Foster City, California, USA). In chapter 3.5, in which hardware aspects are discussed, also results from the qTower 2.2 (Analytik Jena AG, Jena, Germany) are presented. The qTower 2.2 is a RT-PCR machine used in addition to the RT7300 in chapter 4. For DSF experiments with the qTower 2.2, two customized filter modules were supplied by the manufacturer that are both optimized for the detection of SYPRO® Orange. One filter module contains an optical density filter which reduces the overall fluorescence intensity to avoid saturation of the detector when higher protein concentrations are investigated. For differentiation, this filter module is referred to as the “attenuated” SYPRO® Orange filter.

3.2.3 3D fluorescence spectra of fluorescent dyes used for DSF

A standard (20 – 96°C) DSF experiment was performed to achieve a typical sample of denatured protein. The formulation in 10 mM sodium phosphate buffer at pH 5.0 of 4 mg/ml MAb was selected due to low turbidity after exposure to high temperatures (see chapter 6). Samples with SYPRO® Orange, CCVJ, and DCVJ (all Sigma-Aldrich, Steinheim, Germany) were investigated. Three wells of each 20 µl were pooled and transferred into a submicro fluorescence glass cuvette (Hellma Analytics, Müllheim, Germany). A Cary Eclipse spectrofluorimeter (Varian, now Agilent Technologies, Santa Clara, California, USA) with a temperature controlled cuvette holder was used (20 °C). Prior to the 3D scan, the optimal settings for the slids and the photomultiplier tube (PMT) voltage were evaluated to achieve a suitable signal intensity of the sample in the region of interest. The 3D scan was performed in steps of 1 nm with 1 s signal averaging, from 300 – 600 nm excitation and 400 – 700 nm emission wavelength to cover the entire spectroscopic characteristic of the dye in presence of the denatured protein. Although the solutions were clear to the naked eye, first and second order light scattering of the excitation light, which is many times stronger than the fluorescent light from the sample, was observed. For graphical illustration, the scattered light from a MAb sample without the extrinsic dye was subtracted as background. All calculations and graphing were performed using GNU

octave version 3.6.2 (https://www.gnu.org/software/octave/) under Debian Linux (http://www.debian.org/).

3.3 Aspects of data analysis

3.3.1 Analysis of the protein melting temperature

In a simplified model, the protein molecule can populate either the native (N) or the unfolded state (U), and both states are linked by a reversible reaction. The native state is favored due to stabilizing (noncovalent) interactions of the protein. In thermodynamic equilibrium, each concentration is defined by the equilibrium constant of unfolding K_{unf} at the given temperature

$$K_{unf} = \frac{[U]}{[N]} \tag{3-1}$$

At low temperatures, the concentration of the unfolded protein is low and most molecules populate the native state. With increasing temperature, the reaction is shifted towards the unfolded state as the stabilizing interactions are compensated. The equilibrium constant is linked to the Gibbs (free) energy change of unfolding ΔG_{unf} via equation (3-2)

$$\Delta G_{unf} = -RT \ln K_{unf} \tag{3-2}$$

where R is the gas constant and T the absolute temperature [K]. As can be seen from equation (3-2), ΔG_{unf} of the system is zero when K_{eq} equals one. The temperature at which both concentrations of native and unfolded protein are the same is defined as the protein melting temperature (T_m).[27] In a DSC scan, ΔG_{unf} is zero at the midpoint of the endothermic unfolding transition (see chapter 4).

DSF is based on the interaction of the environmental sensitive fluorescent probe with the unfolding protein structure upon heating. The exposure of hydrophobic structure leads to more pronounced interaction and higher fluorescence intensity. Assuming that the highest fluorescence intensity is observed in the unfolded state, the midpoint of the transition represents the apparent T_m value. This fluorescence increase can be monitored using a common RT-PCR machine (see chapter 3.5) that also facilitates the temperature ramp. In contrast to protein unfolding, DNA melting results in a descending fluorescence intensity of the probe upon heating, and thus a positive sign

of the first derivative. The possibility to invert the sign of the first derivative in most RT-PCR software allows T_m analysis of proteins. But performing HTS with numerous samples in multi well plates raise the need for automatized data analysis to handle the magnitude of data points in a reasonable amount of time. Using scientific graphing and data analysis software such as Origin® (Originlab Corporation, Northampton, Massachusetts, USA) as described below, or other programs,[28-30] scripts for automatized data analysis can be programmed. Furthermore, routines like nonlinear (Boltzmann) functions can be adapted for advanced data analysis, which are typically not supported by RT-PCR software. In the following paragraphs, two methods for the determination of the apparent T_m value will be demonstrated, which were automatized using LabTalk on Origin® 8 SR6 (Originlab) (see Appendix for the full LabTalk code of the "OpenTM" script).

First, the sigmoidal shape of the fluorescence transition can be investigated by fitting a model function. The Boltzmann function was described in literature for T_m determination of DSF experiments.[6,19] This equation describes the sigmoidal transition of the native protein with low fluorescence intensity values to the unfolded structure with high fluorescence intensity in a reversible, two-state one-step reaction. Despite the common irreversibility and noncooperativity of the unfolding process, the Boltzmann analysis is known to produce good results.[4] The fluorescence intensity (I) is described by the Boltzmann function via four parameters:

$$I(T) = \frac{A_L - A_U}{1 + e^{\left(\frac{T - T_m}{dT}\right)}} + A_U \tag{3-3}$$

A_L is the lower and A_U the upper limit of the fluorescence intensity*, T_m is the temperature at the midpoint of the transition, and dT is the slope factor. Figure 3-1 A exemplarily presents the fitted Boltzmann functions to both transitions of 4 mg/ml MAb in 25 mM histidine buffer pH 7.7. Initially, local minima and maxima of the fluorescence intensity were determined (54, 74, 77, 84 °C). These temperatures were then used as starting points for A_L and A_U. Next, χ^2 was minimized during the fit while all four parameters are free for maximum conformity. The apparent T_m values were determined as 68.26 °C and 81.31 °C for T_{m1} and T_{m2}, respectively (Figure 3-1 A).

* Note: To prevent confusion with the osmotic second virial coefficient (A_2) from the parametric expansion of the osmotic pressure (chapter 6), the upper and lower limits A_2 and A_1 as published in Menzen and Friess[31] (chapter 5) are renamed in this thesis to A_U and A_L, respectively.

Second, the midpoint can be determined by investigation of the first derivative of the fluorescence intensity. Figure 3-1 B illustrates the apparent T_m values of both transitions of 4 mg/ml MAb in 25 mM histidine buffer pH 7.7 with T_{m1} and T_{m2} of 68.97 °C and 81.28 °C, respectively. These results were obtained by analysis of the first derivative for peak maxima. To obtain a higher temperature resolution, the first derivative was splined (interpolated). Furthermore, absolute values of the first derivative were necessary for the peakfind algorithm and thus negative signs were inversed (see inlet graph of Figure 3-1 B).

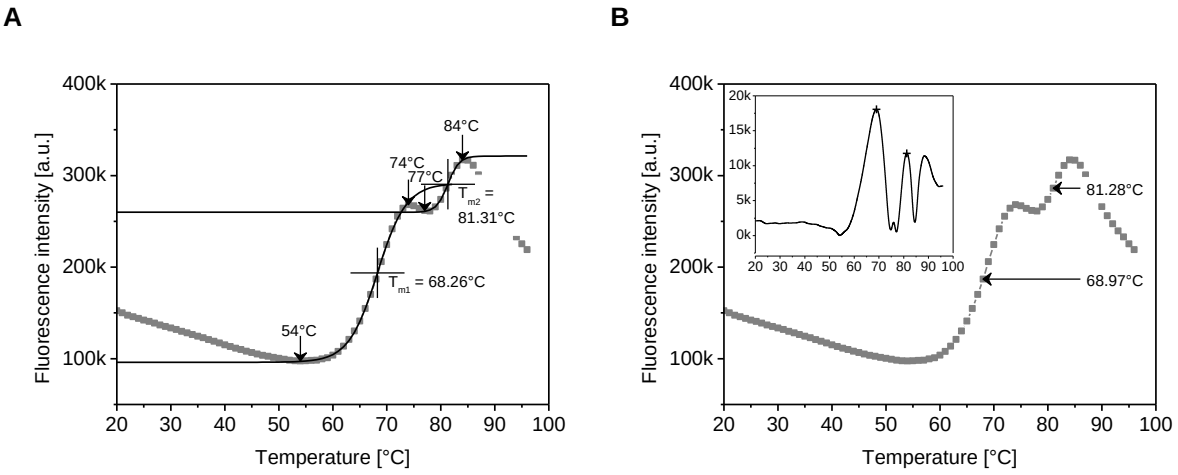

Figure 3-1. Common techniques to determine apparent T_m values from DSF melting transitions are illustrated in the example of 4 mg/ml MAb in 25 mM histidine buffer pH 7.7. The Boltzmann equation was fitted to both melting transitions (A). The T_m values as the midpoint of the fits are marked with a cross. The inflection point of the transitions were analyzed by the first derivative of the fluorescence data (B). The T_m values are the local maxima of the first derivative as illustrated in the insert graph.

The results from T_m analysis of 96 samples of 4 mg/ml MAb in 25 mM histidine buffer pH 7.7 are presented in Figure 3-2. The histograms illustrate a small difference in the apparent T_{m1} value between Boltzmann fit and first derivative analysis. Such difference was not observed for T_{m2}. Similar histograms were obtained for the RT7300 and the qTower 2.2 system. The standard deviations ranged between 0.2 and 0.3 °C. A normal distribution of the obtained T_m values was confirmed by Shapiro-Wilk test ($p = 0.05$) for both analysis methods and both RT-PCR machines. Consequently, about 99.73 % of all values are within the range of three-sigma (3σ). That means with a typical standard deviation of a DSF experiment as described above (< 0.3 °C), 3σ is about 0.6 - 0.9 °C. Therefore, as a practical rule, a difference

of > 1 °C is with high probability a significant result, and the thermal shift is assumed to be caused by a stabilizing or destabilizing effect on the protein structure.

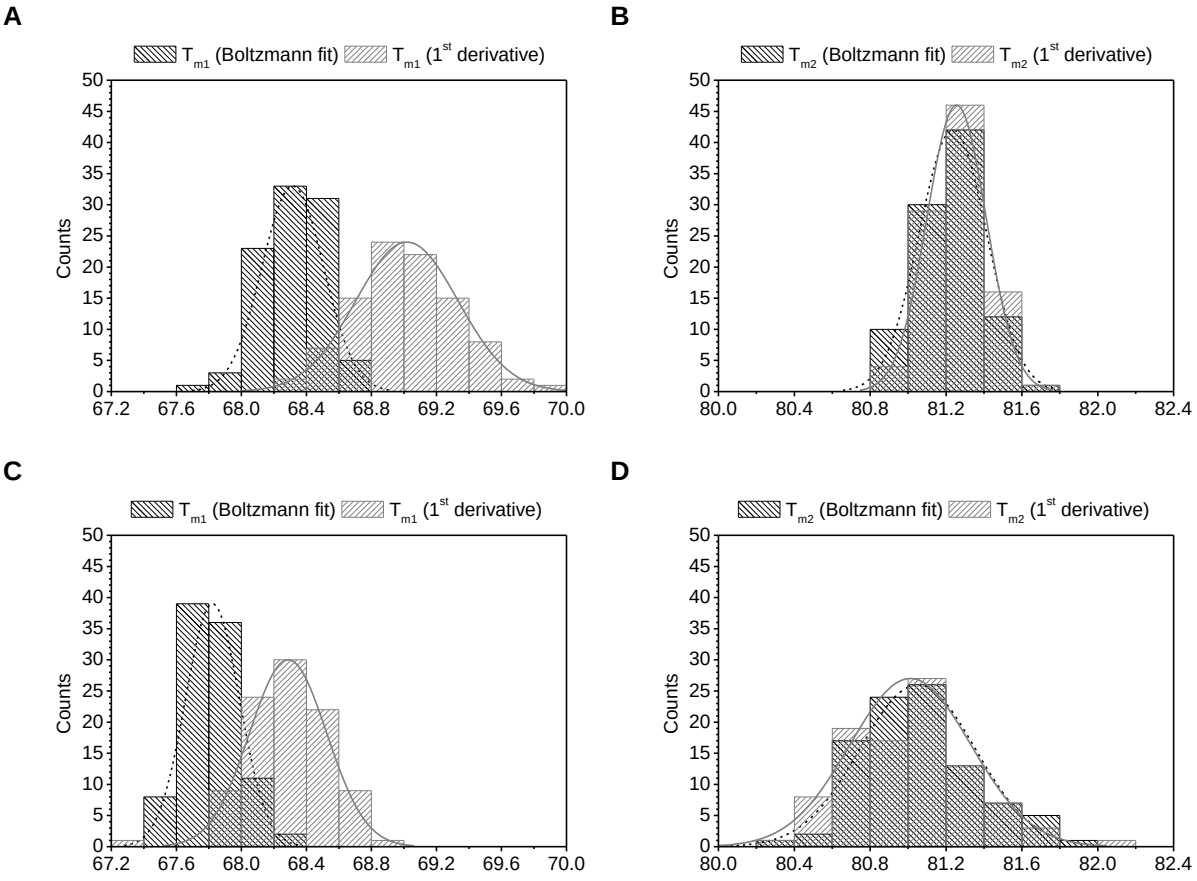

Figure 3-2. Histograms of apparent T_m values of 4 mg/ml MAb in 25 mM histidine buffer pH 7.7 determined by Boltzmann fit and first derivative analysis. T_m values of the first melting transition (A) and second melting transition (B) were obtained with the RT7300 (Filter C). Data from T_{m1} (C) and T_{m2} (D) were obtained with the qTower 2.2 (attenuated SYPRO® Orange filter).

The interpretation of the melting transitions of the multi-domain mAb molecules will be discussed in detail in chapter 4. It is important to note that the T_m value depends on the formulation conditions of the protein such as pH and ionic strength. These effects can increase or decrease the T_m value due to stabilizing or destabilizing conditions, respectively, and can affect individually the domains of the mAb. It is therefore possible to obtain overlapping unfolding transitions. Overlapping transitions are difficult to analyze. In this case and also when apparent T_m values are close, first derivative analysis might be more sensitive and easier to automatize than Boltzmann fitting. Furthermore, the first unfolding transition is typically very strong, whereas higher transitions are often less pronounced.

3.3.2 Analysis of the onset temperature of unfolding

The first investigation on a value similar to the onset temperature of unfolding was described by King et al.[26] They studied the thermal stability of various mAbs and concluded that the temperature at which 1 % of the protein was unfolded ($T_{1\%}$), is more predictive than the common T_m value.[26] Their procedure included a novel approach to analyze the fluorescence transitions obtained by DSF. By simultaneous fitting of three Gaussian curves to the unfolding transitions, they were able to deconvolute the unfolding of each mAb domain. Based on the total area under the curve (AUC) of unfolding protein, the temperature at which 1 % of the area is reached is referred to $T_{1\%}$. Figure 3-3 illustrates this type of data analysis on the example of 4 mg/ml MAb in 25 mM histidine buffer pH 7.7. Three Gaussians were fitted to the melting transitions of the MAb molecule using Origin® 8 SR6 (Originlab). After integration in temperature steps of 0.01 °C, the $T_{1\%}$ value was determined as 62.56 °C.

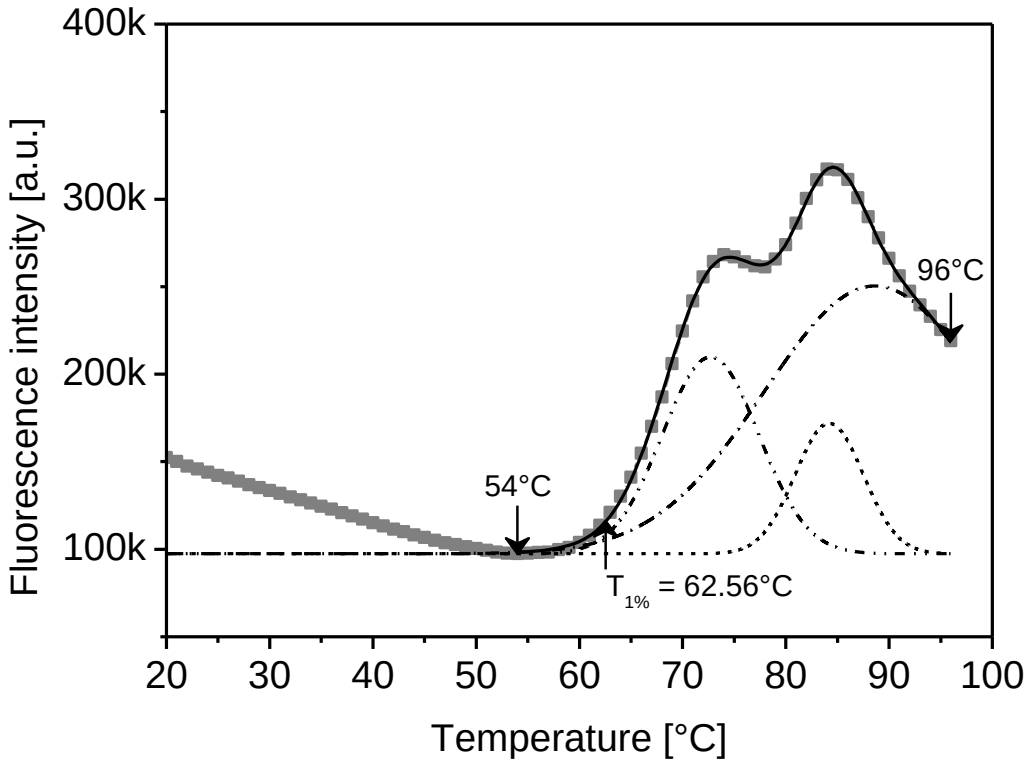

Figure 3-3. Illustration of the procedure to determine $T_{1\%}$ as described by King et al.[26], on the example of 4 mg/ml MAb in 25 mM histidine buffer pH 7.7. Three Gaussian curves were simultaneously fitted to the unfolding transitions (54 – 96 °C). The resulting Gaussians suggest the unfolding of the three individual mAb domains (CH2, CH3, Fab; see chapter 4). The temperature at 1 % of the total AUC ($T_{1\%}$) is indicative for 1 % of unfolding.[26]

The advantage of the procedure from King et al. is the introduction of a parameter that is analogous to the energy from DSC experiments and which is not obtained by common T_m analysis. Furthermore, this AUC value enables the derivation of an onset temperature by defining a threshold, at which a certain percentage of unfolding has occurred (e.g., $T_{1\%}$). The disadvantage of the simultaneous Gaussian analysis is its complexity and nonrobustness with respect to the numerous shapes of melting profiles which typically appear for multi-domain proteins in HTS scenarios. Automated data analysis for this procedure is not available in marketed RT-PCR software so far. As Origin® supports nonlinear fitting including multiple Gaussian functions as presented in Figure 3-3, the analysis of $T_{1\%}$ similar to King et al. could be automatized and included in the OpenTM LabTalk script presented in this work.

The analysis of T_m by Boltzmann fitting is a common procedure for the analysis of DSF melting profiles (see chapter 3.3.1). It is therefore desirable to obtain the onset temperature based on the results of the Boltzmann fit. The following section will introduce a procedure to calculate $T_{m,onset}$ from the fitted parameters of the Boltzmann function that allows the determination of T_m and $T_{m,onset}$ in one step. The procedure is illustrated in Figure 3-4 on the example of 4 mg/ml MAb in 25 mM histidine buffer pH 7.7. The $T_{m,onset}$ value is defined as twice the distance between T_m and the intersection of the tangents through T_m and the base line. The equation to obtain $T_{m,onset}$ from the fitted parameters of the Boltzmann function is derived in the following section.

The Boltzmann function f is used to describe the fluorescence intensity as a function of the temperature. The Boltzmann function was already introduced in equation (3-3) but should be repeated here for derivation of $T_{m,onset}$.

$$f(T) = \frac{A_L - A_U}{1 + e^{\left(\frac{T - T_m}{dT}\right)}} + A_U \tag{3-4}$$

A_L and A_U are the lower and upper fluorescence intensity limits, respectively. T_m is the temperature at the inflection point, and dT is a slope factor at T_m. Equation (3-4) was derived using Maxima version 5.26.0 (http://maxima.sourceforge.net/) to obtain f'(T)

$$f'(T) = -\frac{e^{\left(\frac{T-T_m}{dT}\right)}(A_L - A_U)}{dT\left(e^{\left(\frac{T-T_m}{dT}\right)} + 1\right)^2} \tag{3-5}$$

The slope of the Boltzmann function at T_m is obtained from the derived function f'(T) with $T=T_m$

$$f'(T_m) = -\frac{A_L - A_U}{4dT} = \frac{A_U - A_L}{4dT} \tag{3-6}$$

Next, the fluorescence intensity at T_m is obtained from the Boltzmann function f (equation (3-4))

$$f(T_m) = \frac{A_L - A_U}{2} + A_U = \frac{A_U + A_L}{2} \tag{3-7}$$

Using the results from equation (3-6) and (3-7), the tangent g through T_m is described by a linear equation

$$g(T_m) = \frac{A_U + A_L}{2} = a + \frac{A_U - A_L}{4dT} T_m \tag{3-8}$$

whereas a is the intercept of the tangent. Subsequently, the intersection T' of the tangent with the baseline ($=A_L$) is obtained from

$$T' = \frac{A_L - a}{\frac{A_U - A_L}{4dT}} = \frac{A_L - \left(\frac{A_U + A_L}{2} - \frac{A_U - A_L}{4dT} T_m\right)}{\frac{A_U - A_L}{4dT}} \tag{3-9}$$

The onset temperature $T_{m,onset}$ is calculated by subtracting twice the distance between T_m and T' (equation (3-9)) from T_m

$$T_{m,onset} = T_m - 2(T_m - T') = \frac{8dT\left(A_L - \frac{A_U + A_L}{2} + \frac{A_U - A_L}{4dT} T_m\right)}{A_U - A_L} - T_m \tag{3-10}$$

Equation (3-10) is described only by parameters that are obtained from the fitted Boltzmann function, and therefore $T_{m,onset}$ is calculated without further procedures.

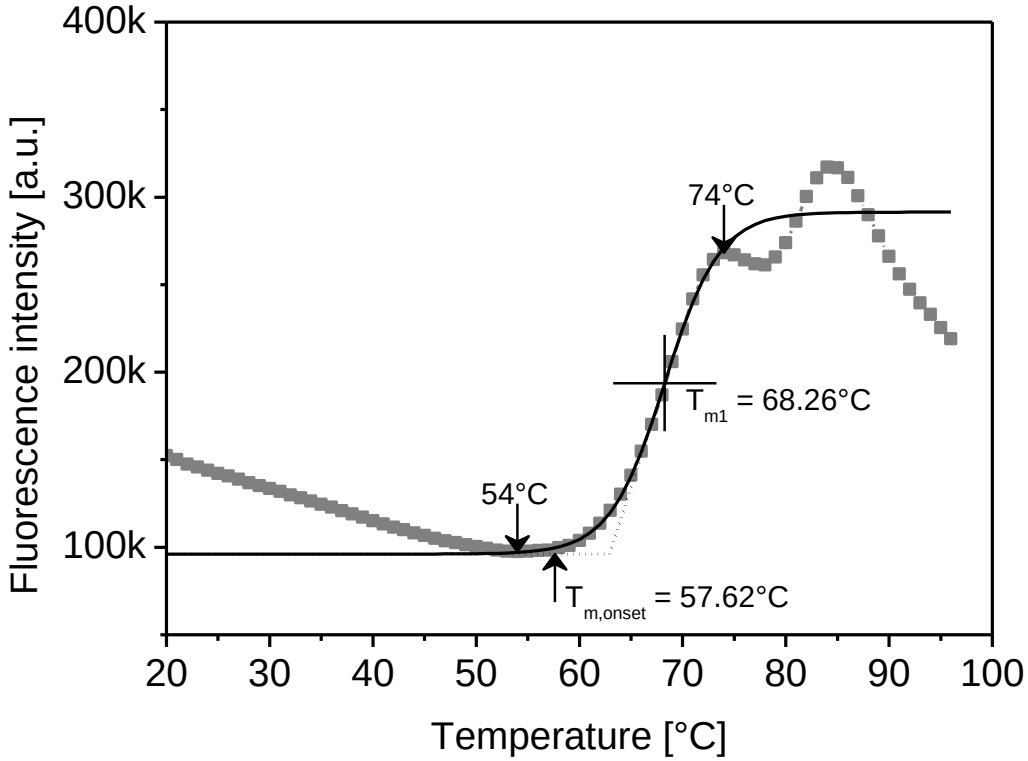

Figure 3-4. DSF melting profile of 4 mg/ml MAb in 25 mM histidine buffer pH 7.7. The Boltzmann function was fitted to the first melting transition (black line). To restrain the data to the first transition, the local minimum and maximum at 54 °C and 74 °C were used as lower and upper limits, respectively. All four parameters were free during the fit. The obtained apparent T_m value at the inflection point is marked with a cross. Dotted lines mark the tangents leading to the $T_{m,onset}$ value (upper arrow) as calculated by equation (3-10).

Of course, $T_{m,onset}$ can be calculated for every transition observed upon thermal unfolding of the protein. In this case, the nomenclature $T_{m1,onset}$, $T_{m2,onset}$, etc. is suggested to differentiate the events. For the HTS of therapeutic proteins, typically the lowest observed transition is of interest. Thus, $T_{m,onset}$ is represented as the onset temperature of the first transition, i.e., the temperature at which the first change of the structure is detected by the fluorescent dye. Figure 3-5 illustrates the analysis of $T_{m2,onset}$ of the second unfolding transition on the same example as presented in Figure 3-4 for the first unfolding transition.

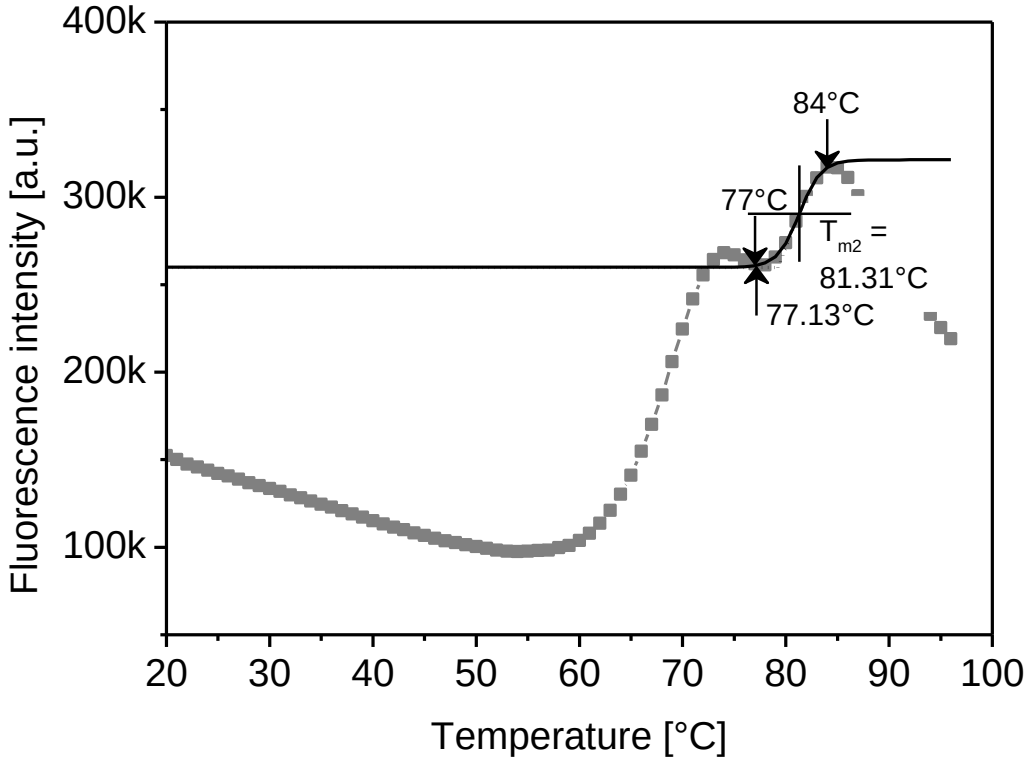

Figure 3-5. Boltzmann fit to the second melting transition of the MAb of the same sample as presented in Figure 3-4. As the "overall" onset of unfolding is marked by the $T_{m,onset}$ value, the value obtained at 77.13 °C is therefore not named. If onset temperatures of different domains are of interest, the value can be referred to as $T_{m2,onset}$.

3.4 The effect of experimental parameters on the apparent T_m value

SYPRO® Orange, which is sensitive to the increasing hydrophobicity upon protein unfolding, is the most frequently used fluorescent dye in DSF. However, the use of probes with different environmental sensitivity can change the outcome as different processes are monitored. As the measured fluorescence intensity originates from protein-dye interaction, also the influence of the concentration of both protein and SYPRO® Orange on the DSF results needs to be evaluated. Furthermore, the heating ramp affects the apparent T_m value as the process of unfolding during DSF is supposedly not in equilibrium. Consequently, experimental parameters were systematically varied to achieve an optimal DSF protocol.

3.4.1 Popular dyes used for DSF

The environmental sensitivity of a fluorescent dye is key for its applicability as a probe in DSF experiments. Upon protein unfolding, interaction of the dye with the

protein molecules must lead to a change in the fluorescence properties. In case of the dyes from the anilinonaphthalene sulfonic acid family (1,8-ANS; 2,6-ANS; Bis-ANS; 2,6-TNS), the switchover from a medium with high dielectric constants (polar environment) to a medium with low dielectric constants (nonpolar, hydrophobic environment) leads to a blue shift in emission maximum and increase in quantum yield.[1] The fluorescence spectra of other small molecules can interfere with the low excitation and emission wavelength of these dyes which limit their application. The sensitivity towards “hydrophobicity” is also the case for Nile red, Dapoxyl sulfonic acid, and SYPRO® Orange. SYPRO® Orange is the most often used dye for DSF,[32] due to its high photostability, chemical stability, and high fluorescence increase during DSF which is beneficial over Nile red and Dapoxyl sulfonic acid.[6] Comparable results to SYPRO® Orange were also reported for the related dye NanoOrange®.[33-36] As these probes rely on an increase in protein hydrophobicity with unfolding, they have limitations for proteins which are rather hydrophobic by nature (high fluorescence intensity of the native protein) or when surfactants are present (high background fluorescence due to interactions with micelles or hydrophobic structures). In both cases, an increase in fluorescence intensity upon unfolding can be concealed. For these applications, dyes with different environmental sensitivity are reported. The use of CCVJ,[37] and DCVJ,[31] for DSF in the presence of surfactants was recently reported, which is comprehensively discussed in chapter 5. Alexandrov et al. described the application of CPM, a dye that reacts covalently with free thiol-groups (cysteines) of the protein upon thermal unfolding.[38] It allows the analysis of very hydrophobic proteins, such as membrane proteins, which are reported to be challenging.[33,39] Although CPM could be applied for samples in the presence of surfactants, the reaction is limited to pH 6 to 8.[38] Thioflavine T is a dye which is known to interact primarily with fibrils and amyloid structures.[40,41] It was recently applied to DSF to monitor the formation of amorphous, fibrillar aggregates upon thermal unfolding.[42] Especially for proteins with high β-sheet content, such as mAbs, Thioflavin T is a promising dye for the assessment of the conformational and colloidal stability.[42] ProteoStat® (Enzo Life Science, Plymouth Meeting, Pennsylvania, USA) is a molecular rotor dye that was developed for DSF, and is proposed for the analysis of protein aggregation. Already applied during the structural characterization of first nucleotide binding domain (NBD1),[35] the application of ProteoStat® for the development of therapeutic proteins, e.g., in the presence of surfactants, needs to be

shown. The analysis of a protein with a set of dyes with different environmental sensitivity may be promising to obtain both conformational and colloidal stability data.[37,42]

3.4.2 Aspects of sample preparation

The simple and direct sample preparation is one major advantage of the DSF method. Typically, there a no preparative steps on the protein sample necessary. In combination with the multi-well plate format, the fast forward sample handling is one of the key features to allow HTS with this method. For a DSF experiment, three single liquid handling steps are necessary: i) the protein containing sample solution needs to be dispensed into the well, ii) a working solution of the fluorescent dye needs to be prepared from a concentrated stock solution, and iii) the working solution of the fluorescent dye needs to be added and mixed.

The necessary sample volume for one well depends on the well plate size and instrumental setup. It needs to be considered that with addition of the fluorescent probe as a solution, the total volume increases and a dilution of the sample is inevitable. Furthermore, other components like ligands or excipients can be spiked into the samples from stock solutions to prepare the final formulation directly in the wells. A sample volume of 20 µl was found to give robust results for the optical 96-well reaction plates with the RT7300 RT-PCR. By addition of 1 µl of the working solution of the dye, the resulting dilution was minimized to 5 %. The influence of 5 % sample dilution on the apparent T_m value can be neglected for low concentration samples (compare Figure 3-6 B).

Table 3-1 summarizes the results for three different ways of sample preparation, admixing 1 µl working solution of the dye to 20 µl protein solution, admixing 20 µl protein solution to 1 µl working solution of the dye, and admixing 10 µl working solution of the dye to 10 µl protein solution. With one exception at 2 mg/ml MAb, the standard error was very low for all samples prepared by mixing the 10 µl solutions. The drawback of this approach is that the MAb stock solution needs to be double concentrated, which might be a hurdle. Moreover, the working solution of the dye should be prepared in the corresponding placebo buffer to avoid changing the formulation parameters like ionic strength, excipient concentration, or pH value. This is cumbersome when many different formulations are to be screened. Starting with

the 1 µl drop of working solution bears the risk of drying while preparing the well plate. Furthermore, smaller volumes are more easily pipetted into a solution than the other way round. This is most likely responsible for the slightly lower standard deviation of the approach starting with a larger volume of protein solution. Finally, the working solution of the dye was freshly prepared immediately before the experiment, because a slight decrease in S/N ratio over time was observed upon storage of the aqueous solution.

Table 3-1. Three different sample preparation protocols were compared.

MAb conc.	20 µl MAb + 1 µl dye		1 µl dye + 20 µl MAb		10 µl MAb + 10 µl dye	
	T_{m1} (CH2) [°C]	T_{m2} (Fab) [°C]	T_{m1} (CH2) [°C]	T_{m2} (Fab) [°C]	T_{m1} (CH2) [°C]	T_{m2} (Fab) [°C]
2 mg/ml	66.7±0.1	80.7±0.3	68.3±0.6	80.8±0.1	65.5±0.7	80.8±0.1
800 µg/ml	66.6±0.2	80.7±0.1	67.1±0.2	80.9±0.1	66.7±0.1	80.8±0.1
400 µg/ml	67.3±0.2	80.6±0.1	67.6±0.6	80.8±0.1	67.0±0.1	80.6±0.1
160 µg/ml	67.2±0.2	80.3±0.1	67.9±0.8	80.4±0.2	67.1±0.1	80.4±0.1
80 µg/ml	67.6±0.3	80.2±0.4	67.7±0.4	80.4±0.1	67.3±0.1	80.3±0.3
40 µg/ml	67.5±0.2	80.1±0.2	67.0±0.3	80.4±0.1	66.3±0.1	80.7±0.1

MAb in 25 mM histidine buffer pH 7.7 with 5x SYPRO® Orange. The presented T_m values are mean values with standard deviation of a sample triplicate.

3.4.3 The effect of SYPRO® Orange and protein concentration

The molecular structure and concentration of SYPRO® Orange are undisclosed. It is supplied by the manufacturer in a five thousand times (5000x) concentrated stock solution in dimethyl sulfoxide (DMSO). SYPRO® Orange was developed for gel staining after SDS-PAGE, and a dilution of 1:5000 (corresponding to 1x) is suggested by the manufacturer for this purpose.[43] For DSF applications, SYPRO® Orange concentrations between 1 – 5x are most commonly used. The DSF method was designed as a screening platform with low material consumption, which is especially important when purified drug substance is limited or the cost-of-goods are high. In this case, the application of low protein concentrations is beneficial. In contrast, when the drug product concentration is high, the analysis without dilution is desirable.

Figure 3-6 A shows the DSF melting profiles of a dilution series of the MAb in 25 mM histidine buffer pH 7.7 at various concentrations ranging from 80 µg/ml to 58 mg/ml.

With higher protein concentration more hydrophobic surface becomes available upon unfolding, and thus the fluorescence intensity increased because more dye molecules were able to interact. Additionally, the unfolding transition was shifted with increasing MAb concentration to lower apparent T_m values at higher initial and baseline fluorescence readings (Figure 3-6 B). Furthermore, lower T_m values were observed with 3x and 5x SYPRO® Orange. As SYPRO® Orange binds to the unfolded state of the protein, the interaction of the dye might be responsible for the reduced thermal stability of the MAb. However, DSC analysis of protein unfolding did demonstrate that T_m was not affected by the presence of up to 5x SYPRO® Orange (see chapter 4).

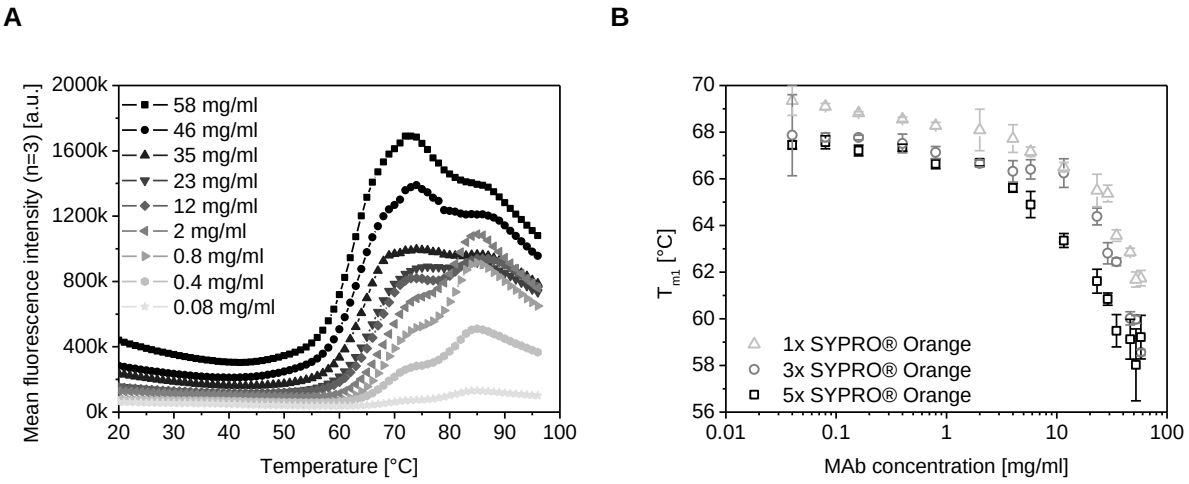

Figure 3-6. DSF melting profiles of various MAb concentrations in 25 mM histidine buffer pH 7.7 between 0.08 – 58 mg/ml with 1x SYPRO® Orange (A). Apparent T_m values obtained by Boltzmann fitting to the first melting transition of the MAb samples with SYPRO® Orange concentrations between 1 – 5x (B).

As the SYPRO® Orange stock solution is supplied in DMSO, residual amounts of the organic solvent are present in the sample. Sorrel et al. showed that DMSO has a negative effect on the stability of anthrax protein protective antigen, leading to a T_m values decreased by 3 °C and 4 °C in the presence of 1 % and 20 % DMSO, respectively.[44] DMSO is a typical solvent used for small molecules during FBDD and Niesen et al. suggest a final DMSO below 2 % during DSF experiments.[6]

To investigate the effect of DMSO on the apparent T_m values of the MAb, samples with 1x SYPRO® Orange were prepared and DMSO was spiked into the samples to obtain a concentration 0.06, 0.1, and 0.2 % DMSO, mimicking 3x, 5x, and 10x of the dye. The thermal stability of the MAb was not significantly reduced (Figure 3-7).

Especially the apparent T_m values of the low concentrated samples, where the effect of DMSO is expectedly high, were in good agreement. The large deviations for the samples in high MAb concentration of T_{m2} illustrate the diminishing second transition as presented in Figure 3-6 A and are independent on the addition of DMSO. That means the presence of DMSO due to a high amount of SYPRO® Orange did not negatively affect the thermal stability of the MAb during DSF. This finding was confirmed by DSC experiments which are presented in chapter 4.

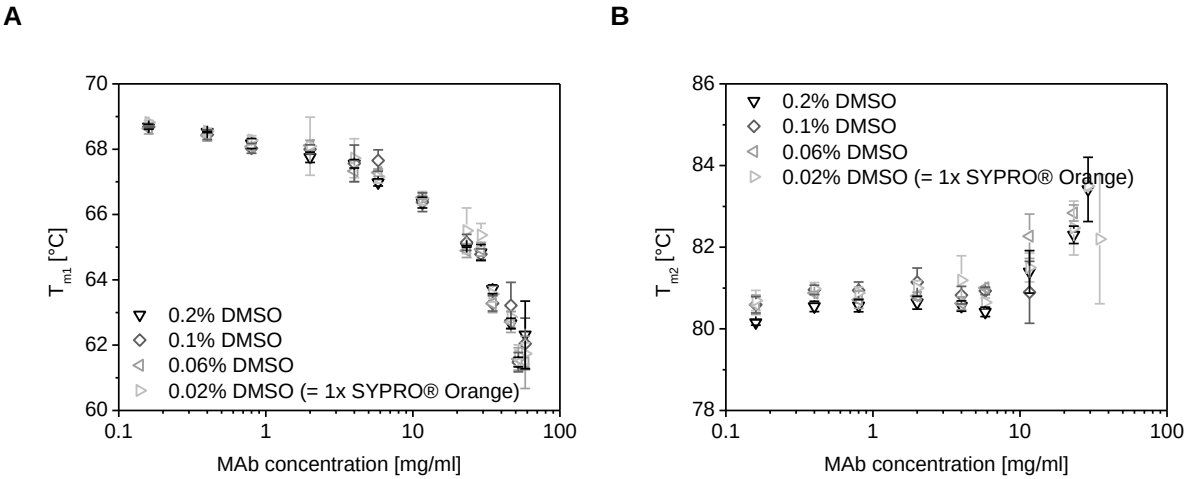

Figure 3-7. The T_{m1} and T_{m2} from Boltzmann analysis of the MAb in 25 mM histidine buffer pH 7.7 in the presence of 0.06, 0.1, and 0.2 % DMSO.

The observation that the second melting transition is more difficult to detect at higher MAb concentration (Figure 3-6 A) suggests that the amount of SYPRO® Orange may have been too low to monitor the full unfolding process in these samples. Figure 3-8 A shows the DSF melting profiles of 28 mg/ml MAb in 25 mM histidine buffer pH 7.7 with 5x and 25x SYPRO® Orange. Because the protein concentration was the same, the higher absolute mean fluorescence intensity of the 25x SYPRO® Orange suggests that a higher number of dye molecules could interact. The first fluorescence increase was much more pronounced than the second for both dye concentrations. It is important to note that the presented fluorescence curves were recorded at an emission wavelength of 530 nm because the high dye concentration in combination with a high protein concentration lead to saturation of the detector when the optimal filter settings at 578 nm were applied. This limitation by saturation will depend on the RT-PCR machine and the setting used. For 0.28 mg/ml MAb, the expected two subsequent transition profile was observed (Figure 3-8 B). Interestingly, a lower absolute fluorescence intensity of the second unfolding transition was obtained with

25x SYPRO® Orange. This may be due to attenuation of the incident light through absorption by the dye in solution (static quenching) and potentially interaction of the dye molecules with each other in the presence of only small protein amount (collisional quenching).[45]

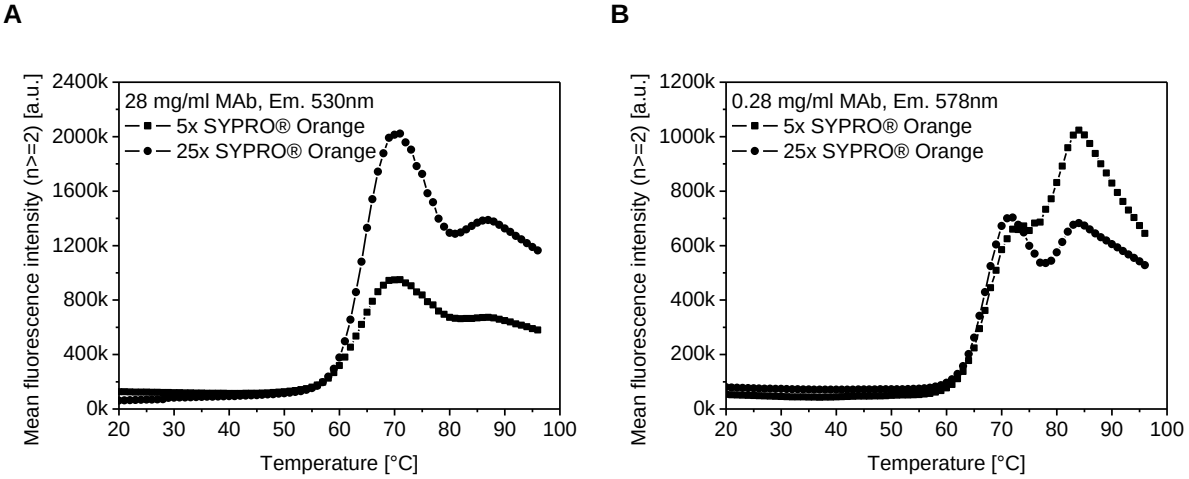

Figure 3-8. DSF melting profiles of the MAb in 25 mM histidine buffer pH 7.7 with 5x and 25x SYPRO® Orange. Emission filter at 530 nm was used for the 28 mg/ml sample to avoid saturation of the detector (A). The 1:100 diluted sample was analyzed with the standard filter setting at 578 nm (B).

Interestingly, the molecular rotor-dye DCVJ showed promising results for high concentration protein samples. As illustrated in Figure 3-9 A, at the high 35 mg/ml and 175 mg/ml MAb, the fluorescence increase upon thermal unfolding of the MAb resulted in a single transition for SYPRO® Orange (see also Figure 3-6 A). Probably, protein-protein interactions via the exposed hydrophobic patches of the highly crowded protein solution at this high concentration interfere with SYPRO® Orange. In contrast, the two expected transitions of the MAb were obtained when DCVJ was used (Figure 3-9 B). Furthermore, the fluorescence gain upon unfolding was much higher in case of DCVJ in comparison to SYPRO® Orange at 175 mg/ml MAb. A similar observation of higher signals with increasing protein concentration was made by Nashine et al. with Thioflavine T and referred to the formation of amorphous aggregates.[42] Furthermore, the fluorescence drop and the disappearance of second/higher melting transitions with increasing MAb concentration (see Figure 3-6 A) may be due to protein aggregation. Niesen et al. suggest that the fluorescence drop after unfolding is caused by aggregation of the protein. This aggregation is driven by the hydrophobic patches which become exposed upon unfolding, and consequently the hydrophobic surface for the interaction with SYPRO® Orange is

reduced.[6] This would explain the higher sensitivity of DCVJ which monitors the consecutive process of protein unfolding and aggregation of the MAb molecule.

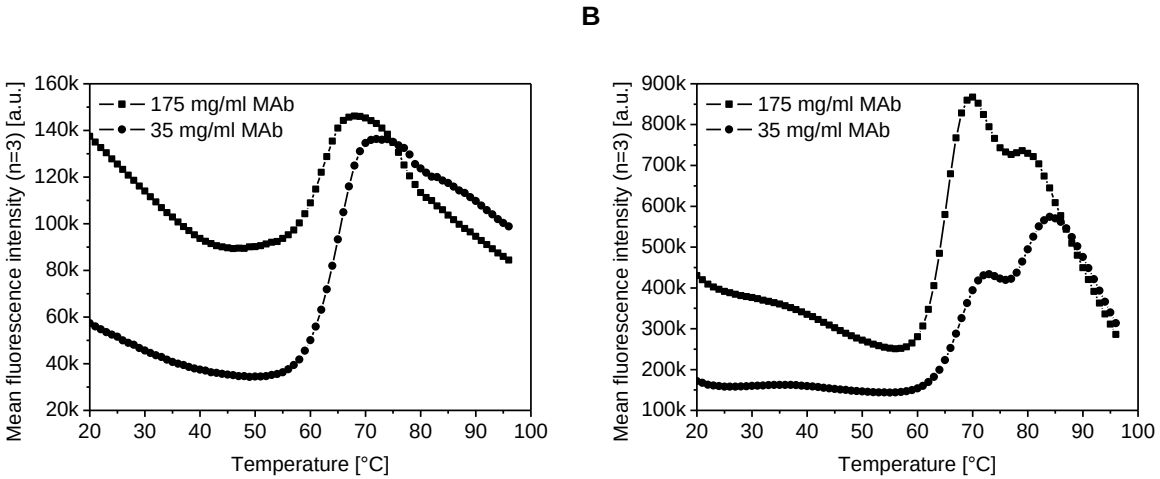

Figure 3-9. DSF melting curves of highly concentrated MAb formulations in 1 mM phosphate buffer pH 6.0. Results were obtained with 1x SYPRO® Orange (A) and 100µM DCVJ (B).

In conclusion, for HTS at low protein concentration, it can be recommended to use the lowest applicable SYPRO® Orange concentration (1x). This ensures that the interference of the dye and its solvent is minimized (c(DMSO) = 0.02 %). The detector settings should be optimized to result in a high S/N ratio, which is typically achieved by choosing the optimum excitation and emission filters as long as saturation is excluded. DSF is not limited to diluted samples, although the apparent T_m values were found to be dependent on the MAb concentration. In case of high protein concentrations, higher dye concentrations might be beneficial to avoid depletion of free dye and more clearly resolve higher unfolding transitions. But the higher amounts of both dye and solvent might negatively influence the protein stability. Furthermore, the absolute fluorescence intensity needs to be monitored for saturation effects of the detector, and an emission wavelength setting aside the fluorescence maximum may be necessary. In case of very high MAb concentrations, also other probes like DCVJ can be beneficial to monitor the process of unfolding.

3.4.4 The effect of the temperature ramp

After a first heating of 0.8 mg/ml MAb in 25 mM histidine buffer pH 7.7 to 96 °C during DSC and cooling, the second heating scan did not show an endothermic transition (Figure 3-10 A). This indicates irreversible unfolding which is known for multi-domain proteins such as mAbs after thermal denaturation.[46,47] In this case, no

equilibrium with a defined ratio between folded and unfolded state exists. As a consequence, the heating rate was observed to affect the apparent T_m value (Figure 3-10 B). Applying a lower heating rate of 0.3 °C/min resulted in lower apparent T_m values, whereas higher values were observed when the rate was increased to 1.5 °C/min. The extent of the shift was comparable for both DSC and DSF. At higher heating rate less time is available for the unfolding process, and thus the apparent T_m value is shifted to higher temperature. Interestingly, the scan rate dependence was more pronounced for the second unfolding transition (Figure 3-10 B).

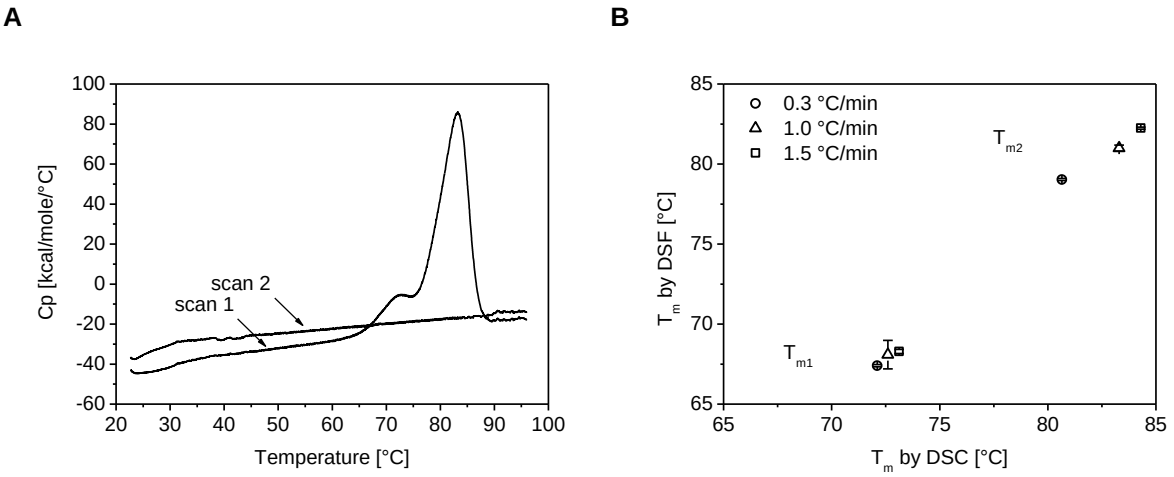

Figure 3-10. Repetitive DSC scans of 0.8 mg/ml MAb in 25 mM histidine buffer pH 7.7 (A). Effect of the heating rate on the apparent T_m values by DSC and DSF (B). The MAb samples in 25 mM histidine buffer pH 7.7 had a concentration of 1 mg/ml for DSC and 2 mg/ml for DSF.

The Microcal VP-DSC used (see chapter 4.2.10), is limited to a maximum heating rate of 1.5 °C/min, but the capillary models are capable of faster heating at 4 °C/min. In DSC experiments, a faster scan rate is commonly applied when small enthalpies are studied to narrow the unfolding range and thus increase the signal intensity. In contrast, slow heating may improve the resolution of multiple transitions.[48] The quick thermo controllers of RT-PCR machines allow for very fast DSF experiments, but the optical detection system becomes rate limiting. A good resolution of the MAb unfolding transitions was obtained at 1 °C/min in reasonable runtimes, and therefore was applied for both DSC and DSF experiments to compare the results.

3.5 Hardware settings and test for DSF

There are two requirements of DSF that are matched RT-PCR machines, a precise and fast temperature controller as well as a fluorescence detector. In combination

with multi-well plate formats, RT-PCR machines represent ideal hardware for the DSF technique.

3.5.1 Fluorescence excitation and emission settings

RT-PCR machines are optimized for the detection of fluorescent probes which are either dyes covalently linked to sequence specific probes or dyes that bind nonspecifically to nucleic acids.[49] These probes are used as reporter signal to monitor the progress of amplification. To serve in simple single-color to multiplex PCR assays,[50] marketed machines are typically equipped with several filter sets to allow for the detection of various fluorescent dyes. These dyes have a high excitation and emission wavelength in common, to minimize background fluorescence effects from biologic material. In case of the RT3700, a single excitation filter at 490 nm and four emission filter (510, 554, 578, and 610 nm) are available, and a halogen lamp is used as light source. The qTower 2.2 uses three LED light sources (blue, white, and red) and excitation and emission filters. Incandescent lamps with their broad spectrum of irradiated light,[51] offer a higher flexibility to customize filter modules with tailored excitation wavelength. LEDs, on the other hand, are more economic with lower price and very long life times.

The spectroscopic properties of SYPRO® Orange and of the molecular rotor dyes CCVJ and DCVJ were investigated in the presence of denatured MAb to extract the optimal excitation and emission settings (Figure 3-11). The obtained excitation and emission maxima are presented in Table 3-2. Because of the high excitation and emission wavelengths that are similar to common PCR dyes like SYBR® Green, FAM, and TAMRA,[50] SYPRO® Orange is applicable in all marketed RT-PCR machines. The highest fluorescence intensities with SYPRO® Orange were obtained with Filter C of the RT7300 (Ex. 490 / Em. 578 nm) and the SYPRO® Orange filter for the qTower 2.2 (Ex. 490 / Em. 580 nm). When saturation effects were observed with this very sensitive module, the yellow filter for TAMRA (Ex. 535 / Em. 580 nm) showed good results. In case of CCVJ and also DCVJ, the lower excitation and emission wavelengths, closer to the blue range of the visible spectrum, do not match common PCR dyes well and might raise the need for a customized filter module. As presented in chapter 5, Filter A (Ex. 490 / Em. 530 nm) of the RT7300 was suitable for the detection of DCVJ, and allowed for the application of DSF in the presence of surfactants.

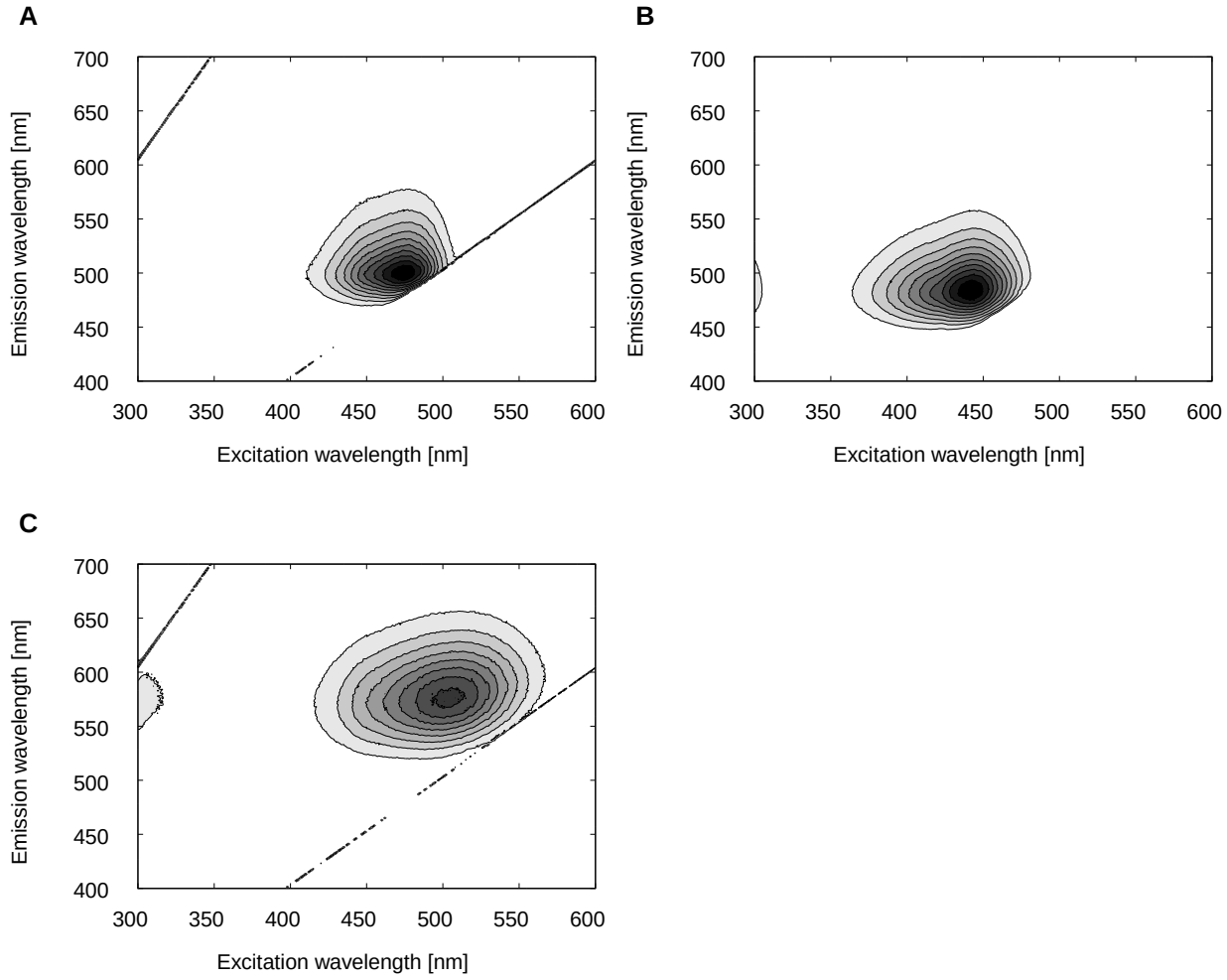

Figure 3-11. Three-dimensional fluorescence excitation and emission spectra of DCVJ (A), CCVJ (B), and SYPRO® Orange (C) in the presence of denatured MAb. The background spectrum of a MAb sample without the dye was subtracted to eliminate the effects from first and second order stray light in the graphs.

Table 3-2. The excitation and emission maxima in the presence of denatured MAb were obtained from the 3D scans presented in Figure 3-11.

	Excitation / emission maximum [nm]	
	In the presence of denatured MAb	Literature reports
SYPRO® Orange	500 / 575	470 / 569 [43]
DCVJ	470 / 500	450 / 480-505 [52]
CCVJ	440 / 470	437 / 490 [53]

The reported SYPRO® Orange data was obtained in an aqueous SDS-PAGE buffer with 0.05 % SDS and 150 µg/ml BSA.[43] Kung et al. reported emission wavelengths of DCVJ dependent on the dielectric constant of the solvent (high dielectric constant (glycerol): 505 nm; low dielectric constant (benzene): 480 nm).[52] The data of CCVJ was obtained in glycerol by Haviv et al.[53]

3.5.2 Homogeneity of the recorded fluorescence signal and apparent T_m within well plates

Any analytical machine based on well plate sample handling is prone to variations from well to well due to temperature differences across the well plate, moving optics, or other aspects of hardware design. Figure 3-12 shows the distribution of the maximum fluorescence intensities and the apparent T_{m1} values for the same sample of 4 mg/ml MAb in 25 mM histidine pH 7.7 across a 96-well plate. For the RT7300 system, which uses a CCD camera that captures the fluorescence readings of the whole plate, spots of lower maximum fluorescence intensity occurred in the corners of the well plate (Figure 3-12 A). In contrast, horizontal lines of similar maximum fluorescence intensities were observed as the qTower 2.2 scans the eight wells of a column simultaneously via optical fibers and subsequently moves the detector head column by column across the plate. When the machine is initialized, detector settings for the eight fibers are verified and adjusted to an internal intensity reference. Therefore it is likely, that similar values occurred in the same row (Figure 3-12 B).

But the absolute fluorescence intensity is less important than the obtained apparent T_m values. Since the relative fluorescence increase is analyzed for T_m determination, the T_{m1} and T_{m2} values were randomly distributed across the well plate (Figure 3-12 C - F). Thus, also other variations, e.g., in the amount of fluorescent dyes in the wells leading to differences in absolute fluorescence intensity, show minor effects. Furthermore, Seo and coworkers recently demonstrated the application of DSF to quantify proteins in cell lysates using absolute fluorescence readings.[54]

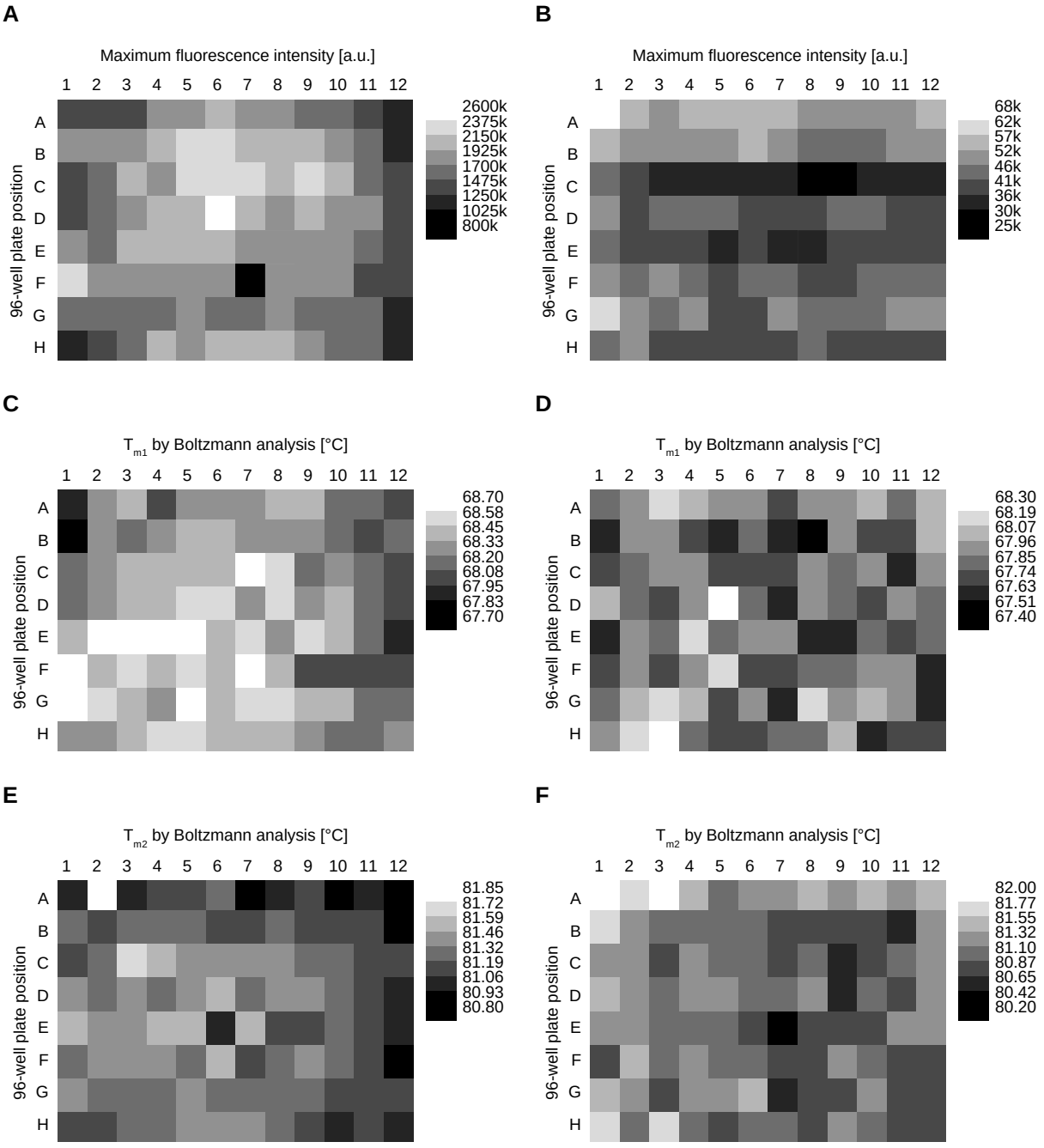

Figure 3-12. Maximum fluorescence intensity distribution of 4 mg/ml MAb in 25 mM histidine buffer pH 7.7 across the 96-well plate from the RT7300 with Filter C (Em. 578 nm) (A) and from the qTower 2.2 (attenuated SYPRO® Orange filter) (B). In addition, the corresponding apparent T_{m1} (C + D) and T_{m2} (E + F) values from Boltzmann analysis are presented.

3.6 Summary and conclusion

An extrinsic fluorescent dye, most often SYPRO® Orange, is used to monitor the unfolding process of proteins upon heating in DSF. Especially for formulation development of therapeutic protein drugs, the onset temperature of unfolding is of interest as it marks the temperature where first structural changes are observed. A

method to calculate the $T_{m,onset}$ value from the Boltzmann fit, which is routinely used to determine the apparent T_m value, was generated. Based on a RT7300 RT-PCR machine, a robust DSF method was developed and critical parameters were evaluated. For optimal sample handling and minimal dilution effects, the addition of a small volume of an aqueous working solution of the dye into the sample solution dispensed in the wells is beneficial. The dye concentration was kept as low as possible, to avoid saturation effects of the fluorescence detector, and to minimize the amount of DMSO, which is the solvent of dye in the stock solution. Protein concentrations as low as 40 µg/ml up to 175 mg/ml MAb were investigated. High protein concentrations are no limitation for DSF, although a higher dye concentration may be beneficial to monitor the unfolding process of multiple domains. In this case, and when surfactants are present, also probes with different environmental sensitivity like the molecular rotor dyes DCVJ and CCVJ are promising (see chapter 5). Because of aggregation and irreversible denaturation, the unfolding process upon heating was not at equilibrium, and increasing the heating rate resulted in higher apparent T_m values. Although faster heating rates are possible, the overall heating rate of 1 °C/min was applied to allow for comparison of the obtained results to DSC measurements. The multi-well plate format with low sample and time consumption, and automatized data analysis allows HTS of thermal stabilities. A standard deviation as low as 0.3 °C was found across a 96-well plate for both the RT7300 and the qTower 2.2. As the spectroscopic properties of SYPRO® Orange in the presence of denatured protein are well within the spectroscopic range of common dyes used for DNA analysis, probably all marketed RT-PCR machines are capable to obtain DSF data.

3.7 References

1. Stryer L 1965. The interaction of a naphthalene dye with apomyoglobin and apohemoglobin: A fluorescent probe of non-polar binding sites. J Mol Biol 13(2):482-495.

2. Poklar N, Lah J, Salobir M, Maček P, Vesnaver G 1997. pH and Temperature-Induced Molten Globule-Like Denatured States of Equinatoxin II: A Study by UV-Melting, DSC, Far- and Near-UV CD Spectroscopy, and ANS Fluorescence†. Biochemistry (Mosc) 36(47):14345-14352.

3. Pantoliano MW, Petrella EC, Kwasnoski JD, Lobanov VS, Myslik J, Graf E, Carver T, Asel E, Springer BA, Lane P, Salemme FR 2001. High-Density Miniaturized Thermal Shift Assays as a General Strategy for Drug Discovery. J Biomol Screen 6(6):429-440.

4. Lo M-C, Aulabaugh A, Jin G, Cowling R, Bard J, Malamas M, Ellestad G 2004. Evaluation of fluorescence-based thermal shift assays for hit identification in drug discovery. Anal Biochem 332(1):153-159.

5. Matulis D, Kranz JK, Salemme FR, Todd MJ 2005. Thermodynamic Stability of Carbonic Anhydrase: Measurements of Binding Affinity and Stoichiometry Using ThermoFluor. Biochemistry (Mosc) 44(13):5258-5266.

6. Niesen FH, Berglund H, Vedadi M 2007. The use of differential scanning fluorimetry to detect ligand interactions that promote protein stability. Nat Protocols 2(9):2212-2221.

7. Ciulli A. 2013. Biophysical Screening for the Discovery of Small-Molecule Ligands. In Williams MA, Daviter T, editors. Protein-Ligand Interactions, ed.: Humana Press. p 357-388.

8. Mashalidis EH, Śledź P, Lang S, Abell C 2013. A three-stage biophysical screening cascade for fragment-based drug discovery. Nat Protocols 8(11):2309-2324.

9. Winter A, Higueruelo AP, Marsh M, Sigurdardottir A, Pitt WR, Blundell TL 2012. Biophysical and computational fragment-based approaches to targeting protein–protein interactions: applications in structure-guided drug discovery. Q Rev Biophys 45(04):383-426.

10. Breuer S, Chang MW, Yuan J, Torbett BE 2012. Identification of HIV-1 Inhibitors Targeting the Nucleocapsid Protein. J Med Chem 55(11):4968-4977.

11. Cala O, Remy MH, Guillet V, Merdes A, Mourey L, Milon A, Czaplicki G 2013. Virtual and biophysical screening targeting the gamma-tubulin complex--a new target for the inhibition of microtubule nucleation. PLoS ONE 8(5):e63908.

12. Barman S, You L, Chen R, Codrea V, Kago G, Edupuganti R, Robertus J, Krug RM, Anslyn EV 2014. Exploring naphthyl-carbohydrazides as inhibitors of influenza A viruses. Eur J Med Chem 71(0):81-90.

13. Fagan RL, Wu M, Chédin F, Brenner C 2013. An Ultrasensitive High Throughput Screen for DNA Methyltransferase 1-Targeted Molecular Probes. PLoS ONE 8(11): e78752.

14. Fung S-PS, Wang H, Tomek P, Squire CJ, Flanagan JU, Palmer BD, Bridewell DJA, Tijono SM, Jamie JF, Ching L-M 2013. Discovery and characterisation of hydrazines as inhibitors of the immune suppressive enzyme, indoleamine 2,3-dioxygenase 1 (IDO1). Bioorg Med Chem 21(24):7595-7603.

15. Pizarro JC, Hills T, Senisterra G, Wernimont AK, Mackenzie C, Norcross NR, Ferguson MA, Wyatt PG, Gilbert IH, Hui R 2013. Exploring the Trypanosoma brucei Hsp83 potential as a target for structure guided drug design. PLoS Negl Trop Dis 7(10):e2492.

16. Amaning K, Lowinski M, Vallee F, Steier V, Marcireau C, Ugolini A, Delorme C, Foucalt F, McCort G, Derimay N, Andouche C, Vougier S, Llopart S, Halland N, Rak A 2013. The use of virtual screening and differential scanning fluorimetry for the rapid identification of fragments active against MEK1. Bioorg Med Chem Lett 23(12):3620-3626.

17. Eadsforth TC, Gardiner M, Maluf FV, McElroy S, James D, Frearson J, Gray D, Hunter WN 2012. Assessment of Pseudomonas aeruginosa N5,N10-methylenetetrahydrofolate dehydrogenase-cyclohydrolase as a potential antibacterial drug target. PLoS ONE 7(4):25.

18. Brvar M, Perdih A, Renko M, Anderluh G, Turk D, Solmajer T 2012. Structure-Based Discovery of Substituted 4,5′-Bithiazoles as Novel DNA Gyrase Inhibitors. J Med Chem 55(14):6413-6426.

19. Ericsson UB, Hallberg BM, DeTitta GT, Dekker N, Nordlund P 2006. Thermofluor-based high-throughput stability optimization of proteins for structural studies. Anal Biochem 357(2):289-298.

20. Mezzasalma TM, Kranz JK, Chan W, Struble GT, Schalk-Hihi C, Deckman IC, Springer BA, Todd MJ 2007. Enhancing Recombinant Protein Quality and Yield by Protein Stability Profiling. J Biomol Screen 12(3):418-428.

21. Crowther GJ, Napuli AJ, Thomas AP, Chung DJ, Kovzun KV, Leibly DJ, Castaneda LJ, Bhandari J, Damman CJ, Hui R, Hol WGJ, Buckner FS, Verlinde CLMJ, Zhang Z, Fan E, van Voorhis WC 2009. Buffer Optimization of Thermal Melt Assays of Plasmodium Proteins for Detection of Small-Molecule Ligands. J Biomol Screen 14(6):700-707.

22. Ablinger E, Hellweger M, Leitgeb S, Zimmer A 2012. Evaluating the effects of buffer conditions and extremolytes on thermostability of granulocyte colony-stimulating factor using high-throughput screening combined with design of experiments. Int J Pharm 436(1–2):744-752.

23. He F, Hogan S, Latypov RF, Narhi LO, Razinkov VI 2010. High throughput thermostability screening of monoclonal antibody formulations. J Pharm Sci 99(4):1707-1720.

24. Goldberg DS, Bishop SM, Shah AU, Sathish HA 2011. Formulation development of therapeutic monoclonal antibodies using high-throughput fluorescence and static light scattering techniques: Role of conformational and colloidal stability. J Pharm Sci 100(4):1306-1315.

25. Li Y, Mach H, Blue JT 2011. High throughput formulation screening for global aggregation behaviors of three monoclonal antibodies. J Pharm Sci 100(6):2120-2135.

26. King AC, Woods M, Liu W, Lu Z, Gill D, Krebs MRH 2011. High-throughput measurement, correlation analysis, and machine-learning predictions for pH and thermal stabilities of Pfizer-generated antibodies. Protein Sci 20(9):1546-1557.

27. Becktel WJ, Schellmann JA 1987. Protein Stability Curves. Biopolymers 26:1859-1877.

28. Moreau MJJ, Schaeffer PM 2013. Dissecting the salt dependence of the Tus-Ter protein-DNA complexes by high-throughput differential scanning fluorimetry of a GFP-tagged Tus. Mol Biosyst 9(12):3146-3154.

29. Niesen F. 2012. DSF Analysis v3.0.2. Accessed 06/14/2012, at: ftp://ftp.sgc.ox.ac.uk/pub/biophysics/.

30. Wang CK, Weeratunga SK, Pacheco CM, Hofmann A 2012. DMAN: a Java tool for analysis of multi-well differential scanning fluorimetry experiments. Bioinformatics 28(3):439-440.

31. Menzen T, Friess W 2013. High-throughput melting-temperature analysis of a monoclonal antibody by differential scanning fluorimetry in the presence of surfactants. J Pharm Sci 102(2):415-428.

32. Boivin S, Kozak S, Meijers R 2013. Optimization of protein purification and characterization using Thermofluor screens. Protein Expr Purif 91(2):192-206.

33. Yeh AP, McMillan A, Stowell MHB 2006. Rapid and simple protein-stability screens: application to membrane proteins. Acta Crystallographica Section D 62(4):451-457.

34. Epps DE, Sarver RW, Rogers JM, Herberg JT, Tomich PK 2001. The Ligand Affinity of Proteins Measured by Isothermal Denaturation Kinetics. Anal Biochem 292(1):40-50.

35. Rabeh Wael M, Bossard F, Xu H, Okiyoneda T, Bagdany M, Mulvihill Cory M, Du K, di Bernardo S, Liu Y, Konermann L, Roldan A, Lukacs Gergely L 2012. Correction of Both NBD1 Energetics and Domain Interface Is Required to Restore ΔF508 CFTR Folding and Function. Cell 148(1–2):150-163.

36. Kornhaber GJ, Tropak MB, Maegawa GH, Tuske SJ, Coales SJ, Mahuran DJ, Hamuro Y 2008. Isofagomine Induced Stabilization of Glucocerebrosidase. Chembiochem 9(16):2643-2649.

37. Ablinger E, Leitgeb S, Zimmer A 2013. Differential scanning fluorescence approach using a fluorescent molecular rotor to detect thermostability of proteins in surfactant-containing formulations. Int J Pharm 441(1–2):255-260.

38. Alexandrov AI, Mileni M, Chien EYT, Hanson MA, Stevens RC 2008. Microscale Fluorescent Thermal Stability Assay for Membrane Proteins. Structure 16(3):351-359.

39. Senisterra GA, Ghanei H, Khutoreskaya G, Dobrovetsky E, Edwards AM, Privé GG, Vedadi M 2010. Assessing the Stability of Membrane Proteins to Detect Ligand Binding Using Differential Static Light Scattering. J Biomol Screen 15(3):314-320.

40. Biancalana M, Koide S 2010. Molecular mechanism of Thioflavin-T binding to amyloid fibrils. Biochimica et Biophysica Acta (BBA) - Proteins and Proteomics 1804(7):1405-1412.

41. Voropai ES, Samtsov MP, Kaplevskii KN, Maskevich AA, Stepuro VI, Povarova OI, Kuznetsova IM, Turoverov KK, Fink AL, Uverskii VN 2003. Spectral Properties of Thioflavin T and Its Complexes with Amyloid Fibrils. Journal of Applied Spectroscopy 70(6):868-874.

42. Nashine V, Kroetsch A, Sahin E, Zhou R, Adams M 2013. Orthogonal High-Throughput Thermal Scanning Method for Rank Ordering Protein Formulations. AAPS PharmSciTech 14(4):1360-1366.

43. Steinberg TH, Jones LJ, Haugland RP, Singer VL 1996. SYPRO Orange and SYPRO Red Protein Gel Stains: One-Step Fluorescent Staining of Denaturing Gels for Detection of Nanogram Levels of Protein. Anal Biochem 239(2):223-237.

44. Sorrell FJ, Greenwood GK, Birchall K, Beining C 2010. Development of a differential scanning fluorimetry based high throughput screening assay for the discovery of affinity binders against an anthrax protein. J Pharm Biomed Anal 52(5):802-808.

45. Lakowicz JR. 2006. Principles of Fluorescence Spectroscopy. 3rd ed.: Springer.

46. Lazar KL, Patapoff TW, Sharma VK 2010. Cold denaturation of monoclonal antibodies. mAbs 2(1):42-52.

47. Andersen CB, Manno M, Rischel C, Thórólfsson M, Martorana V 2010. Aggregation of a multidomain protein: A coagulation mechanism governs aggregation of a model IgG1 antibody under weak thermal stress. Protein Sci 19(2):279-290.

48. MicroCal. 2003. VP-DSC MicroCalorimeter User's Manual. Rev. B ed., Northampton, MA: MicroCal, LLC.

49. Lind K, Stahlberg A, Zoric N, Kubista M 2006. Combining sequence-specific probes and DNA binding dyes in real-time PCR for specific nucleic acid quantification and melting curve analysis. Biotechniques 40(3):315-319.

50. Logan J, Edwards K, Saunders NA. 2009. Real-time PCR: Current Technology and Applications. ed., Norfolk, UK: Caister Academic Press.

51. Ojanen M, Kärhä P, Ikonen E 2010. Spectral irradiance model for tungsten halogen lamps in 340-850 nm wavelength range. Appl Opt 49(5):880-886.

52. Kung CE, Reed JK 1989. Fluorescent molecular rotors: a new class of probes for tubulin structure and assembly. Biochemistry (Mosc) 28(16):6678-6686.

53. Haviv S. 2007. Master Thesis. CCVJ's fluorescence lifetime as a viscosity measurement tool and its possible application as a tunable picoseconds reference lifetime standard. Missouri, Columbia: University of Missouri, Biological engineering

54. Seo D-H, Jung J-H, Kim H-Y, Park C-S 2014. Direct and simple detection of recombinant proteins from cell lysates using differential scanning fluorimetry. Anal Biochem 444(0):75-80.

4 The application of DSC and DSF to the formulation development of therapeutic mAbs

4.1 Introduction

Analysis by means of differential scanning calorimetry (DSC) is the gold standard to investigate the thermal stability of proteins.[1] The small energy amounts associated with structural changes of proteins ask for high sensitivity, and DSC is therefore often referred to as microcalorimetry. From a DSC thermogram, thermodynamic parameters such as the enthalpy of unfolding (ΔH), the change in heat capacity (ΔC_p), and the midpoint of the melting transition, referred to as the protein melting temperature (T_m), are calculated.[2] A high T_m value is commonly considered as beneficial for the stability of therapeutic protein formulations, because the probability of conformational changes of the protein molecules is low (chapter 1.3). The T_m value depends on intrinsic factors of the protein, like primary sequence as well as secondary and tertiary structural elements. Furthermore, the protein environment affects the T_m value; consequently, during formulation development of therapeutic protein drugs, the influence of external factors like pH, ionic strength, and excipient addition at different concentrations are screened to assess the optimally stabilizing conditions. Moreover, the T_m value is suggested to be a predictor for long-term stability.[3,4]

Although miniaturization,[5] automation, and methodological improvements were achieved, DSC is still a time and material consuming technique, and the pharmaceutical industry is in need of high-throughput techniques which allow rapid thermal stability screenings of a high number of samples with low cost of goods.[6,7]

In terms of stability screening for formulation development, differential scanning fluorimetry (DSF) was first described by He and coworkers.[8] DSF analyzes the fluorescence intensity of a fluorescent dye that interacts with the protein as a function of temperature.[9] Upon thermal unfolding of the protein, the fluorescence intensity increases and an apparent T_m value can be derived. In the meantime, DSF was successfully applied for thermal stability screening of therapeutic proteins and

monoclonal antibodies (mAbs) in particular.[10-12] For a detailed introduction into DSF, please refer to chapter 3.

In this chapter, the fluorescence melting curves resulting from DSF are compared to the thermograms obtained by DSC. As the most important outcome parameter, the T_m and $T_{m,onset}$ values are investigated in order to correlate both methods. Two model IgG1 type mAbs were investigated. Cetuximab (CX) is a human/mouse chimeric mAb against the epidermal growth factor receptor (EGRF) and is used for the treatment of EGFR expressing cancer types, such as colorectal cancer, and head and neck cancer.[13] In 2007, the formulation of the marketed product was changed due to issues with colloidal instability.[14] In contrast to the old PBS buffer, the new polysorbate 80 containing formulation is more stable.[15] In a first step, it was necessary to purify the market product to remove the surfactant that otherwise interferes with DSF analysis. Additionally, a therapeutic mAb produced in CHO cells, which is referred to as “MAb”, was used.

To understand the individual melting transitions of the multi-domain mAb, the molecules were cleaved into Fab and Fc via enzymatic digestion. After purification, the isolated fragments were investigated to characterize the thermal stability of the individual mAb domains. This enables a better understanding of results from excipient screenings for formulation development and the effects on the different domains in DSC and DSF of the full mAb molecule.

Next, the effect of the glycans attached to the mAb molecules as an intrinsic factor of the thermal stability was investigated. The glycan moieties are crucial for the biologic activity and mediate receptor functions, e.g., at the Fcγ receptor and C1 component of the complement system for antigen clearance, and the neonatal receptor (FcRn) for catabolism and salvation.[16] Thus, glycoengineering can be applied for prolonging the half-life. The antibody-dependent cellular cytotoxicity can be increased by defucosylation,[17] or production in nonfucosylating cell lines.[18] Thus, glycosylation is a promising target of mAb engineering to produce next-generation molecules with tailored characteristics.[19,20] The effect of glycans on the chemical, colloidal, and conformational stability of therapeutic proteins was extensively reviewed by Solá and Griebenow.[21] For many proteins including mAbs, an enhanced stability caused by glycosylation was reported.[21,22] Correspondingly, cleavage of the Fc-glycan results in a reduced thermal stability of mAbs.[8,23-28] Recently, Alsenaidy and coworkers focused

on the high-throughput aspect for formulation development, and screened the pH effect on the thermal stability of an IgG1 mAb upon complete and partial deglycosylation of the Fc part.[29] In contrast, little is known about the role of glycosylation in the Fab region in thermal stability. CX is a therapeutic mAb with two glycosylation sites. The thermal stability of CX and its Fab and Fc fragments was investigated by DSF before and after deglycosylation. The results were compared to MAb which is only glycosylated at the Fc site.

Subsequently, a broader variety of MAb formulations was studied in terms of the effect of pH, salt, and excipient on the thermal stability. Especially, the potentially stabilizing effect of arginine and also histidine was investigated. It has been reported by Falconer et al. that the basic amino acids in particular are beneficial excipients for mAb formulations.[30] A special focus was on the effect of the counterions, which are essential for pH adjustment.

Finally, the focus was on the comparability of the outcome of DSC and DSF. T_m and $T_{m,onset}$ values of both methods were explored towards a correlation between DSC and DSF. The existence of such a correlation allows for a head to head comparison of results obtained with both techniques. This would render DSF a high-throughput screening method for the thermal stability of proteins with low time and material consumption, and also orthogonal to DSC for R&D of therapeutic protein drugs.

4.2 Materials and methods

4.2.1 mAb model proteins

The therapeutic IgG1 model monoclonal antibody (“MAb”) produced in CHO cells is supplied in a 25 mM histidine buffer at pH 7.7 in a stock concentration of about 55 mg/ml with ε_{280nm} of 1.49 ml g^{-1} cm^{-1}.

Erbitux® was purchased at the local pharmacy containing 5 mg/ml Cetuximab (CX) in a citrate buffer at pH 5.5 containing polysorbate 80, glycine, and sodium chloride (NaCl). Using a reference solution of 2 mg/ml CX, an ε_{280nm} value of 1.39 ml $mg^{-1}cm^{-1}$ was determined via ultraviolet light (UV) absorption measurement with an Agilent 8453 spectrophotometer (Agilent Technologies, Santa Clara, California, USA). Prior to further use, protein A affinity chromatography was applied for purification (see chapter 4.2.2).

4.2.2 Protein purification by protein A affinity chromatography

Protein A affinity chromatography was applied to i) purify CX marketed product from polysorbate 80, ii) purify the mAb molecules after incubation with PNGase F, and iii) to separate the Fc fragment from Fab and other unwanted species after incubation with papain.

Therefore, an ÄKTA purifier 10 (GE Healthcare, Uppsala, Sweden) was equipped with a Pierce Protein A chromatography cartridge (Thermo Fisher Scientific, Bonn, Germany) (column volume, CV = 5 ml). The binding buffer was composed of 100 mM sodium phosphate with additional 150 mM NaCl at pH 7.2. The column was equilibrated with 2 CV of binding buffer with a flow of 2 ml/min. The protein solution was mixed 1:1 with binding buffer and about 50 - 70 mg of the protein were loaded onto the protein A column at a flow rate of 2 ml/min. During the injection phase and additional 2 CV of washout, fractions were collected in 15-ml PP tubes using a Frac 920 fraction collector (GE Healthcare) capturing any unbound species (e.g., Fab). For surfactant removal from market CX, the flow was increased to 4 ml/min and the column was flushed with 40 CV of binding buffer to remove any unspecifically adsorbed material. Elution of the specifically bound protein from the protein A resin was achieved by switching to a 100 mM sodium phosphate buffer pH 3 at a flow rate of 2 ml/min with a linear gradient from 0 % to 100 % over 2 CV. The elution buffer was kept at 100 % over 7 CV. The eluting protein was collected in 15-ml PP tubes using the fraction collector, and was immediately neutralized with a 1 M sodium phosphate buffer pH 8.5 to result in approx. 175 mM sodium phosphate buffer at a measured pH value of 6.5. Finally, the column was reequilibrated for 6 CV with binding buffer at a flow rate of 2 ml/min. This purification protocol was performed several times, pooling the protein containing fractions, until the desired amount of purified protein was obtained. Typically, further preparative steps like volume reduction and dialysis followed as described in the corresponding methods chapters.

4.2.3 Preparation of deglycosylated samples of MAb and CX and their fragments

Deglycosylation of both mAb molecules was achieved by enzymatic cleavage using PNGase F. Therefore, 75 µl corresponding to 37.500 units PNGase F (New England Biolabs, Ipswich, Massachusetts, USA) were added to 33 ml of approx. 3 mg/ml mAb solution in a 50-ml PP tube. In case of MAb, a 50 mM sodium phosphate buffer

pH 7.2 and in case of CX, a 175 mM sodium phosphate buffer pH 6.5 was used. The reaction mixture was incubated at 37 °C and gently shaken for 24 h using a Certomat IS (B. Braun Biotech International, now Sartorius AG, Göttingen, Germany). The enzymatic reaction was stopped by cooling the tube to 2 – 8 °C. Subsequently, the deglycosylated mAb molecules were purified using protein A affinity chromatography (see chapter 4.2.2). By this means, the Fc-carrying mAb species was retained while the cleaved glycans and PNGase F were washed out. After protein A affinity purification, parts of the neutralized mAb samples were further treated with papain to obtain the deglycosylated Fab and Fc fragments (see chapter 4.2.4).

Finally, different formulations of the full mAb molecules and their Fab and Fc fragments were prepared. The same procedure was applied to both glycosylated and deglycosylated species. Vivaspin® 20 tubes (Sartorius Stedim Biotech, Göttingen, Germany) were used to reduce the volume and to dialyze the protein into a 10 mM sodium phosphate buffer pH 7.2 or pH 5.0. For full mAb molecules, tubes with a PES membrane of 30 kDa MWCO and for the fragments 10 kDa MWCO were applied. Afterwards, the pH of the protein solutions was adjusted, the solutions were filtrated through a 0.2 µm PVDF membrane filter (Aerodisc® LV, Pall Life Sciences, Port Washington, New York, USA), and the concentration was determined by A_{280nm} measurements with the NanoDrop 2000 photometer (Thermo Scientific, Wilmington, Delaware, USA) and adjusted with the appropriate buffer. Next, the samples were split into two parts and concentrated stock solutions of NaCl in 10 mM phosphate buffers at pH 7.2 or pH 5.0 were added to one part of the protein solutions to obtain a set of samples at a final concentration of 140 mM NaCl. Protein concentrations of 1.5 mg/ml of the full mAbs, 1.0 mg/ml of Fab, and 0.5 mg/ml of the Fc fragments were adjusted. Subsequently, the pH value of the samples was checked and adjusted if necessary. Finally, all samples were filtrated through a 0.2 µm RC membrane filter (Minisart® RC4, Sartorius Stedim Biotech). Untreated and deglycosylated MAb molecules were analyzed by SDS-PAGE. A slightly reduced molecular weight after removal of the glycans was found indicating the success of the deglycosylation procedure.

4.2.4 Preparation and purification of Fab and Fc fragments

Papain was used to prepare Fab and Fc fragments of both CX and MAb. A pilot study revealed that the digestion was independent of the buffer (phosphate or histidine)

and mAb concentrations of up to 20 mg/ml were successfully cleaved in 24 h of incubation time with 20 µg/ml papain. Excellent yields were achieved when 10 mM cysteine and 2 mM disodium ethylenediaminetetraacetate (Na_2EDTA) were present in the reaction mixture.

A reaction medium was prepared by addition of 10 µl of papain suspension (from papaya latex, Sigma-Aldrich, Steinheim, Germany) to 448 µl of a solution containing 300 mM cysteine and 60 mM Na_2EDTA. Of this reaction medium, 353 µl was added to 10 ml of 20 mg/ml MAb solution in 40 mM histidine buffer pH 7.0. The reaction mixture was incubated at 37 °C and gently shaken using a Certomat IS (B. Braun Biotech International, now Sartorius AG, Göttingen, Germany). For in-process control, aliquots of 60 µl of the reaction mixture were taken after 0 h, 2 h, and 21 h of incubation, and 20 µl of a 160 mM iodoacetamide solution was added to stop the reaction. After 24 h 3.3 ml of 160 mM iodoacetamide solution was added to the reaction mix, and the mix was stored at 2 – 8 °C until purification. The in-process controls and the terminated reaction mixture were analyzed by HP-SEC (chapter 4.2.6).

The analogous protocol was applied to fragment 50 ml of 2 mg/ml CX in phosphate buffer, and also 30 ml of deglycosylated MAb and CX after protein A affinity chromatography in 175 mM phosphate buffer at pH 6.5 at a protein concentration of about 3 mg/ml (see chapter 4.2.3).

Purification of the reaction mixture was performed by means of protein A affinity chromatography in order to separate Fab from Fc (see chapter 4.2.2). The fraction containing the Fab fragment also contains the enzyme, iodoacetamide, cysteine, and Na_2EDTA. To remove these reagents, ultrafiltration was applied using Vivaspin® tubes with a 10 kDa MWCO PES membrane (Sartorius Stedim Biotech, Göttingen, Germany). Success of the purification was monitored by HP-SEC (chapter 4.2.6). After acidic elution from the protein A resin, the fraction contains any species carrying Fc, which is the full mAb ("$(Fab)_2Fc$"), Fc with a single cleaved Fab fragment ("(Fab)Fc"), and the completely cleaved Fc fragment. If HP-SEC analysis after 24 h revealed a content of more than 1 % of undigested mAb monomer, all fractions of the Fc species were pooled and the volume was reduced to approx. 100 – 200 µl. This concentrated protein solution containing the full mAb, (Fab)Fc, and the Fc fragment was purified by means of SEC. Therefore, a Sephacryl® 16/60 column (CV =

120 ml), was connected to an ÄKTA purifier 10 system (GE Healthcare, Uppsala, Sweden). The column was equilibrated with 0.4 CV of 100 mM sodium phosphate buffer with additional 150 mM NaCl pH 7.2 as mobile phase at a flow rate of 1 ml/min. The sample was injected using a 250 µl glass syringe (Hamilton, Reno, Nevada, USA) into a 500 µl sample loop, and upon injection, the loop was emptied with 2 ml mobile phase. The eluted species was fractionated by peak detection at 280 nm and collected in 15-ml PP tubes. The main fraction consisting of the pure Fc fragment, which eluted last due to the smallest molecular weight, was used for further preparative steps.

Finally, different formulations of Fab and Fc were prepared with 10 mM sodium phosphate buffers at pH 7.2 and pH 5.0 with and without additional 140 mM NaCl. This was achieved by either buffer exchange using Vivaspin® tubes with a 10 kDa MWCO PES membrane (Sartorius Stedim Biotech) right into the final formulation buffer or by spiking a concentrated buffered NaCl solution into the sample solution, similar to the protocol described in chapter 4.2.3.

4.2.5 Sample preparation for MAb formulation screening

The stock solution of about 55 mg/ml MAb in 25 mM histidine buffer at pH 7.7 was dialyzed into 10 mM sodium phosphate buffer pH 7.2 using Vivaflow® 50 dialysis cassettes with a 30 kDa MWCO PES membrane (Sartorius Stedim Biotech, Göttingen, Germany) at 2 - 8 °C. Subsequently, the pH of the solution was adjusted, the solution was filtrated through a 0.2 µm PES membrane filter (VWR International, West Chester, Pennsylvania, USA), and the protein concentration was adjusted via A_{280nm} measurements using the NanoDrop 2000 photometer (Thermo Scientific, Wilmington, Delaware, USA). Parts of this solution were used to prepare 10 mM phosphate buffer solutions at pH 5.0 using Vivaspin® tubes with a 30 kDa MWCO membrane (Sartorius Stedim Biotech).

Twice concentrated stock solutions of arginine and histidine were prepared in 10 mM phosphate buffer, and the pH was adjusted with either hydrochloric acid, acetic acid, citric acid, aspartic acid, or glutamic acid to pH 7.2 and pH 5.0. The arginine stock solutions were filtrated through a 0.2 µm PES membrane filter (VWR). Subsequently, the arginine or histidine stock solutions were added at a 1:1 ratio to a stock solution of 8 mg/ml MAb in 10 mM phosphate buffer to obtain a final concentration of 4 mg/ml

MAb at both pH values with different types of counterions. As a reference, the same amounts of acid were added to 10 mM phosphate buffers at pH 5.0 and 7.2 to prepare formulations without arginine or histidine. In this case, the pH was adjusted with sodium hydroxide.

4.2.6 High performance size exclusion chromatography (HP-SEC)

HP-SEC was performed on an Agilent 1200 series HPLC system (Agilent Technologies, Santa Clara, California, USA). The autosampler and the column were temperature controlled at 18 °C and 20 °C, respectively. Of each sample solution, 20 µl were injected onto a Tosoh TSKgel® G2000SW$_{XL}$ column (7.8x300 mm) (Tosoh Bioscience, Stuttgart, Germany) using a mobile phase of 100 mM sodium phosphate buffer with additional 100 mM sodium sulfate pH 6.8 at a flow rate of 0.5 ml/min. The eluted sample was detected by means of UV absorption at 280 nm. The chromatograms were analyzed regarding retention times and the area under the curve (AUC) with ChemStation® B.02.01-SR2 (Agilent Technologies).

4.2.7 Hydrophobic interaction chromatography (HIC)

An HIC protocol similar to Wakankar et al. was used.[31] A Tosoh TSKgel® Phenyl-5PW (7.5x75 mm) (Tosoh Bioscience, Stuttgart, Germany) was connected to an Agilent 1100 series HPLC system (Agilent Technologies, Santa Clara, California, USA). The temperature of the column was controlled at 40 °C. Channel B was loaded with a 10 mM sodium phosphate buffer at pH 7.2 and channel A was loaded with a 10 mM sodium phosphate buffer with additional 2 M ammonium sulfate adjusted to pH 7.2. The protein samples were diluted with 10 mM sodium phosphate buffer + 2 M ammonium sulfate pH 7.2, and 10 – 25 µg of the protein were injected onto the column at a flow rate of 1 mg/ml. The mobile phase ratio was adjusted as the following: i) 5 min equilibration at 25 % B, ii) linear gradient from 25 % to 100 % B over 30 min, iii) 5 min at 100 % B, iv) linear gradient from 100 % B to 25 % B over 5 min, v) 5 min reequilibration at 25 % B. Detection was performed via UV adsorption at 280 nm. The chromatograms were analyzed regarding retention times and AUC with ChemStation® B.02.01-SR2 (Agilent Technologies). The obtained chromatograms were corrected by subtraction of a chromatogram after injection of a placebo sample without protein using Origin® 8 SR6 (Originlab Corporation, Northampton, Massachusetts, USA).

4.2.8 Isoelectric focusing (IEF)

The IEF protocol provided by the manufacturer Serva Electrophoresis (Heidelberg, Germany) was applied. The Servalyt Precotes® gel 125x125x0.3 mm pH 6-9 (Serva Electrophoresis) was cooled at 5 °C on a Multiphor II equipped with an MultiTemp III water bath (GE Healthcare, Buckinghamshire, UK). The samples in 10 mM phosphate buffers were diluted to 0.5 mg/ml, and 10 µl were loaded onto the gel in the center between the electrodes. In addition, 5 µl Serva marker mix 3-10 (Serva Electrophoresis) was applied 2 – 3 times across the gel. Using an Electrophoresis power supply EPS 3501 XL (GE Healthcare, Buckinghamshire, UK) 6 mA and 2000 V were applied for 5000 Vh. Next, the gel was immediately fixed with 20 % (w/V) trichloroacetic acid and stained with Serva Blue (Serva Electrophoresis) according to the manufacturer's protocol. After background destaining, the gels were scanned in the wet state using an Epson Perfection V750 PRO (Seiko Epson Corp, Suwa, Japan) scanner. The isoelectric points (pI) of the proteins were obtained by relating the positions to the marker bands. Each sample was at least tested on two gels.

4.2.9 Differential scanning fluorimetry (DSF)

DSF was performed with two different RT-PCR machines. The qTower 2.2 (Analytik Jena, Jena, Germany) was exclusively used to analyze CX, including the deglycosylation study and the formulation screening study. The RT7300 RT-PCR (Applied Biosystems, Foster City, California, USA) was used initially to analyze MAb and its fragments.

Typically, protein concentrations of 4 mg/ml of the full mAb molecules, 2.66 mg/ml of Fab, and 1.33 mg/ml of Fc were investigated. The protein concentrations were reduced to 1.5 mg/ml of the full mAbs, 1.0 mg/ml of Fab, and 0.5 mg/ml of the Fc fragments for analysis after deglycosylation.

In either case, 20 µl of the sample was pipetted into 96-well reaction plates (Applied Biosystems) and skirted white plates (Biometra, Göttingen, Germany) for use with the RT7300 and the qTower 2.2 RT-PCR machine, respectively. An aqueous working dilution of SYPRO® Orange (Sigma-Aldrich, Steinheim, Germany) was prepared and 1 µl of the working solution was added to the well plate and mixed by aspiration. The final SYPRO® Orange concentration in the well was 1x (1:5000 dilution of the supplied stock solution). The well plate was sealed with an optical adhesive (Applied

Biosystems; Biometra) and centrifuged at 2000 g for 2 min to remove air bubbles and to focus the volume on the bottom of the well plates. The RT-PCR machines were utilized to record the fluorescence intensity while heating the well plates. With both machines, a stepwise heating ramp of 1 °C with an overall heating rate of 1 °C/min was applied. The experiment was performed from 20 °C to 96 °C. The recorded fluorescence intensity raw data was exported from both machines, and subsequent data analysis was performed with Origin® 8 SR6 (Originlab Corporation, Northampton, Massachusetts, USA). The resulting melting curves were analyzed regarding transitions (increase in fluorescence intensity) by Boltzmann fitting and first derivative analysis. In case of the RT7300, data from Filter C (Em. 578 nm) and case of the qTower 2.2 data from color module 3 (Ex. 535 nm, Em. 580 nm) was used for determination of T_m and $T_{m,onset}$. The apparent T_m value is the temperature at the inflection point of the Boltzmann function fitted to the data. Furthermore, the apparent T_m value was obtained from the peak maximum of the interpolated first derivative. $T_{m,onset}$ is the temperature at the onset of unfolding derived from Boltzmann fit data as described in chapter 3. Presented results are mean values of three wells with standard deviation of the mean.

4.2.10 Differential scanning calorimetry (DSC)

The sample and the reference cell of a VP-DSC MicroCalorimeter (MicroCal, Northampton, Massachusetts, USA; now Malvern Instruments) were filled with the protein formulation and the corresponding placebo, respectively. The investigated samples were at the same protein concentration as described in the DSF method. Using the ThermoVac station (MicroCal), sample and reference were degassed for at least 30 s. Subsequently, the solutions were injected at 25 °C using a gastight glass syringe (Hamilton, Reno, Nevada, USA). The prescan thermostat time was set to 15 min to allow for equilibration of the sample. DSC thermograms were recorded from 20 °C to 96 °C at a scan rate of 1 °C/min. After each protein scan, both cells were heated up with about 50 % (V/V) nitric acid to 90 °C. The cells were washed subsequently with 1 % (w/V) sodium dodecyl sulfate (SDS) solution and water. The thermogram of the protein scan was corrected by subtraction of a water-versus-water scan and normalized for the protein concentration using Origin® 7 SR2 (OriginLab Corporation, Northampton, Massachusetts, USA) with MicroCal VPViewer2000® version 1.4.10 (MicroCal). The T_m value is represented by the peak maximum of the

endothermic transition. To calculate $T_{m,onset}$, a linear baseline was subtracted and the Boltzmann function was fitted to the ascending slope of the first transition. From the obtained parameters of the fit, the $T_{m,onset}$ value was calculated using the equation presented in chapter 3.3.2.

4.2.11 DFFITS outlier test

In the case of bivariate data sets, parameters like the Cook's distance or DFFITS ("difference in fit, standardized") can be used to identify outliers. The DFFITS parameter was calculated using the following equations.[32]

The residuals e_i of the i-th value were calculated as

$$e_i = y_i - \hat{y}_i \tag{4-1}$$

where y_i is the true value from the experiment and $\hat{y}_i$ is the predicted value based on the linear regression. The residual reflects the distance from the true value to the line of the linear regression in the direction of x. Subsequently, the leverage h_i of every value i was calculated based on the following formula

$$h_i = \frac{1}{n} + \frac{(x_i - \bar{x})^2}{SS_x} \tag{4-2}$$

where n is the total number of samples, x_i is the true value i-th sample, $\overline{x}_i$ is the mean of all x, and SS_x is the sum of squares of all x values. The leverage is a measure of the distance of the particular sample from the mean. From the residual and leverage, the scalar version of the Cook's distance D_i was derived according to

$$D_i = \frac{e_i^2}{(k+1)MS_e}\left[\frac{h_i}{1-h_i}\right] \tag{4-3}$$

where k is the number of independent variable (k=1) and MS_e is the mean square error which is the sum of squares of the residuals divided by the degrees of freedom n-k-1. To obtain the DFFITS value, the MS_e of the data set with omitted potential outlier ($MS_{e(i)}$) is calculated, which was achieved by means of the following equation

$$MS_{e(i)} = \left(\frac{n-k-1}{n-k-2}\right)MS_e - \frac{e_i^2}{(1-h_i)(n-k-2)} \tag{4-4}$$

Next, the studentized residuals s was calculated based on the outlier omitted $MS_{e(i)}$ value

$$s_i = \frac{e_i}{\sqrt{MS_{e(i)}(1-h_i)}} \tag{4-5}$$

Finally, the DFFITS parameter is given by the studentized residuals and the leverage as

$$DFFITS_i = s_i \sqrt{\frac{h_i}{1-h_i}} \tag{4-6}$$

The magnitude of DFFITS reflects the influence of the sample on the results of the linear regression. DFFITS is zero in the case when the omission of the i-th sample has no influence on the linear regression, which means that the prediction $\hat{y}_i$ equals the true y value. In that case, the sample is exactly on the regression line. DFFITS shows a positive sign when $y_i > \hat{y}_{i(i)}$ and vice versa. Absolute values of DFFITS > 1 indicate a large influence on the linear regression.[33]

To identify values with a high influence on the linear regression in the interaction coefficients data set, DFFITS was calculated and the sample with the highest absolute DFFITS value was omitted. Subsequently, the DFFITS analysis was repeated with the obtained reduced data set until no sample resulted in absolute DFFITS values above the threshold of 1.

4.3 Results and discussion

4.3.1 General comparison of DSF melting profiles and DSC thermograms

Figure 4-1 A presents the results of 4 mg/ml MAb in 25 mM histidine buffer pH 7.2. At this neutral pH, the thermogram obtained from DSC measurements showed two distinct transitions. The first transition (T_{m1}) occurred at about 72 °C and a second transition (T_{m2}) with a larger enthalpy was found at about 83 °C. Lower apparent T_m values were obtained when the pH of the solution was lowered to pH 5.0. Furthermore, the DSC method indicates that unfolding of the MAb occurred in three distinct steps, which were separated and resolved as single transitions (Figure 4-1 C). In case of CX, the DSC transition with the largest peak had a much lower T_m

value compared with the MAb. This led to the observation of three distinct transitions at both pH values (Figure 4-1 B and D). A comprehensive study on the role of the mAb domains on the unfolding transitions is described in chapter 4.3.2.

As can be seen from the graphs in Figure 4-1, the DSC thermograms and DSF melting profiles were in good agreement as reported by other authors.[8,10,12] The DSF method predominantly detected the first melting transition with a strong fluorescence increase (see chapter 3). Additional unfolding transitions at higher temperature were hardly detectable, especially in the case of CX. The midpoint of the fluorescence increase, representing the apparent T_m value by DSF, showed that the values obtained by DSF were at 2 - 4 °C lower temperatures (dotted lines in Figure 4-1).

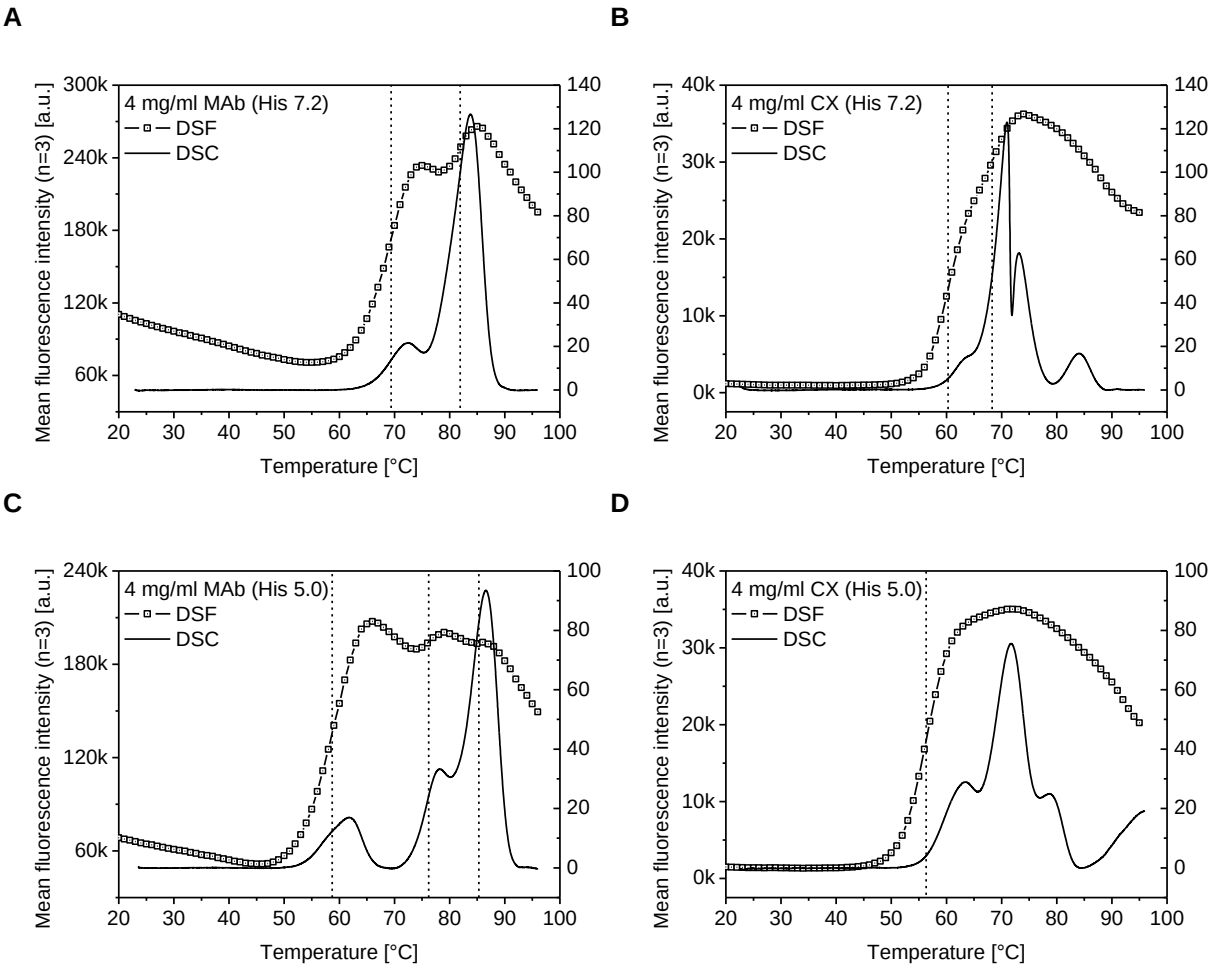

Figure 4-1. DSC thermograms and DSF melting profiles of MAb and CX in 25 mM histidine buffer pH 7.2 (A + B) and 25 mM histidine buffer pH 5.0 (C + D).

A discussion on the correlation and comparability of absolute T_m values obtained by DSC and DSF is given in chapter 4.3.4 and 4.3.6, respectively. Interestingly, all DSF melting curves reveal a decrease in fluorescence intensity after the energetically

most pronounced transition. It was suggested by Niesen and coworker that protein aggregation via the exposed hydrophobic patches diminishes the accessible hydrophobic surface. This effect leads to reduced interaction with the dye and subsequently a decrease in fluorescence intensity.[9] Furthermore, the disruption of the DSC signal (drop/downshift of Cp) suggests that aggregates form, disturbing the heat convection in the cells. Thus, both phenomena indicate that protein aggregation occurs at this temperature and affects both DSC and DSF (see also chapter 4.3.2).

4.3.2 Identification of mAb domains involved in the unfolding process

In the following sections, the results from DSC and DSF analyses of enzymatic fragments of MAb and CX are presented. From the obtained thermograms, the transitions seen with mAbs were to be assigned to the distinct domains, and the changes in energy and hydrophobicity detected by DSC and DSF were to be correlated with the structural segments.

4.3.2.1 Enzymatic fragmentation of the mAb molecules

Enzymatic cleavage of the mAb molecules using papain and subsequent purification rendered the isolated Fab and Fc fragments. Both fragments with a similar molecular weight of about 50 kDa were analytically separated by hydrophobic interaction chromatography (HIC). The HIC chromatograms of the fragments from both MAb and CX demonstrate successful cleavage and purification (Figure 4-2).

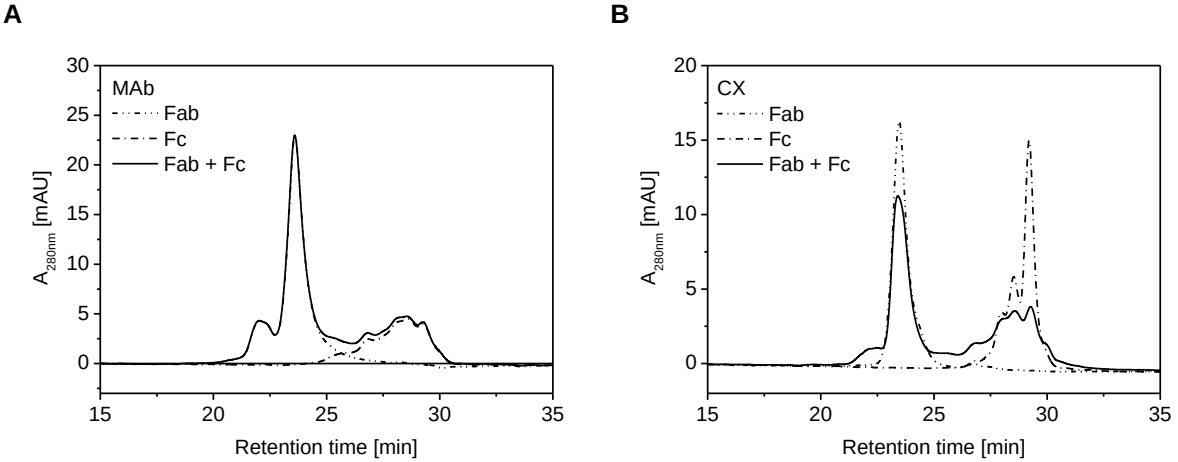

Figure 4-2. HIC chromatograms of Fab, Fc, and a 1:1 mixture of Fab and Fc originating from MAb (A) and CX (B)

Complete baseline separation, as demonstrated by Wakankar et al.,[31] could not be achieved. The finding that especially the Fc fragment with different subspecies

showed charge or hydrophobic heterogeneity is in good agreement with the presence of (heavy-chain) variants with different N- or C-termini,[34] different glycosylation patterns containing charged sugars (sialylation),[34] asparagine isomerization (Asp → iso-Asp and cyclic imides),[31,35-37] deamidation,[34] oxidization (of methionine in CH2),[36] or reduction (disulfide residue reduction to free thiol groups).[31] These modifications lead to the fingerprint characteristics observed especially by methods sensitive to charges,[38,39] and corresponds to the IEF results (chapter 4.3.3.1).

4.3.2.2 Identification of the distinct mAb domains by DSC

Figure 4-3 and Figure 4-4 present an overlay of the DSC thermograms of both mAb molecules and their fragments at pH 5.0 and 7.2 with 140 mM and without NaCl. In all formulations two transitions of the Fc fragment were observed for both mAb molecules. The sequence and nature of the domain unfolding of the Fc fragment were investigated by Tischenko and coworkers.[40] Using a fluorescent label, they were able to assign the first and second melting transition to the CH2 and CH3 domain, respectively. The peak broadening of CH2 domain at low pH, which in some cases also forms a shoulder, suggests that the CH2 domain did not unfold in a cooperative manner. It was reported by Tischenko that the inter-chain interactions via glycans is rather weak, and that the stabilization of CH2 is mainly caused by inter-domain interactions at the CH2-CH3 interface.[40] In contrast, they found that the CH3 domains of the Fc part forms a unique block with strong inter-chain interactions that unfolds cooperatively.[40] Ghirlando and coworkers made another observation upon thermal unfolding of a Fc fragment. In contrast to Tischenko et al., they used PBS buffer pH 7.4 with high ionic strength and observed aggregation of the Fc fragment upon unfolding of the CH3 domain.[28] Due to the aggregation, the reversible two-state model was not applicable and cooperativeness should not be investigated.[28] These findings are in good agreement with the results presented in Figure 4-3. Furthermore, it has to be noted that the Fc sequence is conserved in most mAb molecules and thus the DSC thermograms of MAb and CX are similar. Differences in their melting thermograms can be assigned to differences in the glycosylation patterns.

The Fab fragment, which is unique for both mAb molecules, is responsible for the characteristic DSC thermograms of MAb and CX. At pH 7.2, independent of the addition of 140 mM NaCl, a single melting transition of Fab from MAb is observed (Figure 4-3 A and C). An important study was performed by Ionescu et al., who

compared the DSC thermograms of different mAbs molecules and their Fab and Fc fragments.[25] They demonstrated that the melting temperature of the Fab part can significantly vary between different mAbs due to their unique antigen binding domains.[25] Furthermore, they found that the melting transition with the highest enthalpy is typically caused by the Fab fragment and therefore suggest to use this as an indicator when full mAb molecules with unknown structure are investigated.[25] Similarly, Fab of CX showed a strong unfolding transition, but with a leading small pre-peak before the main transition suggesting a noncooperative unfolding of the domains (Figure 4-3 B and D).

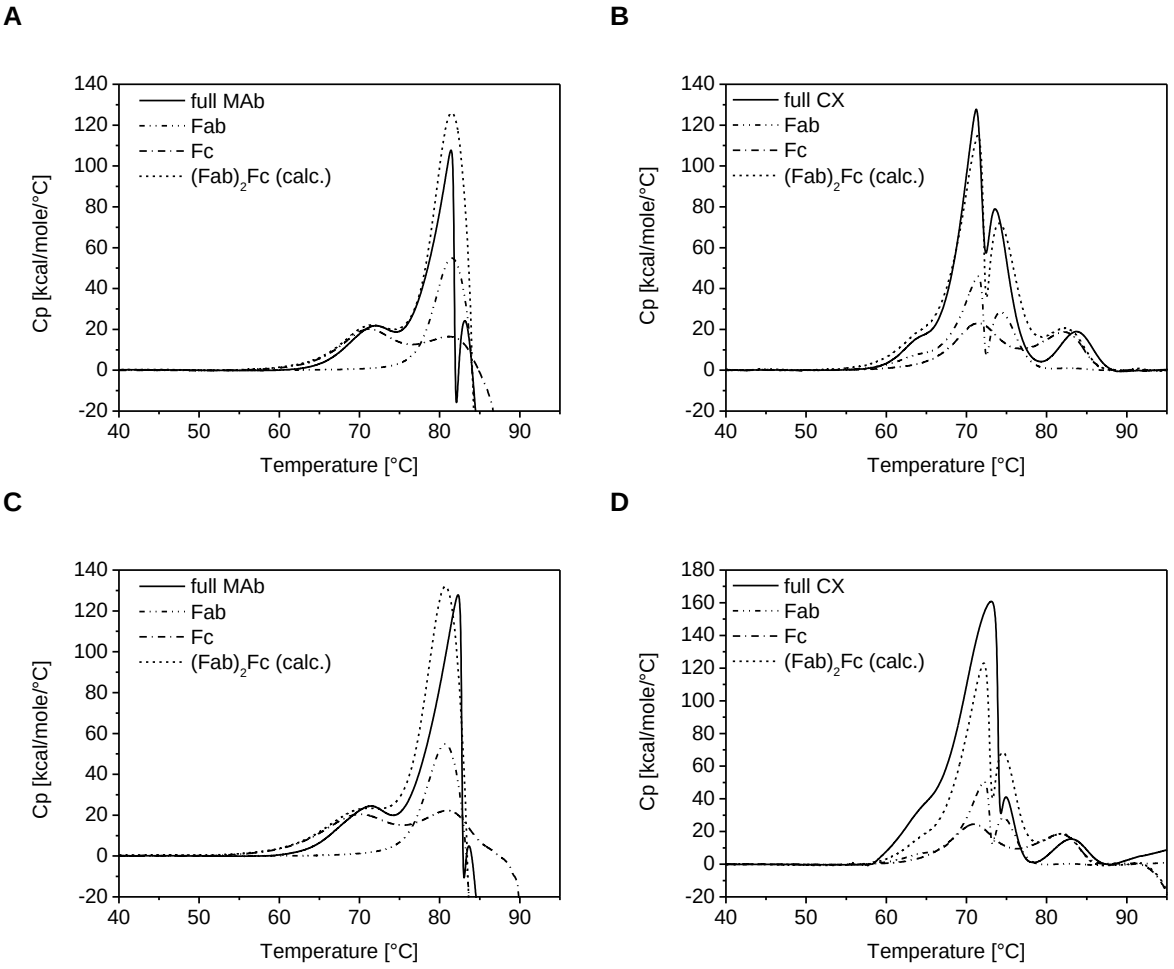

Figure 4-3. DSC thermograms of MAb and CX and their corresponding Fab and Fc fragments in 10 mM phosphate buffers at pH 7.2 (A + B) and in 10 mM phosphate buffer pH 7.2 + 140 mM NaCl (C + D). "$(Fab)_2Fc$ (calculated)" represents the sum of the Fab and the Fc fragment at 2:1.

Especially at the neutral pH of 7.2 and independent of the addition of NaCl, the melting transitions of the full mAb molecules and their fragments were in excellent agreement. The sum of the thermograms of $(Fab)_2Fc$, representing the full mAb molecule, mirrored the DSC thermogram of the full intact molecules (Figure 4-3).

Therefore, a clear assignment of the transitions was possible: The first observed melting transition of MAb was caused by the CH2 domain. The second transition was represented by an overlay of CH3 and Fab, which both melt at about the same temperature (Figure 4-3 A and C). This was in contrast to the CX molecule where T_m of Fab was lower and three transitions were observed. In this case, the first transition was composed of the pre-transition of Fab. The large main peak was represented by the main transition of Fab and CH3. The CH3 domain formed the third transition (Figure 4-3 B and D).

When the pH was lowered to 5.0 (Figure 4-4), a strong destabilization of the Fc part was observed. The T_m values were several degrees lower than for the samples at pH 7.2. In contrast, the T_m of the Fab fragment was less affected by pH, and even a small shift to higher temperature was observed in case of MAb. These pH effects resulted in slightly changing orders in the unfolding sequence. In case of MAb, unfolding of CH3 was resolved at pH 5.0, and the three transitions were assigned to CH2, CH3, and Fab (Figure 4-4 A and C). In case of CX at pH 5.0, the unfolding of the CH2 domain did overlap with the pre-transition of Fab, followed by the main Fab and CH3 transitions (Figure 4-4 B and D). Furthermore, the absence or presence of 140 mM NaCl significantly changed the results. At low ionic strength, the net positive charge of MAb at pH 5.0 resulted in repulsive electrostatic interactions which prevented the protein from aggregation (suggested by the absence of Cp signal breakdown). When NaCl was added, repulsive charges were shielded and the breakdown of the Cp signal suggested strong protein precipitation. Similar effects were observed for the CX molecules (compare Figure 4-4 A, B and C, D).

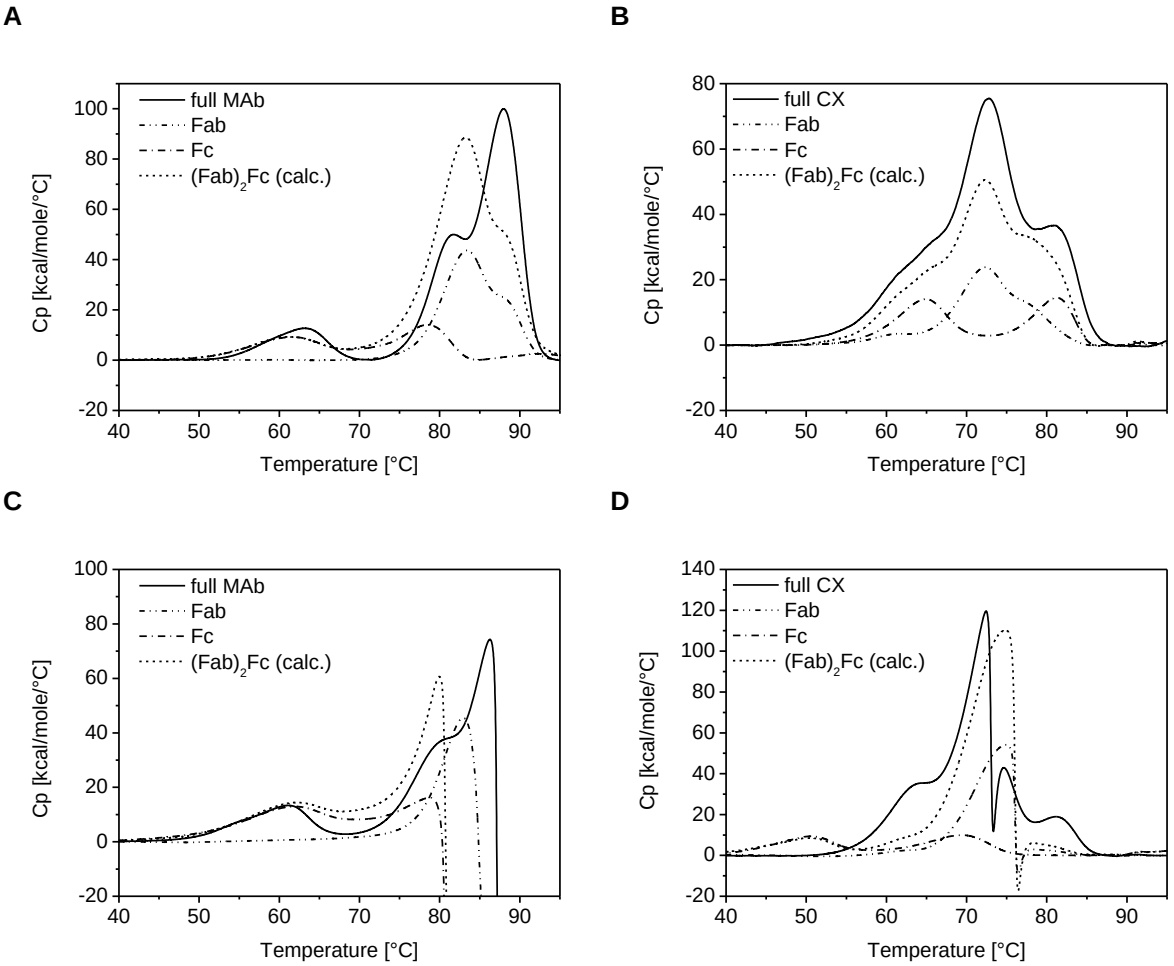

Figure 4-4. DSC thermograms of MAb and CX and their corresponding Fab and Fc fragments in 10 mM phosphate buffers at pH 5.0 (A + B) and in 10 mM phosphate buffer pH 5.0 + 140 mM NaCl (C + D). "$(Fab)_2Fc$ (calculated)" represents the sum of the Fab and the Fc fragment at 2:1.

The effect of presumably electrostatic protein-protein interactions at low pH was also observed for a 2:1 Fab and Fc mixture from MAb in DSC, as presented in Figure 4-5. A good agreement between full MAb, the calculated sum of the fragments, and the mixture in solution was obtained at pH 7.2 (Figure 4-5 A and B). This suggests that each domain unfolds individually without interference. In contrast, at the low pH of 5.0, a strong destabilizing effect on each domain was observed as indicated by a shift of the melting transitions to lower temperature (Figure 4-5 C and D). The mismatch of the DSC thermograms of full intact MAb and the fragment mixture points to the fact that the cleaved protein was able to interact at interfaces which were not accessible when the hinge region of the mAb molecule was intact. Interestingly, the presence of 140 mM NaCl at pH 5.0 increased the T_m value of the CH2 domain of the Fab and Fc mixture. Both effects of pH and salt demonstrate the importance of electrostatic forces.

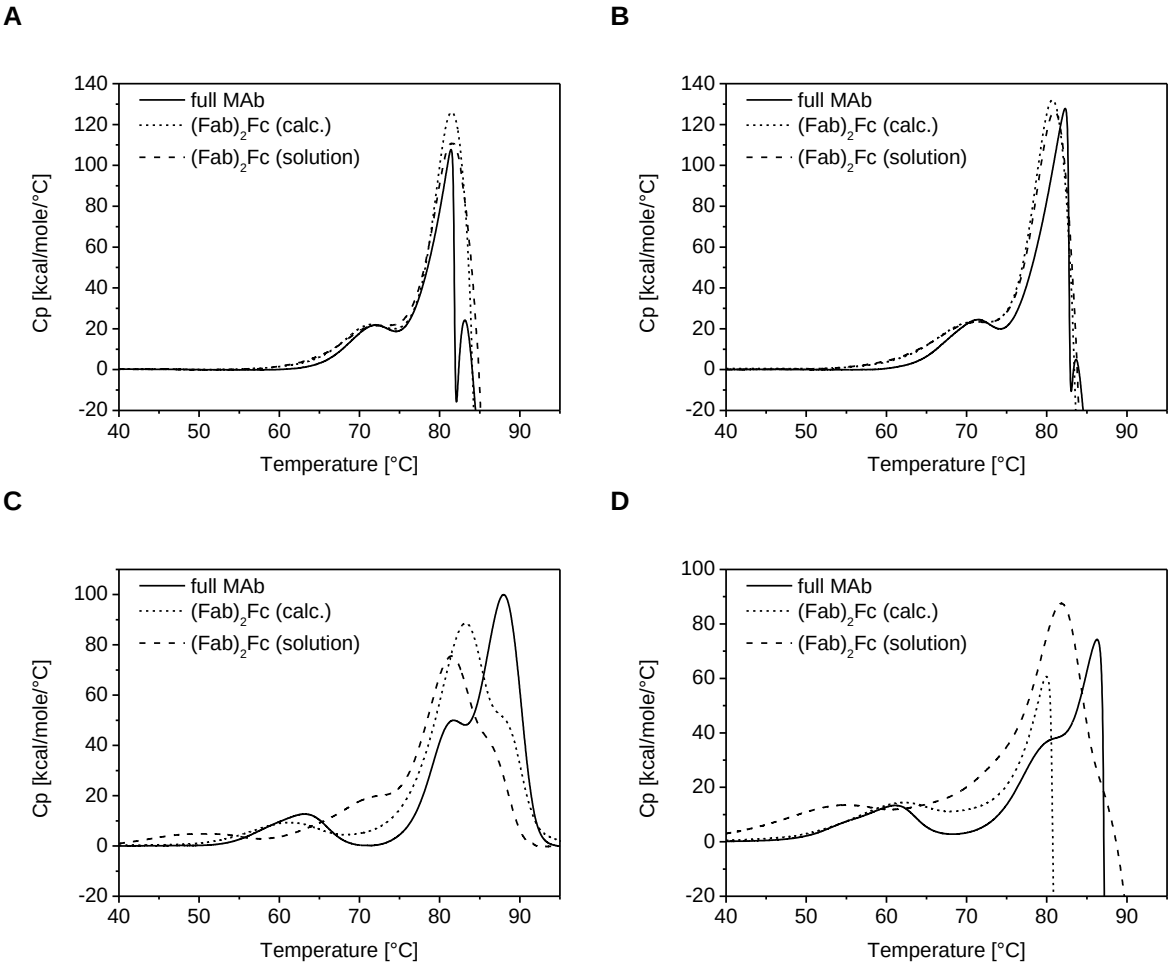

Figure 4-5. DSC thermograms of the full MAb, the calculated curve from the results of the isolated Fab and Fc fragments at 2:1 ("$(Fab)_2Fc$"), and the experimental results of the 2:1 mixture of both fragments in solution. 10 mM phosphate buffer pH 7.2 (A) and with 140 mM NaCl (B). 10 mM phosphate buffer pH 5.0 (C) and with 140 mM NaCl (D).

4.3.2.3 Unfolding of mAb fragments in DSF

The results from DSF experiments, studying the Fab and Fc fragments, are presented in Figure 4-6 and Figure 4-7 for the formulations at pH 7.2 and 5.0, respectively. Especially for the full MAb, the melting process of multiple domains is reflected by two fluorescence transitions at pH 7.2 (Figure 4-6 A and C) and three transitions at pH 5.0 (Figure 4-7 A and C). Due to the overlapping melting transitions of the CX domains, only one transition was observed for CX (Figure 4-6 B and D, Figure 4-7 B and D). Interestingly, the melting profile of the purified Fc fragment from both mAb molecules showed one transition at the expected temperature of the CH2 domain. Thus, in contrast to the DSC thermograms, unfolding of the CH3 domain was not recorded with DSF (compare Figure 4-3). Thermal unfolding of the Fab fragment resulted in one transition. The high T_m value of the Fab fragment from MAb, and the

matching T_m values of the Fab fragment and the CH2 domain from CX were confirmed. Furthermore, the two melting transitions of the full MAb were obtained when both fragments were mixed in a 2:1 ratio in solution. Thus, the first and second melting transitions could be identified as the Fc (CH2) and Fab part of MAb, respectively.

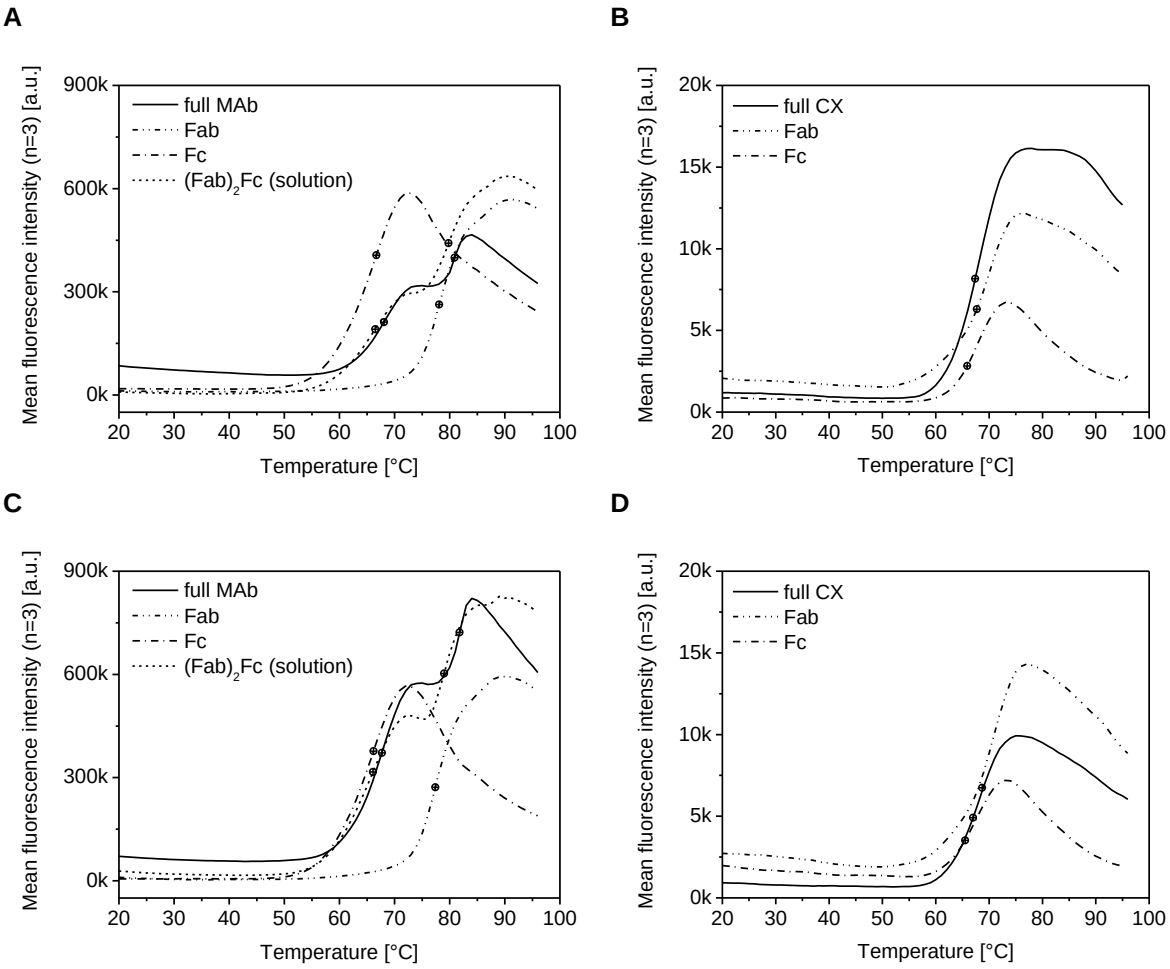

Figure 4-6. DSF melting profiles of MAb and CX and their corresponding Fab and Fc fragments in 10 mM phosphate buffers at pH 7.2 (A + B) and in 10 mM phosphate buffer pH 7.2 + 140 mM NaCl (C + D).

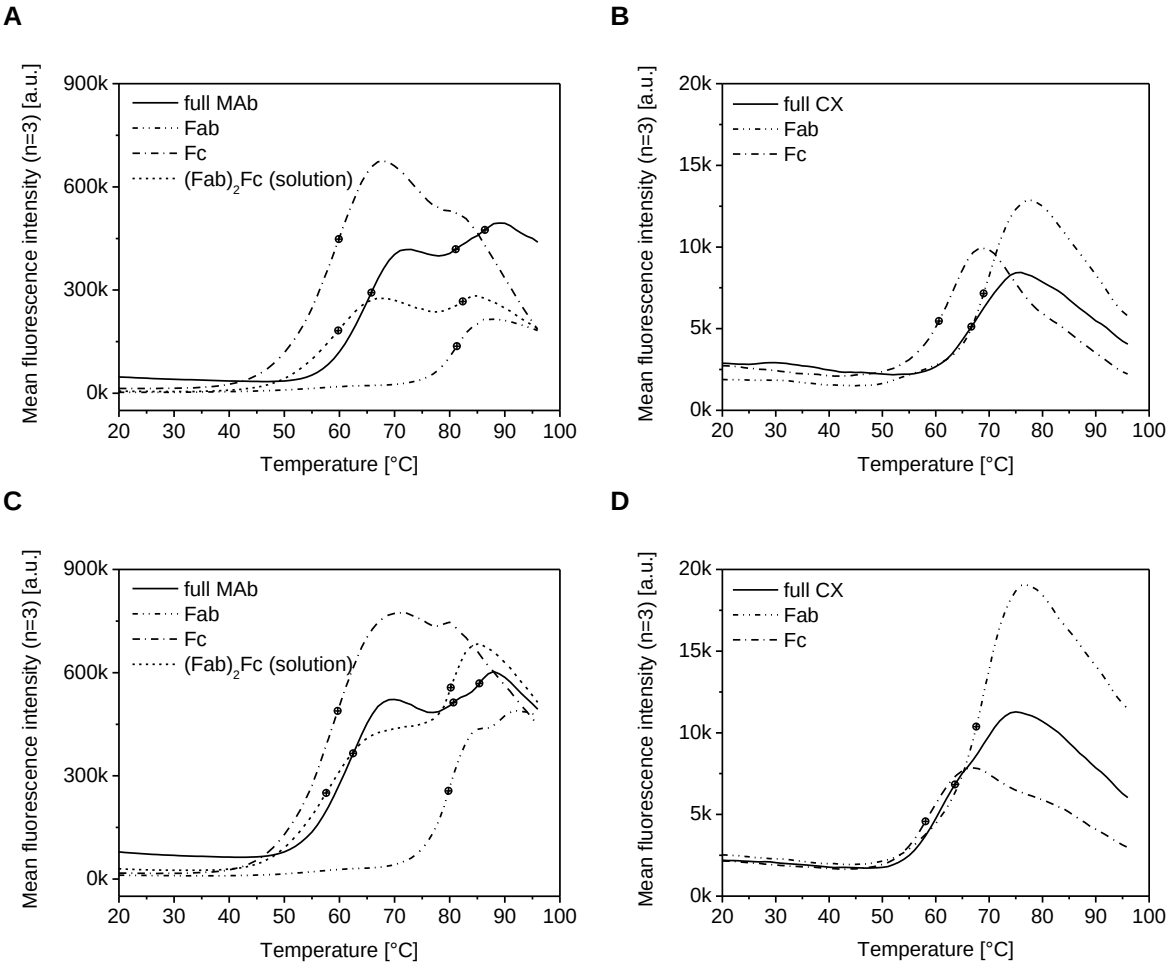

Figure 4-7. DSF melting profiles of MAb and CX and their corresponding Fab and Fc fragments in 10 mM phosphate buffers at pH 5.0 (A + B) and in 10 mM phosphate buffer pH 5.0 + 140 mM NaCl (C + D).

Overall, the structural changes observed by DSC and DSF were in good agreement despite their different physicochemical principles. For example, the strong destabilization of the Fc fragment at the low pH of 5.0, especially in the presence of NaCl, was observed by both DSC and DSF. But DSF did not show a high resolution of the multiple transitions of all mAb domains when compared with DSC and unfolding of the CH3 domain was not observed. The finding that the CH2 domain and also Fab fragment lead to a strong fluorescence transition might be helpful for the identification and interpretation of melting profiles of unknown mAb molecules. Furthermore, the low sample and time consumption of DSF allows for the analysis of Fab and Fc fragments after rapid cleavage and purification at small scale. A comprehensive discussion on the correlation of DSC and DSF results is given in chapter 4.3.4.

4.3.3 The effect of deglycosylation on the thermal stability of mAbs and their Fab and Fc fragments

Pioneering work of Mimura and coworkers revealed that complete deglycosylation significantly reduced the thermal stability of the CH2 domain of an IgG1 mAb.[23] Deglycosylation of mAb molecules was also performed by Ionescu et al.[25] They used the shift of the first DSC melting transition due to sugar removal as a proof that the first transition is caused by the CH2 domain at which the protein is glycosylated. An interesting study was performed by Ha and coworkers investigating the effect of a hemi-glycosylated mAb, i.e., one heavy chain is glycosylated whilst the other is glycan-free.[41] They observed a slightly reduced thermal stability of the asymmetrical, hemi-glycosylated form in comparison to the symmetrical, full-glycosylated mAb molecule. Wen et al. tried to investigate the effect of the glycosylation site.[24] They presented data for a mAb molecule that is also glycosylated in the variable region and its nonglycosylated form. Unfortunately, their model antibody showed an overlap of all three main transitions of the CH2 domain, the CH3 domain, and the Fab fragment, so that a shift of T_m is difficult to assign to one of the domains. They concluded, after careful inspection of the DSC thermograms, a small reduction in thermal stability upon deglycosylation of the Fab site.[24]

In this study, CX was used as a model protein to investigate the effect of the glycan on the thermal stability of the domains of the full mAb and of the domains of the isolated Fab and Fc fragments. The CX molecule of IgG1 type is glycosylated at two sites of the heavy chain, at the asparagine residue Asn299 within the CH2 domain, and at Asn88 of the variable region of Fab.[42] Glycosylation at Asn299 is a distinctive feature of CX, as most IgGs are glycosylated at Asn297.[42] The composition of the CH2 domain-glycan of CX was reported to be similar to the N-glycans found in other recombinant therapeutic mAb molecules.[43] Interestingly, the Fab-glycans show a high amount of galactose-α-1,3-galactose structures,[44] which are unfavorable due to potential immunogenic reactions.[45]

PNGase F was used to prepare a completely deglycosylated form of the mAb molecule. By means of the papain cleavage after the deglycosylation procedure, T_m values of the isolated fragments were obtained. DSF was chosen as a material and time saving technique for T_m analysis. Moreover, the results from CX were compared to a second model protein MAb, an IgG1 type mAb molecule, with common Fc glycosylation pattern.

4.3.3.1 Determination of the isoelectric point of the mAbs and their fragments

Isoelectric focusing (IEF) was performed to investigate the isoelectric point (pI) of the proteins (Figure 4-8). Several isoforms of the full mAbs, as well as of both Fc fragments, and the Fab fragment of CX were observed (Table 4-1). Because of a lower resolution in the high pH range of the gel (pH > 9), the Fab fragment of MAb supposedly consisted of one (probably two) isoforms. The appearance of charge isoforms is in good agreement with the results obtained from HIC analysis (see Figure 4-2). The different pI values of the mAb molecules can be explained by their unique primary sequence. The Fab fragment of MAb showed a much higher pI value compared with the CX Fab fragment. Interestingly, basic amino acids seemed to prevail in the Fab region, whereas the net charge of Fc was in the neutral pH range. As a result, the pI of the full mAb molecules settled in between the pIs of their Fab and Fc fragments. After deglycosylation, a small shift of the protein bands towards lower pI values was observed, especially in case of the full mAb molecules. Thus, the observed isoforms are presumably not caused by varying glycosylation pattern (e.g., sialylation).

Table 4-1. Results from IEF experiments with glycosylated and deglycosylated full mAb molecules and their Fab and Fc fragments.

Species	Appearance	pI value
MAb	4 bands	8.3 – 9.5
Fab (MAb)	1 (-2) band(s)	9.5 – 10.7
Fc (MAb)	> 4 bands	6.9 – 7.8
CX	7 bands	7.4 – 8.0
Fab (CX)	3 (-4) bands	8.0 – 9.5
Fc (CX	> 4 bands	6.9 – 7.8

pI, Isoelectric point.

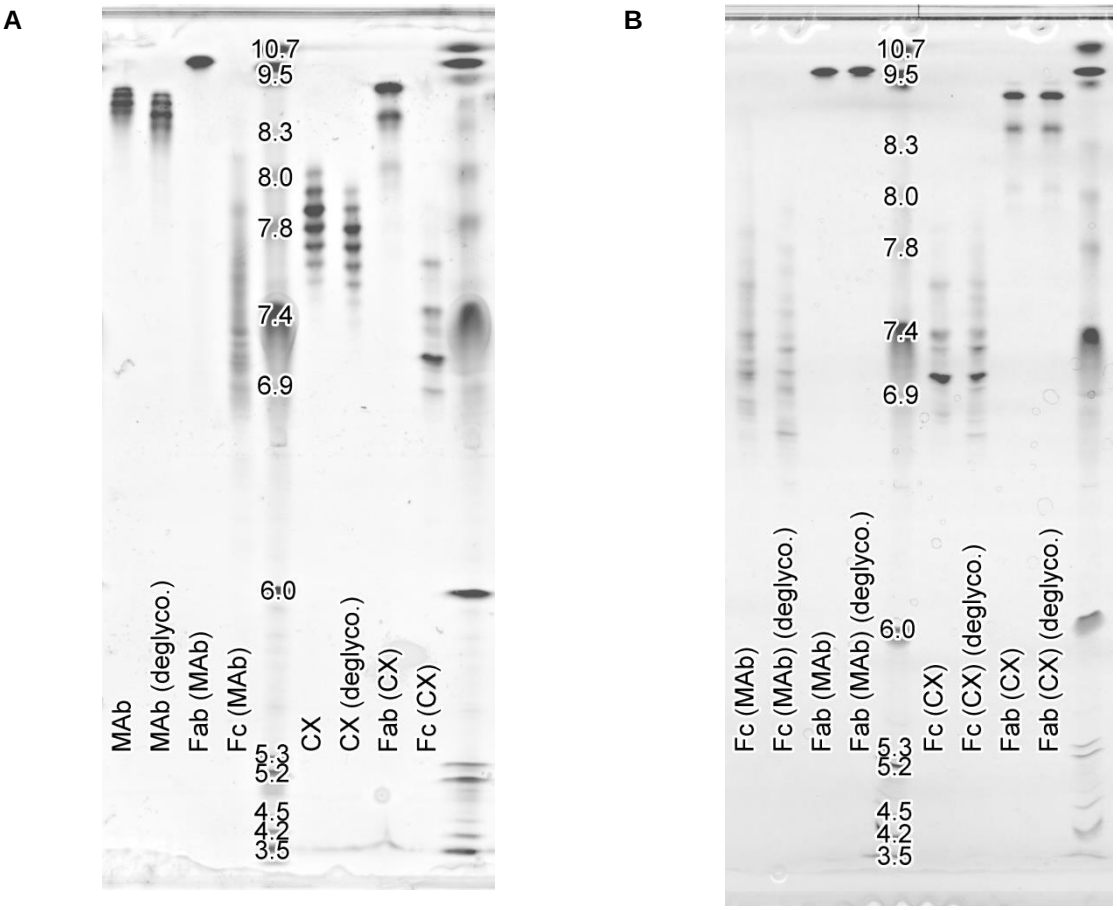

Figure 4-8. Decolorized scans of the IEF gels after Serva blue staining. The full mAb molecules and their fragments were tested before and after deglycosylation. Cathode (-) and anode (+) were located at the top and bottom of the scans, respectively.

4.3.3.2 Effect of deglycosylation on the Fc fragment

The T_{m1} values from the first melting transition obtained by DSF, resembling the unfolding of the CH2 domain of both mAb molecules (compare chapter 4.3.2) and the isolated Fc fragments, were analyzed before and after removal of the glycans. For a better comparison, the thermal shift ΔT_m of untreated minus deglycosylated form was calculated, and the results are presented in Figure 4-9. All samples showed a negative shift of T_m suggesting a reduced thermal stability upon deglycosylation. Thermal stability was lowered independently of the formulation, although the degree of the T_m shift and the absolute T_m values were pH and salt dependent. Both mAb molecules in 10 mM phosphate buffer pH 7.2 showed a reduction of T_m of about -4 °C. The effect of deglycosylation was less pronounced when the isolated Fc fragments were investigated with a ΔT_m of approx. -1 °C. The Fc fragment of MAb and the full CX molecule were particulary sensitive to low pH. Addition of 140 mM NaCl negatively affected the thermal stability in all cases. This suggests that higher

ionic strength was detrimental even at neutral pH where charge effects and subsequent charge shielding by salt addition are less pronounced.

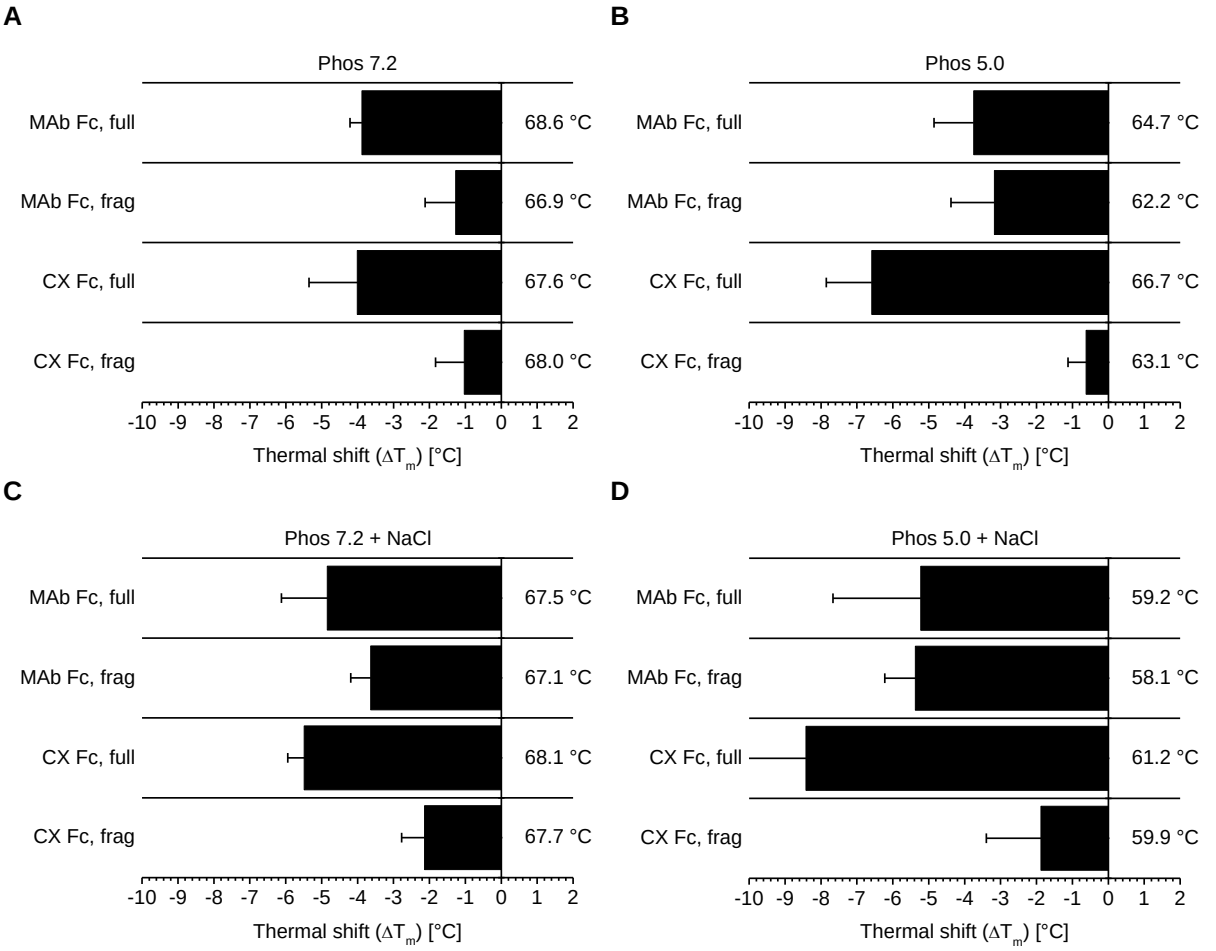

Figure 4-9. Thermal shift (ΔT_m) as the result of deglycosylation of the Fc fragment. The ΔT_m value was calculated for Fc of the full mAb as well as the purified Fc fragment. A negative ΔT_m value means a reduced thermal stability after removal of the glycan structure. The effect of deglycosylation on the thermal stability was investigated in different formulations (A – D).

The CH2 domain of the mAb showed a strong destabilization at the low pH of 5.0 compared with the formulation at pH 7.2. This holds true for the full MAb and CX, as well as the isolated Fc fragments (compare chapter 4.3.2). Deglycosylation further reduced the T_m value of both species (Figure 4-9). The same effect of pH and deglycosylation on CH2 was also reported by other authors.[8,24,26,29] Thus, it is likely that the observed unfavorable trends of low pH and deglycosylation are common to all mAbs, and IgG1 in particular. It was proposed that the glycans attached to the CH2 domain are located in a groove between both heavy chains of the Fc fragment.[16,23,46] A closed conformation of the CH2 domain was found after removal of the glycans,[46] whereas large glycan moieties lead to a more open CH2 domain

structure.[46,47] Truncation of the glycans also influences the FcγR binding which is mediated via the carbohydrates.[46] Furthermore, it was concluded that the α-1,6-mannose branch is firmly bound to the protein surface.[46,48] A recent NMR study suggests that the CH2-glycan is more dynamic and exposed to the solvent than initially expected, and may switch between a bound and an unbound state.[49]

Considering these interaction of the glycans with the protein structure, it is reasonable that the thermal stability is (negatively) affected by deglycosylation. Either stabilization of the native state or destabilization of the unfolded state would lead to a higher overall thermal stability.[21,22,50] Stabilization of the native state, which is most likely, could be achieved by additional noncovalent attractive interactions and a decrease in structural dynamics.[22] The results from Mimura et al. with truncated glycan forms confirm that the reduction in thermal stability is supposedly due to a loss of protein-glycan interactions.[23] Similarly, Ionescu et al. suggest that the reason for the lower T_m might not be an “intrinsic” destabilization but rather omission of stabilizing inter-domain interactions.[25] Additional destabilization of the unfolded state might be possible due to steric hindrance.[22,51]

4.3.3.3 Effect of deglycosylation on the Fab fragment

The T_m shift of the Fab domain after deglycosylation is presented in Figure 4-10. For MAb, where no glycans are attached to this domain, no change of the T_m value was expected. The results demonstrate that no significant change was observed, either for the full mAb or the isolated Fab fragment. Furthermore, this finding confirmed that the enzymatic digestion with PNGase F and the subsequent purification procedure did not negatively affect the thermal stability of the protein. Unfortunately, the overlapping melting transitions of the native CX molecule inhibit the discrimination between the unfolding of the CH2 domain and the Fab fragment (see chapter 4.3.2). Additionally, the CH2 domain was found to be strongly destabilized after removal of the glycans. Therefore, it was not possible to refer the T_m values before and after deglycosylation to the Fab domain in the full CX molecule. The results of the purified Fab fragment, however, clearly indicate that no significant T_m shift occurred upon removal of the glycans in the Fab region of CX (Figure 4-10). Thus, glycosylation of the protein at the site of Asn88 did not enhance the thermal stability of the mAb molecule.

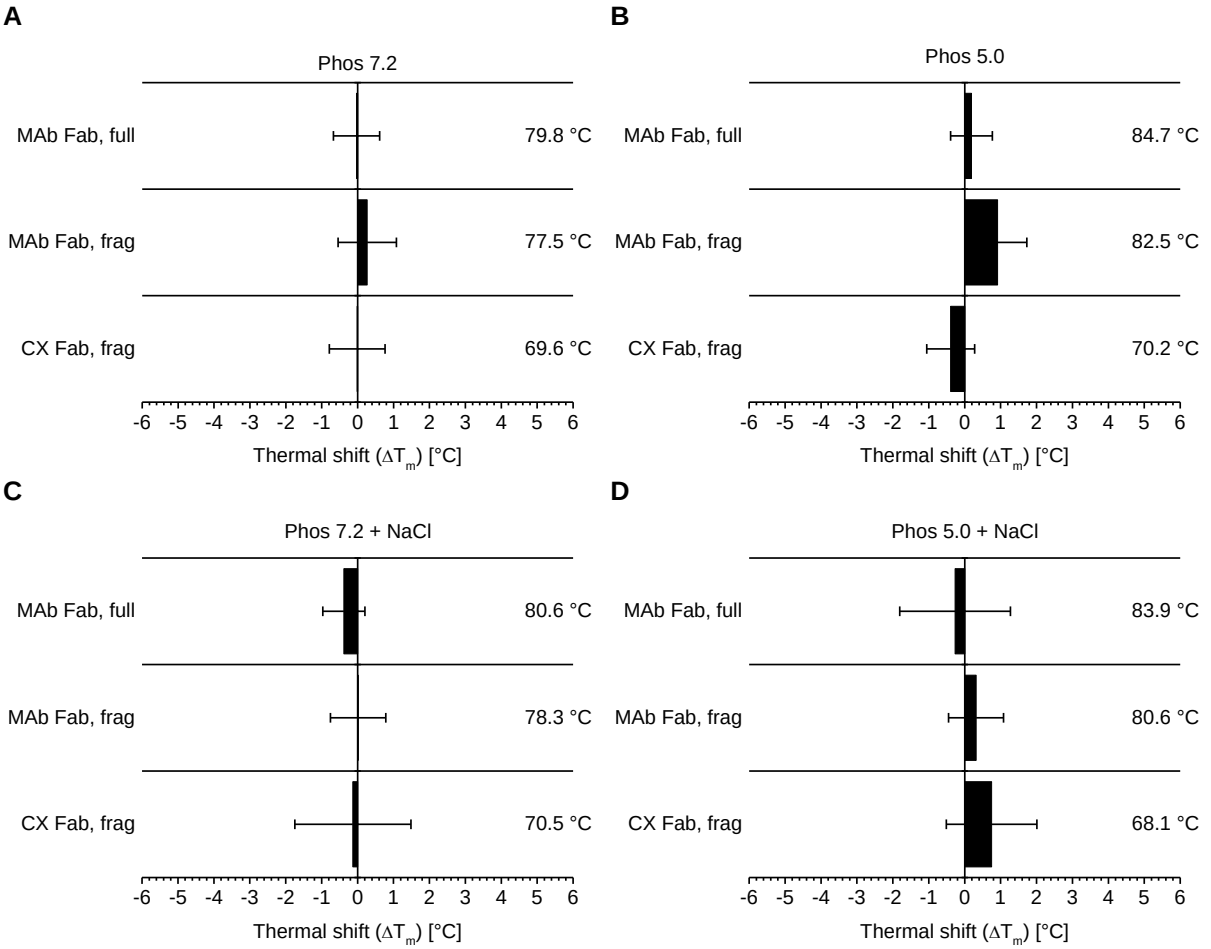

Figure 4-10. Thermal shift (ΔT_m) as the result of deglycosylation of the Fab fragment. In case of full MAb where the melting transition of Fab is resolved with DSF, ΔT_m of the full mAb was calculated. A negative ΔT_m value means a reduced thermal stability after removal of the glycan structure. The effect of deglycosylation on the thermal stability was investigated of the protein in different formulations (A – D).

The Fab-glycan was reported to be larger than the CH2-glycan and contains also α-galactose and N-glycolylneuraminic acid, which are not involved in CH2-glycan structure.[42-44] In contrast to the conserved, symmetrical, dimeric Fc fragment with its identical heavy chains, the Fab fragment is inherently more heterogeneous in structure. The dimeric form of Fc allows also for interaction of the glycans with each other via H-bonds,[46] which is not possible for the Fab-glycan. Furthermore, only 15 - 20 % of human serum IgG is approximately glycosylated at the Fab domain,[52] suggesting that glycosylation at this site is less important *in vivo*. The crystal structure of Fab from CX was resolved by Li and coworkers using X-ray crystallography,[53] and is available via the RCSB Protein Data Bank (1YY8, http://www.rcsb.org). Investigation of the crystal structure using the PyMOL Molecular Graphics System version 1.3 (Academic license, Schrodinger LLC, http://pymol.sourceforge.net)

revealed that Asn88 is located on the outside of a small α-helix and is oriented towards the environment (Figure 4-11). Although in proximity to the gap between the Fab domains, the exposed position suggests that the glycans are easily accessible by solvent molecules. Thus, the glycans attached to Fab might be less shielded and less interactive with the protein surface compared with the Fc-glycans. Subsequently, deglycosylation is supposedly less affecting the thermal stability of the Fab part in contrast to the Fc part.

Figure 4-11. 3D structure of Fab from CX. The observer is looking onto the domains of the light chain ("front row"). The heavy chain is settled behind in the "back row". Asn88 is located on a small α-helix facing upwards into the solvent space (dark color). The structure originates from PDB 1YY8 and was generated using PyMOL.

In conclusion, it was demonstrated that the stabilizing effect of the glycan moieties on the mAb molecules is domain specific. Both mAbs showed a reduced thermal stability after deglycosylation of the CH2 domain. The negative shift of T_m was more pronounced for MAb in comparison to CX. The effect was immanent for both the full mAb and the isolated Fc fragment. Thus, the presence of the glycan is important for the overall thermal stability of the full mAb but the stabilizing effect is limited to the CH2 region. The T_m values of Fab were not significantly changed upon

deglycosylation. Thus, CX did not gain a higher thermal stability due to the glycan attached to the VL domain.

4.3.4 Thermal screening for the effect of excipients on the T_m value of MAb

Formulation screenings for optimal thermal stability typically consider pH, ionic strength, and selected excipients at varying concentrations. It is known that arginine interacts with and stabilizes or destabilizes protein structure presumably due to the guanidine-group. Unlike guanidinium hydrochloride (GdnHCl), it was demonstrated by Ishibashi et al. that arginine is not a denaturant.[54] Although there is evidence that the T_m value is lower for some proteins in the presence of arginine,[55,56] Falconer et al. reported basic amino acids to be beneficial for the stability of a mAb resulting in an increase in T_m.[30] Consequently, we investigated arginine and histidine for their potential application as stabilizing agents for MAb against thermal unfolding. First, increasing amounts of arginine were added to analyze the concentration dependency of any effect. Next, the effect of the counterion was studied at either 100 mM arginine or histidine.

4.3.4.1 Effect of arginine concentration in the presence of chloride

Figure 4-12 shows the T_m values obtained by DSF for the CH2 domain and the Fab part, and DSC thermograms of MAb at pH 7.2 and 5.0. Using a 4 mg/ml MAb sample in 10 mM phosphate buffer as a reference, an increasing amount of arginine resulted in a T_m (CH2) lowering by up to 7 to 8 °C for the 1 M arginine containing formulation at both pH values. This was confirmed by the DSC measurements (Figure 4-12). Yancey also demonstrated lower T_m values up to 2 °C for bovine pancreatic ribonuclease upon addition of 0.4 M arginine.[56] No change of T_m of lysozyme was observed by DSC, but only up to 60 mM arginine was tested.[57] The thermal stability of the Fab part was marginally increased at low arginine concentrations (apparent T_m increase by 1.1 °C at 50 mM arginine pH 5.0 in DSF). As demonstrated by the DSC thermograms, the higher apparent T_m values of the Fab part were likely due to an increased colloidal stability as the T_m analysis was less perturbed by protein aggregation (chapter 4.3.2). At pH 5.0, the positive net charge of the MAb molecules led to repulsion and higher colloidal stability as long as the charges were not shielded by the addition of salt (100 mM arginine). In presence of 1 M arginine, the DSC thermogram returned to baseline after unfolding of the Fab part at both pH values suggesting reduced precipitation (Figure 4-12). For the two model proteins RNase

and lysozyme Arakawa et al. found a concentration dependent T_m reduction of 1 - 3 °C but an increase in solubility of the thermally unfolded protein.[55] They suggested that arginine suppresses the aggregation of the unfolded species supposedly via binding of the guianidino-moiety to the protein.[55] Shiraki et al. found arginine to be the best candidate among 15 amino acids in the prevention of aggregation upon thermal denaturation of proteins, and speculate that the guanidine-group might interfere with intermolecular or intramolecular H-bonds.[57] In conclusion, arginine reduced the apparent T_m value of the CH2 domain, but supposedly stabilized the MAb via solubilization upon thermal unfolding of the Fab fragment with reduced aggregation of the protein.

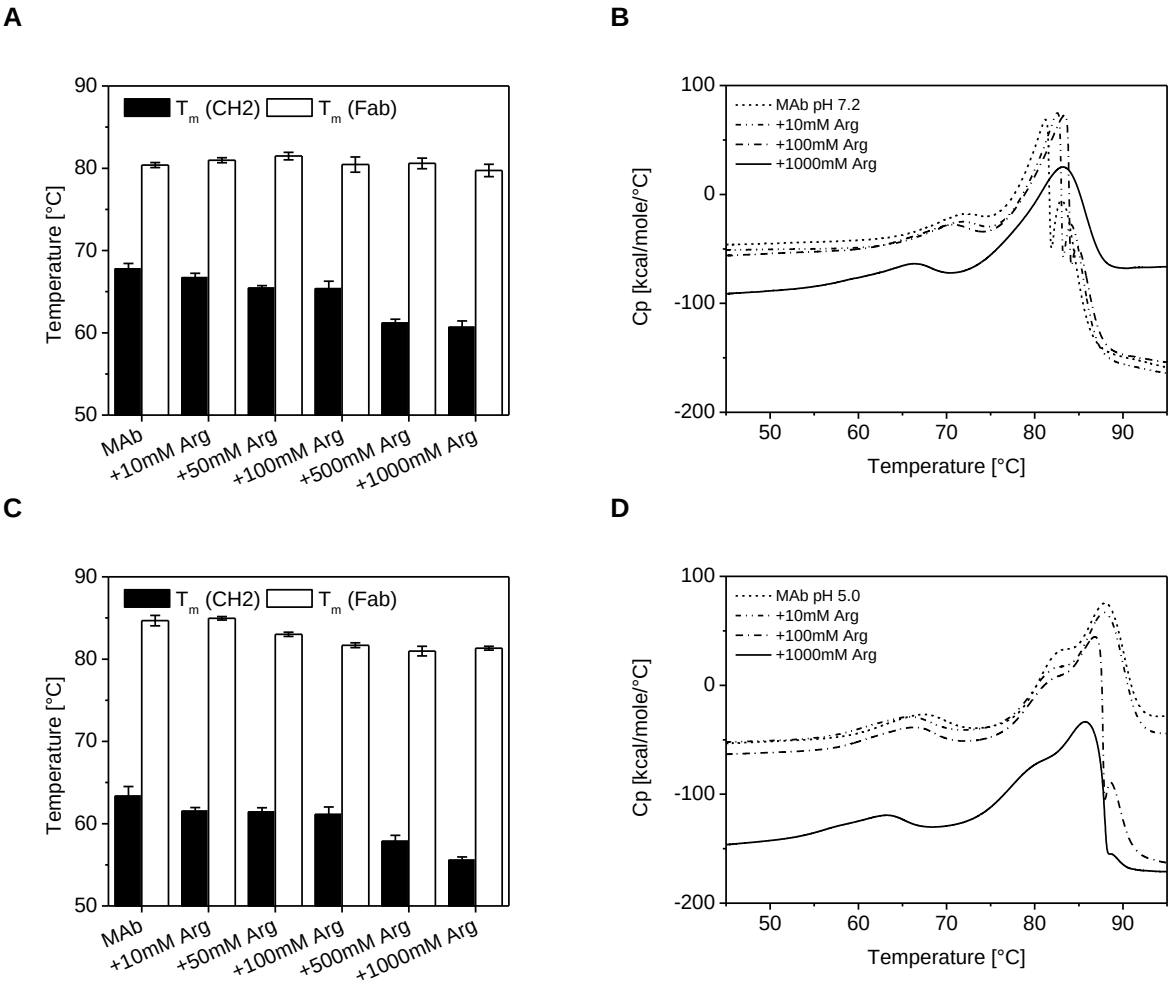

Figure 4-12. Apparent T_m values obtained by DSF and DSC thermograms of 4 mg/ml MAb in 10 mM phosphate buffer and with additional 10 mM to 1 M arginine at pH 7.2 (A + B) and pH 5.0 (C + D). The pH was adjusted with hydrochloric acid.

4.3.4.2 Effect of the counterion of arginine after pH adjustment

Adjustment of the solution pH is necessary to maintain a desired value after addition of the basic amino acid to the 10 mM phosphate buffer that corresponds to the buffer of the MAb stock solution. Ishibashi and coworkers have noted that the choice of acid needs to be considered during pH adjustment of arginine solutions due to possible counterion specific effects.[54] The DSF results of the samples at pH 7.2 are presented in Figure 4-13 A. Compared with the arginine-free reference sample of the MAb in 10 mM phosphate buffer, all 100 mM arginine containing samples showed a T_m (CH2) which is reduced at an average of 2.5 °C, regardless of the acid used for pH adjustment. T_m of the Fab fragment was slightly increased by about 1 °C for all samples except the citrate containing formulation. This finding was confirmed by DSC measurements which especially promote the stabilizing effect in the presence of aspartate and glutamate (Figure 4-13 B). At pH 5.0, the effects of the different ion partners were more pronounced (Figure 4-13 C). Citrate in the presence of 100 mM arginine reduced T_m (CH2) by about 5 °C, whereas a reduction about 2 - 3 °C was seen for the other samples. Interestingly, T_m (Fab) was reduced in case of chloride, acetate, and citrate. In agreement with the result obtained at pH 7.2, the amino acids aspartate and glutamate increased T_m (Fab) about 1 °C. The DSC thermogram of arginine-free MAb sample showed the expected progression without signal breakdown due to the net repulsion at the low pH value (Figure 4-13 D). The addition of 100 mM arginine in the presence of chloride, acetate, or citrate as the counterion resulted in the breakdown of the Cp signal suggesting aggregation. Interestingly, the samples containing either aspartate or glutamate were again supposedly stabilized. Possibly, the smaller chloride and acetate counterions lead to a more efficient shielding effect and subsequently the net repulsion at the low pH is reduced. Citrate with its three carboxyl moieties has a strong effect on the ionic strength of the solution. The acidic amino acids aspartic acid and glutamic acid also have a strong effect on the ionic strength and their positive stabilizing effect suggests a specific interaction. In conclusion, the presence of a specific ion partner for arginine was more important at the low pH compared with neutral pH value. Thus, presumably electrostatic interactions play a role in the observed synergistic stabilizing effect of arginine and both acidic amino aspartate and glutamate in case of the Fab fragment.

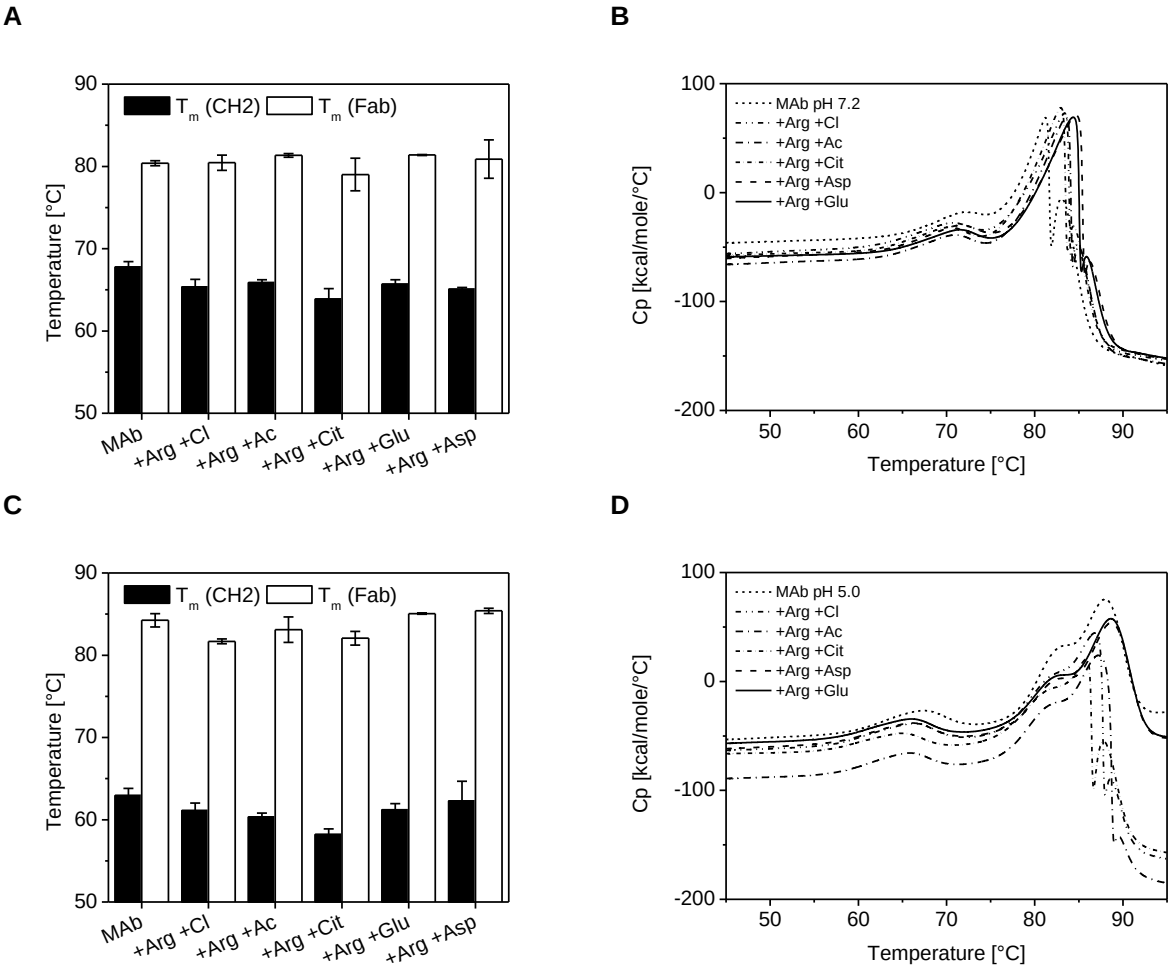

Figure 4-13. Apparent T_m values obtained by DSF and DSC thermograms of 4 mg/ml MAb in 10 mM phosphate buffer and with additional 100 mM arginine at pH 7.2 (A + B) and pH 5.0 (C + D). The pH was adjusted with hydrochloric acid (Cl), acetic acid (Ac), citric acid (Cit), glutamic acid (Glu), or aspartic acid (Asp).

4.3.4.3 The effect of histidine and different counterion partners

Amino acids including both arginine and histidine were reported by Tian et al. to protect mAbs from conformational changes upon freeze-drying via noncovalent interactions.[58] Furthermore, histidine was found to increase the stability and enhance the physical properties of an IgG2 mAb in both lyophilized and liquid state.[59] Finally, Falconer reported that especially histidine among the basic amino acids increased the T_m values of a mAb.[30] At pH 7.2, the addition of 100 mM histidine did not result in a significant change of T_m (CH2), and T_m (Fab) was increased by about 1 °C independent of the counterion (Figure 4-14 A). Thus, the addition of histidine resulted in a similar stabilizing effect of the Fab fragment but in contrast to arginine, no destabilization of the Fc part was observed. An increase of T_m (Fab) comparable to the one in the arginine study was observed for the 100 mM histidine samples

containing aspartate and glutamate at pH 5.0 (Figure 4-14 B). Interestingly, the combination of histidine and chloride was found to be particularly perturbing with a T_m reduction of about 8 °C for the CH2 domain. A rather pronounced destabilization of 5.5 °C was observed when the formulations at 25 mM histidine buffer and 10 mM phosphate buffer at pH 5.0 were compared (chapter 5). A control experiment was performed without the presence of the basic amino acids in which the tested acids were neutralized with sodium hydroxide and showed that the anions alone did hardly effect the apparent T_m values of the MAb (Figure 4-14 C and D). These findings suggest that a broad excipient screening is necessary to comprehensively study individual specific formulation effects.

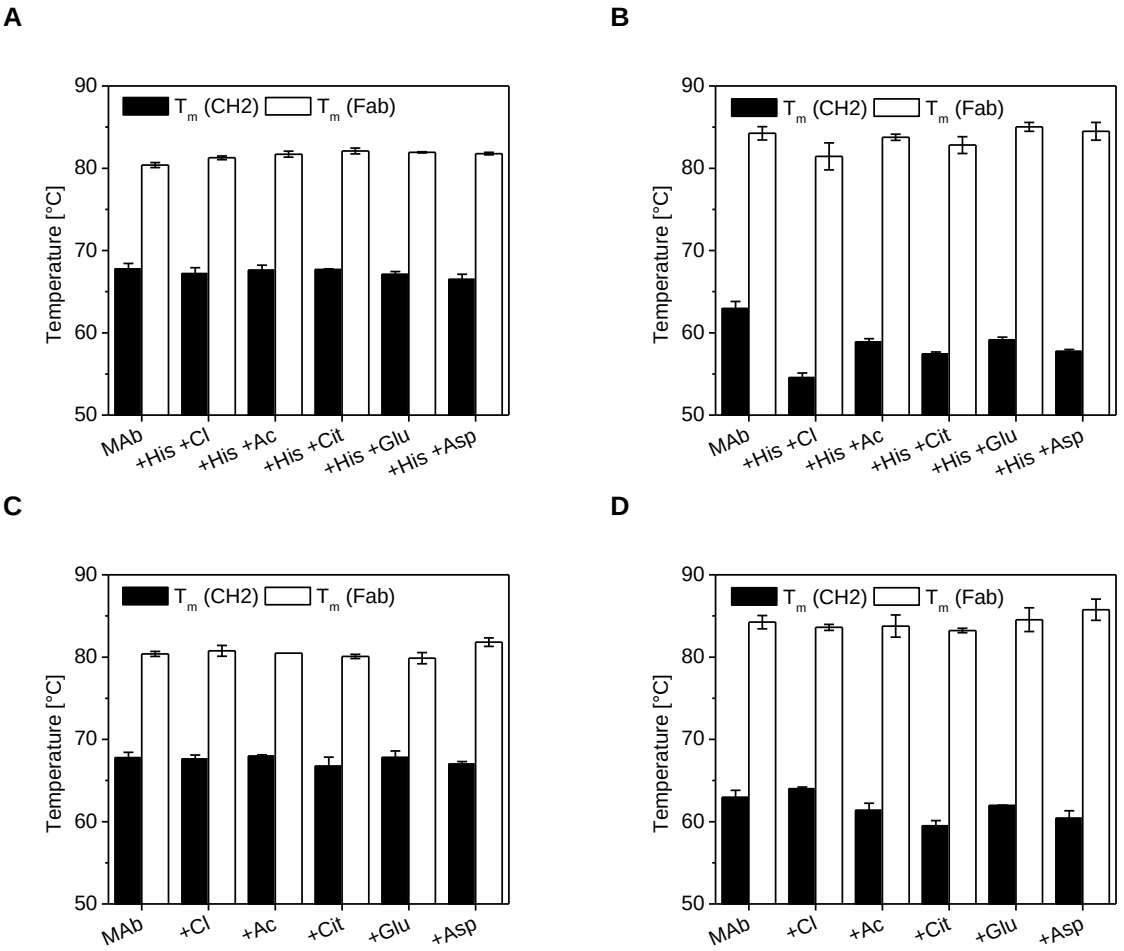

Figure 4-14. Apparent T_m values obtained by DSF of 4 mg/ml MAb in 10 mM phosphate buffer and with additional 100 mM histidine at pH 7.2 (A) and pH 5.0 (B). The pH was adjusted with hydrochloric acid (Cl), acetic acid (Ac), citric acid (Cit), glutamic acid (Glu), or aspartic acid (Asp). As a control, sodium hydroxide was used to neutralize the tested acids in 10 mM phosphate buffer at pH 7.2 (C) and pH 5.0 (D).

4.3.5 Correlation of T_m and $T_{m,onset}$ values from DSF and DSC

The protein melting temperature (T_m) is defined as the temperature at which half of the protein is in the unfolded state. This point is represented by the peak maximum of an ideally Gaussian shaped DSC melting transition for a two-state reaction from the native to the unfolded state. In a case where multiple unfolding processes occur simultaneously, mathematical models might be applied to analyze T_m values of overlapping transitions. As extensively discussed in chapter 3 and in this chapter, the apparent T_m value of DSF is based on a different physicochemical principle. However, it was reported by many authors that a linear correlation between T_m values from DSC and DSF exist, particularly for mAb molecules.[8,10-12] Moreover, it was also reported that DSC lead to higher values compared to DSF.[8,10,12] Figure 4-15 A presents the results of a T_m screening of nine different formulations of 4 mg/ml MAb. The formulations included six 10 mM phosphate buffer systems at pH 7.2 and pH 5.0 with or without additional 280 mM mannitol or 140 mM NaCl. Additionally, three 25 mM histidine buffers at pH 7.7, pH 7.2, and pH 5.0 were analyzed. The interpretation of the T_m values is comprehensively discussed in chapter 5. The linear fit to the data with a coefficient of determination (R^2) of 0.979 suggests that the outcome parameters of both methods were in very good agreement. Therefore, T_m values obtained by DSF can be correlated to the results from DSC and vice versa as long as the detected melting transitions can be directly assigned to a specific mAb domain, as it is the case for MAb.

Figure 4-15 B shows the correlation between the onset temperatures determined by DSC and DSF. The $T_{m,onset}$ values were in both cases determined via the empiric equation based on tangents from Boltzmann fit data, which is derived in detail in chapter 3.3.2. A linear correlation between both methods for both model mAbs with the equation of the linear fit of

$$T_{m,onset}(DSF) = 1.007\, T_{m,onset}(DSC) - 3.9\,°C \qquad (4\text{-}7)$$

suggests that both values were in good agreement (R^2 = 0.884). One sample of MAb (10 mM phosphate pH 5.0 + 140 mM NaCl) did not fit into the observed linear correlation and a much lower $T_{m,onset}$ was observed by DSC measurements. Possibly, the unfavorable sample conditions of low pH and high salt concentration were responsible for the early energetic changes. Furthermore, a broad transition with a slow ascending slope also lead to a very low $T_{m,onset}$ value using the tangent based

approach. In such an extreme case, the presented equation tends to overestimate (value too low) the $T_{m,onset}$ of the transition. For equation (4-7), this sample was omitted after a positive DFFITS outlier test result.

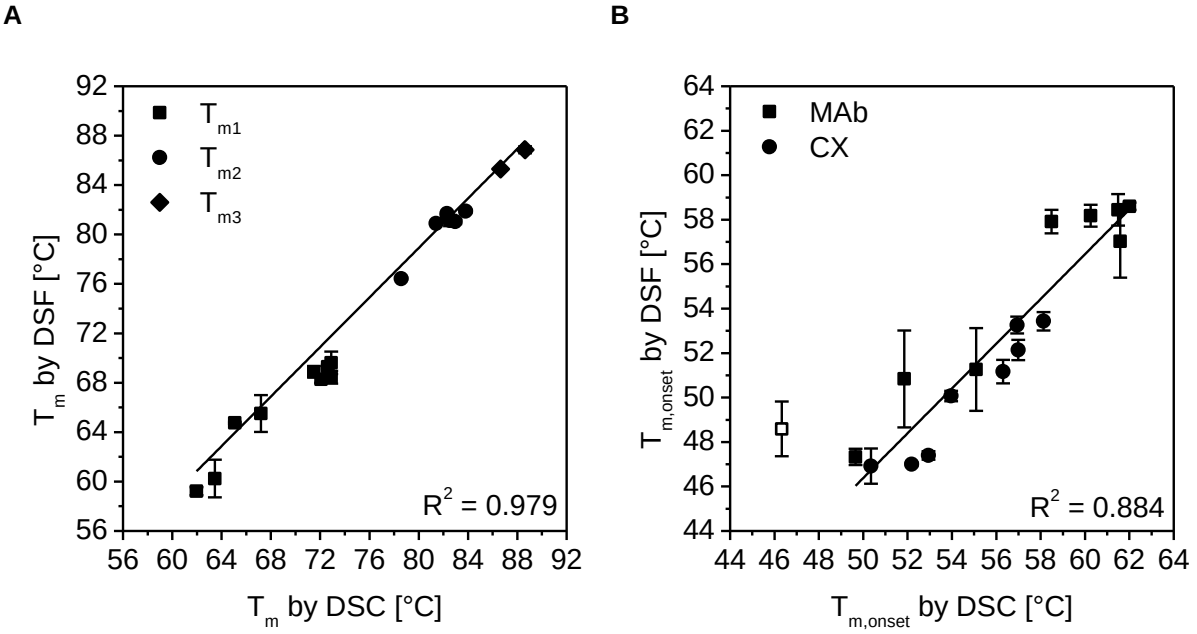

Figure 4-15. Linear correlation of the results from DSF and DSC. T_m values from 4 mg/ml MAb (A) and $T_{m,onset}$ values from 4 mg/ml MAb and 4 mg/ml CX (B) in various formulations (His 7.7; His 7.2; His 5.0; Phos 7.2 +/- NaCl, mannitol; Phos 5.0 +/- NaCl, mannitol).

It is worth noting that the results presented in Figure 4-15 B for MAb and CX were obtained on different RT-PCR machines. MAb samples were analyzed using the RT73000, whereas the qTower 2.2 was exclusively used for the CX samples. Therefore, the comparison of onset temperatures is likely to be a very robust method in terms of protein molecule and hardware setup. Furthermore, the scientific conclusions from $T_{m,onset}$ in comparison to T_m might be stronger: In contrast to the T_m value, $T_{m,onset}$ takes also the width of the transition into consideration. A sharp transition, i.e. a small $T_{1/2}$ value, is indicative for cooperative unfolding,[60] and would result in a higher $T_{m,onset}$ value in contrast to broad transitions. As the onset value corresponds to the temperature at which first structural changes occur, it is highly evident that this parameter is a better indicator and probably predictor of overall thermal stability of proteins.[10] It is therefore highly recommended to include $T_{m,onset}$ analysis into thermal stability screenings, especially during formulation development of therapeutic protein drugs. In conclusion, trends of stabilization or destabilization obtained by T_m screenings of various samples during pharmaceutical R&D can be

easily performed by DSF with low time and material consumption. The finding that values from DSF are systematically lower than those from DSC is discussed in the following chapter (4.3.6).

4.3.6 Investigation on the absolute comparability of T_m values

It was demonstrated in the previous chapter that the T_m results from DSF are consistently lower compared to the results from DSC. This finding was also reported by other authors for mAb molecules.[8,10,12] The T_m of a protein is related to its thermodynamic equilibrium between the folded and the unfolded state. There are presumably three main reasons for systematically lower T_m values arising from DSF experiments in direct comparison to DSC: i) method variations, such as heating ramp or protein concentration, ii) a strong interaction of the dye with the unfolded protein, and iii) the physicochemical difference of both methods to monitor the unfolding process. In the following paragraphs, each aspect is individually discussed.

4.3.6.1 Method variations

The effect of method variations are extensively discussed in chapter 3 during the development of the DSF method. Especially, the heating ramp and the protein concentration were found to affect the apparent T_m value of the same protein in the same formulation. It is therefore important to maintain a comparable environment when directly correlating T_m values between both methods. Therefore, the heating ramp of DSF was optimized to achieve an overall heating rate of 1 °C/min despite stepwise temperature increments. Although, only results of samples of the same protein concentrations were directly compared, method variations are assumed to be not responsible for the observed systematic deviation between the T_m results from DSC and DSF.

4.3.6.2 Strong interaction of the dye with the unfolded protein

Assuming the simplest case of a one-step reaction between a single/unique native (N) and a single/unique unfolded state (U), any ligand (L) binding to and thus stabilizing the unfolded protein, should lead to a destabilization of the native state by shifting the equilibrium to the right hand side of the equation

$$[N] + [L] \rightleftharpoons [U] + [L] \rightleftharpoons [UL] \tag{4-8}$$

As a result, the T_m value is shifted to lower temperatures in the presence of the destabilizing ligand. This scenario represents just the opposite case of a typical ligand screening, where any low molecular weight species binding to the native state of the protein leads to a positive shift of T_m. Considering the fact that SYPRO® Orange binds to the hydrophobic sites of the protein, which become exposed upon thermal unfolding, it its suspected that the probe leads to a negative shift of T_m. This effect might therefore be responsible for the systematically lower apparent T_m values observed by DSF (compare chapter 4.3.4). In order to investigate the effect of SYPRO® Orange on the T_m, DSC thermograms of the MAb in the absence and the presence of dye were analyzed. Furthermore, the influence of DMSO was checked, because the organic solvent is always present in the same volume fraction as the dye in any sample. In case of the typical SYPRO® Orange concentration of 1x, meaning a 1:5000 dilution of the stock solution supplied by the manufacturer, the protein is exposed to 0.02 % DMSO. Figure 4-16 A shows the results of a DSC scan of 4 mg/ml MAb in 25 mM histidine buffer pH 7.7 with either 0.1 % DMSO or 0.1 % SYPRO® Orange (= 5x) and also a reference scan of a sample spiked with the same amount of water. Both water and DMSO scans showed a perfect overlay with matching T_m values (Table 4-2). The T_m values of the SYPRO® Orange containing sample were in excellent agreement, although a minimally lower enthalpy of the first melting transition was observed. Furthermore, the study was performed with 4 mg/ml MAb in 10 mM phosphate buffer at pH 7.2 (Figure 4-16 B). The presence of 0.1 % DMSO did not show an effect on the DSC results similar to the findings in the histidine formulation. Interestingly, 5x SYPRO® Orange was found to slightly alter the shape of the thermogram, leading to a lower $T_{m,onset}$ value, whereas T_{m1} and T_{m2} were unchanged. Lowering the SYPRO® Orange concentration to 1x, which is the typical concentration used for DSF in this study, no significant effect could be demonstrated. These results confirm the claim of He et al. who observed no change in the melting transitions investigated by intrinsic fluorescence, SLS, and DSC in their work.[8] In terms of a practical application of DSF, a significant influence of SYPRO® Orange on the T_m value can be ruled out.

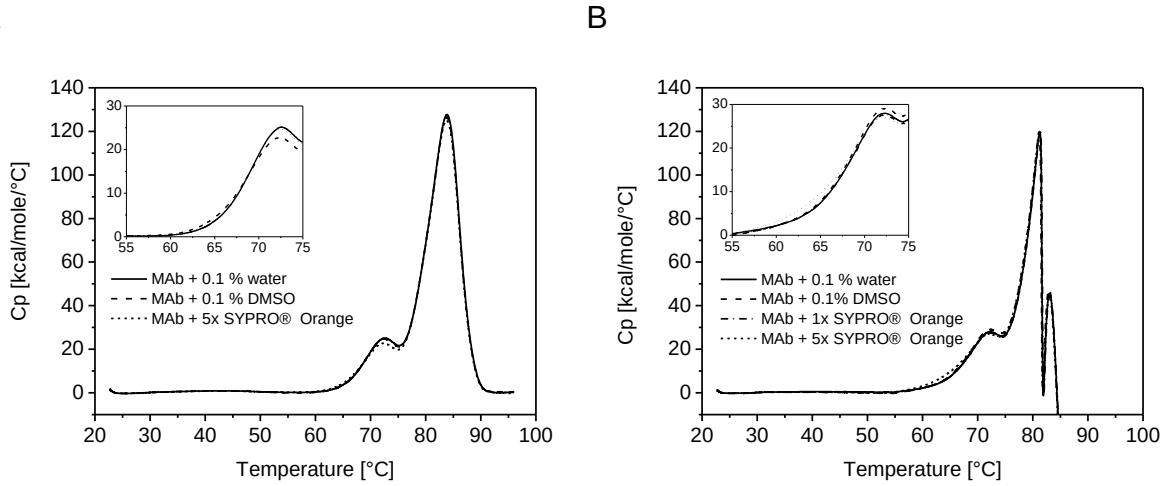

Figure 4-16. DSC thermograms of 4 mg/ml MAb spiked up to 5x SYPRO® Orange, 0.1 % DMSO, and 0.1 % water in 25 mM histidine buffer pH 7.7 (A) and 10 mM phosphate buffer pH 7.2 (B).

Table 4-2. T_m values obtained from the DSC scans presented in Figure 4-16.

4 mg/ml MAb	$T_{m,onset}$ [°C]	T_{m1} [°C]	T_{m2} [°C]
His 7.7 + 0.1 % water	60.0	72.8	83.9
His 7.7 + 0.1 % DMSO	59.5	72.7	83.8
His 7.7 + 0.1 % SYPRO® Orange (5x)	58.5	72.7	83.8
Phos 7.2 + 0.1 % water	59.4	72.3	81.3
Phos 7.2 + 0.1 % DMSO	59.1	72.3	81.1
Phos 7.2 + 0.02 % SYPRO® Orange (1x)	59.1	72.3	81.3
Phos 7.2 + 0.1 % SYPRO® Orange (5x)	56.3	72.0	81.2

4.3.6.3 Analysis of different physicochemical end points

To investigate the physicochemical differences of DSC and DSF, one first needs to consider the process of protein folding and unfolding. Theories regarding the process of protein folding are extensively reviewed and only a rough description of current understanding should be given in this work. A method referred to as “zipping and assembly method” (ZAM) for the molecular dynamic simulation of protein folding recently showed promising results to match *in silico* calculations with experimental results.[61] Beginning with a random coil, the algorithm detects starting points where initial secondary structure elements form in parallel, mainly driven by hydrophobic interaction. These blocks will grow and interact with each other in order to form larger structures (“zipping and assembly”). In this process native as well as nonnative interactions unite and break as the tertiary structure forms. This finalization process

of the conformation can induce secondary structure changes so that those elements are subject to changes until the end of the folding process. Due to computational limitations, although impressive results were recently obtained using supercomputers as well as distributed computing platform, complex proteins such as mAbs are still challenging to simulate. The same is true for simulation of protein unfolding. Ren and coworker simulated the thermal unfolding of Rhodanase, a 2-domain protein of 33 kDa, and found that the α-helix is more sensitive to heat than β-sheets.[62] Another simulation revealed that the cofactor binding site of *E. coli* dihydrofolate reductase (1 domain, 19 kDa), which is formed by an α-helix and β-sheet, was most susceptible to heat, and the protein subsequently formed molten globule like intermediates with decreasing secondary structure, until the structure at high temperature was completely depleted.[63] Consequently, the secondary structure elements play a crucial role during thermal unfolding. Figure 4-17 illustrates the amino acid composition involved in secondary structure elements based on the data reported by Otaki and coworkers.[64]

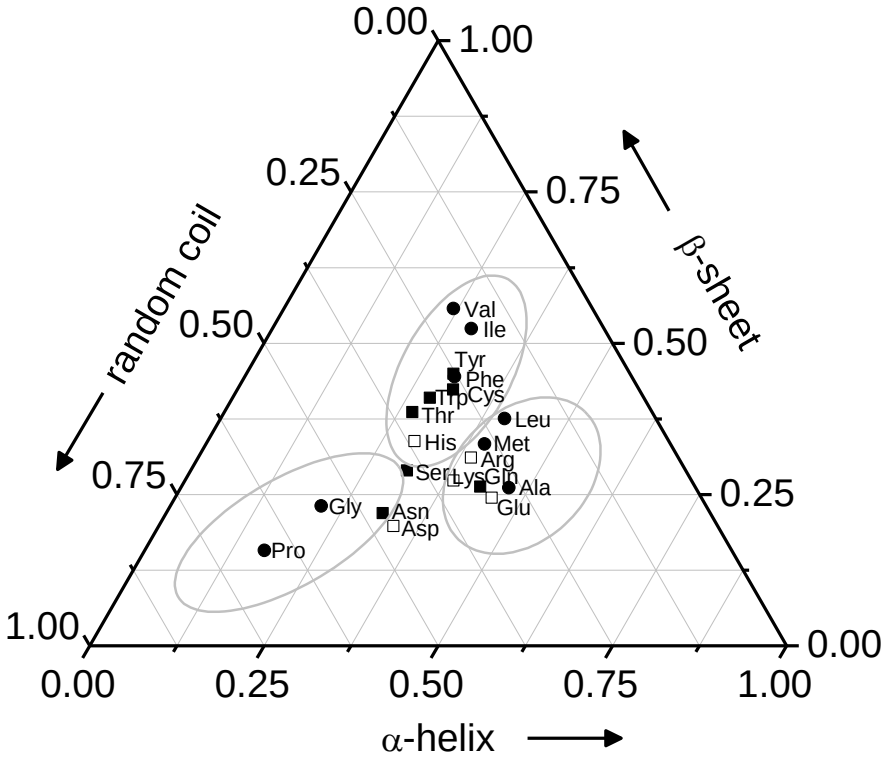

Figure 4-17. The composition of the amino acids in α-helix, β-sheet, and random coil structure. The amino acids are grouped into charged polar (open squares), uncharged polar (closed squares), and nonpolar (closed circles) characteristic. Aliphatic and nonpolar residues are involved in all secondary structure elements. The graph is based on the data from Otaki et al.[64]

Several amino acids show a tendency towards certain secondary structure elements.[64,65] The α-helix is the preferred secondary structure. In cases of steric hindrance due to bulky side chains, β-strands are favored (valine, threonine, isoleucine). Competing H-bonds are unfavorable for α-helix structures (serine, aspartic acid, asparagine) and proline is known as a secondary structure breaker due the restricted angle of the ring structure. It was stated that the α-helix tends towards aliphatic and hydrophilic amino acids, whereas β-strands are likely consisting of both aliphatic and aromatic residues (Figure 4-17).[64] Fluorescent probes like Bis-ANS and SYPRO® Orange are assumed to interact mainly with the hydrophobic, nonpolar residues that are present in all secondary structure parts.

In analogy to the postulated process of protein folding, thermal unfolding is presumably starting with a perturbation of secondary structure elements. Subsequently, the conformation is loosened to molten globule like intermediate which finally break contact and a random coil would be obtained if not for other interfering processes. Aggregation is typically observed upon unfolding of the protein via hydrophobic interactions of the exposed hydrophobic patches (see chapter 6). Whereas DSC monitors every subtle energy change upon thermal unfolding, DSF relies on the interaction of the fluorescent probe. That means the unfolding process is monitored by DSF as long as a change in exposed hydrophobic structure occurs. In case all interaction sites are accessible to the dye, no further fluorescence intensity increase is possible. The hypothesis is that this stage of unfolding is reached before the last structural interaction is abolished. Furthermore, the initiation of protein aggregation upon unfolding, as discussed in chapter 6, will perturb the end point. While the protein molecules aggregate via the exposed hydrophobic patches, this surface is no longer accessible for the interaction with the dye.[9] In all the cases, the maximum of hydrophobic exposure is reached before a completely unordered, random coil structure is obtained. This can explain the observation that the apparent T_m value, where half of the observed change occurred, is lower in case of hydrophobic exposure (DSF) compared to enthalpy change (DSC).

However, the suggested endpoint detection at lower temperatures in case of DSF cannot explain all effects, because also $T_{m,onset}$ values from DSF were found to be lower compared to the results from DSC (Figure 4-15 B). DSF might be particularly sensitive to the suggested initial perturbation of secondary structure elements. Thus,

small deviations from the native structure associated with low enthalpies would give a higher signal in DSF compared to DSC, and thus detect the onset of unfolding at lower temperatures.

Finally, both methods are based on different physicochemical processes but the results are in good agreement and can be linearly correlated. DSC and DSF can be stated as orthogonal methods for the assessment of protein thermal stability. Especially $T_{m,onset}$ is very promising to detect thermal instability issues during high-throughput screenings. Interesting candidates, e.g., with particularly low or high values, could be crosschecked by one or the other method.

4.4 Conclusion

Thermal analysis is essential for the assessment of the thermal stability of proteins. Especially with multi-domain molecules such as mAbs, the process of unfolding consists of multiple steps. The melting profiles of DSF and the thermograms from DSC enabled a more detailed characterization with respect to the thermal sensitivity of the different fragments and domains. Typically, a different thermal stability of Fab and Fc is observed. Intrinsic factors, for instance, the glycosylation pattern of the Fc that interacts with the protein structure, affect the T_m value. Enzymatic removal of the Fc-glycans resulted in a reduction of the thermal stability of both the isolated Fc fragment and Fc of the full mAbs. Host cells and process parameters therefore have an influence on the thermal stability of the mAb. Furthermore, this suggests why Fc fragments from humanized mAbs can show different melting profiles. At the same time, the thermal stability of the Fab fragment is unique for every mAb molecule. The Fab fragment of MAb had higher T_m values compared to Fab of CX. Interestingly, the additional glycosylation of CX in the Fab region did not affect the thermal stability. Presumably the Fab-glycans are not involved in the conformational structure of the Fab domains as suggested by the crystal structure (PDB 1YY8). The low sample amounts necessary for a DSF experiment and the high-throughput design allowed the investigation of costly samples (e.g., the deglycosylated fragments) or screenings of various external factors that influence the thermal stability. Different pH values, ionic strength conditions, and excipients were investigated. Interestingly, lower T_m values of the CH2 domain were observed at pH 5.0 in the presence of arginine and histidine, including a significant effect of the counter-anions. Moreover, arginine and

histidine showed a stabilization of the Fab part supposedly via reduced aggregate formation upon thermal unfolding, with special synergistic effects by the counter-anions aspartate and glutamate. It was demonstrated that the results from DSC and DSF can be linearly correlated, although consistently lower values were obtained by DSF. Especially, the $T_{m,onset}$ value indicating the first change in conformational structure, which is supposedly a better predictive parameter than T_m,[10] can be obtained from both methods. Because of the different physicochemical measurements, DSC and DSF are valuable, orthogonal, and complimentary methods for thermal stability analysis of therapeutic proteins.

4.5 References

1. Schön A, Velázquez-Campoy A. 2005. Calorimetry. In Jiskoot W, Crommelin DJA, editors. Methods for Structural Analysis of Protein Pharmaceuticals, ed., Arlington, VA: American Association of Pharmaceutical Scientists.

2. Gill P, Moghadam TT, Ranjbar B 2010. Differential Scanning Calorimetry Techniques: Applications in Biology and Nanoscience. J Biomol Tech 21(4):167-193.

3. Nashine V, Kroetsch A, Sahin E, Zhou R, Adams M 2013. Orthogonal High-Throughput Thermal Scanning Method for Rank Ordering Protein Formulations. AAPS PharmSciTech 14(4):1360-1366.

4. Youssef AMK, Winter G 2013. A critical evaluation of microcalorimetry as a predictive tool for long term stability of liquid protein formulations: Granulocyte Colony Stimulating Factor (GCSF). Eur J Pharm Biopharm 84(1):145-155.

5. Wang L, Wang B, Lin Q 2008. Demonstration of MEMS-based differential scanning calorimetry for determining thermodynamic properties of biomolecules. Sensors and Actuators B: Chemical 134(2):953-958.

6. He F, Razinkov VI, Middaugh CR, Becker GW. 2013. High-Throughput Biophysical Approaches to Therapeutic Protein Development. In Narhi LO, editor Biophysics for Therapeutic Protein Development, ed., New York: Springer.

7. Samra HS, He F 2012. Advancements in High Throughput Biophysical Technologies: Applications for Characterization and Screening during Early Formulation Development of Monoclonal Antibodies. Mol Pharm 9(4):696-707.

8. He F, Hogan S, Latypov RF, Narhi LO, Razinkov VI 2010. High throughput thermostability screening of monoclonal antibody formulations. J Pharm Sci 99(4):1707-1720.

9. Niesen FH, Berglund H, Vedadi M 2007. The use of differential scanning fluorimetry to detect ligand interactions that promote protein stability. Nat Protocols 2(9):2212-2221.

10. King AC, Woods M, Liu W, Lu Z, Gill D, Krebs MRH 2011. High-throughput measurement, correlation analysis, and machine-learning predictions for pH and thermal stabilities of Pfizer-generated antibodies. Protein Sci 20(9):1546-1557.

11. Li Y, Mach H, Blue JT 2011. High throughput formulation screening for global aggregation behaviors of three monoclonal antibodies. J Pharm Sci 100(6):2120-2135.

12. Goldberg DS, Bishop SM, Shah AU, Sathish HA 2011. Formulation development of therapeutic monoclonal antibodies using high-throughput fluorescence and static light scattering techniques: Role of conformational and colloidal stability. J Pharm Sci 100(4):1306-1315.

13. Mierzwa ML, Nyati MK, Morgan MA, Lawrence TS 2010. Recent Advances in Combined Modality Therapy. The Oncologist 15(4):372-381.

14. EMA. 2013. Erbitux - Procedural steps taken and scientific information after the authorisation. London: EMA. Accessed 12/16/2013, at: http://www.ema.europa.eu/docs/en_GB/document_library/EPAR_-_Procedural_steps_taken_and_scientific_information_after_authorisation/human/000558/WC500029115.pdf.

15. Lahlou A, Blanchet B, Carvalho M, Paul M, Astier A 2009. Mechanically-induced aggregation of the monoclonal antibody cetuximab. Ann Pharm Fr 67(5):340-352.

16. Jefferis R 2012. Isotype and glycoform selection for antibody therapeutics. Arch Biochem Biophys 526(2):159-166.

17. Mizushima T, Yagi H, Takemoto E, Shibata-Koyama M, Isoda Y, Iida S, Masuda K, Satoh M, Kato K 2011. Structural basis for improved efficacy of therapeutic antibodies on defucosylation of their Fc glycans. Genes Cells 16(11):1071-1080.

18. Ha S, Wang Y, Rustandi RR 2011. Biochemical and biophysical characterization of humanized IgG1 produced in Pichia pastoris. mAbs 3(5):453-460.

19. Robak T 2009. GA-101, a third-generation, humanized and glyco-engineered anti-CD20 mAb for the treatment of B-cell lymphoid malignancies. Curr Opin Investig Drugs 10(6):588-596.

20. Morgan C, Fernandes D 2009. Designing Biobetter Monoclonal Antibody Therapeutics By Glycoengineering. International Pharmaceutical Industry (IPI):38-44.

21. Solá RJ, Griebenow K 2009. Effects of glycosylation on the stability of protein pharmaceuticals. J Pharm Sci 98(4):1223-1245.

22. Solá RJ, Rodríguez-Martínez JA, Griebenow K 2007. Modulation of protein biophysical properties by chemical glycosylation: biochemical insights and biomedical implications. Cell Mol Life Sci 64(16):2133-2152.

23. Mimura Y, Church S, Ghirlando R, Ashton PR, Dong S, Goodall M, Lund J, Jefferis R 2000. The influence of glycosylation on the thermal stability and effector function expression of human IgG1-Fc: properties of a series of truncated glycoforms. Mol Immunol 37(12–13):697-706.

24. Wen J, Jiang Y, Narhi L 2008. Effect of Carbohydrate on Thermal Stability of Antibodies. American Pharmaceutical Review 11(6):98-104.

25. Ionescu RM, Vlasak J, Price C, Kirchmeier M 2008. Contribution of variable domains to the stability of humanized IgG1 monoclonal antibodies. J Pharm Sci 97(4):1414-1426.

26. Hari SB, Lau H, Razinkov VI, Chen S, Latypov RF 2010. Acid-induced aggregation of human monoclonal IgG1 and IgG2: molecular mechanism and the effect of solution composition. Biochemistry (Mosc) 49(43):9328-9338.

27. Liu H, Bulseco G-G, Sun J 2006. Effect of posttranslational modifications on the thermal stability of a recombinant monoclonal antibody. Immunol Lett 106(2):144-153.

28. Ghirlando R, Lund J, Goodall M, Jefferis R 1999. Glycosylation of human IgG-Fc: influences on structure revealed by differential scanning micro-calorimetry. Immunol Lett 68(1):47-52.

29. Alsenaidy MA, Kim JH, Majumdar R, Weis DD, Joshi SB, Tolbert TJ, Middaugh CR, Volkin DB 2013. High-Throughput Biophysical Analysis and Data Visualization of Conformational Stability of an IgG1 Monoclonal Antibody After Deglycosylation. J Pharm Sci 102(11):3942-3956.

30. Falconer RJ, Chan C, Hughes K, Munro TP 2011. Stabilization of a monoclonal antibody during purification and formulation by addition of basic amino acid excipients. J Chem Technol Biotechnol 86(7):942-948.

31. Wakankar AA, Borchardt RT, Eigenbrot C, Shia S, Wang YJ, Shire SJ, Liu JL 2007. Aspartate Isomerization in the Complementarity-Determining Regions of Two Closely Related Monoclonal Antibodies. Biochemistry (Mosc) 46(6):1534-1544.

32. Zaiontz C. 2013. Real Statistics Using Excel. Accessed 10/23/2013, at: http://www.real-statistics.com/multiple-regression/outliers-and-influencers/.

33. Cohen J, Cohen P, West SG, Aiken LS. 2003. Applied Multiple Regression/Correlation Analysis for the Behavioral Sciences. ed., Mahawah, NY: Erlbaum.

34. Lyubarskaya Y, Houde D, Woodard J, Murphy D, Mhatre R 2006. Analysis of recombinant monoclonal antibody isoforms by electrospray ionization mass spectrometry as a strategy for

streamlining characterization of recombinant monoclonal antibody charge heterogeneity. Anal Biochem 348(1):24-39.

35. Cacia J, Keck R, Presta LG, Frenz J 1996. Isomerization of an Aspartic Acid Residue in the Complementarity-Determining Regions of a Recombinant Antibody to Human IgE: Identification and Effect on Binding Affinity. Biochemistry (Mosc) 35(6):1897-1903.

36. Valliere-Douglass J, Wallace A, Balland A 2008. Separation of populations of antibody variants by fine tuning of hydrophobic-interaction chromatography operating conditions. J Chromatogr A 1214(1–2):81-89.

37. Zhang W, Czupryn MJ 2003. Analysis of isoaspartate in a recombinant monoclonal antibody and its charge isoforms. J Pharm Biomed Anal 30(5):1479-1490.

38. Vlasak J, Ionescu R 2008. Heterogeneity of monoclonal antibodies revealed by charge-sensitive methods. Curr Pharm Biotechnol 9(6):468-481.

39. Lin J, Tan Q, Wang S 2011. A high-resolution capillary isoelectric focusing method for the determination of therapeutic recombinant monoclonal antibody. J Sep Sci 34(14):1696-1702.

40. Tischenko VM, Abramov VM, Zav'yalov VP 1998. Investigation of the Cooperative Structure of Fc Fragments from Myeloma Immunoglobulin G†. Biochemistry (Mosc) 37(16):5576-5581.

41. Ha S, Ou Y, Vlasak J, Li Y, Wang S, Vo K, Du Y, Mach A, Fang Y, Zhang N 2011. Isolation and characterization of IgG1 with asymmetrical Fc glycosylation. Glycobiology 21(8):1087-1096.

42. Qian J, Liu T, Yang L, Daus A, Crowley R, Zhou Q 2007. Structural characterization of N-linked oligosaccharides on monoclonal antibody cetuximab by the combination of orthogonal matrix-assisted laser desorption/ionization hybrid quadrupole–quadrupole time-of-flight tandem mass spectrometry and sequential enzymatic digestion. Anal Biochem 364(1):8-18.

43. Stadlmann J, Pabst M, Kolarich D, Kunert R, Altmann F 2008. Analysis of immunoglobulin glycosylation by LC-ESI-MS of glycopeptides and oligosaccharides. Proteomics 8(14):2858-2871.

44. Ayoub D, Jabs W, Resemann A, Evers W, Evans C, Main L, Baessmann C, Wagner-Rousset E, Suckau D, Beck A 2013. Correct primary structure assessment and extensive glyco-profiling of cetuximab by a combination of intact, middle-up, middle-down and bottom-up ESI and MALDI mass spectrometry techniques. mAbs 5(5):699-710.

45. Chung CH, Mirakhur B, Chan E, Le Q-T, Berlin J, Morse M, Murphy BA, Satinover SM, Hosen J, Mauro D, Slebos RJ, Zhou Q, Gold D, Hatley T, Hicklin DJ, Platts-Mills TAE 2008. Cetuximab-Induced Anaphylaxis and IgE Specific for Galactose-α-1,3-Galactose. N Engl J Med 358(11):1109-1117.

46. Krapp S, Mimura Y, Jefferis R, Huber R, Sondermann P 2003. Structural Analysis of Human IgG-Fc Glycoforms Reveals a Correlation Between Glycosylation and Structural Integrity. J Mol Biol 325(5):979-989.

47. Sondermann P, Huber R, Oosthuizen V, Jacob U 2000. The 3.2-A crystal structure of the human IgG1 Fc fragment–FcγRIII complex. Nature 406(6793):267-273.

48. Nagae M, Yamaguchi Y 2012. Function and 3D Structure of the N-Glycans on Glycoproteins. Int J Mol Sci 13(7):8398-8429.

49. Barb AW, Prestegard JH 2011. NMR analysis demonstrates immunoglobulin G N-glycans are accessible and dynamic. Nat Chem Biol 7(3):147-153.

50. Kwon K-S, Yu M-H 1997. Effect of glycosylation on the stability of α1-antitrypsin toward urea denaturation and thermal deactivation. Biochimica et Biophysica Acta (BBA) - General Subjects 1335(3):265-272.

51. Høiberg-Nielsen R, Fuglsang CC, Arleth L, Westh P 2006. Interrelationships of Glycosylation and Aggregation Kinetics for Peniophora lycii Phytase†. Biochemistry (Mosc) 45(15):5057-5066.

52. Stadlmann J, Weber A, Pabst M, Anderle H, Kunert R, J. Ehrlich H, Peter Schwarz H, Altmann F 2009. A close look at human IgG sialylation and subclass distribution after lectin fractionation. Proteomics 9(17):4143-4153.

53. Li S, Schmitz KR, Jeffrey PD, Wiltzius JJW, Kussie P, Ferguson KM 2005. Structural basis for inhibition of the epidermal growth factor receptor by cetuximab. Cancer Cell 7(4):301-311.

54. Ishibashi M, Tsumoto K, Tokunaga M, Ejima D, Kita Y, Arakawa T 2005. Is arginine a protein-denaturant? Protein Expr Purif 42(1):1-6.

55. Arakawa T, Tsumoto K 2003. The effects of arginine on refolding of aggregated proteins: not facilitate refolding, but suppress aggregation. Biochem Biophys Res Commun 304(1):148-152.

56. Yancey P, Clark M, Hand S, Bowlus R, Somero G 1982. Living with water stress: evolution of osmolyte systems. Science 217(4566):1214-1222.

57. Shiraki K, Kudou M, Fujiwara S, Imanaka T, Takagi M 2002. Biophysical Effect of Amino Acids on the Prevention of Protein Aggregation. J Biochem (Tokyo) 132(4):591-595.

58. Tian F, Middaugh CR, Offerdahl T, Munson E, Sane S, Rytting JH 2007. Spectroscopic evaluation of the stabilization of humanized monoclonal antibodies in amino acid formulations. Int J Pharm 335(1–2):20-31.

59. Chen B, Bautista R, Yu K, Zapata G, Mulkerrin M, Chamow S 2003. Influence of Histidine on the Stability and Physical Properties of a Fully Human Antibody in Aqueous and Solid Forms. Pharm Res 20(12):1952-1960.

60. GE Healthcare. 2010. Preformulation and stability studies of biotherapeutics using DSC. MicroCal application note 28-9755-22 AA. Accessed 05/13/2013, at: www.gelifesciences.com.

61. Dill KA, Ozkan SB, Shell MS, Weikl TR 2008. The protein folding problem. Annu Rev Biophys 37:289-316.

62. Ren Y, Gao J, Ge W, Li J 2008. Thermal Unfolding of a Double-Domain Protein: Molecular Dynamics Simulation of Rhodanese. Ind Eng Chem Res 48(19):8865-8871.

63. Sham YY, Ma B, Tsai C-J, Nussinov R 2002. Thermal unfolding molecular dynamics simulation of Escherichia coli dihydrofolate reductase: Thermal stability of protein domains and unfolding pathway. Proteins: Struct, Funct, Bioinf 46(3):308-320.

64. Otaki JM, Tsutsumi M, Gotoh T, Yamamoto H 2010. Secondary Structure Characterization Based on Amino Acid Composition and Availability in Proteins. J Chem Inf Model 50(4):690-700.

65. Berg JM, Tymoczko JL, Stryer L. 2002. Section 3.6, The Amino Acid Sequence of a Protein Determines Its Three-Dimensional Structure. Biochemistry, 5th edition, ed., New York: W H Freeman.

5 High-throughput T_m analysis of a mAb by DSF in the presence of surfactants

This chapter has been published as Tim Menzen and Wolfgang Friess, 2013, High-throughput melting-temperature analysis of a monoclonal antibody by differential scanning fluorimetry in the presence of surfactants, J Pharm Sci 102(2): 415-428.

5.1 Abstract

Differential scanning fluorimetry (DSF) is successfully used as a high-throughput screening method for the analysis of the protein melting temperature (T_m) in the development of therapeutic monoclonal antibody (mAb) formulations. Typically, surfactants are utilized in mAb formulations as a stabilizer, but the commonly applied polarity sensitive dye SYPRO® Orange shows bright fluorescence in the presence of micelles, concealing the signal of protein unfolding. Studying various mAb formulations containing polysorbate 20, polysorbate 80, or poloxamer 188, the molecular rotor probe DCVJ (9-(Dicyanovinyl)julolidine) was investigated. Although limited to higher mAb concentrations, DCVJ enabled the determination of T_m in many formulations where SYPRO® Orange failed. It is important to note that careful background correction of placebo formulations is essential for the precise determination of T_m and especially $T_{m,onset}$. Thermal shifts of T_{m1} (lowest observed thermal transition) indicating stabilizing or destabilizing effects of pH or excipient were in good agreement across all tested formulations and correlated well with DSC measurements. Additionally, the micellization temperature of poloxamer 188 was confirmed, which leads to a nonproteinous transition. With this new method, it is possible to apply DSF during the development of therapeutic proteins in surfactant containing formulations.

5.2 Introduction

Since the introduction of the first generation of therapeutic monoclonal antibodies (mAbs) to the market in the 1990s, a variety of products were approved by the authorities and many more are in late stages of development.[1] Protein stability is a

crucial parameter during development and production. Besides chemical instability, conformational and colloidal instability can lead to aggregation which is often linked to a loss of efficiency.[2] Furthermore, immunological reactions are most likely dependent on protein aggregates.[3] Because of the complex structure of proteins as compared to small molecules, a large arsenal of analytical tools is necessary for comprehensive analysis. Conformational structure can be typically studied with spectroscopic methods like intrinsic and extrinsic fluorescence, circular dichroism (CD), Fourier transform infrared (FTIR), and Raman[4,5]. By analysis of structural changes of the protein upon thermal unfolding, a protein melting temperature (T_m) can be defined at which half of the protein is in an unfolded state. T_m is commonly associated with conformational stability.[6] Typically differential scanning calorimetry (DSC), tracing thermal events during heating, is used to determine T_m ($T_{m\,DSC}$).[7,8] However, DSC is limited to low sample throughput and comparably high sample volumes. Consequently, there is a demand for alternative, high-throughput screening (HTS) methods of stabilizing or destabilizing factors. In 2001, Pantoliano and coworkers introduced a HTS based on extrinsic fluorescence to screen large libraries of small molecule ligands.[9] The polarity sensitive dye 1-anilinonaphthalene-8-sulfonic acid (ANS) is used to analyze protein unfolding as ANS changes its fluorescence properties upon binding to newly exposed hydrophobic surfaces that appear upon denaturation. Already utilized in cuvettes with common spectrofluorimeters,[10,11] Pantoliano et al. adapted a special instrumental setup to analyze samples in microplates. The thermal transitions observed by the interaction of the fluorescent dye with the unfolding protein do not represent melting transitions from DSC, but the obtained apparent melting temperatures can be closely interpreted in terms of the calorimetric values. Since the introduction of this method in literature, referred to as ThermoFluor® or differential scanning fluorimetry (DSF), substantial development occurred. Making use of the temperature controller and fluorescence detector of common real-time polymerase chain reaction (RT-PCR) machines,[12] in the last decade, DSF found its application in the wide field of protein science, ranging from identification of stabilizing buffer conditions,[13-15] optimal crystallization parameters[16] or ligands,[12,17,18] to the determination of binding constants[19] as well as protein-protein complexes.[20] A review was dedicated to this topic by Senisterra et al. this year.[21] More recently, various authors, predominately from the pharmaceutical industry, reported that DSF is a powerful tool for the development of mAb formulation. By

comparing the data from accelerated stress tests, Goldberg et al. could demonstrate that both DSF and differential static light scattering (DSLS) are HTS methods to screen conformational and colloidal stability and are synergistic for mAb formulation optimization and stability prediction.[22] Li and coworkers applied DSF, among other methods, and extensively studied the aggregation propensity of three mAbs. They found that T_m alone is not able to predict aggregation pathways, e.g., when aggregate growth is the rate determining kinetic step, but is essential in combination with a size-based assay to understand the aggregation behavior of the protein.[23] He and coworkers similarly analyzed the formulation conditions of mAbs by DSF,[24,25] whereas King et al. collected thermal stability data for numerous mAbs with this method.[26] All these DSF studies in formulation development have used SYPRO® Orange as fluorescent dye because of its environmental sensitivity, bright fluorescence, chemical stability, and spectral properties in the range of the typical RT-PCR machine filter sets. However, none of the authors included surface active excipients, although surfactants are often used as stabilizing agents during production and storage of therapeutic proteins.[27] This is because in the presence of a surfactant above the critical micelle concentration (CMC), SYPRO® Orange is transferred into the hydrophobic core of the micelles resulting in bright fluorescence of the dye and consequently high background. The comparatively small increase of the fluorescence intensity due to the unfolding of the protein is concealed. To overcome this major limitation in DSF as HTS in formulation development, the aim of this study was to implement the use of a fluorescent probe which is sensitive to protein folding but shows less micelle interaction. As a so called fluorescent molecular rotor, 9-(Dicyanovinyl)julolidine (DCVJ) shows environmentally sensitive properties. Nonradiative relaxation after twisted intramolecular charge transfer (TICT) is dependent on the system. In a low viscosity polar environment, radiationless decay after intramolecular rotation is favored, and thus only weak fluorescence occurs. In solvents of high viscosity and “spatially restricted” environment, torsional rearrangement is suppressed and an increased fluorescence is observed.[28,29] The general feasibility of DCVJ in the analysis of protein unfolding and aggregation in the presence of a surfactant has been shown many times.[30,31] Therefore, we tested whether the physicochemical and photochemical properties of DCVJ enable its application for T_m determination with DSF of a mAb in the presence of a surfactant with a common RT-PCR machine. Concentrations of 0.8 mg/ml, 4 mg/ml, or 40 mg/ml

of the mAb were formulated with and without either polysorbate 20 (PS 20), or polysorbate 80 (PS 80), or poloxamer 188 (PX 188) in pharmaceutically relevant concentration in nine different buffer systems based on either phosphate or histidine, including sodium chloride (NaCl) or mannitol. $T_{m\,DSF}$ values obtained with DCVJ and SYPRO® Orange after careful background correction in the presence of surfactants were compared with the values of surfactant-free formulations. Furthermore, the effect of background correction on the resulting apparent onset temperature of unfolding in the presence of surfactants based on the Boltzmann fit ($T_{m,onset}$) was evaluated. In addition, T_m measurements by DSC were performed to confirm the DSF results and to understand the formulation effects. Furthermore, the temperature dependent micelle formation of PX 188 was analyzed by dynamic light scattering (DLS) measurements.

5.3 Materials and Methods

DCVJ (9-(Dicyanovinyl)julolidine) and SYPRO® Orange were purchased from Sigma-Aldrich (Steinheim, Germany). Lutrol® F-68 (poloxamer 188, PX 188) was purchased from BASF (Ludwigshafen, Germany), Tween® 80 (polysorbate 80, PS 80) and Tween® 20 (polysorbate 20, PS 20) by Merck (Darmstadt, Germany). All other excipients were purchased from BDH Prolabo/VWR (Darmstadt, Germany) and were of HPLC grade or better. Highly purified water was prepared by an ELGA Purelab system (ELGA LabWater, Celle, Germany) and exclusively used as a solvent if not otherwise mentioned.

5.3.1 Sample preparation

The formulations at 0.8 mg/ml, 4 mg/ml, and 40 mg/ml of a humanized IgG1 type monoclonal antibody (“MAb”) produced in CHO ($\varepsilon_{280\,nm}$ = 1.49 ml mg^{-1} cm^{-1}) in 25 mM histidine at pH 7.7, 7.2, and 5.0 as well as in 10 mM phosphate buffer with and without 140 mM NaCl or 280 mM mannitol at pH 7.2 and pH 5.0 were prepared from stock solutions. All formulations were filtrated through a 0.2 µm PES syringe filter prior to use. Surfactant containing formulations were prepared by either adding 8.4 mg of PX 188, or 10 µl of PS 20 or PS 80 working solutions to 1000 µl MAb solution to achieve a surfactant concentration of 0.84 % PX 188 and 0.18 % or 0.04 % PS 20 and PS 80, respectively.

5.3.2 Differential scanning fluorimetry (DSF)

For DSF, a 220 mM DCVJ stock solution in dimethyl sulfoxide (DMSO) was prepared. SYPRO® Orange was supplied by the manufacturer as a 5000x concentrated stock solution in DMSO. Working solutions of both fluorescent dye stock solutions were prepared in water immediately prior to the experiment. 1 µl fluorescent dye working solution was pipetted to 20 µl sample solution in MicoroAmp® Optical 96-Well Reaction Plates (Applied Biosystems, Foster City, California, USA) and mixed by aspiration. The final dye concentrations were 100 µM for DCVJ or 1x (corresponding to a 1:5000 dilution of the provided stock solution) for SYPRO® Orange. Well plates were sealed with MicroAmp® Optical Adhesive Film (Applied Biosystems) and centrifuged at 2000 g for 1 min to remove air bubbles. A RT 7300 Real-Time PCR machine (Applied Biosystems) at a temperature ramp of 1 °C/min from 20 °C to 96 °C in steps of 1 °C was utilized. The emitted fluorescence intensity was read out across all 96 wells at every step. Raw data were exported for further processing with Origin® 8 SR6 (Originlab Corporation, Northampton, Massachusetts, USA) to obtain melting curves of fluorescence intensity at 530 nm for DCVJ and 578 nm for SYPRO® Orange as a function of temperature. A placebo sample without MAb was recorded for each system and subtracted from the melting curve of the verum samples. The background corrected melting curves were differentiated, smoothed (polynomial order = 1, number of points = 5), and splined (cubic spline with 99 interpolated points in between two data points). Peak centers of the resulting first derivative were used as melting temperatures ($T_{m\,DSF}$). The presented $T_{m\,DSF}$ are the mean of three independent values. Using Origin®, the Boltzmann function[17] was fitted to the averaged fluorescence traces of three independent samples. The local minimum and maximum of the fluorescence intensity associated with the apparent transition were used as input values, while all parameters were unconstrained during the fit. The onset temperature $T_{m,onset}$ was calculated using the following empiric equation

$$T_{m,onset} = \frac{8dT\left(A_L - \frac{A_U + A_L}{2} + \frac{T'_m(A_U - A_L)}{4dT}\right)}{A_U - A_L} - T'_m \qquad (5\text{-}1)$$

with T'_m the inflection point, dT the slope factor, A_L the lower fluorescence intensity, and A_U the upper fluorescence intensity of the sigmoidal curve. $T_{m,onset}$ resembles twice the distance on the x-scale of T'_m, and the point of intersection between the tangents through T'_m and A_L (see also chapter 3.3.2).

5.3.3 Differential scanning calorimetry (DSC)

The sample and the reference cell of a VP-DSC MicroCalorimeter (MicroCal, Northampton, Massachusetts, USA, now Malvern Instruments) were filled with the 4 mg/ml MAb formulation and the corresponding placebo, respectively. Prescan thermostat time was set to 15 min to allow for equilibration of the sample. DSC thermograms were recorded from 20 °C to 96 °C at a scan rate of 1 °C/min. After each protein scan, both cells were heated up with nitric acid and washed subsequently with 1 % SDS solution and water. The thermogram was corrected by subtraction of a water-versus-water scan and normalized for the protein concentration using Origin® 7 SR2 (Originlab) with MicroCal VPViewer2000® version 1.4.10. $T_{m\,DSC}$ is represented by the peak maximum of the endothermic transition.

5.3.4 Dynamic light scattering (DLS)

A DynaPro Plate Reader from Wyatt Technologies (Dernbach, Germany) with Dynamics software version 7.1.5.6 was used to determine the hydrodynamic radius of particulate species in solution. A sample solution of 20 µl was pipetted into a 384 well plate (Corning Incorporated, Corning, New York, USA), covered with paraffin and centrifuged at 2000 g for 2 min. Each well was analyzed with five acquisitions and an acquisition time of 5 s. A continuous temperature ramp from 20 °C to 80 °C with a temperature rate of 0.1 °C/min was applied with analysis of each well every 1 °C.

5.4 Results

At first, the DSF results obtained with DCVJ of the 40 mg/ml MAb formulations with and without surfactant were compared to DSC results followed by the application of DCVJ and SYPRO® Orange in the presence of a surfactant at decreasing MAb concentrations. Supplementary results characterizing the micellization of PX 188 will be presented. Finally, the effect of background correction on $T_{m\,DSF}$ and $T_{m,onset}$ was investigated.

Depending on the formulation pH, the mAb showed 2 or 3 unfolding transitions and the T_m values were enumerated, beginning with the lowest protein unfolding transition observed. The DSC thermogram of the histidine formulation is exemplarily presented in Figure 5-1. At pH 7.7 as well as pH 7.2, the first transition ($T_{m1\,DSC}$) was caused by the melting of the CH2 domain, whereas the second transition ($T_{m2\,DSC}$) represented

the unfolding of the CH3 domain and the Fab fragment.[32-34] Decreasing the pH value to 5.0 resulted in a shift of the $T_{m\,DSC}$ of both CH2 and CH3 domain to lower temperatures leading to a distinct transition for CH3 ($T_{m2\,DSC}$) and Fab ($T_{m3\,DSC}$).

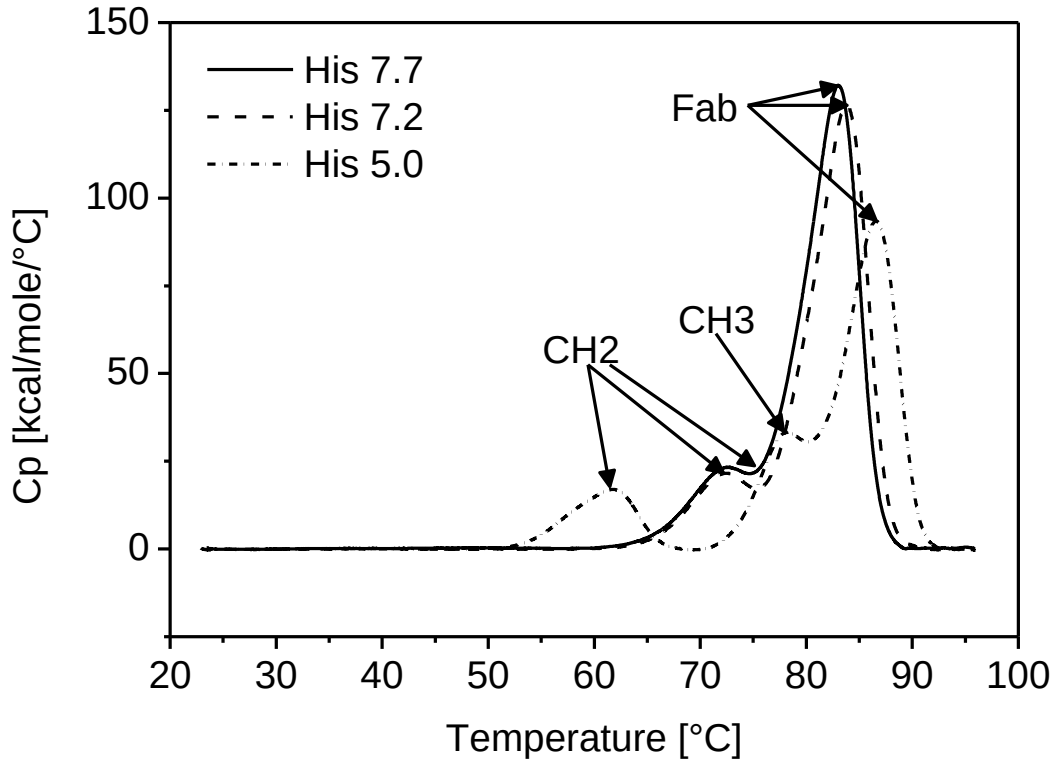

Figure 5-1. DSC melting curves of 4 mg/ml MAb in histidine buffer at pH 7.7, 7.2, and 5.0. With decreasing pH, the first transition ($T_{m1\,DSC}$) corresponding to the CH2 domain is shifted to lower temperatures and the second transition splits into $T_{m2\,DSC}$ (CH3) and $T_{m3\,DSC}$ (Fab). In contrast, the transition with the highest area resembling the Fab fragment is shifted to higher temperatures at lower pH value.

Independent of the addition of a surfactant, the transitions observed by DSF with DCVJ and DSC were in good agreement, as represented in Figure 5-2 A, with $T_{m\,DSF}$ consistently 4 °C lower than $T_{m\,DSC}$. The thermal shift of T_{m1} (ΔT_{m1}) of the different formulations related to the histidine pH 7.7 system is presented in Figure 5-3 A and B for DSF and DSC, respectively. The common trends of stabilizing and destabilizing effects of the varied formulation parameters were in good agreement. Both methods revealed a large negative ΔT_{m1} at low pH, also in presence of sodium chloride. Mannitol reduced the negative ΔT_{m1} and even resulted in a positive ΔT_{m1} in case of the mAb formulated in phosphate buffer at pH 7.2. Although $T_{m1\,DSF}$ values were 1 - 2 °C higher in the presence of a surfactant than in the surfactant-free formulation,

$T_{m1\ DSC}$ was lower in some samples, especially at pH 5.0. This discrepancy between both methods is also responsible for the outliers of the presented correlation in Figure 5-2 A.

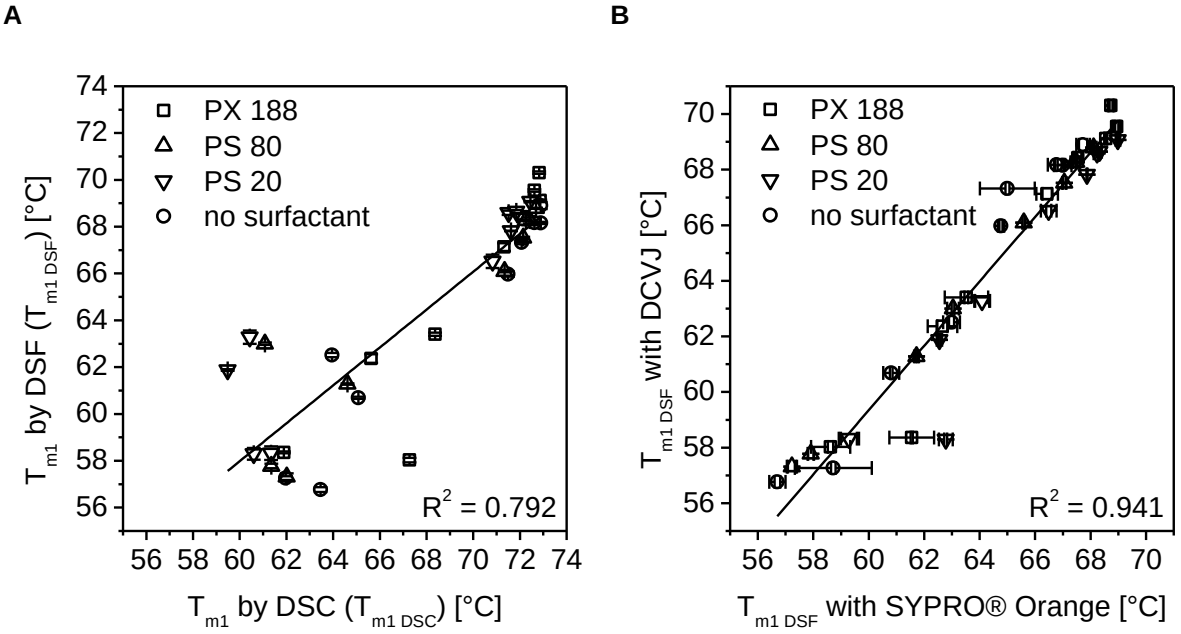

Figure 5-2. Linear correlation of $T_{m1\ DSF}$ with DCVJ of 40 mg/ml and $T_{m1\ DSC}$ of 4 mg/ml MAb in formulations with and without surfactant (A). Linear correlation of $T_{m1\ DSF}$ determined by DSF with SYPRO® Orange and with DCVJ of 40 mg/ml MAb of the surfactant-free formulations and in the presence of PX 188, PS 80, and PS 20 (B).

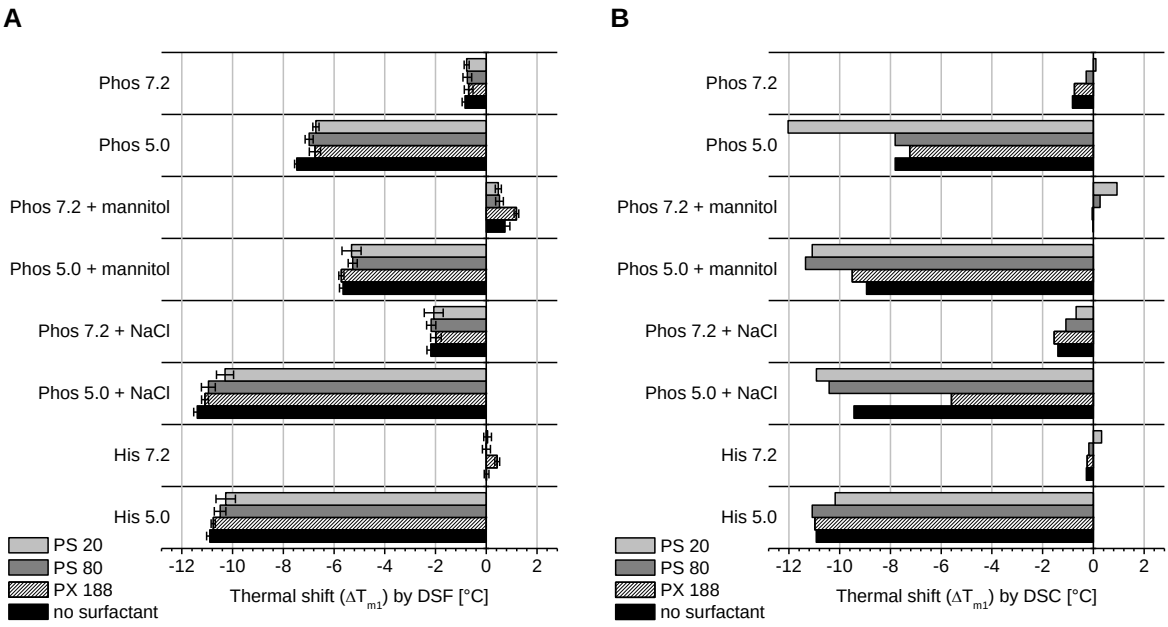

Figure 5-3. Thermal shift ΔT_{m1} of the different MAb formulations in relation to the histidine pH 7.7 formulation obtained by DSF with DCVJ (40 mg/ml) (A) and DSC (4 mg/ml) (B).

To estimate the error of the DSC values, the histidine pH 7.2 sample was injected four times, and the standard deviation was found to be 0.02 °C for both $T_{m1\ DSC}$ and $T_{m2\ DSC}$. This confirms the reported high reproducibility of DSC,[35] and justifies the validity of single measurements for the sake of time and material. The $T_{m\ DSF}$ values obtained with SYPRO® Orange and DCVJ were in excellent agreement, and a linear correlation of $T_{m1\ DSF}$ was found resembling all nine different formulations of 40 mg/ml MAb with and without surfactant (Figure 5-2 B).

Figure 5-4 exemplarily presents the fluorescence signal trace of the histidine samples at pH 7.2 analyzed with SYPRO® Orange (A - D) and DCVJ (E - H).

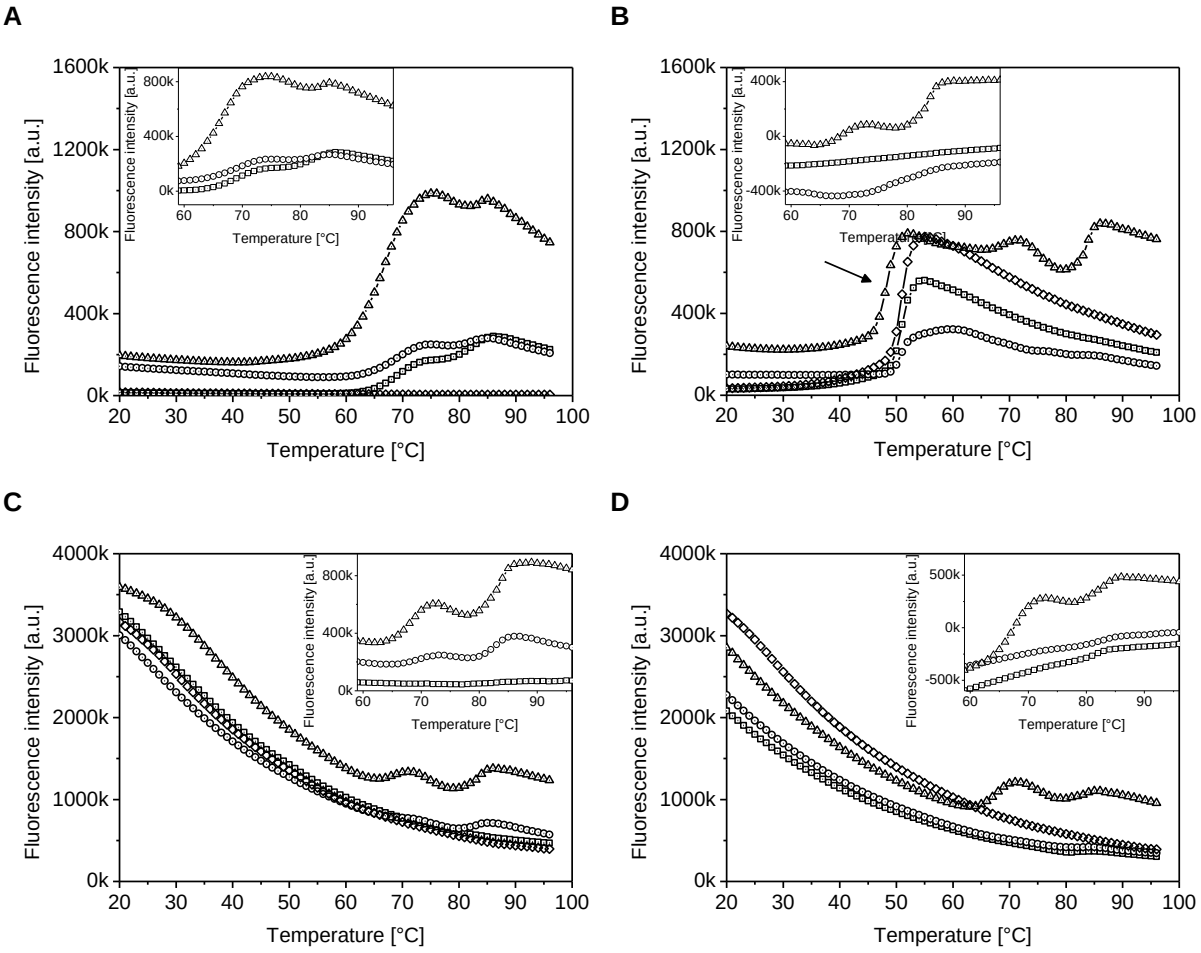

Figure 5-4. DSF melting curves of MAb in histidine pH 7.2 without surfactant (A) and with PX 188 (B), PS 80 (C), and PS 20 (D) obtained by SYPRO® Orange. The graphs show the raw data traces of the placebo sample (diamonds) and with 0.8 mg/ml (squares), 4 mg/ml (circles), and 40 mg/ml MAb (pyramids). The black arrow indicates the signal caused by the interaction of the dye with PX 188 at the critical micellization temperature. The small inserted graphs show the protein transition after background correction by subtraction of the placebo signal from the raw data.

Without a surfactant, the increase of the fluorescence intensity is more distinct with higher protein concentration. SYPRO® Orange resulted in a significant signal even at the lowest applied MAb concentration of 0.8 mg/ml (Figure 5-4 A), whereas 4 mg/ml MAb was necessary for DCVJ (Figure 5-4 E).

The presence of a surfactant resulted in an interfering background fluorescence signal. In case of PS 80 (Figure 5-4 C and G) and PS 20 (Figure 5-4 D and H), high initial background fluorescence was observed, which declined with increasing temperature. In case of PX 188, the background signal showed a sharp and intense fluorescence increase when the critical micellization temperature of the poloxamer was exceeded at about 50 °C (Figure 5-4 B and F, black arrow).

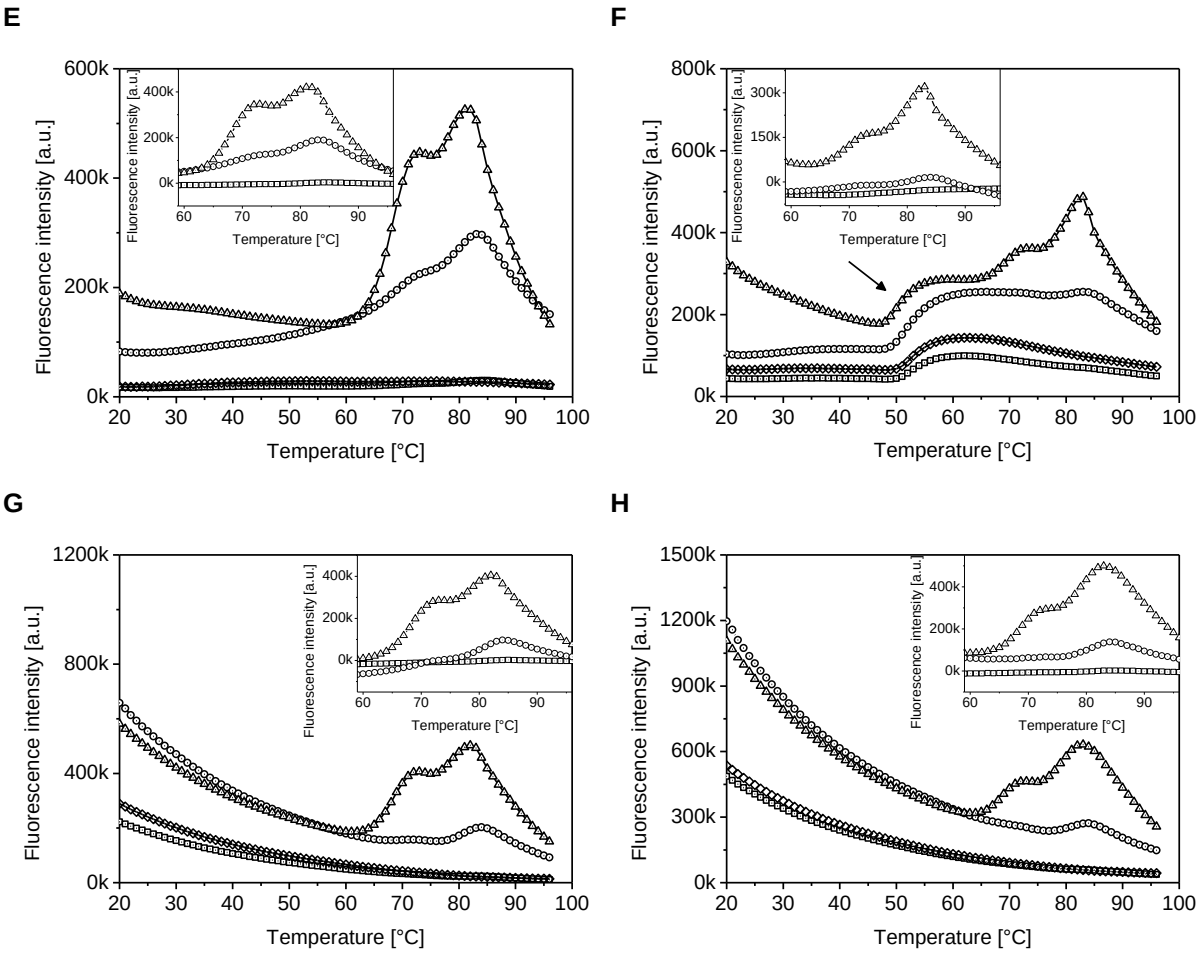

Figure 5-4 (continued). DSF melting curves of MAb in histidine pH 7.2 without surfactant (E) and with PX 188 (F), PS 80 (G), and PS 20 (H) obtained by DCVJ. The graphs show the raw data traces of the placebo sample (diamonds) and with 0.8 mg/ml (squares), 4 mg/ml (circles), and 40 mg/ml MAb (pyramids). The black arrow indicates the signal caused by the interaction of the dye with PX 188 at the critical micellization temperature. The small inserted graphs show the protein transition after background correction by subtraction of the placebo signal from the raw data.

The transformation of single surfactant molecules to micellar structures was further investigated by means of DSC and DLS. Figure 5-5 shows the results from a protein free solution of PX 188 in histidine buffer at pH 7.2.

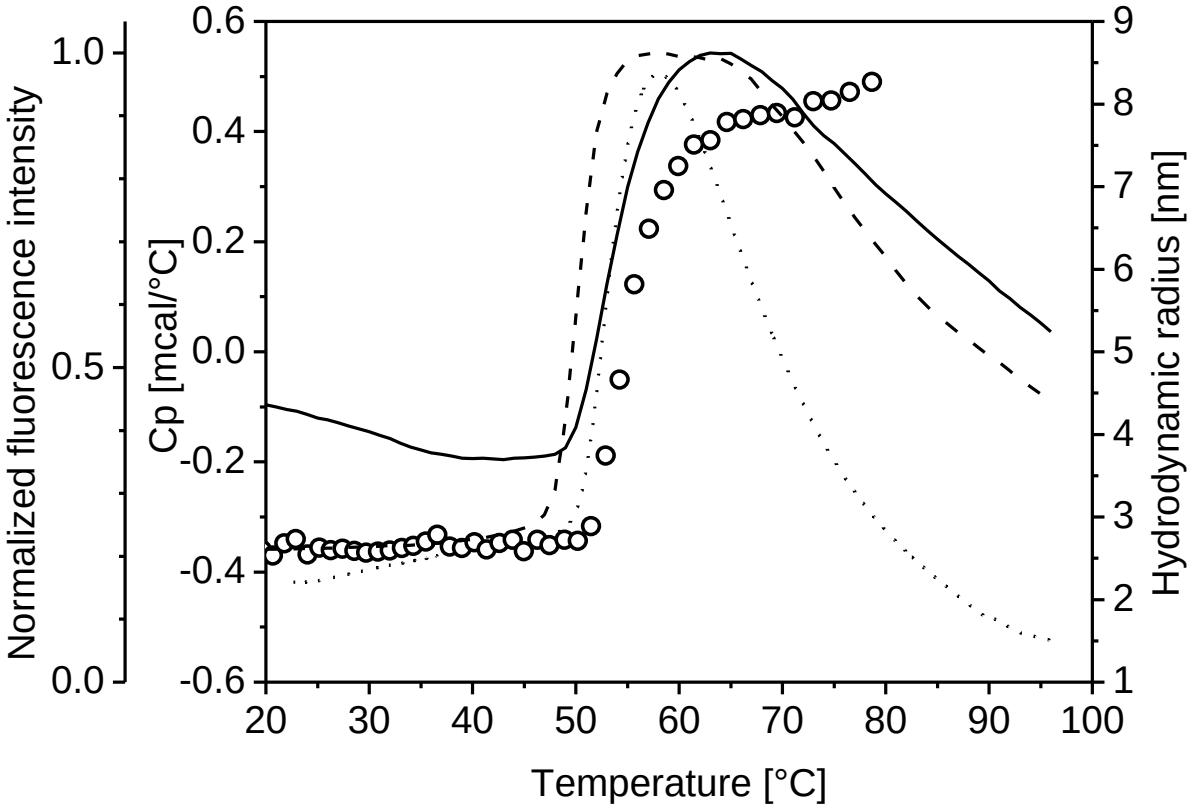

Figure 5-5. Micellization behavior of PX 188 in histidine pH 7.2 analyzed by DSF with DCVJ (solid line) and with SYPRO® Orange (dashed line), DSC (dotted line), and DLS (circles).

The fluorescence increase of DCVJ was sharper and occurred at slightly lower temperatures than that of SYPRO® Orange. The endothermic transition observed by DSC was in good agreement although the midpoint of the transition occurred at higher temperatures compared to DSF. In DLS, the association of single PX 188 molecules with an apparent hydrodynamic radius of about 2.4 nm to micellar structures of an apparent hydrodynamic radius of about 8 nm started at a slightly higher temperature (52 °C). With respect to nonequilibrium conditions, the temperatures at which the micellization process starts was in overall good accord between the different methods.

Background correction was performed by subtracting the fluorescence trace of a placebo sample from the signal of the protein containing formulation (inserted graphs in Figure 5-4), and the obtained $T_{m\,DSF}$ values are presented in Table 5-1.

Table 5-1. $T_{m\ DSF}$ of MAb (0.8 mg/ml, 4 mg/ml, and 40 mg/ml) in nine different formulations with and without surfactant analyzed by DSF with either SYPRO® Orange or DCVJ.

MAb conc.	40 mg/ml								4 mg/ml						0.8 mg/ml			
Fluoresc. dye	DCVJ				SYPRO® Orange				DCVJ				SYPRO® Orange		DCVJ		SYPRO® O.	
Formulation	no surfact.	PX 188	PS 80	PS 20	no surfact.	PX 188	PS 80	PS 20	no surfact.	PS 80	PS 20		no surfact.	PS 20	no surfact.		no surfact.	
	$T_{m1\ DSF}$ [°C]				$T_{m1\ DSF}$ [°C]				$T_{m1\ DSF}$ [°C]				$T_{m1\ DSF}$ [°C]		"		"	
His 7.7	68.2±0.1	69.1±0.1	68.3±0.1	68.6±0.1	67.0±0.3	68.6±0.1	67.4±0.1	68.2±0.1	68.9±0.1	69.3±0.2	72.2±1.1		68.5±0.5	69.5±0.1	69.6±0.4		69.3±0.2	
His 7.2	68.2±0.1	69.6±0.1	68.3±0.1	68.7±0.1	66.8±0.3	68.9±0.1	67.5±0.1	68.3±0.1	68.8±0.1	69.7±0.1	69.0±1.0		69.3±0.2	69.4±0.1	68.9±0.8		69.6±0.1	
His 5.0	57.3±0.1	58.4±0.1	57.8±0.1	58.3±0.3	58.7±1.4	61.6±0.8	57.9±0.1	59.3±0.4	56.2±0.1	57.0±0.2	56.1±0.3		59.2±0.3	58.6±0.2	56.2±0.1		60.1±0.2	
Phos 5.0 + NaCl	56.8±0.1	58.0±0.1	57.3±0.2	58.3±0.3	56.7±0.3	58.6±0.7	57.2±0.2	62.8±0.1	57.7±0.1	59.2±0.2	55.1±0.3		60.2±1.5	60.2±0.1			62.3±0.6	
Phos 7.2 + NaCl	66.0±0.1	67.1±0.2	66.1±0.1	66.5±0.3	64.8±0.1	66.4±0.4	65.6±0.1	66.5±0.1	66.1±0.2	67.0±0.1	66.1±0.2		68.9±0.5	67.3±1.1			67.7±0.2	
Phos 5.0 + mannitol	62.5±0.1	63.4±0.1	63.0±0.1	63.3±0.3	63.0±0.3	63.5±0.8	63.0±0.2	64.1±0.3	63.5±0.2	64.1±0.2	64.1±0.7		65.5±1.5	65.7±0.1			66.2±1.9	
Phos 7.2 + mannitol	68.9±0.2	70.3±0.1	68.8±0.1	69.1±0.1	67.7±0.3	68.7±0.1	68.1±0.1	69.0±0.1	68.3±1.1	69.4±0.3	70.5±1.0		69.6±0.9	69.5±0.8			69.6±0.2	
Phos 5.0	60.7±0.1	62.4±0.2	61.3±0.1	61.9±0.1	60.8±0.3	62.7±0.5	61.7±0.1	62.6±0.1	62.1±0.4	62.7±0.4	64.9±0.1		64.7±0.1	63.9±1.0	56.9±1.1		65.1±0.2	
Phos 7.2	67.3±0.1	68.4±0.1	67.5±0.1	67.8±0.1	65.0±1.0	67.5±0.2	67.1±0.1	67.9±0.1	68.0±0.7	68.6±0.1	68.7±0.3		68.3±0.3	68.9±0.5	61.5±0.4		68.3±0.1	
	$T_{m2\ DSF}$ [°C]				$T_{m2\ DSF}$ [°C]				$T_{m2\ DSF}$ [°C]				$T_{m2\ DSF}$ [°C]		"		"	
His 7.7	77.3±0.1	78.7±0.1	77.6±0.2	77.8±0.1		82.4±0.1	82.4±0.2	82.2±0.1	78.5±0.1	79.1±0.1	79.4±0.2		81.1±0.2	81.8±0.1	78.8±0.1		81.3±0.1	
His 7.2	78.4±0.2	80.2±0.1	78.8±0.1	79.2±0.1		83.5±0.1	82.5±0.4	83.3±0.1	79.7±0.1	80.7±0.1	80.8±0.2		81.9±0.1	82.6±0.1	80.6±0.4		82.1±0.1	
His 5.0	77.8±0.1	78.8±0.1	77.9±0.1	78.3±0.1				79.4±0.2	76.9±0.1	76.7±0.2	77.2±0.1		76.4±0.1	76.6±0.2	76.5±0.1		76.6±0.2	
Phos 5.0 + NaCl	77.3±0.1	79.4±0.1	77.3±0.2	76.3±0.1	66.9±1.2	84.7±1.3	84.6±0.2	84.5±0.6	79.3±0.1	79.5±0.6	80.0±0.4		85.6±0.2	85.8±0.1			80.2±0.1	
Phos 7.2 + NaCl	76.3±0.1	77.1±0.1	76.7±0.1	77.2±0.1		81.6±0.3	81.7±0.1	81.5±0.1	78.1±0.3	79.4±0.3	80.1±0.1		81.7±0.1	81.9±0.1			81.6±0.1	
Phos 5.0 + mannitol	81.4±0.1	82.0±0.1	81.5±0.1	81.7±0.1		87.1±0.2		87.3±0.1	83.3±0.1	83.4±0.1	84.5±0.2		82.3±0.1	81.6±2.0			81.9±0.3	
Phos 7.2 + mannitol	76.8±0.1	77.6±0.1	77.5±0.1	78.0±0.2	81.7±0.1	82.2±0.1	82.3±0.1	82.2±0.1	80.3±0.1	80.2±0.3	80.7±0.2		81.5±0.1	82.1±0.1			81.7±0.2	
Phos 5.0	80.3±0.1	81.2±0.1	80.4±0.1	80.7±0.1		86.0±0.1	86.0±0.1	86.8±0.1	82.0±0.2	82.1±0.2	83.9±0.2		72.0±1.5	81.5±0.9	81.4±0.1		82.0±0.3	
Phos 7.2	76.3±0.1	76.6±0.1	76.7±0.1	80.2±0.1	80.6±0.1	81.4±0.1	81.5±0.2	81.3±0.1	79.3±0.2	79.5±0.1	79.8±0.1		80.9±0.1	81.3±0.1	80.5±0.1		80.8±0.1	
	$T_{m3\ DSF}$ [°C]				$T_{m3\ DSF}$ [°C]				$T_{m3\ DSF}$ [°C]				$T_{m3\ DSF}$ [°C]		"		"	
His 5.0		85.5±0.1	85.2±0.2	84.6±0.4					83.6±0.4	84.4±0.1	84.4±0.1		85.3±0.1	85.3±0.1	83.5±0.3			
Phos 5.0 + NaCl			85.9±0.4	85.3±0.3					85.4±0.1	85.1±0.1	85.1±0.1						85.1±0.8	
Phos 5.0 + mannitol													86.9±0.3	87.5±0.5			87.4±1.3	
Phos 5.0													81.1±0.5	86.9±0.1	85.6±0.2		85.9±0.1	

no PX 188 | no PX 188, PS 80 | no PX 188, PS 80, PS 20 | no PX 188, PS 80, PS 20

Blank cell means data analysis revealed no $T_{m\ DSF}$ value. His, histidine buffer; Phos, phosphate buffer with and without additional sodium chloride or mannitol; PX, poloxamer; PS, polysorbate

After background correction, it was possible to determine $T_{m1\ DSF}$ precisely for all formulations with both dyes at 40 mg/ml MAb. As expected, the data analysis was hindered when the protein concentration was reduced, because the fluorescence intensity of the background conceals the lowered protein signal. Consequently for some formulations, the $T_{m\ DSF}$ values could not be determined (Table 5-1). Although it was possible with DCVJ to analyze $T_{m\ DSF}$ for both polysorbates at 4 mg/ml MAb, SYPRO® Orange allowed the determination only in presence of PS 20. The nonproteinous signal of PX 188 hampered the determination of $T_{m\ DSF}$ at lower protein concentrations, and no $T_{m\ DSF}$ values were obtained even after careful background correction. A further reduction of the protein concentration to 0.8 mg/ml completely concealed the protein transition in the presence of a surfactant. The appearance of $T_{m2\ DSF}$ was more distinct with DCVJ, especially at higher MAb concentrations. In contrast, $T_{m2\ DSF}$ could be clearly detected with SYPRO® Orange at low MAb concentration but diminished at 40 mg/ml. The change in fluorescence intensity resembling $T_{m3\ DSF}$ in case of MAb formulations at pH 5.0 was very weak, thus difficult to analyze and only precisely detectable in a few cases (Table 5-1).

The influence of background correction on $T_{m1\ DSF}$ and $T_{m,onset}$ was investigated and the difference between the values obtained from raw data and after placebo subtraction is presented in Table 5-2 for 40 mg/ml MAb. Whereas background correction of the surfactant free samples did not result in marked changes, the pronounced background fluorescence signal in case of formulations containing surfactant was expected to render a shift. Although $T_{m1\ DSF}$ values obtained from Boltzmann fitting shifted between 0.1 and 0.5 °C, the values resulting from analysis of the first derivative showed the smallest difference ranging from 0 to 0.3 °C. The onset of $T_{m\ DSF}$ was calculated based on the Boltzmann function fitted to the fluorescence traces. As the calculated value $T_{m,onset}$ depends on the slope factor of the transition, it is more susceptible to the curve change caused by the mathematical process of background subtraction compared to the inflection point of the curve itself.

Table 5-2. Difference in $T_{m1\ DSF}$ values before and after background correction (40 mg/ml MAb with DCVJ).

	$T_{m1\ DSF}$ [°C] first derivative analysis				$T_{m1\ DSF}$ [°C] Boltzmann fit				$T_{m,onset}$ [°C] Onset temperature			
40 mg/ml with DCVJ	no surf	PX 188	PS 80	PS 20	no surf	PX 188	PS 80	PS 20	no surf	PX 188	PS 80	PS 20
His 7.7	0	0.3	0	0.3	0.1	-0.1	0.2	0.1	0	1.0	1.7	1.1
His 7.2	-0.1	-0.3	0	0	0	-0.3	0.2	0.1	-0.1	0.5	2.1	1.7
His 5.0	0	n.a.	-0.1	0	0	n.a.	0.2	0.2	-0.3	n.a.	1.9	2.3
Phos 5.0 + NaCl	0	n.a.	0	0.2	-0.1	n.a.	0.1	0.3	-0.2	n.a.	1.4	2.4
Phos 7.2 + NaCl	0	-0.2	0.1	0.2	0	0.1	0.1	0.4	-0.3	0.9	1.5	2.3
Phos 5.0 + mannitol	0	n.a.	0.1	0.3	0	n.a.	0.2	0.3	-0.3	n.a.	1.4	3.1
Phos 7.2 + mannitol	0.1	-0.8	0	-0.1	-0.2	-0.7	0.1	0.2	0.1	2.5	1.8	3.2
Phos 5	0	n.a.	0	-0.2	-0.1	n.a.	0.1	0.5	-0.4	n.a.	1.3	4.6
Phos 7.2	0	-0.4	0	0.1	0	-0.2	0.1	0.2	-0.3	0.6	0.9	2.3

A positive result indicates that $T_{m1\ DSF}$ was shifted to lower temperature placebo subtraction. Because no $T_{m1\ DSF}$ could be obtained without background correction for the samples with PX 188 at pH 5.0, a comparison is not available (n.a.) in this case. His, histidine buffer; Phos, phosphate buffer with and without additional sodium chloride or mannitol; PX, poloxamer; PS, polysorbate; Surf, surfactant.

As presented in Table 5-2, $T_{m,onset}$ was shifted substantially up to 4.6 °C indicating a significant overestimation without background correction. This effect is illustrated in Figure 5-6, which exemplarily compares the original melting trace of 40 mg/ml MAb in histidine at pH 7.2 with DCVJ in the presence of PS 80 with the resulting trace after background correction. Although $T_{m,onset}$ is significantly reduced by 2 °C from 61.9 °C to 59.9 °C after background subtraction, the inflection point of the Boltzmann fit shifts insignificantly from 68.2 °C to 68.0 °C. The analysis of the first derivative is even less affected by the background correction procedure delivering a $T_{m1\ DSF}$ of 68.4 °C before and after subtraction of the placebo trace.

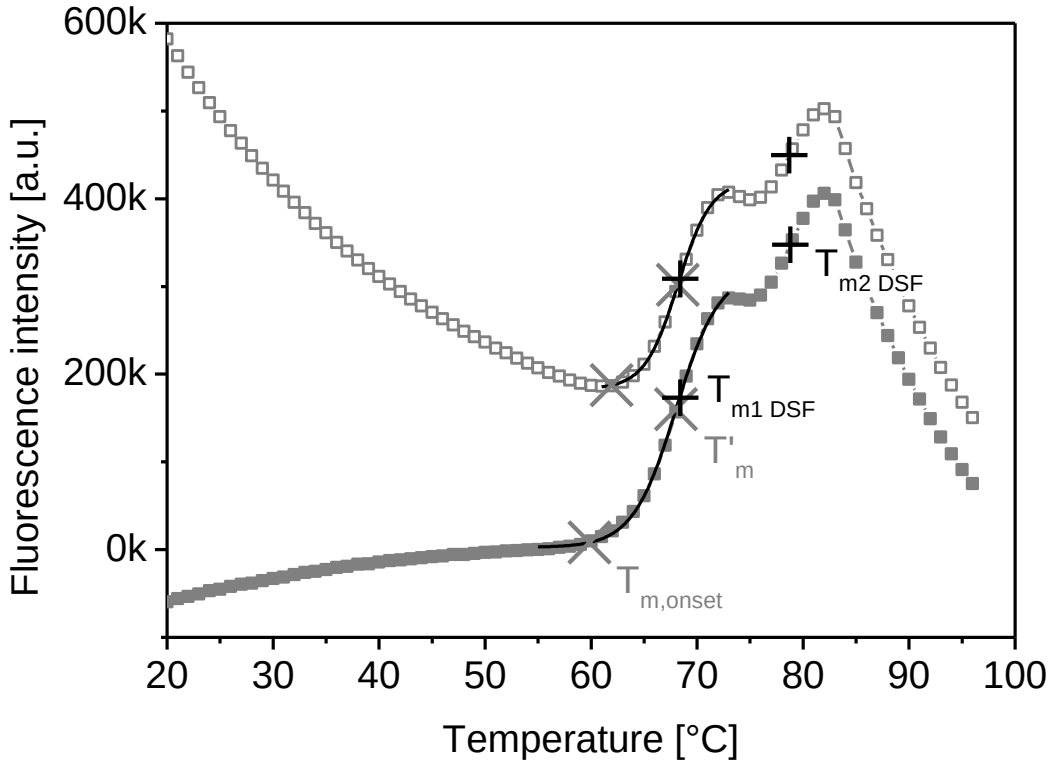

Figure 5-6. Illustration of the T_m values of 40 mg/ml MAb in histidine buffer pH 7.2 in the presence of PS 80. Open and closed squares resemble the raw data and background corrected melting trace, respectively. $T_{m1\ DSF}$ and $T_{m2\ DSF}$ values determined as the maxima of the first derivative are marked with a black "+". The black line displays the result of the Boltzmann fit to the first transition. A grey "x" marks the inflection point (T'_m) of the sigmoidal function, while $T_{m,onset}$ is calculated based on the parameters of the fit. $T_{m1\ DSF}$ and T'_m are usually in good agreement. Although the process of background correction had a minor influence $T_{m1\ DSF}$, $T_{m,onset}$ was significantly lower because the slope is affected because of the subtraction of the signal caused by the surfactant.

5.5 Discussion

5.5.1 DSF in presence of surfactant

In this study, T_m values of a mAb in three concentrations between 0.8 and 40 mg/ml were determined in nine different formulations with and without PS 20, PS 80, and PX 188 both by DSF and DSC. At the higher pH values tested (pH 7.2 and 7.7), the mAb typically showed two distinct transitions; whereas at pH 5.0, a third transition occurred at rather high temperatures. In case of mAbs the Fab fragment, the CH2 and the CH3 domain of the Fc fragment unfolded individually resulting in particular endothermic melting transitions in DSC. The order in which these segments unfold is determined by their independent stability. Ionescu et al. and Garber et al. used the

melting enthalpy to identify the fragments and propose that the Fab fragment is responsible for the largest peak.[32,33] The CH2 domain, especially in the aglycosylated form, is strongly destabilized at low pH (chapter 4.3.3).[34] Although the CH3 domain and the Fab fragment are likely to unfold simultaneously at higher pH values (7.2, 7.7), three distinct transitions at lower temperatures result at pH 5.0. The transitions could be clearly detected in DSC experiments, whereas the appearance of a second or third transition was not consistent in DSF because the increase in fluorescence intensity was frequently rather small and thus difficult to resolve. Multiple transitions of a mAb with DSF were also reported by Li et al. and He et al., but they focused only on the first transition, which resembles the domain with the lowest thermal stability.[23,24] Goldberg et al. also reported two clearly separated transitions in DSC and DSF for one mAb, and for a second mAb, they found up to three transitions, depending on pH similar to our results.[22] Because of the linear correlation of T_{m1} between DSC and DSF as presented in Figure 5-2 A, $T_{m1\ DSF}$ is most likely caused by unfolding of CH2. Experiments with isolated Fab and Fc fragments are necessary to ultimately assign a certain MAb segment to $T_{m2\ DSF}$ and $T_{m3\ DSF}$ (chapter 4.3.2).

As a common trend found by both methods, T_{m1} of the mAb at a pH of 5.0 was lower than that at pH 7.2 and 7.7 denoting a protein destabilization presumably due to a reduction of stabilizing attractive intramolecular electrostatic interactions. The addition of mannitol resulted in a slight increase of the T_{m1} value corresponding to the stabilizing effect of the sugar alcohol presumably by preferential exclusion. The addition of sodium chloride increased the ionic strength of the solution and led to a reduced T_{m1}, destabilizing the mAb, which is likely due to shielding of stabilizing attractive electrostatic interactions. Low pH and high salt concentrations also turned out to be unfavorable for mAb stability in a study by He et al.[24] Goldberg demonstrated a concentration dependent stabilization by trehalose, whereas a destabilization by sodium chloride was observed.[22] The effects of sodium chloride and mannitol on T_{m2} were less pronounced. Interestingly, the effect of pH was inversed with respect to $T_{m2\ DSF}$, resulting in higher values at pH 5.0.

Excipients interacting with the protein influence T_m by either stabilizing the native or the unfolded state. Surfactants occupy interfaces preventing protein aggregation at these very interfaces and only marginally influence the conformational stability of the protein molecules.[36] The results from DSF suggest that the presence of a surfactant

potentially stabilized the mAb as can be seen by the increase in $T_{m1\ DSF}$ by approx. 1 - 2 °C (Figure 5-3 A). In contrast, with DSC (Figure 5-3 B), surfactant containing samples showed slightly lower $T_{m1\ DSC}$ values, predominately at pH 5.0. Similar results were reported by Bam et al. studying the effect of polysorbates on the stability of recombinant human growth hormone.[36] They also found a reduced T_m by DSC suggesting binding of polysorbate to hydrophobic patches, wheras FTIR and CD analysis revealed no change in secondary structure.[36] DSC reveals all thermal events during unfolding of the secondary and tertiary structure, wheras DSF is sensitive only to changes of hydrophobic exposure or the microenvironment at the surface (chapter 4.3.6). The transitions determined by DSF are in good agreement with DSC data and as presented in Figure 5-2 A, a linear correlation exists, although $T_{m1\ DSC}$ is typically slightly higher than the $T_{m1\ DSF}$ (compare chapter 4.3.5), which was also found by He et al.,[20] Goldberg et al.,[22] and King et al.[26] The absolute T_m values depend on the heating rate in DSF and DSC because unfolding is not at equilibrium. Therefore, the analyzed T_m should be treated as apparent values. Although the heating rate was 1 °C/min in DSF and DSC, the heat transfer into the different sample volumes is likely to be different. The systematic difference between $T_{m\ DSC}$ and $T_{m\ DSF}$ may also be due to preferred binding of the dye to the unfolded protein. In a simple two-state model, the unfolded state is consequently preferred, the native state destabilized and the apparent T_m shifted to lower temperatures by the dyes. Assuming a competitive binding of the nonionic surfactant with the dye for hydrophobic patches at the surface of the unfolded protein, the slight apparent increase of $T_{m1\ DSF}$ observed in presence of a surfactant can be explained. However, in HTS a threshold, e.g., set to a thermal shift > 1 °C[21] suggesting stabilizing or destabilizing conditions should be carefully evaluated to avoid misinterpretations when comparing surfactant containing and free formulations.

The precise determination of the apparent T_m via DSF is based upon a significant increase of the fluorescence intensity while the protein unfolds. Beside factors of the protein itself, e.g., hydrophobic nature and folding, the method also depends on experimental factors like concentrations (protein, dye, and excipients), sensitivity of the dye, instrumental features, and others. Based on the assumption that the recorded fluorescence intensity resembles the sum of the dye's fluorescence caused by interaction with the protein and the surfactant or other excipients, a discrimination of the protein related signal and the unwanted background signal should always be

possible. In practice, no linear dependence was found and the background fluorescence conceals the protein transition at lower protein concentrations. Background correction by subtraction of placebo samples is essential to enable a precise analysis of the melting transition of the protein. By this means, it was possible to determine $T_{m\,DSF}$ of lower concentrated MAb solutions (4 mg/ml), even with the polarity-sensitive dye SYPRO® Orange in presence of a surfactant. The molecular rotor DCVJ rendered melting curves of superior quality and also enabled $T_{m\,DSF}$ determination in case of PS 80, where SYPRO® Orange failed. The characteristics of DCVJ and its correlation with SYPRO® Orange, background signals of the surfactants, the process of background correction, and further T_m analysis will be discussed in the sections below.

5.5.2 Comparison of the fluorescent dyes SYPRO® Orange and DCVJ

DSF is based on the environmental sensitive property of a fluorescent dye. Typically polarity sensitive dyes are used, which are quenched in aqueous polar media and show low fluorescence intensity. Upon protein thermal unfolding, hydrophobic residues typically resting within the core of the native protein get exposed to the solvent. SYPRO® Orange and other polarity sensitive dyes bind to hydrophobic patches and the fluorescence intensity increases. The transition from low intensity of the native, folded protein and the high intensity after unfolding is analyzed to determine the temperature at which 50 % of the protein is in its unfolded state. The highest fluorescence intensity does not necessarily indicate the state at which the protein is completely unfolded. The hydrophobic patches, which are responsible for the interaction with SYPRO® Orange, also favor protein aggregation and may be capped by intermolecular interactions.[17] Additionally, multiple domains and binding sites per protein molecule with different dye affinity and also the depletion of unbound dye at high protein concentration might add to the effect that the transition observed in DSF occurs at lower temperature compared to the $T_{m\,DSC}$ (Figure 5-2). To distinguish DSF from calorimetric methods, other authors suggest a different nomenclature, such as “apparent melting (point) temperature”[23] or “temperature of hydrophobic exposure”.[24,25] The different affinity of the presented dyes even complicates the interpretation of the thermal events and consequently in simple analogy the term “$T_{m\,DSF}$” was chosen. Free rotation of the dicyanovinyl moiety of DCVJ allows TICT and the molecule leaves the excited state predominately by

radiationless deactivation.[29] Instead, fluorescence is favored when intramolecular rotation is limited, e.g., in highly viscous media or the rigid microenvironment of unfolded or aggregated protein.[30] Hawe and coworker used DCVJ and the related CCVJ to detect heat induced aggregates in IgG formulations. They found molecular rotor dyes superior in comparison to polarity-sensitive dyes like ANS, Bis-ANS, and Nile Red especially in formulations containing polysorbate.[31] In surfactant-free environments, DCVJ was successfully used for DSF by Li et al. recently.[23] They claimed a good correlation between the T_m values determined with both dyes, but no data was presented.[23] The results of this study also support the reported linear correlation, even in presence of surfactants (Figure 5-2 B). This suggests that both dyes show a similar sensitivity to structural changes upon thermal unfolding of the mAb. As presented in Figure 5-4 and described by other authors for SYPRO® Orange, the fluorescence intensity of both dyes typically drops after the final transition of the unfolded protein. This decrease was, on the one hand, supposed to be due to protein aggregation by hydrophobic protein-protein interactions reducing the hydrophobic surface available for dye binding[17,22] and, on the other hand, assumed to be caused by common temperature quenching which was shown by He et al. for SYPRO® Orange in a hydrophobic environment (Isopropanol and chemically unfolded protein by guanidine hydrochloride).[24] Yet et al. additionally attributed a second exponential decay to the disassociation of the dye from the micelles with increasing temperature.[16] In case of DCVJ, higher temperatures lead to an accelerated TICT and lower viscosity of the solution, which both favor nonradiative solvent relaxation. Aside from temperature, excipients, pH, protein concentration, aggregation, and other protein-protein interactions strongly influence the viscosity of the solution.[25,37,38] In preceding experiments, it was shown for this mAb via turbidity measurements that strong aggregation of the protein occurred exactly at $T_{m2\ DSF}$.[39] Protein aggregation might therefore explain the different sensitivities of both dyes towards $T_{m2\ DSF}$. Although the fluorescence intensity is decreased in case of SYPRO® Orange by depletion from the hydrophobic patches that are prone to aggregate, a resulting change in microviscosity by aggregation might be responsible for the clear $T_{m2\ DSF}$ with DCVJ. Further investigation on the mechanism of interaction between the fluorescent dye, the protein, and the solution especially with respect to viscosity at elevated temperatures is necessary but is beyond the aim of this article. In addition, weaker fluorescence intensities of DCVJ compared to SYPRO® Orange

in the same samples were detected, which Li and coworkers related to the suboptimal excitation and emission filters for DCVJ used by the RT-PCR machine.[23] RT-PCR optics is usually optimized for intercalating dyes to track the amplification of nucleotides. Excitation and emission filters are conveniently limited to a certain set of wavelength. In this study, a RT 7300 RT-PCR equipped with the standard excitation and emission filters was used. Excitation wavelength is fixed to about 490 nm and four emission wavelengths are available, of which the lowest of 530 nm was chosen for the detection of DCVJ and 578 nm were selected for SYPRO® Orange because of the strongest signal. Whereas the emission maximum of SYPRO® Orange fits well, higher fluorescence intensity could be achieved with more appropriate filter sets for DCVJ. The resulting higher sensitivity would enable a further reduction of the necessary protein concentration. Furthermore, other dyes like the related CCVJ can be applied with customized filters as recently presented by Ablinger et al. with G-CSF in presence of surfactants.[40] But such a hardware change requires careful evaluation.

5.5.3 The surfactant background signal

SYPRO® Orange is known to show a bright fluorescence in presence of micelles,[41] which results in a high initial fluorescence intensity. This problem was already reported in literature, especially in the field of membrane protein science.[16,42-44] To overcome this problem, Kean and coworker carefully titrated the free surfactant concentration to a level with a sufficient signal-to-noise ratio, at which the determination of melting event was possible.[43] After this, Senisterra et al. demonstrated that DSLS is a suitable alternative to DSF with respect to the applicability of high throughput thermal stability screenings in the presence of surfactants or notably hydrophobic proteins, such as membrane proteins, because no fluorescent probe is needed.[42] Mezzasalma and coworker name surfactants (including polysorbate) as a parameter of their protein stability profiling, a ThermoFluor® assay with customized instrumentation based on ANS, but did not present any surfactant-related data.[45] As exemplarily presented in Figure 5-4, pure buffer systems exhibit marginal fluorescence, whereas surfactants and potentially other components lead to a significant background signal as a function of the temperature. Calculating the apparent T_m based on the original data without subtraction of the background would lead to false results. By using background correction, the unique trace of the fluorescent dye response to only protein unfolding

is obtained, which is the key for the accurate determination of apparent T_m by DSF. By comparing the four placebo formulations, a different behavior of the surfactants can be derived. PX 188 shows a sharp and intense fluorescence increase with the inflection at about 48 - 50 °C. DSC measurement of the PX 188 containing placebo confirms an endothermic transition at similar temperatures (Figure 5-5). The CMC of PX 188 and other Poly(ethylene oxide)-poly(propylene oxide)-poly(ethylene oxide) block polymers depends strongly on the temperature. The CMC as a function of polymer concentration and temperature decreases with increasing temperature.[46] By means of light-scattering, Zhou and Chu investigated the transition from the unimer to the formation of micelles and found micellar structures above about 50 °C for 1.25 % PX 188.[47] The additional DLS measurements show an increase of the apparent hydrodynamic radius from 2.4 nm to about 8 nm starting at approx. 52 °C, as presented in Figure 5-5 for the histidine system at pH 7.2, reflecting the transition from single polymer coils to micelles. Hydrodynamic radii as well as the critical micellization temperature (CMT) are in excellent agreement with the results found by Zhou and Chu[47] and the theoretical CMT of an aqueous solution of 0.84 % PX 188, which can be calculated as 50.49 °C based on the empirical correlation presented by Alexandridis et al.[48] This temperature induced micelle formation can be explained by enhanced dehydration of PX 188 with increasing temperature, which results in an increasing aggregation number.[47] This process can be clearly traced with DSF with both fluorescent dyes. Poloxamers were already investigated by means of a fluorescent environmental probe (DPH) by Alexandridis et al. in a common cuvette spectrofluorimeter but not in HTS using RT-PCR machines.[49]

Both PS 20 and PS 80 show similar background traces. Starting at very high initial fluorescence intensity, the value decreases with increasing temperature. This holds true for both dyes although the decline by temperature dependent quenching is much more pronounced with SYPRO® Orange. Surfactant concentrations of the PS 20 and PS 80 were chosen to be approx. 25 times above the corresponding CMC at room temperature.[50] It is reported that the CMC is decreased in buffered solutions due to the ionic strength of the salts,[51] also for nonionic surfactants.[52] Because of the binding of surfactant molecules to the protein surface, the CMC can also be increased, although hydrophobic interactions of nonionic surfactants are likely to be weak compared to the electrostatic interactions of charged detergents like SDS.[53,54] Surfactant concentrations were chosen in the range of marketed products. Referring

to literature, concentrations of PS 20 and PS 80 in biopharmaceutical products are usually between 0.0003 - 0.3 % (w/v).[27] PX 188 is stated to be preferably used in amounts of 0.001 – 1 % (w/v).[55]

5.5.4 Background correction and T_m analysis

The Boltzmann function was reported by many authors to be an adequate tool to determine the apparent T_m from the melting curves obtained by DSF.[13,15,17,18] The Boltzmann function describes a two stage one-step reaction (folded ↔ unfolded). The equation is valid only for reversible reactions. The results reported in literature demonstrate that it is applicable in most cases, although protein unfolding is typically an irreversible or multistep reaction. Other authors used more complex models to describe the underlying thermodynamic processes, and thus, by fitting the data to these equations, additional information on the enthalpy of unfolding or binding constants can be derived in addition to the melting temperature.[9,12,19,45,56] Other groups determine the apparent T_m by analysis of the first[14,16,24,25,57] or second[22,23] derivative of the obtained melting curves. Describing the slope of the melting curves, the peak centers of the first derivative reflect the steepest ascensions of the raw melting curve. Preceding experiments showed that the first derivative is typically in very good agreement with the inflection point of the fitted Boltzmann function. In case of the surfactant containing solutions, it also turned out that the first derivative method is more robust. Especially in situations wherein the data resulted in a poor fit because of small transitions, analysis of the first derivative resulted in closer and more reproducible results. Data analysis is a major aspect of successful DSF experiments with common RT-PCR machines, because further processing of the fluorescence intensity readings has to be performed by the user. A user-friendly solution would push the application of DSF. Just recently, Wang and coworker proposed a Java-based application to simplify data analysis of DSF experiments.[58] Niesen also provided a free Microsoft Excel® template to facilitate T_m analysis for a set of RT-PCR machines.[59] The advantage of using scientific graphing and analysis software like Origin® in combination with scripting languages (LabTalk) is the control of every single parameter and the analysis can be adapted to the experimental needs like subtraction of background data, nonlinear fitting, or triplicate handling. Particularly, the feature to automatically process placebo samples and subtract the fluorescence from the corresponding protein signals is a key feature to analyze $T_{m\ DSF}$

in the presence of a surfactant in high-throughput fashion. However, a reasonable effort has to be taken initially to implement such an algorithm (see Appendix for the OpenTM LabTalk script).

Using a different algorithm based on the area of a Gaussian fit, King et al. calculated the onset temperature at which 1 % of the protein is unfolded ($T_{1\%}$).[26] The authors found that $T_{1\%}$ is a more powerful predictor for protein stability than the common midpoint values. Additionally, $T_{1\%}$ as low as body temperature was found, meaning that a small amount of the protein is likely to be unfolded *in vivo* while T_m was well in an acceptable range. Thus, $T_{m,onset}$ should be monitored on a routine basis in addition to T_m. The presented empiric equation to calculate the onset temperature is based on the fitted parameters of the Boltzmann equation (T'_m, dT, A_L, and A_U) (chapter 3.3.2). Depending on the slope factor of the transition, $T_{m,onset}$ is affected by the process of background correction as exemplarily illustrated in Figure 5-6. Although the analysis of the first derivative is less affected by the background correction procedure, in case of excipients with significant influence on the fluorescence intensity, the T_m of the protein might be overestimated. Although $T_{m1\ DSF}$ did not change markedly, $T_{m,onset}$ might be shifted significantly making careful background correction particularly important.

5.6 Summary and outlook

Surfactants are challenging in DSF because the fluorescent dye can interact with micellar structures, and the resulting background fluorescence disturbs the analysis of the unfolding protein. With careful background correction by subtraction of the background fluorescence of placebo formulations from the protein melting curves, the apparent T_m of the protein can be analyzed even in the presence of PS 20, PS 80, and PX 188. The obtained $T_{m\ DSF}$ values were in good agreement with DSC measurements, and a linear correlation for T_{m1} with and without surfactant was presented. Thermal shifts of T_{m1} due to formulation parameters followed common trends with destabilization of the mAb at low pH with and without sodium chloride, whereas mannitol was found to be slightly stabilizing. $T_{m\ DSF}$ analysis in the presence of PX 188 was notably difficult, because the temperature dependent micellization of PX 188 resulted in a misleading and disturbing signal in DSF, which was confirmed by additional DSC and DLS measurements. DCVJ enabled the determination of

$T_{m\,DSF}$ in the presence of surfactants in many cases where SYPRO® Orange failed and showed superior melting curves in higher protein concentrations. Its fluorescence as a molecular rotor is predominantly depending on the viscosity and spatial restriction, whereas the commonly used SYPRO® Orange and other polarity sensitive dyes show fluorescence in nonpolar environment also present in micelles. This benefit is limited by a lower sensitivity of DCVJ than that of SYPRO® Orange regarding the protein concentration.

5.7 Conclusion

We recommend using DCVJ for $T_{m\,DSF}$ analysis if surfactants are present and the protein concentration is high enough to achieve an adequate fluorescence signal. This protein concentration also depends on the used RT-PCR machine. SYPRO® Orange is necessary for low protein concentrations in the absence of surfactants and possibly at a lower surfactant content. The occurring background fluorescence should be corrected by subtraction of a placebo sample in all cases with both dyes. Background correction had minor influence on the inflection point but enabled the determination of correct $T_{m\,onset}$ values. Furthermore, the empiric equation for $T_{m\,onset}$ calculation based on the common Boltzmann fit is beneficial for automatized data analysis enabling an easy routine analysis of $T_{m\,onset}$. The high-throughput fashion of DSF with low consumption of time and material is now adaptable to a more flexible and comprehensive screening including surfactants that are typically used as stabilizing agents. Therefore, this method may find its application during the development of therapeutic biologics in either surfactant containing formulations or inherently hydrophobic proteins.

5.8 Acknowledgements

We gratefully thank Prof. Angelika Vollmar for the opportunity to use the RT-PCR machine and Wyatt Technologies (Dernbach, Germany) for temporally providing the DynaPro plate reader and software for the DLS measurements.

5.9 References

1. Beck A, Wurch T, Bailly C, Corvaia N 2010. Strategies and challenges for the next generation of therapeutic antibodies. Nat Rev Immunol 10(5):345-352.

2. Mahler H-C, Friess W, Grauschopf U, Kiese S 2009. Protein aggregation: Pathways, induction factors and analysis. J Pharm Sci 98(9):2909-2934.

3. Filipe V, Hawe A, Schellekens H, Jiskoot W. 2010. Aggregation and immunogenicity of therapeutic proteins. In Wang W, Roberts CJ, editors. Aggregation of Therapeutic Proteins, ed., New York: John Wiley & Sons, Inc. p 403-433.

4. Pace CN, Shirley BA, Thomson JA. 1989. Measuring the Conformational Stability of a Protein. In Creighton TE, editor Protein Structure: A Practical Approach, ed., Oxford: RL Press at Oxford University Press. p 311-330.

5. Pelton JT, McLean LR 2000. Spectroscopic Methods for Analysis of Protein Secondary Structure. Anal Biochem 277(2):167-176.

6. Youssef Mohamed AMK. 2010. PhD Thesis. Systematic Studies to Correlate Microcalorimetry with Stability Studies on Liquid Formulations of Various Protein Drugs. Munich, Germany: LMU München, Fakultät für Chemie und Pharmazie

7. Brandts JF, Lin LN 1990. Study of strong to ultratight protein interactions using differential scanning calorimetry. Biochemistry (Mosc) 29(29):6927-6940.

8. Plotnikov V, Rochalski A, Brandts M, Brandts JF, Williston S, Frasca V, Lin L-N 2002. An Autosampling Differential Scanning Calorimeter Instrument for Studying Molecular Interactions. Assay Drug Dev Technol 1(1):83-90.

9. Pantoliano MW, Petrella EC, Kwasnoski JD, Lobanov VS, Myslik J, Graf E, Carver T, Asel E, Springer BA, Lane P, Salemme FR 2001. High-Density Miniaturized Thermal Shift Assays as a General Strategy for Drug Discovery. J Biomol Screen 6(6):429-440.

10. Leung S-M, Senisterra G, Ritchie KP, Sadis SE, Lepock JR, Hightower LE 1996. Thermal activation of the bovine Hsc70 molecular chaperone at physiological temperatures: physical evidence of a molecular thermometer. Cell Stress Chaperones 1(1):78-89.

11. Poklar N, Lah J, Salobir M, Maček P, Vesnaver G 1997. pH and Temperature-Induced Molten Globule-Like Denatured States of Equinatoxin II: A Study by UV-Melting, DSC, Far- and Near-UV CD Spectroscopy, and ANS Fluorescence†. Biochemistry (Mosc) 36(47):14345-14352.

12. Lo M-C, Aulabaugh A, Jin G, Cowling R, Bard J, Malamas M, Ellestad G 2004. Evaluation of fluorescence-based thermal shift assays for hit identification in drug discovery. Anal Biochem 332(1):153-159.

13. Vedadi M, Niesen FH, Allali-Hassani A, Fedorov OY, Finerty PJ, Wasney GA, Yeung R, Arrowsmith C, Ball LJ, Berglund H, Hui R, Marsden BD, Nordlund P, Sundstrom M, Weigelt J, Edwards AM 2006. Chemical screening methods to identify ligands that promote protein stability, protein crystallization, and structure determination. Proceedings of the National Academy of Sciences 103(43):15835-15840.

14. Crowther GJ, Napuli AJ, Thomas AP, Chung DJ, Kovzun KV, Leibly DJ, Castaneda LJ, Bhandari J, Damman CJ, Hui R, Hol WGJ, Buckner FS, Verlinde CLMJ, Zhang Z, Fan E, van Voorhis WC 2009. Buffer Optimization of Thermal Melt Assays of Plasmodium Proteins for Detection of Small-Molecule Ligands. J Biomol Screen 14(6):700-707.

15. Ericsson UB, Hallberg BM, DeTitta GT, Dekker N, Nordlund P 2006. Thermofluor-based high-throughput stability optimization of proteins for structural studies. Anal Biochem 357(2):289-298.

16. Yeh AP, McMillan A, Stowell MHB 2006. Rapid and simple protein-stability screens: application to membrane proteins. Acta Crystallographica Section D 62(4):451-457.

17. Niesen FH, Berglund H, Vedadi M 2007. The use of differential scanning fluorimetry to detect ligand interactions that promote protein stability. Nat Protocols 2(9):2212-2221.

18. Sorrell FJ, Greenwood GK, Birchall K, Beining C 2010. Development of a differential scanning fluorimetry based high throughput screening assay for the discovery of affinity binders against an anthrax protein. J Pharm Biomed Anal 52(5):802-808.

19. Matulis D, Kranz JK, Salemme FR, Todd MJ 2005. Thermodynamic Stability of Carbonic Anhydrase: Measurements of Binding Affinity and Stoichiometry Using ThermoFluor. Biochemistry (Mosc) 44(13):5258-5266.

20. Kopec J, Schneider G 2011. Comparison of fluorescence and light scattering based methods to assess formation and stability of protein-protein complexes. J Struct Biol 175(2):216-223.

21. Senisterra G, Chau I, Vedadi M 2012. Thermal Denaturation Assays in Chemical Biology. Assay Drug Dev Technol 10(2):128-136.

22. Goldberg DS, Bishop SM, Shah AU, Sathish HA 2011. Formulation development of therapeutic monoclonal antibodies using high-throughput fluorescence and static light scattering techniques: Role of conformational and colloidal stability. J Pharm Sci 100(4):1306-1315.

23. Li Y, Mach H, Blue JT 2011. High throughput formulation screening for global aggregation behaviors of three monoclonal antibodies. J Pharm Sci 100(6):2120-2135.

24. He F, Hogan S, Latypov RF, Narhi LO, Razinkov VI 2010. High throughput thermostability screening of monoclonal antibody formulations. J Pharm Sci 99(4):1707-1720.

25. He F, Woods C, Litowski J, Roschen L, Gadgil H, Razinkov V, Kerwin B 2011. Effect of Sugar Molecules on the Viscosity of High Concentration Monoclonal Antibody Solutions. Pharm Res 28(7):1552-1560.

26. King AC, Woods M, Liu W, Lu Z, Gill D, Krebs MRH 2011. High-throughput measurement, correlation analysis, and machine-learning predictions for pH and thermal stabilities of Pfizer-generated antibodies. Protein Sci 20(9):1546-1557.

27. Kerwin BA 2008. Polysorbates 20 and 80 used in the formulation of protein biotherapeutics: Structure and degradation pathways. J Pharm Sci 97(8):2924-2935.

28. Loutfy RO, Arnold BA 1982. Effect of viscosity and temperature on torsional relaxation of molecular rotors. J Phys Chem 86(21):4205-4211.

29. Loutfy RO, Law KY 1980. Electrochemistry and spectroscopy of intramolecular charge-transfer complexes. p-N,N-Dialkylaminobenzylidenemalononitriles. J Phys Chem 84(21):2803-2808.

30. Hawe A, Sutter M, Jiskoot W 2008. Extrinsic Fluorescent Dyes as Tools for Protein Characterization. Pharm Res 25(7):1487-1499.

31. Hawe A, Filipe V, Jiskoot W 2010. Fluorescent Molecular Rotors as Dyes to Characterize Polysorbate-Containing IgG Formulations. Pharm Res 27(2):314-326.

32. Ionescu RM, Vlasak J, Price C, Kirchmeier M 2008. Contribution of variable domains to the stability of humanized IgG1 monoclonal antibodies. J Pharm Sci 97(4):1414-1426.

33. Garber E, Demarest SJ 2007. A broad range of Fab stabilities within a host of therapeutic IgGs. Biochem Biophys Res Commun 355(3):751-757.

34. Wen J, Jiang Y, Narhi L 2008. Effect of Carbohydrate on Thermal Stability of Antibodies. American Pharmaceutical Review 11(6):98-104.

35. Wen J, Arthur K, Chemmalil L, Muzammil S, Gabrielson J, Jiang Y 2012. Applications of differential scanning calorimetry for thermal stability analysis of proteins: Qualification of DSC. J Pharm Sci 101(3):955-964.

36. Bam NB, Cleland JL, Yang J, Manning MC, Carpenter JF, Kelley RF, Randolph TW 1998. Tween protects recombinant human growth hormone against agitation-induced damage via hydrophobic interactions. J Pharm Sci 87(12):1554-1559.

37. Liu J, Nguyen MDH, Andya JD, Shire SJ 2005. Reversible self-association increases the viscosity of a concentrated monoclonal antibody in aqueous solution. J Pharm Sci 94(9):1928-1940.

38. Kanai S, Liu J, Patapoff TW, Shire SJ 2008. Reversible self-association of a concentrated monoclonal antibody solution mediated by Fab–Fab interaction that impacts solution viscosity. J Pharm Sci 97(10):4219-4227.

39. Menzen T, Frieß W. Poster Presentation. *8th PBP World Meeting*, Istanbul, Turkey, 03/20/2012.

40. Ablinger E, Leitgeb S, Zimmer A. Poster Presentation. *Workshop on Protein Aggregation and Immunogenicity*, Breckenridge, CO, 07/10/2012.

41. Malone JP, Radabaugh MR, Leimgruber RM, Gerstenecker GS 2001. Practical aspects of fluorescent staining for proteomic applications. Electrophoresis 22(5):919-932.

42. Senisterra GA, Ghanei H, Khutoreskaya G, Dobrovetsky E, Edwards AM, Privé GG, Vedadi M 2010. Assessing the Stability of Membrane Proteins to Detect Ligand Binding Using Differential Static Light Scattering. J Biomol Screen 15(3):314-320.

43. Kean J, Cleverley RM, O'Ryan L, Ford RC, Prince SM, Derrick JP 2008. Characterization of a CorA Mg2+ transport channel from Methanococcus jannaschii using a Thermofluor-based stability assay. Mol Membr Biol 25(8):653-661.

44. Senisterra GA, Finerty JPJ 2009. High throughput methods of assessing protein stability and aggregation. Mol Biosyst 5(3):217-223.

45. Mezzasalma TM, Kranz JK, Chan W, Struble GT, Schalk-Hihi C, Deckman IC, Springer BA, Todd MJ 2007. Enhancing Recombinant Protein Quality and Yield by Protein Stability Profiling. J Biomol Screen 12(3):418-428.

46. Alexandridis P, Hatton TA 1995. Poly(ethylene oxide)-poly(propylene oxide)-poly(ethylene oxide) block copolymer surfactants in aqueous solutions and at interfaces: thermodynamics, structure, dynamics, and modeling. Colloids and Surfaces A: Physicochemical and Engineering Aspects 96(1–2):1-46.

47. Zhou Z, Chu B 1988. Light-scattering study on the association behavior of triblock polymers of ethylene oxide and propylene oxide in aqueous solution. J Colloid Interface Sci 126(1):171-180.

48. Alexandridis P, Holzwarth J, Hatton TA 1995. A correlation for the estimation of critical micellization concentrations and temperatures of polyols in aqueous solutions. J Am Oil Chem Soc 72(7):823-826.

49. Alexandridis P, Holzwarth JF, Hatton TA 1994. Micellization of Poly(ethylene oxide)-Poly(propylene oxide)-Poly(ethylene oxide) Triblock Copolymers in Aqueous Solutions: Thermodynamics of Copolymer Association. Macromolecules 27(9):2414-2425.

50. Sigma Life Science. 2008. Detergents and Solubilization Reagents. BioFiles. Accessed 02/24/2012, at: http://www.sigmaaldrich.com/life-science/learning-center/biofiles.html#detergents.

51. Fuguet E, Ràfols C, Rosés M, Bosch E 2005. Critical micelle concentration of surfactants in aqueous buffered and unbuffered systems. Anal Chim Acta 548(1–2):95-100.

52. Palladino P, Ragone R 2011. Ionic Strength Effects on the Critical Micellar Concentration of Ionic and Nonionic Surfactants: The Binding Model. Langmuir 27(23):14065-14070.

53. Lee HJ, McAuley A, Schilke KF, McGuire J 2011. Molecular origins of surfactant-mediated stabilization of protein drugs. Adv Drug Delivery Rev 63(13):1160-1171.

54. Otzen D 2011. Protein–surfactant interactions: A tale of many states. Biochimica et Biophysica Acta (BBA) - Proteins and Proteomics 1814(5):562-591.

55. Saito A, Miyauchi E. 2009. Stabilized Protein-Containing Formulations. In Kita-Ku J, Chuo-Ku J, editors., US 20090264629A1 ed.: Chugai Seiyaku Kabushiki Kaisha

56. Cimmperman P, Baranauskiene L, Jachimoviciute S, Jachno J, Torresan J, Michailoviene V, Matuliene J, Sereikaite J, Bumelis V, Matulis D 2008. A Quantitative Model of Thermal Stabilization and Destabilization of Proteins by Ligands. Biophys J 95(7):3222-3231.

57. Uniewicz KA, Ori A, Xu R, Ahmed Y, Wilkinson MC, Fernig DG, Yates EA 2010. Differential Scanning Fluorimetry Measurement of Protein Stability Changes upon Binding to Glycosaminoglycans: A Screening Test for Binding Specificity. Anal Chem 82(9):3796-3802.

58. Wang CK, Weeratunga SK, Pacheco CM, Hofmann A 2012. DMAN: a Java tool for analysis of multi-well differential scanning fluorimetry experiments. Bioinformatics 28(3):439-440.

59. Niesen F. 2012. DSF Analysis v3.0.2. Accessed 06/14/2012, at: ftp://ftp.sgc.ox.ac.uk/pub/biophysics/.

6 Temperature-ramped studies on the aggregation, unfolding, and interaction of a therapeutic mAb

This chapter has been published as Tim Menzen and Wolfgang Friess, 2014, Temperature-ramped studies on the aggregation, unfolding, and interaction of a therapeutic monoclonal antibody, J Pharm Sci 103(2): 445-455.

6.1 Abstract

Investigations on thermal behavior are essential during the development of therapeutic proteins. Understanding the link between thermal unfolding and aggregation might help to minimize conformational and colloidal instabilities. In this study, a therapeutic monoclonal antibody and its Fab and Fc fragments were investigated. The apparent melting temperature of a protein and its onset were determined by differential scanning fluorimetry. Temperature-ramped turbidity measurements were performed to assess the temperature of aggregation, where large protein particles occurred. The formation of small aggregates was monitored and the interaction parameter k_D at low, ambient, and high temperature was calculated by temperature-ramped dynamic light scattering. Transformation of k_D into A_2^* based on literature findings allowed the interpretation of net repulsive or attractive conditions. Repulsive net charges at low pH increased the colloidal stability, although a reduction of the conformational stability was observed. At neutral conditions and in the presence of salt, unfolding was followed by precipitation of the protein. A sharp decrease of k_D and negative A_2^* values suggest that the aggregation was driven by hydrophobic interactions. Thus, the presented methods described and explained the thermal behavior of the protein and demonstrated their value for the development of pharmaceutical protein products.

6.2 Introduction

The therapeutic and commercial success of protein drugs, especially monoclonal antibodies (mAbs), is well known today. The development of new drugs, biosimilars of marketed products, or other forms such as antibody drug conjugates (ADCs), is

still challenging because of the outstanding complexity of the stability and function of the protein molecule.[1] mAbs commonly face different types of instability reactions, including chemically altered material, changed conformational structures, or the formation of native or nonnative protein aggregates.[2-5] All of these instabilities can reduce the efficiency and safety of the product. For example, immunogenic reactions in patients are assumed to be caused by “altered protein,” although clear evidence is still lacking and the topic is in hot discussion.[6,7] It is reasonable to minimize the occurrence of unwanted altered protein during the development of a protein drug. Spectroscopic methods such as fluorescence, ultraviolet-visible (UV-Vis), circular dichroism, and Fourier-transform infrared spectroscopy are typically applied to characterize the conformational structure of the protein.[8] Additionally, a thermal analysis by differential scanning calorimetry (DSC) or differential scanning fluorimetry (DSF) reveals the apparent melting temperature (T_m) of a protein, which is commonly linked to the overall thermal stability of the protein.[9-12] Because of the vast distribution of particle size, many methods are necessary to describe protein aggregates comprehensively. Typically, high performance size exclusion chromatography (HP-SEC) and light scattering techniques are applied for small, soluble aggregates; nanoparticle tracking analysis, light obscuration, and microflow imaging are applied for subvisible particles; and visual inspection is applied for large particles, to name some prominent examples.[5,13]

A net attraction between protein molecules leads to aggregation although multiple individual forces are involved. The interaction potential is composed of long (Coulomb) and short range forces (van-der-Waals, solvation and hydrogen-bonds, hard-sphere repulsion/excluded volume, and other specific interactions).[14,15] Instead of assessing each single force, a common approach is the determination of the osmotic second virial coefficient A_2 from the parametric expansion of the osmotic pressure (also referred to as B_{22}). A_2 describes the deviation from the ideal solution due to overall pairwise molecular interactions between the particles.[16] Although crystallization and solubility were thoroughly investigated in relation to A_2 for many proteins,[17-25] research on mAbs focused mainly on the effect of intermolecular interactions at the low concentration on the viscosity of highly concentrated mAb solutions. Saito and coworker demonstrated that A_2 is dependent on the surface properties of mAbs, and a high negative A_2 value correlated with a high viscosity of concentrated mAb solutions, and an increased tendency of the mAb for aggregation

due to the attractive interactions.[26] Also, a strong correlation between A_2 and the viscosity of highly concentrated mAb solutions was found by Connolly et al.[27] They concluded that weak interactions are responsible because the net charge of the mAb was in no correlation.[27] In their work, the assessment of A_2 via static light scattering (SLS) or analytical ultracentrifugation (AUC) is of low throughput and other methods such as self-interaction chromatography (SIC) have been proposed to reduce time and material consumption.[24,28-31] Yadav and coworkers recently published a different approach to determine A_2 based on measurements only using a dynamic light scattering (DLS) instrument.[32] With careful consideration of the attenuation factor, the recorded scatter intensity signal is used to create Debye plots to calculate A_2. Although this elegant approach enables A_2 measurements in a single machine, it is limited by a low throughput and cannot be adopted to well plate readers. On the contrary, the diffusion interaction parameter k_D, which is easily accessible via DLS, is used as an alternative screening parameter. The k_D value can be expressed as [33]

$$k_D = 2A_2M - (\zeta_1 + 2\upsilon_{sp}) \tag{6-1}$$

where A_2 is the osmotic second virial coefficient, M is the molar mass of the protein, ζ_1 is the coefficient from the linear term of the virial expansion of the concentration dependent friction coefficient, and υ_{sp} is the partial specific volume of the protein. Thus, the k_D value consist of a first, thermodynamic part expressed by A_2 and a second, hydrodynamic part. To determine k_D, the mutual diffusion coefficient D is determined for several dilutions of the protein sample. From the slope of the linear fit to the data points, k_D can be determined based on the following equation

$$D = D_0(1 + k_D c) \tag{6-2}$$

where D is the mutual diffusion coefficient, D_0 is the diffusion coefficient at infinite dilution, and c is the protein concentration.

Yadav and coworkers investigated the interactions of mAbs at low ionic strength and suggest that close to the isoelectric point (pI), specific attractive forces are responsible for self-association and also lead to high viscosity in high mAb concentrations, although a correlation to k_D was not found under these latter conditions.[34] Chari et al. involved k_D measurements to demonstrate that at high mAb concentrations and low ionic strength, both long-range and short-range electrostatic interactions are responsible for viscosity effects.[35] Although long-range electrostatic

interactions were responsible for mAb aggregation at low concentration, Kumar and coworker found that at high mAb concentrations, short-range hydrophobic interactions predominate the aggregation kinetics.[36] Although Arzenšek and coworker intensively investigated the effects of pH and ionic strength on k_D by the addition of sodium chloride,[37] Rubin et al. recently studied the aggregation of a mAb with respect to the ionic strength from salts of the Hofmeister series.[38] They found that a lower k_D value is suggestive for a lower relative colloidal stability of the mAb.[38] However, because of the hydrodynamic component, the sign of k_D does not indicate net attractive or net repulsive intermolecular interaction.[26] Lehermayr et al. and also Connolly et al. present a linear fit of the data to transform k_D into A_2.[27,39] In this article, a linear fit was performed on the united data set of A_2 and k_D values published in literature on mAbs to obtain an equation to transform the interaction parameters. This equation was used to estimate the thermodynamic interaction parameter (A_2^*) and thus the net attraction or net repulsion.

To understand the role of intermolecular interactions during the process of thermal unfolding and aggregation of mAbs, k_D and A_2^* values were investigated at low, ambient, and elevated temperature by DLS. The absolute values and their change upon heating were used to interpret the results from DSF regarding the conformational stability and the exposure of hydrophobic patches upon unfolding. The results from the DLS and temperature-ramped turbidity experiments were linked to characterize and interpret the aggregation behavior. Additionally, the Fab and the Fc domain were isolated to study the influence of the individual domains on the overall stability of the mAb. A strong effect of pH and ionic strength was observed. At the low pH of 5.0 and low ionic strength, a high k_D value was observed suggesting strong electrostatic repulsion, which prevented the protein from precipitation. Despite this colloidal stabilization, a reduced conformational stability was found with respect to the negative shift of the T_m value compared with the neutral pH. At pH 7.2 and 5.0 in the presence of salt, lower k_D values were found. Furthermore, different aggregation behaviors for Fab and Fc or the full mAb were observed. In the case of Fab, k_D values did not change with increasing temperatures until presumably minimal perturbation of the structure below the onset temperature of unfolding resulted in substantial aggregation. In the case of Fc and the full mAb, unfolding and aggregation coincided at similar temperatures and were associated with a reduction of k_D suggesting that the conformational change induced new interaction spots. At the

neutral pH or when the charges were shielded in the presence of a salt at the low pH, precipitation of the protein occurred.

6.3 Materials and methods

6.3.1 mAb fragmentation and protein formulation

A therapeutic monoclonal antibody of IgG1 type produced in CHO cells (“MAb”) was digested with 0.1 % (w/w) of papain from papaya latex (Sigma Aldrich, Steinheim, Germany) in a 40 mM histidine buffer containing 10 mM cysteine and 2 mM disodium ethylenediaminetetraacetic acid at pH 7.0. The mixture was incubated for 24 h at 37 °C and the reaction was stopped by the addition of an aqueous iodoacetamide solution to reach a concentration of 40 mM iodoacetamide. To isolate the fragments, the mixture was purified by chromatography using an ÄKTA purifier 10 system (GE Healthcare, Uppsala, Sweden) and ultrafiltration steps. First, all Fc carrying species were retained by protein A affinity chromatography using a 5 ml Pierce protein A cartridge (Thermo Fisher Scientific, Bonn, Germany). Second, size exclusion chromatography (SEC) using a Sephacryl® 16/60 column (GE Healthcare) was performed to separate Fc from residual full MAb or partly fragmented MAb. Finally, the protein was dialyzed by means of Vivaspin® 20 tubes with a 10 kDa molecular weight cut-off PES membrane (Sartorius Stedim Biotech, Göttingen, Germany) to remove all low molecular weight species with the target formulation buffer (10 mM phosphate at pH 5.0 and pH 7.2, with or without 140 mM sodium chloride (NaCl) and 280 mM mannitol). The pH of the samples was adjusted and filtration was performed using 0.2 µm syringe filter (Pall, Port Washington, New York, USA). The protein concentration was determined using an extinction coefficient of 1.49 ml g^{-1} cm^{-1}. Isoelectric focusing using a Servalyt Precotes® gel (Serva Electrophoresis, Heidelberg, Germany) resulted in isoelectric points (pI) between 8.3 - 9.5 for the full MAb, 9.5 - 10.7 for Fab, and 6.9 - 7.8 for Fc. The purity of the isolated Fab and Fc fragments was confirmed by hydrophobic interaction chromatography using a TSKgel® Phenyl-5PW column (Tosoh Bioscience, Stuttgart, Germany) on an Agilent 1200 series HPLC system (Agilent Technologies, Santa Clara, California, USA) as described by Wakankar et al.[40]

6.3.2 Differential scanning fluorimetry (DSF)

DSF was performed using a RT7300 Real-Time PCR machine (Applied Biosystems, Foster City, California, USA) as recently described (chapter 5).[41] In short, 20 µl of the sample (0.8 mg/ml MAb, 2.6 mg/ml Fab, and 1.3 mg/ml Fc) was pipetted into a 96-well plate (Applied Biosystems) and 1 µl of an aqueous working solution of SYPRO® Orange (Sigma Aldrich) was added to a final dye dilution of 1:5000 in relation to the supplied stock solution by the manufacturer. The temperature was increased from 20 °C to 96 °C at 1 °C/min in steps of 1 °C. The fluorescence intensity at 578 nm was analyzed with Origin® 8.0 SR6 (Originlab Corporation, Northampton, Massachusetts, USA) regarding the temperature at the inflection point (T_m) and the onset temperature of unfolding ($T_{m,onset}$) using a nonlinear Boltzmann fit to the melting transitions (see also chapter 3.3).[41] A placebo sample was used for background correction, and the presented values are mean values of three wells. A negative impact of the dye on T_m was ruled out as the T_m value of the MAb in 10 mM phosphate buffer pH 7.2 obtained by DSC was not significantly changed ($\Delta T_m < 0.1$ °C) by either the presence of 1x SYPRO® Orange or 0.1 % dimethyl sulfoxide (DMSO) (chapter 4.3.6.2).

6.3.3 Temperature-ramped turbidity measurements

Turbidity measurements were performed with an Agilent 8453 UV-Vis Spectrophotometer equipped with a Peltier temperature controller (Agilent Technologies) in a 500 µl glass micro cuvette with PTFE stopper (Hellma Analytics, Müllheim, Germany). Samples of 0.8 mg/ml MAb, 2.6 mg/ml Fab, and 1.3 mg/ml Fc were used. The temperature was gradually increased by 1 °C from 20 °C to 97 °C. The absorption values at 350 nm were exported and the first derivative of the data was calculated and splined with Origin® LabTalk 8.0 SR6. The maximum and the onset (10% of maximum) of the interpolated first derivative curve resemble the temperature of aggregation (T_{agg}) and the onset temperature of aggregation ($T_{agg,onset}$), respectively.

6.3.4 Dynamic light scattering (DLS)

DLS measurements were performed in 384-well plates (Corning Incorporated, Corning, New York, USA) using a DynaPro plate reader (Wyatt Technologies, Santa Barbara, California, USA). A triplicate of three wells was measured for every sample with 20 acquisitions of 2 s for every well. The machine was cooled with gaseous

nitrogen, and a temperature protocol was applied starting with 4 °C, 8 °C, and 10 °C, followed by a stepwise increase by +5 °C up to 85 °C. The DYNAMICS® software version 7.1.7.16 (Wyatt Technologies) was used to analyze the recorded autocorrelation function by means of cumulants analysis to determine the diffusion coefficient (D) and the derived hydrodynamic radius (R_h) via the Stokes-Einstein equation. For phosphate buffers with and without NaCl, a viscosity of 1.019 mPa s at 20 °C and a refractive index of 1.333 were used. The viscosity of the 280 mM mannitol containing buffers was calculated as 1.017 mPa s at 25 °C according to Liu et al.[42] and a refractive index of 1.340 as typical for 280 mM sugar solutions was applied in the DYNAMICS® software. The effect of the temperature dependent reduction of the refractive index was tested based on the findings of Schiebener et al. for water.[43] The deviation of k_D was found to be below 0.1 ml/g when considering a heating induced reduction of the refractive index from 1.333 to 1.320. Because of the insignificance of this difference, no temperature corrections of the refractive index were made. The presented results of R_h are mean values with standard error determined from the triplicate sample with a protein concentration in a comparable range between 1.2 – 2.5 mg/ml. The measurements were repeated at 4 °C of all samples and at 25 °C for the samples at pH 5.0.

6.3.5 Calculation of the interaction parameter k_D and A_2

The diffusion coefficients D of a series of at least seven samples with protein concentrations ranging from about 0.4 mg/ml to about 12 mg/ml were determined as triplicates by DLS. A linear fit was performed on the D versus protein concentration data to obtain the diffusion coefficient at infinite dilution D_0. By normalizing D by D_0, the slope of the linear fit resembles the interaction parameter k_D.[38]

6.3.6 Transformation of the interaction parameters of mAbs

As an alternative to the direct determination of A_2, Lehermayr et al. described a linear correlation of k_D and A_2 for several mAbs and suggested using this empiric correlation for A_2 assessment based on k_D from DLS measurements to save time and material.[39] Connolly et al. confirmed this common linear correlation, although a different method for A_2 determination was used.[27] As presented in Figure 6-1, the combination of the published k_D and A_2 results for mAbs supports the hypothesis of a common linearity between both parameters.

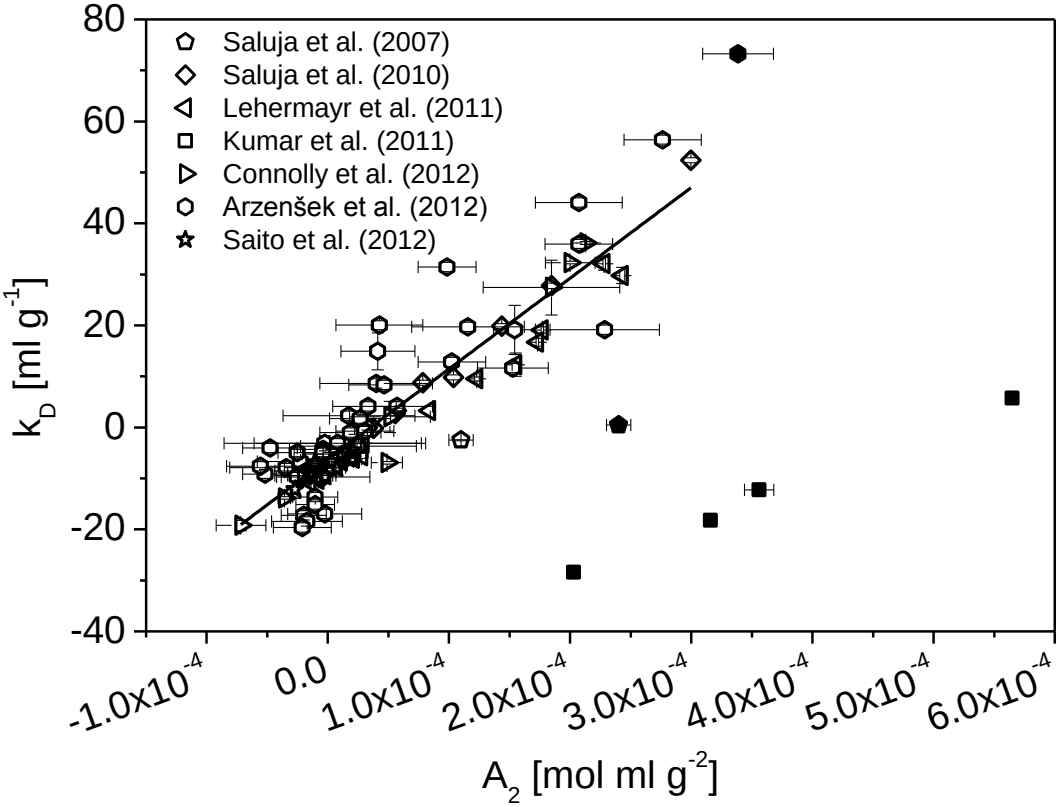

Figure 6-1. Graphical illustration of the equation for the transformation of the interaction parameters of MAbs (TIM). The data points with closed symbols were omitted after DFFITS outlier analysis to result in a linear fit (R^2 = 0.858) across the remaining 93 data points (open symbols). The TIM equation (eq. (6-3)) allows the estimation of the thermodynamic interaction parameter A_2^* from k_D values from DLS measurements. By this means, estimation of net attractive or net repulsive interaction is possible without the experimental determination of A_2.

Thus, based on the published data described in Table 6-1, an equation for the transformation of the interaction parameters of mAbs (short "TIM") was calculated as

$$A_2^* = \frac{k_D + 6.29}{1.19M} \tag{6-3}$$

where A_2^* is the estimated osmotic second virial coefficient and M is the molar mass of the mAb. As summarized in Table 6-1, a multitude of mAb molecules, buffer types, pH, excipient, and analytical methods are included.

Table 6-1. Summary of the experimental conditions from literature where k_D and A_2 of mAbs were described.

Reference	Number and type of mAbs investigated	Number and type of formulations investigated	A_2 deter-min. by
Saluja et al. (2007) [Pfizer] [44]	1 IgG2 (pI 8.5..9.25)	4 (pH 4 - 9; I=4 - 300 mM)	SLS
Saluja et al (2010) [Amgen] [45]	1 IgG2 (pI 8.8)	10 (pH 5.5, I=10 - 110mM)	DLS/ AUC
Lehermayr et al. (2011) [Roche] [39]	7 IgG1 (pIs 7.5..10), 1 IgG4 (pI 6.3-7.8)	2 (pH 6; I=20 - 170 mM)	SLS
Kumar et al. (2011) [Abbott] [36]	1 IgG1	6 (pH 4.5, 6; I=1 - 100 mM)	SLS
Connolly et al. (2012) [Genentech] [27]	6 IgG1, 1 IgG4	1 (pH 5.5, I=20 mM)	DLS/ AUC
Arzenšek et al. (2012) [Sandoz] [37]	1 IgG1 (pI 8.46)	48 (pH 3 - 10; I=15 – 175 mM)	SLS
Saito et al. (2012) [Daiichi Sankyo] [26]	3 IgG1 (pIs 6.7, 8.8, 8.9)	4 (pH 5 - 8; I=150 mM)	AUC

The published data is the basis for the transformation of the interaction parameters of mAbs (TIM) equation (eq. (6-3)) to estimate A_2^* from k_D measurements. The TIM equation is illustrated in Figure 6-1 after the DFFITS outlier test was performed and single measurements were omitted from the linear fit as discussed in the text. Experiments were performed at room temperature and k_D values were obtained by dynamic light scattering (DLS). IgG, Immunoglobulin G; pI, isoelectric point; I, ionic strength; SLS, static light scattering; AUC, analytical ultracentrifugation.

Two exceptions are also presented. The results published by Kumar et al. and Saluja et al. in their early works exhibit a good linearity but are not in agreement with other data.[36,44] In the latter case, the A_2 values are exactly one order of magnitude too high to fit into the correlation but the calculations presented in their article are plausible. Because of the large impact of samples, which do not seem to follow the typical trend, the DFFITS outlier test was performed on the complete data set (compare chapter 4.2.11). In an iterative approach, the sample with the highest absolute DFFITS value suggesting a high influence on the linear regression was eliminated until all cases were within the outlier threshold of 1.[46] By this statistical test, all values

of Kumar et al.,[36] two values with the lowest ionic strength at pH 3 of Arzenšek et al,[37] and all values but the sample at pH 9 from Saluja et. al. (2007),[44] were omitted (Figure 6-1). Thus, the data set was reduced from 103 to 92 different constellations, which are represented in the TIM equation (eq. (6-3)). Interestingly, extreme cases of low pH and low ionic strength seem to be responsible for the observed outliers. These cases may show a deviating ζ_1 value. This could be due to differences in level and distribution of hydration, potential slight changes in protein conformation at extreme pH values, or specific salt interaction affecting the overall size and shape of the antibody molecules.[47] Therefore, the TIM equation is suggested to be only valid in the case of moderate pH and ionic strength conditions. The TIM equation should allow a quick estimation of the quality of the important net attractive or net repulsive interaction based on the thermodynamic parameter A_2^* without the experimental efforts. It has to be noted that some authors[26,27,35,39,45] used the equation postulated by Harding and Johnson which contains υ_{sp} without the factor of 2 as presented in eq. (1-1).[48] It is described by Teraoka that this factor corrects for the backflow of solvent molecules by diffusion into the voids left by protein molecules.[33] However, in the context of the presented conversion with respect to the relatively small value of the partial specific volume of about 0.730 - 0.739 ml/g for mAbs,[26,27,37,49] the difference is assumed to be of minor influence on the overall fit. Moreover, Cheng and coworker just recently investigated the partial specific volume of an IgG2 at two different pH values.[50] They found similar values for a citrate-phosphate formulation buffer at pH 7.0 and pH 4.0.[50] Furthermore, they observed a linear temperature dependence of υ_{sp} and found that a temperature increase from 10 °C to 50 °C resulted in an increase of υ_{sp} by about 2 %.[50] These findings suggest that the solution conditions show only a minor effect on the partial specific volume of a MAb molecule. As expected, the value of 1.19 for the slope of the linear fit (eq. (6-3)) from the TIM equation is well within the range of the slope factors reported by Lehermayr et al. and Connolly et al. of 1.06 and 1.33, respectively, whose data sets are both included (Table 6-1).[27,39] This value of 1.19 is lower than expected from the definition in eq. 1. This deviation was suggested to reflect a protein shape factor as the antibodies deviate from a perfect sphere.[39] According to eq. (6-3), the sign of A_2^* changes from negative (net attraction) to positive (net repulsion) at a k_D value of -6.29 ml/g.

6.4 Results and Discussion

6.4.1 Aggregation, unfolding, and interaction of the mAb in 10 mM phosphate buffer pH 7.2

Table 6-2 contains a comprehensive summary of the results of the thermal stability analysis. On the example of the MAb formulation in 10 mM phosphate buffer at pH 7.2, the results should be explained and discussed in detail. The hydrodynamic radius R_h, based on the diffusion coefficient D obtained from the DLS measurements at increasing temperatures, and the k_D values is presented in Figure 6-2 A. At a MAb concentration of 2.2 mg/ml, the R_h was nearly unchanged with increasing temperatures from 5.23 nm at 4 °C to 5.15 nm at 60 °C. Starting at 65 °C, the radius sharply increased and exceeded 10 nm indicating the formation of small aggregates. On the basis of the diffusion coefficients of a dilution series of seven MAb solutions between 0.4 and 12 mg/ml, the D_0 and k_D values were calculated. The diffusion parameter at infinite dilution D_0 is derived from the intercept of the linear fit of D versus protein concentration. At ambient temperature (20 - 25 °C) the D_0 results between $4.3*10^{-7}$ and $4.8*10^{-7}$ cm^2 s^{-1} are in good agreement with data published for mAbs (compare Table 6-2).[34,37,39,44,45,51,52] As illustrated in Figure 6-2 A, D_0 increased with increasing temperature until it reached a maximum value at 60 °C ($T@D_{0max}$). The observed drop of D_0 when exceeding this temperature is linked to the aggregation of the mAb resulting in smaller diffusion coefficients due to the increase in size as can be seen from the R_h in Figure 6-2 A. This finding suggests that at temperatures below $T@D_{0max}$, the calculated k_D value can be assigned to the MAb monomer. Above $T@D_{0max}$, the calculation is spoiled by MAb aggregates, and mathematically obtained k_D values are incorrect and must not be further interpreted or compared with the ones obtained for the monomeric form. As can be seen in Figure 6-2 A, the k_D value at the initial temperature of 4 °C was about zero (0.8±1.2 ml/g). With increasing temperature, the k_D value was found to be constant until a first small drop occurred at 25 °C (-5.7 ml/g) followed by another plateau up to 60 °C (-8.6 ml/g) with little changes. Exceeding 60 °C, the k_D value dropped sharply to about -70 ml/g at 70 °C. With respect to the TIM equation (eq. 3), the A_2^* values indicate that at the elevated temperatures, the thermodynamic interaction switched from net repulsion to net attraction (compare Table 6-2). Furthermore, the melting profiles from DSF analysis of the mAb and its Fab and Fc fragment are presented in Figure 6-2 B. The graphs demonstrate that at the neutral pH, two prominent unfolding

transitions are observed, which can be linked to and identified by the fragments. The first transition resembles the CH2 domain of the Fc fragment. The second transition of the full mAb is caused by simultaneous unfolding of the Fab and CH3 domain.[41] From the midpoint of the fluorescence transitions tracing the presentation of the hydrophobic patches upon unfolding of the protein, the apparent T_m of the protein is obtained where half of the accessible hydrophobic patches are exposed. With an onset value of 59.3 °C ($T_{m,onset}$) and a T_{m1} of 68.4 °C, the DSF data suggest that the decrease of k_D at 60 °C is linked to the unfolding of the protein. The exposed hydrophobic patches are assumed to face hydrophobic interactions, which will lead to a more attractive net interaction represented by a smaller, i.e., more negative k_D and negative A_2^* value. Moreover, the aggregation of the MAb molecules via the exposed hydrophobic patches can explain the decrease in fluorescence intensity after a maximum has been passed in DSF. The participation of the hydrophobic surface regions in intermolecular interactions results in less interaction with the extrinsic fluorescent dye as was originally postulated by Niesen et al.[53] Unfolding of the Fab domain at about 80 °C (T_{m2} = 81.5 °C) is followed by precipitation of the mAb, which is confirmed by an increase in turbidity (T_{agg} = 79.5 °C) and a decrease in fluorescence intensity (Figure 6-2 B). After filtration through a 0.2 µm PVDF filter, a clear solution was obtained with baseline value for A_{350nm} and 96±1 % of the protein was removed as calculated from A_{280nm}. Thus, the MAb precipitate after heating to 97 °C consisted predominately of large particles.

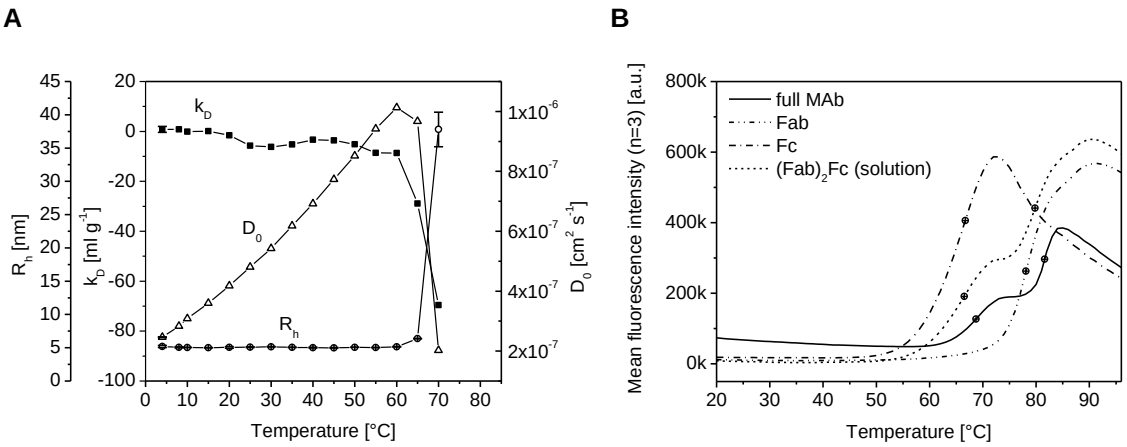

Figure 6-2. Hydrodynamic radius R_h (circles), interaction parameter k_D (black squares), and diffusion coefficient at infinite dilution D_0 (open triangles) as a function of temperature on the example of the mAb in 10 mM phosphate buffer at pH 7.2. The lines should guide the eye. (A). Exemplary melting profiles obtained by DSF of the full MAb, its isolated Fab and Fc fragments, and a 2:1 mixture of Fab and Fc in 10 mM phosphate buffer at pH 7.2. The T_m values obtained by first derivative analysis are marked with crossed circles (B).

6.4.2 Aggregation, unfolding, and interaction of the mAb at other pH and ionic strength conditions

The results for the mAb in the other formulations are in good agreement (Table 6-2 and supplementary Figure 6-4 in chapter 6.8). The addition of 140 mM NaCl or 280 mM mannitol to the 10 mM phosphate buffer at pH 7.2 showed the same trend. For all the three formulations at the neutral pH the R_h values were below 10 nm up to the $T@D_{0max}$ of 65 °C. With the T_{m1} values closely settled between 67.3 and 69.4 °C, the excipients showed only a minor influence on the conformational stability at pH 7.2. Mannitol was found to be slightly stabilizing with ΔT_{m1} of about +1.0 °C, whereas the addition of NaCl destabilized the mAb with ΔT_{m1} of -1.1 °C. As can be seen in Figure 6-3 A, at the neutral pH, the k_D value decreased dramatically when the protein started to aggregate and negative A_2^* occurred. Precipitation of the mAb occurred at approx. 80 °C, which coincides with the second melting transition of the mAb. This finding suggests that aggregation driven by attractive hydrophobic interactions of the full mAb is linked to the unfolding of the Fab and the CH3 domain.

As the pH value is lowered to 5.0 and the mAb net charge becomes positive, the outcome is different. In 10 mM phosphate buffer at pH 5.0 without any excipient, the k_D value was calculated as 37.1±2.1 ml/g at 4 °C. This strong net repulsion prevented the mAb from forming large aggregates as indicated by an R_h value still below 10 nm at 80 °C and by an absent increase in turbidity. The same results were obtained after the addition of mannitol. The neutral sugar alcohol did only slightly reduce the k_D value (34.6±2.1 ml/mg) and had a minor stabilizing effect on the conformational stability (ΔT_{m1} = 1.6 °C) but did not change the aggregation behavior. Similar to the findings at pH 7.2, the k_D values decreased with the onset of unfolding but A_2^* values were always positive (Table 6-2 and Figure 6-3 A). These findings suggest that the hydrophobic patches, which are exposed upon unfolding, mediated attractive intermolecular hydrophobic interactions and reduced the overall net repulsion but the electrostatic interaction still dominated. In contrast, the presence of 140 mM NaCl dramatically reduced the k_D value to -1.5±1.0 ml/g already at 4 °C suggesting interaction forces similar to the conditions at neutral pH. Additionally, strong precipitation was observed by turbidity measurements. These findings suggest that the repulsive positive net charges that prevented the aggregation were shielded by the addition of the salt. Saluja et al. observed that already above an ionic strength of 40 mM, k_D values were leveled independent of the pH of the solution.[44] At pH 5.0,

Arzenšek and coworker presented k_D values of 36 ml/g and -4 ml/g for 15 mM and 175 mM, respectively, and k_D values between -3 ml/g and -10 ml/g at neutral pH,[37] which is in good agreement with our results. This confirms that at the applied ionic strength of 150 mM of the NaCl containing buffer mimicking physiological conditions, repulsive electrostatic forces are effectively shielded. Furthermore, the low pH significantly affected the conformational stability of the mAb. The apparent T_m values were several degrees lower at pH 5.0 compared with pH 7.2 (Table 6-2). The addition of NaCl to the MAb formulation at pH 5.0 resulted in a negative shift of T_{m1} (ΔT_{m1} = -3.3 °C) with $T_{m,onset}$ as low as 48.6 °C. He and coworkers also observed a destabilizing effect of low pH and the addition of NaCl in their T_m screening of mAbs.[10]

6.4.3 Investigation of the isolated Fab and Fc fragments

Especially for the CH2 domain of the Fc fragment, a strong pH dependence of the thermal stability is known[54-57] and the apparent T_m value of the Fc decreased by 6.7 °C when the pH value was changed from pH 7.2 to pH 5.0 (Table 6-2 and supplementary Figure 6-5 and 6-6 in chapter 6.8). In contrast, the apparent T_m of the Fab fragment was increased by 1 °C at the low pH, and the overall high apparent T_m values of about 80 °C suggest that the conformation of the Fab part is rather robust against heat and charge effects. Interestingly, a marked change in R_h of the Fab fragment was already observed at 55 °C and 60 °C at neutral pH and in the presence of salt. This indicates that aggregation occurred at temperatures considerably below the onset of unfolding of the Fab fragment. Additionally, the k_D values of the Fab monomer were constant and close to zero (Table 6-2 and Figure 6-3 B). Thus, the aggregation of Fab was initiated presumably by minimal structural perturbation. At the low pH of 5.0 without the shielding effect of NaCl, no Fab precipitation was observed, and R_h was still below 10 nm at 80 °C, although the k_D value decreased at higher temperatures and negative A_2^* values occurred. This might be a hint that the TIM equation is valid only for the full mAbs and cannot be transferred to individual Fab fragments. In contrast to the Fab part, the Fc fragment showed similar behavior as the full mAb. The CH3 transition was not observed by DSF in the case of the isolated fragment but was confirmed by DSC experiments (chapter 4.3.2). The formation of Fc aggregates started at the same temperature as the midpoint of protein unfolding ($T_m \approx T@R_h < 10$ nm; Table 6-2). Accompanied by the onset of unfolding of Fc, the k_D

value dropped sharply and negative A_2^* values occurred at $T@D_{0max}$, which suggests attractive forces favoring the aggregation that are presumably induced by the conformational change. Therefore, it is likely that the exposed hydrophobic patches of the lower melting CH2 domain are responsible for triggering the aggregation upon heating. As aggregation proceeds above $T@D_{0max}$, the k_D value cannot be discussed beyond this point.

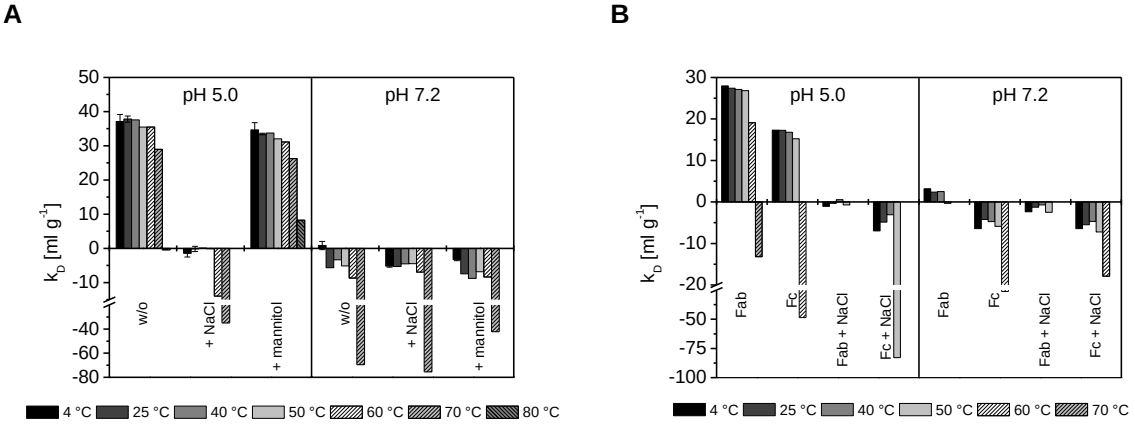

Figure 6-3. Interaction parameter k_D at selected low, ambient, and high temperatures of the mAb (A) and the Fab and Fc fragments (B) in various 10 mM phosphate buffer formulations at pH 7.2 and pH 5.0 with or without 140 mM sodium chloride.

Because of the homology of the Fc part for all human or humanized mAbs, one might assume that changes in thermal stability of the full mAb can be related to the Fab part. As was demonstrated for the mAb in this study, the thermal stability of the full protein is not reflected by simply summing up the behavior of the two separated fragments (compare Figure 6-2 B and also Table 6-2). The higher T_{m1} and $T_{m,onset}$ values of the first transition suggest a mutual stabilization of the Fc domain in the full mAb. Furthermore, the influence of hydrophobic interactions upon unfolding on Fab and Fc differed. With the exception of the strong repulsive conditions at pH 5.0 and low ionic strength, all samples finally precipitated at high temperature. The T_{agg} value corresponded to T_{m2}, which points to the fact that precipitation occurs after unfolding of the Fab and or the CH3 domain.

Table 6-2. Summary of the results from thermal analysis of the full MAb and its isolated Fab and Fc fragments in various formulations.

	pH 5.0							pH 7.2						
	w/o excipient			140 mM NaCl			280 mM mannitol	w/o excipient			140 mM NaCl			280 mM mannitol
	Full MAb	Fab	Fc	Full MAb	Fab	Fc	Full MAb	Full MAb	Fab	Fc	Full MAb	Fab	Fc	Full MAb
Temp. [°C]														
T_{m1}	63.8±0.3	80.8±0.4	58.7±0.1	60.5±0.2	79.4±0.4	58.3±0.3	65.4±0.3	68.4±0.1	78.7±0.1	65.5±0.2	67.3±0.1	78.0±0.1	65.1±0.3	69.4±0.4
T_{m2}	81.6±0.1			80.4±0.1			86.1±0.6	81.5±0.1			82.2±0.1			82.4±0.1
$T_{m,onset}$	54.4±0.4	71.9±0.8	40.5±0.6	48.6±0.2	70.9±0.4	41.0±0.7	56.7±0.9	59.3±0.1	68.8±0.1	50.6±0.2	57.3±0.8	68.2±0.4	50.7±0.6	60.7±0.1
T_{agg}	-	-	-	85.2	77.5	76.8	-	79.5	71.7	76.3	80.5	72.1	80.6	80.5
$T_{agg,onset}$	-	-	-	82.7	75.1	73.9	-	77.1	66.3	70.7	78.2	68.6	78.2	78.1
$T@R_h<10nm$	80	80	70	70	60	50	80	65	55	65	65	55	65	65
$T@D_{0max}$	75	70	60	65	55	50	75	60	55	60	60	55	60	60
k_D [ml g^{-1}]														
k_D (4 °C)	37.1±2.1	28.0	17.3	-1.5±1.0	-1.1	-7.0	34.6±2.1	0.8±1.2	3.2	-6.4	-5.2±0.3	-2.4	-6.4	-3.3±0.3
k_D (25 °C)	37.8±0.9	27.4	17.3	-0.2±0.8	-0.3	-4.9	33.4±0.2	-5.7	2.4	-4.2	-5.3	-1.3	-5.5	-7.4
k_D ($T_{m,onset}$)	36.3	-13.2	16.8	-0.1	n.d.	-3.1	29.1	-8.6	n.d.	-4.7	-5.4	n.d.	-4.7	-8.4
k_D ($T@D_{0max}$)	9.8	-13.2	-48.5	-31.9	-12.2	-82.9	15.0	-8.6	-0.4	-26.2	-6.9	-6.9	-17.9	-8.4
A_2^* [mol ml g^{-}														
A_2^* (4 °C)	$2.4\ 10^{-4}$	$1.9\ 10^{-4}$	$1.3\ 10^{-4}$	$2.7\ 10^{-5}$	$2.7\ 10^{-5}$	$-3.9\ 10^{-6}$	$2.3\ 10^{-4}$	$4.0\ 10^{-5}$	$5.3\ 10^{-5}$	$-7.4\ 10^{-7}$	$6.1\ 10^{-6}$	$2.2\ 10^{-5}$	$-7.4\ 10^{-7}$	$1.7\ 10^{-5}$
A_2^* (25 °C)	$2.5\ 10^{-4}$	$1.9\ 10^{-4}$	$1.3\ 10^{-4}$	$3.4\ 10^{-5}$	$3.4\ 10^{-5}$	$8.0\ 10^{-6}$	$2.2\ 10^{-4}$	$3.3\ 10^{-6}$	$4.9\ 10^{-5}$	$1.2\ 10^{-5}$	$5.6\ 10^{-6}$	$2.8\ 10^{-5}$	$4.5\ 10^{-6}$	$-6.8\ 10^{-6}$
A_2^* ($T_{m,onset}$)	$2.4\ 10^{-4}$	$-3.9\ 10^{-5}$	1.310^{-4}	$3.5\ 10^{-5}$	n.d.	$1.8\ 10^{-5}$	$2.0\ 10^{-4}$	$-1.3\ 10^{-5}$	n.d.	$8.8\ 10^{-6}$	$5.0\ 10^{-6}$	n.d.	$9.1\ 10^{-6}$	$-1.2\ 10^{-5}$
A_2^* ($T@D_{0max}$)	$9.1\ 10^{-5}$	$-3.9\ 10^{-5}$	$-2.4\ 10^{-4}$	$-1.4\ 10^{-4}$	$-3.3\ 10^{-5}$	$-4.3\ 10^{-4}$	$1.2\ 10^{-4}$	$-1.3\ 10^{-5}$	$3.3\ 10^{-5}$	$-1.1\ 10^{-4}$	$-3.4\ 10^{-6}$	$-3.3\ 10^{-6}$	$-6.5\ 10^{-5}$	$-1.2\ 10^{-5}$
D_0 [$cm^2\ s^{-1}$]														
D_0 (25 °C)	$4.6\ 10^{-7}$	$8.2\ 10^{-7}$	$7.5\ 10^{-7}$	$4.8\ 10^{-7}$	$8.2\ 10^{-7}$	$7.5\ 10^{-7}$	$4.3\ 10^{-7}$	$4.8\ 10^{-7}$	$8.2\ 10^{-7}$	$7.5\ 10^{-7}$	$4.8\ 10^{-7}$	$8.2\ 10^{-7}$	$7.5\ 10^{-7}$	$4.4\ 10^{-7}$
R_h [nm]														
R_h (4 °C)	4.8±0.1	2.7±0.1	3.0±0.1	5.0±0.1	2.9±0.1	3.2±0.1	4.9±0.1	5.2±0.2	2.9±0.1	3.2±0.1	5.1±0.1	2.9±0.1	3.2±0.1	5.4±0.1
R_h (25 °C)	4.8±0.1	2.7±0.1	3.0±0.1	5.1±0.1	2.9±0.1	3.2±0.1	4.8±0.1	5.1±0.1	2.9±0.1	3.2±0.1	5.1±0.1	2.9±0.1	3.2±0.1	5.0±0.1
R_h ($T_{m,onset}$)	4.8±0.1	3.2±0.1	3.1±0.1	5.1±0.1	n.d.	3.2±0.1	4.5±0.1	5.2±0.1	n.d.	3.3±0.1	5.1±0.1	n.d.	3.3±0.1	5.0±0.1
R_h ($T@D_{0max}$)	5.6±0.1	3.2±0.1	3.5±0.1	6.1±0.1	2.9±0.1	3.4±0.1	5.4±0.1	5.2±0.1	3.0±0.1	3.5±0.1	5.3±0.1	3.3±0.1	3.5±0.1	5.0±0.1

T_{m1} and T_{m2} are the first and second apparent melting temperatures determined by DSF, respectively. $T_{m,onset}$ is the temperature of unfolding calculated by a tangent based algorithm of the Boltzmann fit function on the first unfolding transition observed by DSF. The temperature of aggregation (T_{agg}) and its onset value ($T_{agg,onset}$) are determined by temperature-ramped turbidity measurements. The hydrodynamic radius (R_h) at various temperatures, the temperature at which R_h of the molecule is still below 10 nm ($T@R_h < 10$ nm), the diffusion coefficient at infinite dilution (D_0), the temperature at which D_0 reached a maximum value ($T@D_{0max}$), and the interaction parameter (k_D) at various temperatures were derived from temperature-ramped DLS measurements. In case of $T_{m,onset} > T@D_{0max}$, the value for R_h and k_D/A_2^* at $T_{m,onset}$ was not determined (n.d.).

6.4.4 Interpretation of k_D at elevated temperatures

The k_D value was also investigated by Rubin and coworkers at 25 °C, 35 °C, and 45 °C in a study on the influence of Hofmeister salts on mAb aggregation.[38] They observed that the formulation induced differences of k_D diminished at the elevated temperatures and therefore suggested that k_D measurements are supposed to be performed at ambient temperatures.[38] As was demonstrated in this study, the analysis of k_D at even higher temperatures allowed the interpretation of aggregation and interaction in combination with conformational stability. A similar temperature-ramped DLS experiment was performed by Kenrick and Some, recently.[58] They also observed a drop of k_D at temperatures where R_h of the protein increased.[58] Because of the increased R_h due to aggregation, we emphasize the interpretation of k_D values only up to $T@D_{0max}$ where the protein is still in its monomeric form. It would be interesting to investigate k_D at temperatures beyond $T@D_{0max}$ to analyze the interaction between the aggregates. But the inhomogeneity of the aggregate population and a nonlinearity of D, e.g., due to concentration dependent aggregation kinetics even in the diluted state create major hurdles. One option to investigate the interaction parameter of oligomers was presented by Printz et al. using HP-SEC in combination with subsequent online SLS/UV detection but this method is only suitable for small soluble aggregates.[59] Interestingly, they found A_2 values of induced dimers and small oligomers that were close to the value of the monomer.

6.4.5 Temperature-ramped analysis for pharmaceutical protein formulation development

During formulation development of a therapeutic protein, material and time consumption are important factors of any analytical method. Table 6-3 compares the investigated methods with respect to these parameters and suggests a value for pharmaceutical formulation development. The analysis of T_m is essential for the assessment of the conformational stability of the protein. It also allows the investigation of mAb domains, which can unfold individually or show a cooperative unfolding. The advantages of DSF compared with conventional DSC are the high-throughput design with small sample volumes and short analysis times, which renders this method essential for formulation development. DSC is needed for the detailed thermodynamic characterization based on heat capacity data with high resolution of all unfolding events or when excipients like surfactants challenge the

application of DSF, although the gaps for application are closing.[41,60,61] Furthermore, DSF in combination with k_D and A_2^* analysis at higher temperatures helps to understand the link between unfolding, intermolecular interactions, and aggregation upon heating.

Table 6-3. Overview of the thermal stability parameters assessed in this study.

Analytical method Outcome parameter	Outcome	Material and time consumption (on the example of this study)	Value for pharm. formulation develop.
DSF T_m, $T_{m,onset}$	Conformational stability; exposure of hydrophobic sites upon thermal unfolding	3x 20 µl = 48 µg Time: low	Essential
DLS k_D	Net intermolecular interactions; prediction of aggregation tendency,[26,36,47,62] viscosity at higher concentration,[26,34,44,52] crystallizability[17,18,21,22,25]	7x (3x 30 µl) = 8.5 mg Time: medium	Essential
DLS (Temp.-ramped) k_D (T)	Interaction tendency at higher temperature and upon thermal unfolding	7x (3x 30 µl) = 8.5 mg Time: high	Remarkable
DLS (Temp.-ramped) R_h (T)	Conformational stability; small aggregates upon thermal unfolding; association of native protein at higher temperature in combination with DSF	3x 30 µl = 108 - 225µg Time: medium/high	Essential
UV-Vis (Temp.-ramped) T_{agg}, $T_{agg,onset}$	Conformational stability; small aggregates upon thermal unfolding	1x 500 µl = 400 µg Time: high	Beneficial

Material and time consumption is based on the methods as used. The value for pharmaceutical formulation development is discussed in detail in the text.

Additionally, this temperature-ramped DLS measurement enables to observe the formation of small aggregates. In combination with the conformational stability data,[12] and HP-SEC data for small aggregates from stress tests at elevated temperatures, a detailed understanding of the aggregation behavior can be achieved. Although the importance of the interaction parameters with respect to aggregation,[26,36,45,62] viscosity at higher concentration,[26,34,44,52] and crystallization[17,18,21,22,25] prediction was demonstrated many times, the use of k_D at higher temperatures for the prediction of storage stability needs to be evaluated in future studies. Another aspect is the occurrence of large aggregates, which can be addressed by temperature-ramped turbidity measurements. The absence of large aggregates is a critical quality attribute of a protein product as demanded by the pharmacopoeias. Preliminary tests showed that the sample volume can be strongly reduced with the use of a 50 µl submicro glass cuvette (Hellma Analytics, Müllheim, Germany) compared with a standard cuvette (T_{agg} (500 µl, n=3) = 79.5±0.1 °C, T_{agg} (50 µl, n=3) = 79.3±0.1 °C; 0.8 mg/ml MAb in 10 mM phosphate buffer pH 7.2). High-throughput screenings of T_{agg} with small volumes can be performed with a temperature-ramp-controlled multiwell plate reader.

6.5 Summary

To investigate the intermolecular interactions during thermal unfolding and aggregation of a mAb and additionally its Fab and Fc fragments, several protein stability parameters were investigated and compared. First, the T_m and $T_{m,onset}$ values were determined by DSF to obtain the information of the process of unfolding. An analysis of the cleaved mAb allowed a clear assignment of the unfolding events of the Fab and the Fc domain. Second, the T_{agg} was assessed by temperature-ramped light absorption measurements at 350 nm detecting the formation of large protein aggregates upon heating. Finally, by performing temperature-ramped DLS measurements, the formation of small aggregates was monitored by the increase in the hydrodynamic radius R_h and additionally, the interaction parameter k_D at refrigerated, ambient, and high temperature was calculated as long as the monomer was observed. On the basis of literature results, an equation for the transformation of the interaction parameters of mAbs (“TIM”) was determined, which allows an empirical translation from k_D into A_2^* for the interpretation of net attraction or repulsion. At the low pH of 5.0 and low ionic strength, electrostatic repulsion reflected

in a high k_D and positive A_2^* values prevented both the full mAb and the fragments from precipitation at high temperatures, despite substantial exposure of hydrophobic patches upon unfolding as demonstrated by DSF. At pH 7.2 as well as at pH 5.0 with charge shielding effect by 150 mM NaCl, MAb, Fab, and Fc showed a different behavior. Already at about 55 - 60 °C, below the onset temperature of unfolding, the Fab fragment started to aggregate. The k_D values of the Fab monomer were constant over the observed temperature range and close to zero, suggesting that the aggregation of Fab was triggered already by a minimal perturbation of the native structure. In contrast, at temperatures where the Fc fragment started to unfold, the k_D dropped strongly to negative k_D and negative A_2^* values. Therefore, the newly exposed hydrophobic patches upon unfolding, which facilitate the interaction with the fluorescent dye, mediated hydrophobic interactions that led to the aggregation of the protein. Finally, all proteins in case of neutral pH or charge shielding by NaCl addition formed a precipitate after CH3 domain and Fab unfolded upon heating. Similar results were observed for the full mAb, although a mutual conformational stabilization in relation to the isolated fragments is suggested by the T_m values. At the same time, a low apparent T_m value was found at the low pH of 5.0, suggesting a conformational destabilization. The addition of excipients such as salt or mannitol was found to be of minor influence on the T_m value compared with the effect of pH. The new and beneficial information from interaction parameter analysis at elevated and high temperatures helped to understand the link between unfolding and aggregation of the MAb as well as the role of the individual Fab and Fc fragments. We emphasize the integration of temperature-ramped screenings for the analysis of unfolding, aggregation, and interaction during formulation development of therapeutic protein drugs.

6.6 Acknowledgements

The DLS measurements using the DnyaPro plate reader were performed at the Wyatt Technologies Europe headquarter in Dernbach, Germany. We gratefully thank Wyatt Technologies for this opportunity.

6.7 References

1. Beck A, Wurch T, Bailly C, Corvaia N 2010. Strategies and challenges for the next generation of therapeutic antibodies. Nat Rev Immunol 10(5):345-352.

2. Manning M, Chou D, Murphy B, Payne R, Katayama D 2010. Stability of Protein Pharmaceuticals: An Update. Pharm Res 27(4):544-575.

3. Wang W 1999. Instability, stabilization, and formulation of liquid protein pharmaceuticals. Int J Pharm 185(2):129-188.

4. Chi EY, Krishnan S, Randolph TW, Carpenter JF 2003. Physical Stability of Proteins in Aqueous Solution: Mechanism and Driving Forces in Nonnative Protein Aggregation. Pharm Res 20(9):1325-1336.

5. Mahler H-C, Friess W, Grauschopf U, Kiese S 2009. Protein aggregation: Pathways, induction factors and analysis. J Pharm Sci 98(9):2909-2934.

6. Wang W, Singh SK, Li N, Toler MR, King KR, Nema S 2012. Immunogenicity of protein aggregates—Concerns and realities. Int J Pharm 431(1–2):1-11.

7. Jiskoot W, Randolph TW, Volkin DB, Middaugh CR, Schöneich C, Winter G, Friess W, Crommelin DJA, Carpenter JF 2012. Protein instability and immunogenicity: Roadblocks to clinical application of injectable protein delivery systems for sustained release. J Pharm Sci 101(3):946-954.

8. Samra HS, He F 2012. Advancements in High Throughput Biophysical Technologies: Applications for Characterization and Screening during Early Formulation Development of Monoclonal Antibodies. Mol Pharm 9(4):696-707.

9. Youssef AMK, Winter G 2013. A critical evaluation of microcalorimetry as a predictive tool for long term stability of liquid protein formulations: Granulocyte Colony Stimulating Factor (GCSF). Eur J Pharm Biopharm 84(1):145-155.

10. He F, Hogan S, Latypov RF, Narhi LO, Razinkov VI 2010. High throughput thermostability screening of monoclonal antibody formulations. J Pharm Sci 99(4):1707-1720.

11. King AC, Woods M, Liu W, Lu Z, Gill D, Krebs MRH 2011. High-throughput measurement, correlation analysis, and machine-learning predictions for pH and thermal stabilities of Pfizer-generated antibodies. Protein Sci 20(9):1546-1557.

12. Goldberg DS, Bishop SM, Shah AU, Sathish HA 2011. Formulation development of therapeutic monoclonal antibodies using high-throughput fluorescence and static light scattering techniques: Role of conformational and colloidal stability. J Pharm Sci 100(4):1306-1315.

13. Zölls S, Tantipolphan R, Wiggenhorn M, Winter G, Jiskoot W, Friess W, Hawe A 2012. Particles in therapeutic protein formulations, Part 1: Overview of analytical methods. J Pharm Sci 101(3):914-935.

14. Saluja A, Kalonia DS 2008. Nature and consequences of protein-protein interactions in high protein concentration solutions. Int J Pharm 358(1-2):1-15.

15. Neal BL, Asthagiri D, Lenhoff AM 1998. Molecular Origins of Osmotic Second Virial Coefficients of Proteins. Biophys J 75(5):2469-2477.

16. Zimm BH 1946. Application of the Methods of Molecular Distribution to Solutions of Large Molecules. The Journal of Chemical Physics 14(3):164-179.

17. Deshpande KS, Ahamed T, ter Horst JH, Jansens PJ, van der Wielen LAM, Ottens M 2009. The use of self-interaction chromatography in stable formulation and crystallization of proteins. Biotechnol J 4(9):1266-1277.

18. George A, Chiang Y, Guo B, Arabshahi A, Cai Z, Wilson WW 1997. Second virial coefficient as predictor in protein crystal growth. Methods Enzymol 276:100-110.

19. Tessier PM, Vandrey SD, Berger BW, Pazhianur R, Sandler SI, Lenhoff AM 2002. Self-interaction chromatography: a novel screening method for rational protein crystallization. Acta Crystallographica Section D 58(10 Part 1):1531-1535.

20. Haas C, Drenth J, Wilson WW 1999. Relation between the Solubility of Proteins in Aqueous Solutions and the Second Virial Coefficient of the Solution. The Journal of Physical Chemistry B 103(14):2808-2811.

21. Guo B, Kao S, McDonald H, Asanov A, Combs LL, William Wilson W 1999. Correlation of second virial coefficients and solubilities useful in protein crystal growth. J Cryst Growth 196(2-4):424-433.

22. Deszczynski M, Harding SE, Winzor DJ 2006. Negative second virial coefficients as predictors of protein crystal growth: Evidence from sedimentation equilibrium studies that refutes the designation of those light scattering parameters as osmotic virial coefficients. Biophys Chem 120(2):106-113.

23. Berger BW, Gendron CM, Lenhoff AM, Kaler EW 2006. Effects of additives on surfactant phase behavior relevant to bacteriorhodopsin crystallization. Protein Sci 15(12):2682-2696.

24. Ahamed T, Ottens M, van Dedem GWK, van der Wielen LAM 2005. Design of self-interaction chromatography as an analytical tool for predicting protein phase behavior. J Chromatogr A 1089(1–2):111-124.

25. Rosenbaum DF, Zukoski CF 1996. Protein interactions and crystallization. J Cryst Growth 169(4):752-758.

26. Saito S, Hasegawa J, Kobayashi N, Kishi N, Uchiyama S, Fukui K 2012. Behavior of Monoclonal Antibodies: Relation Between the Second Virial Coefficient (B 2) at Low Concentrations and Aggregation Propensity and Viscosity at High Concentrations. Pharm Res 29(2):397-410.

27. Connolly Brian D, Petry C, Yadav S, Demeule B, Ciaccio N, Moore Jamie MR, Shire Steven J, Gokarn Yatin R 2012. Weak Interactions Govern the Viscosity of Concentrated Antibody Solutions: High-Throughput Analysis Using the Diffusion Interaction Parameter. Biophys J 103(1):69-78.

28. Martin C, Lenhoff AM 2011. Self-interaction chromatography of proteins on a microfluidic monolith. Biochem Eng J 53(2):216-222.

29. Valente JJ, Payne RW, Manning MC, Wilson WW, Henry CS 2005. Colloidal behavior of proteins: effects of the second virial coefficient on solubility, crystallization and aggregation of proteins in aqueous solution. Curr Pharm Biotechnol 6(6):427-436.

30. Winzor DJ, Scott DJ, Wills PR 2007. A simpler analysis for the measurement of second virial coefficients by self-interaction chromatography. Anal Biochem 371(1):21-25.

31. Deshpande KS, Kuddannaya S, Staginus J, Thüne PC, de Smet LCPM, ter Horst JH, van der Wielen LAM, Ottens M 2012. Biofunctionalization and self-interaction chromatography in PDMS microchannels. Biochem Eng J 67(0):111-119.

32. Yadav S, Scherer TM, Shire SJ, Kalonia DS 2011. Use of dynamic light scattering to determine second virial coefficient in a semidilute concentration regime. Anal Biochem 411(2):292-296.

33. Teraoka I. 2002. Polymer solutions, an introduction to physical properties. ed., New York: Wiley-Interscience.

34. Yadav S, Shire SJ, Kalonia DS 2010. Factors affecting the viscosity in high concentration solutions of different monoclonal antibodies. J Pharm Sci 99(12):4812-4829.

35. Chari R, Jerath K, Badkar A, Kalonia D 2009. Long- and Short-Range Electrostatic Interactions Affect the Rheology of Highly Concentrated Antibody Solutions. Pharm Res 26(12):2607-2618.

36. Kumar V, Dixit N, Zhou L, Fraunhofer W 2011. Impact of short range hydrophobic interactions and long range electrostatic forces on the aggregation kinetics of a monoclonal antibody and a dual-variable domain immunoglobulin at low and high concentrations. Int J Pharm 421(1):82-93.

37. Arzenšek D, Kuzman D, Podgornik R 2012. Colloidal interactions between monoclonal antibodies in aqueous solutions. J Colloid Interface Sci 384(1):207-216.

38. Rubin J, Linden L, Coco WM, Bommarius AS, Behrens SH 2013. Salt-induced aggregation of a monoclonal human immunoglobulin G1. J Pharm Sci 102(2):377-386.

39. Lehermayr C, Mahler H-C, Mäder K, Fischer S 2011. Assessment of net charge and protein–protein interactions of different monoclonal antibodies. J Pharm Sci 100(7):2551-2562.

40. Wakankar AA, Borchardt RT, Eigenbrot C, Shia S, Wang YJ, Shire SJ, Liu JL 2007. Aspartate Isomerization in the Complementarity-Determining Regions of Two Closely Related Monoclonal Antibodies. Biochemistry (Mosc) 46(6):1534-1544.

41. Menzen T, Friess W 2013. High-throughput melting-temperature analysis of a monoclonal antibody by differential scanning fluorimetry in the presence of surfactants. J Pharm Sci 102(2):415-428.

42. Liu Y, Shi M, Cao R, Zhang Y, Hu Y 2007. Densities and Viscosities of the Quaternary System Mannitol-Sorbitol-D-Glucose-H2O and Its Ternary Subsystems at 298.15K. Chin J Chem Eng 15(5):703-709.

43. Schiebener P, Straub J, Sengers JMHL, Gallagher JS 1990. Refractive index of water and steam as function of wavelength, temperature and density. J Phys Chem Ref Data 19(3):677-717.

44. Saluja A, Badkar AV, Zeng DL, Nema S, Kalonia DS 2007. Ultrasonic storage modulus as a novel parameter for analyzing protein-protein interactions in high protein concentration solutions: correlation with static and dynamic light scattering measurements. Biophys J 92(1):234-244.

45. Saluja A, Fesinmeyer RM, Hogan S, Brems DN, Gokarn YR 2010. Diffusion and sedimentation interaction parameters for measuring the second virial coefficient and their utility as predictors of protein aggregation. Biophys J 99(8):2657-2665.

46. Cohen J, Cohen P, West SG, Aiken LS. 2003. Applied Multiple Regression/Correlation Analysis for the Behavioral Sciences. ed., Mahawah, NY: Erlbaum.

47. Zhang L, Tan H, Fesinmeyer RM, Li C, Catrone D, Le D, Remmele RL, Zhang J 2012. Antibody solubility behavior in monovalent salt solutions reveals specific anion effects at low ionic strength. J Pharm Sci 101(3):965-977.

48. Harding SE, Johnson P 1985. The concentration-dependence of macromolecular parameters. Biochem J 231(3):543-547.

49. Jossang T, Feder J, Rosenqvist E 1988. Photon correlation spectroscopy of human IgG. J Protein Chem 7(2):165-171.

50. Cheng W, Joshi SB, Jain NK, He F, Kerwin BA, Volkin DB, Middaugh CR 2013. Linking the Solution Viscosity of an IgG2 Monoclonal Antibody to Its Structure as a Function of pH and Temperature. J Pharm Sci 102(12):4291-4304.

51. Yadav S, Sreedhara A, Kanai S, Liu J, Lien S, Lowman H, Kalonia D, Shire S 2011. Establishing a Link Between Amino Acid Sequences and Self-Associating and Viscoelastic Behavior of Two Closely Related Monoclonal Antibodies. Pharm Res 28(7):1750-1764.

52. Yadav S, Liu J, Shire SJ, Kalonia DS 2010. Specific interactions in high concentration antibody solutions resulting in high viscosity. J Pharm Sci 99(3):1152-1168.

53. Niesen FH, Berglund H, Vedadi M 2007. The use of differential scanning fluorimetry to detect ligand interactions that promote protein stability. Nat Protocols 2(9):2212-2221.

54. Ejima D, Tsumoto K, Fukada H, Yumioka R, Nagase K, Arakawa T, Philo JS 2007. Effects of acid exposure on the conformation, stability, and aggregation of monoclonal antibodies. Proteins: Struct, Funct, Bioinf 66(4):954-962.

55. Ionescu RM, Vlasak J, Price C, Kirchmeier M 2008. Contribution of variable domains to the stability of humanized IgG1 monoclonal antibodies. J Pharm Sci 97(4):1414-1426.

56. GE Healthcare. 2011. Better guidance in antibody therapeutics process development using differential scanning calorimetry. MicroCal application note 28-9870-45 AA. Accessed 05/13/2013, at: www.gelifesciences.com.

57. Latypov RF, Hogan S, Lau H, Gadgil H, Liu D 2012. Elucidation of Acid-induced Unfolding and Aggregation of Human Immunoglobulin IgG1 and IgG2 Fc. J Biol Chem 287(2):1381-1396.

58. Kenrick S, Some D 2013. High-throughput analysis of protein formulations by DLS: thermal stability, colloidal stability and a thermal anomaly in the colloidal stability parameter D1. Colorado Protein Stability Conference Breckenridge, CO:poster presentation.

59. Printz M, Kalonia DS, Friess W 2012. Individual second virial coefficient determination of monomer and oligomers in heat-stressed protein samples using size-exclusion chromatography-light scattering. J Pharm Sci 101(1):363-372.

60. Shi S, Semple A, Cheung J, Shameem M 2013. DSF method optimization and its application in predicting protein thermal aggregation kinetics. J Pharm Sci 102(8):2471-2483.

61. Ablinger E, Hellweger M, Leitgeb S, Zimmer A 2012. Evaluating the effects of buffer conditions and extremolytes on thermostability of granulocyte colony-stimulating factor using high-throughput screening combined with design of experiments. Int J Pharm 436(1–2):744-752.

62. Zhang J, Liu XY 2003. Effect of protein--protein interactions on protein aggregation kinetics. The Journal of Chemical Physics 119(20):10972-10976.

6.8 Supplementary information

The graphs in Figure 6-4 till 6-6 have not been published with the main article and additionally illustrate the data of Table 6-2 to highlight the described effects.

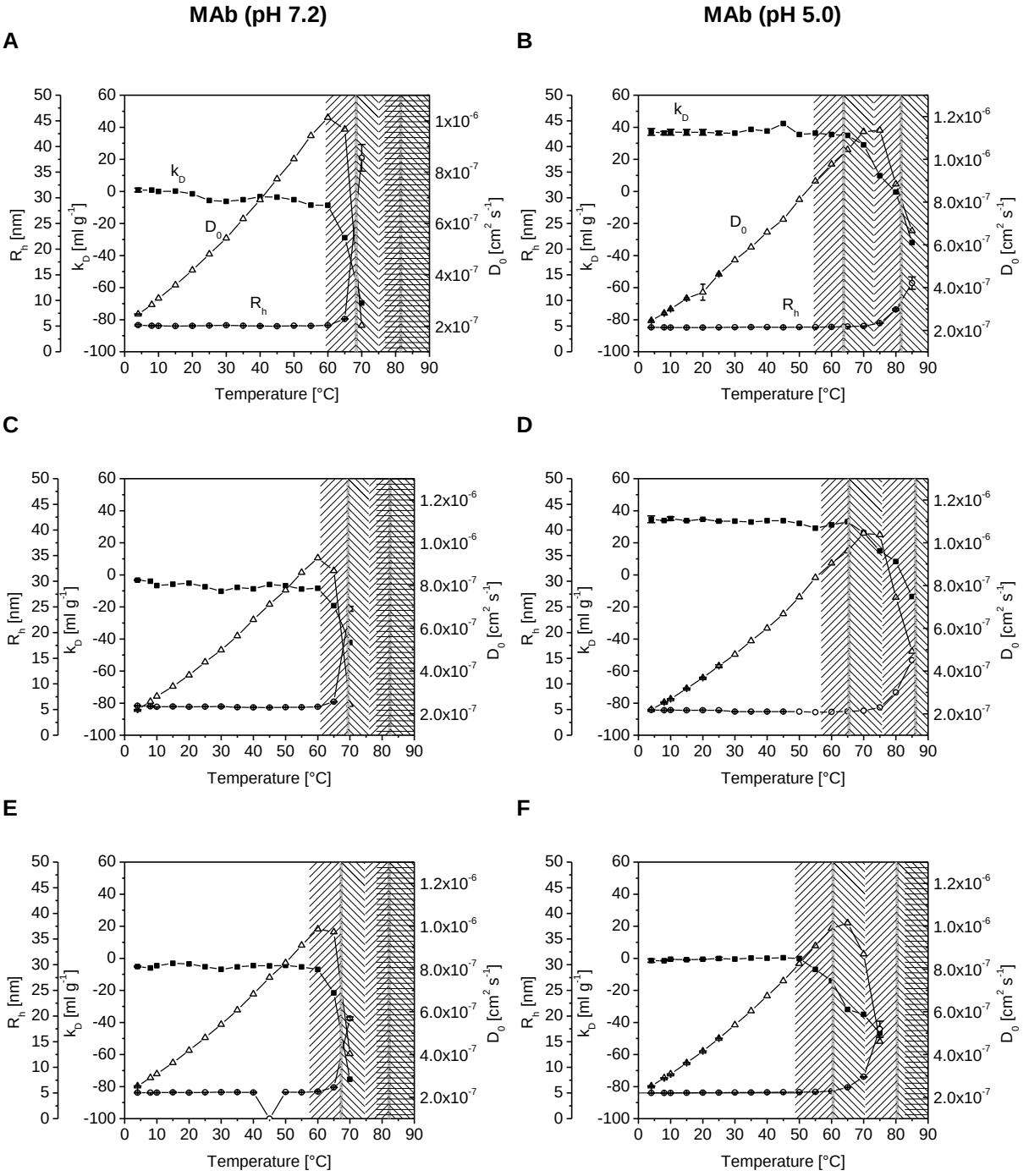

Figure 6-4. Hydrodynamic radius R_h, interaction parameter k_D, and diffusion coefficient at infinite dilution D_0 as a function of temperature of the mAb in 10 mM phosphate buffers (A + B) and with mannitol (C + D) or NaCl (E + F). The onset of unfolding is illustrated by diagonal shades with apparent T_m values in the center as observed by DSF. The occurrence of turbidity is marked by horizontal shades.

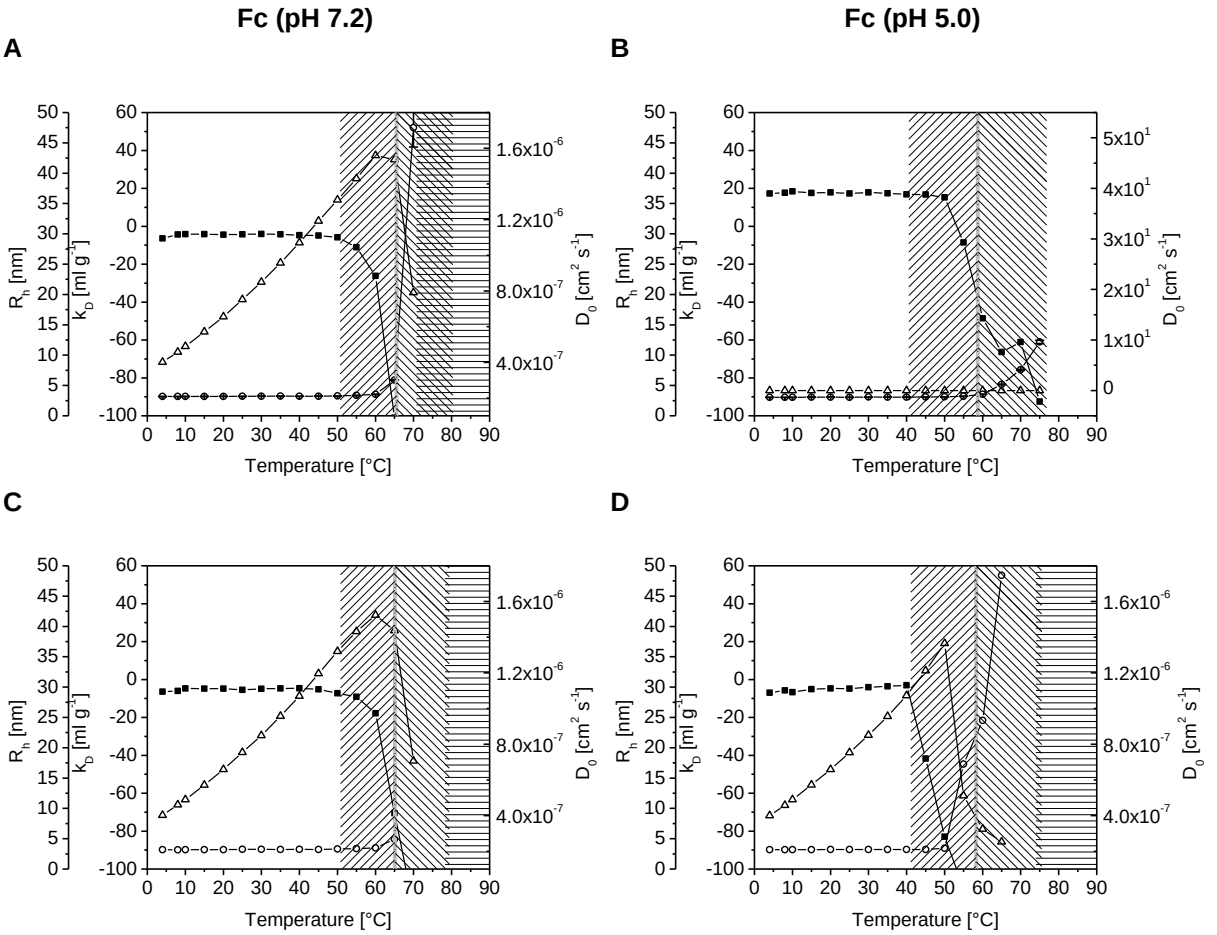

Figure 6-5. Hydrodynamic radius R_h, interaction parameter k_D, and diffusion coefficient at infinite dilution D_0 as a function of temperature of the Fc fragment in 10 mM phosphate buffers (A + B) and with NaCl (C + D). The onset of unfolding is illustrated by diagonal shades with apparent T_m values in the center as observed by DSF. The occurrence of turbidity is marked by horizontal shades.

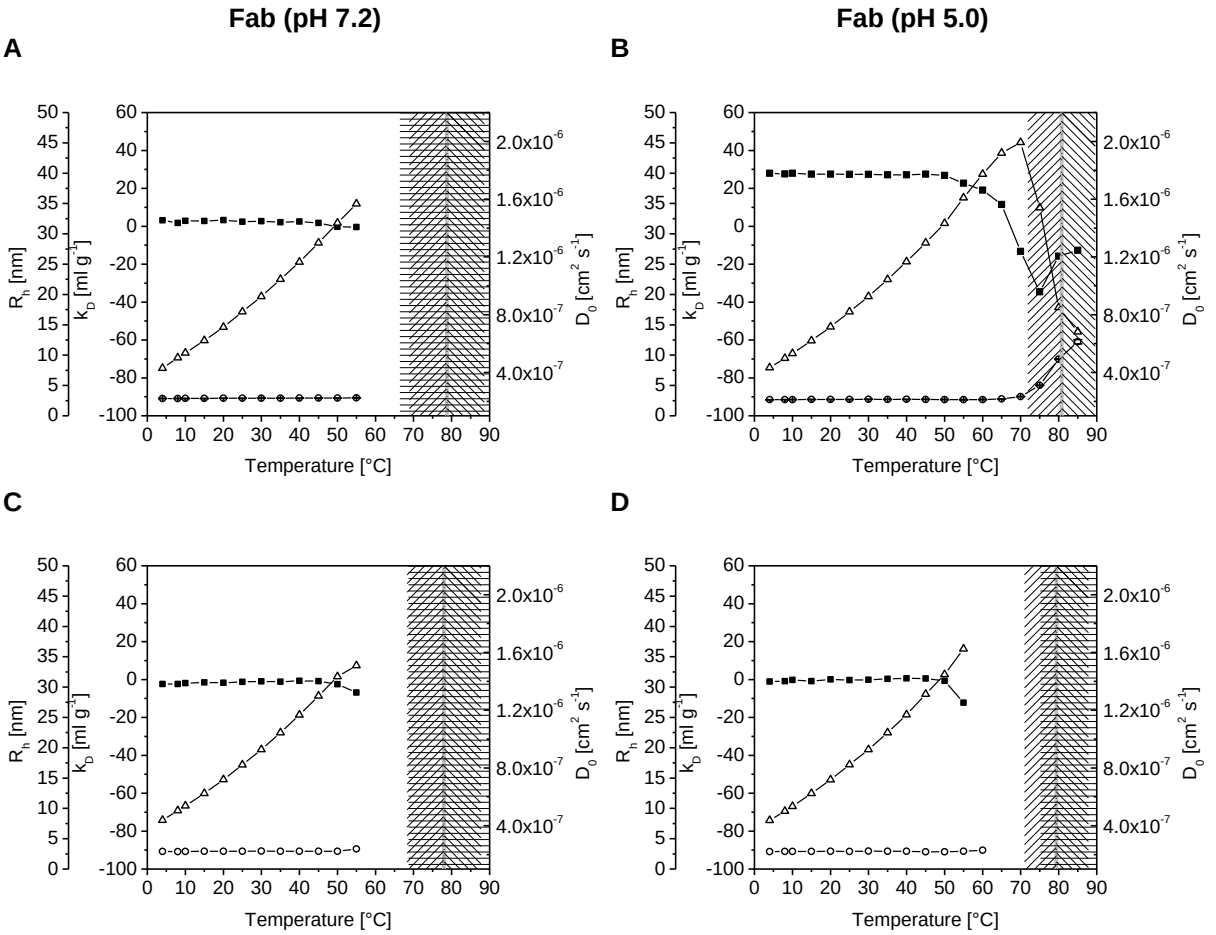

Figure 6-6. Hydrodynamic radius R_h, interaction parameter k_D, and diffusion coefficient at infinite dilution D_0 as a function of temperature of the Fab fragment in 10 mM phosphate buffers (A + B) and with NaCl (C + D). The onset of unfolding is illustrated by diagonal shades with apparent T_m values in the center as observed by DSF. The occurrence of turbidity is marked by horizontal shades.

7 Aggregate growth analyzed by fluorescence (cross-) correlation spectroscopy

7.1 Introduction

The interaction between protein molecules is responsible for protein aggregation, and involves both short- (hard sphere, van der Waals, hydrophobic interactions, etc.) and long range (electrostatic) forces.[1] The interaction parameters k_D or A_2, which are closely related (see TIM equation, chapter 6.3.6), therefore should be investigated routinely during development of therapeutic proteins.[1-5] Negative, i.e., attractive interaction parameters were observed between mAb monomers upon thermal unfolding, leading to irreversible nonnative protein aggregates supposedly due to hydrophobic interactions (chapter 6). Consequently, the analysis of intermolecular interactions between aggregates and monomers is highly appreciated to investigate potential nucleation-driven aggregation as a process for aggregate propagation,[6] as heterogeneous nucleation by sheds from glass and pumps has been reported in literature for other proteins,[7] and mAbs in particular.[8] In contrast, Kiese et al. spiked native-like mAb aggregates from shaking and denatured mAb particles from heat stress to unstressed mAb formulations, and found no indication for homogenous nucleation upon storage.[9] But both k_D and A_2 describe the net effects arising from protein-protein interactions between the same (monomeric) molecules. Printz et al. determined A_2 between small mAb higher molecular weight species after separation by HP-SEC and found preferential interaction between the higher molecular weight species as compared with the interaction between monomeric species.[10] Hence, the interaction parameters between the same (aggregated) species are obtained, but the question regarding the interaction between monomer and aggregates is not addressed. The interaction parameter between two different protein molecules A_{23}, can be analyzed, e.g., by cross-interaction chromatography.[11] Furthermore, surface plasmon resonance and the quartz crystal microbalance are sensitive to interactions between molecules, and can be adapted to investigate cross-species effects.[12-14] The similarity of these methods is the immobilization of one species to a resin or surface while the interaction of the analyte molecule is measured. For the analysis of two different species in solution, a method is necessary that can distinguish both

molecules and subsequently records a change upon interaction. A promising approach is the single particle analysis of fluorescently labeled molecules, which is presented in this chapter.

Fluorescence correlation spectroscopy (FCS) analyzes physicochemical properties of single fluorescent labeled molecules. A laser beam is focused to form a tiny confocal volume in the sample solution. At nanomolar concentrations of the labeled sample, single molecules get excited while diffusing through this illuminated volume, leading to fluctuations of the collected fluorescence intensity over time. By mathematically correlating the fluorescence intensity to itself after increasing lag time τ, an autocorrelation function can be derived. It describes the self-similarity of the signal over time. Thus, short residence in the confocal volume leads to a fast decay of the autocorrelation function. Whereas the diffusion time is related to the Brownian motion, either the viscosity of the solvent or the radius of (spherical) molecules can be calculated by the Stokes-Einstein equation, if the corresponding parameter is known. By extending the setup with a second laser and detector, two spectrally different dyes can be analyzed at the same time. This enables fluorescence cross-correlation spectroscopy (FCCS) in which fluctuations of both signals are correlated with each other. The resulting cross-correlation (CC) function describes the similarity between both colors. A high CC amplitude is observed when both dyes move uniformly. In case of molecules labeled with one distinct dye, a CC signal results from some strong interaction between both molecules, forcing them to move together through the confocal volume. For a fundamental introduction and applications of both FCS and FCCS, the reader is referred to the excellent reviews in literature.[15-17]

Protein aggregation is indicated via FCS by slower diffusion of the molecules due to their increased size. But large differences in molecular weight are necessary for a significant change in diffusion time so that the addition of single monomers to existing aggregates cannot be detected. Therefore, FCCS is used to detect a CC signal when molecules labeled with one dye are bound to aggregates which contain the other label, independent of their size. Consequently, the existing labeled aggregates have grown when CC is observed after addition of differently labeled monomers. A model IgG1 monoclonal antibody “MAb” was labeled with Alexa Fluor® 488 and 647, respectively. Labeled MAb aggregates are obtained by spiking of labeled MAb monomer to 2 mg/ml of the unlabeled MAb and applying thermal stress. FCS and

FCCS measurements are performed before and after the aggregates are formed, and furthermore upon addition of the differently labeled MAb to detect aggregate growth. In this case, the existing aggregates are either exposed to unstressed MAb monomer or a stressed sample.

7.2 Materials and methods

7.2.1 Preparation and purification of labeled protein

An IgG1 type monoclonal antibody MAb was dialyzed into 1 mM sodium phosphate buffer pH 6.0 using Vivaspin® 20 tubes with 30 kDa MWCO (Sartorius Stedim Biotech, Göttingen, Germany) and adjusted to 2 mg/ml using the NanoDrop 2000 photometer (Thermo Scientific, Wilmington, Delaware, USA) based on an extinction coefficient of 1.49 ml g^{-1} cm^{-1}. For covalent linking of the N-hydroxysuccinimide (NHS) ester of the fluorescent dye, the pH value of the solution was adjusted to 8.3 with 1 M sodium hydrogen carbonate. Alexa Fluor® 488 or Alexa Fluor® 647 (Life Technologies, Paisley, United Kingdom) dissolved in dimethyl sulfoxide (DMSO) was added to the MAb solution at a 1.2:1 ratio. The reaction was gently shaken and protected from light for one hour at room temperature. Subsequently, a 10-fold excess of a 1.5 M hydroxylamine solution at pH 8.5 was added. After 1 h of incubation the reaction mix was semi-quantitatively purified by HP-SEC using an Agilent 1100 HPLC system (Agilent Technologies, Santa Clara, California, USA) and a Tosoh TSKgel® G3000SW_{XL} column (7.8x300 mm) (Tosoh Bioscience, Stuttgart, Germany). Fractions of the reaction mix were injected using a mobile phase of 100 mM sodium phosphate buffer with additional 100 mM sodium sulfate pH 6.8 at a flow rate of 0.8 ml/min. The eluate containing the monomer fraction was collected after UV-detection at 280 nm, pooled, concentrated, and dialyzed into a 1 mM phosphate buffer pH 6.0 using a Vivaspin® 6 tube with 30 kDa MWCO. After purification, the degree of labeling (DOL) was determined photometrically using the NanoDrop 2000 photometer via the extinction coefficients and correction factors given by the manufacturer.

7.2.2 Thermal stress for the preparation of protein aggregate

Two formulations of 2 mg/ml MAb in 10 mM sodium phosphate buffer at pH 5.0, 140 mM sodium chloride (NaCl) and at pH 7.2, 280 mM mannitol were prepared.

Furthermore, 2 mg/ml MAb in phosphate buffered saline (PBS) solution pH 7.4 according to Dulbecco's formula containing sodium, potassium, magnesium, calcium, and chloride was used.[18] Labeled MAb (see chapter 7.2.1) was spiked into the samples to obtain the necessary nanomolar concentrations for FCS. Samples were heat stressed at 76 °C in Eppendorf Safe-Lock® tubes (Eppendorf, Hamburg, Germany) using an Eppendorf Thermomixer.

7.2.3 Fluorescence correlation spectroscopy (FCS) and fluorescence cross-correlation spectroscopy (FCCS)

FCS and FFCS were performed with a ConfoCor 3 (Carl Zeiss, Jena, Germany). Prior to the experiments, the z-plane and the x,y-position of the pinhole were adjusted to optimize the confocal volume with a Alexa Fluor® 488 solution. The optimal concentrations of the labeled MAb were evaluated based on the obtained count rates in the corresponding detector channels. A concentration of approx. 60 nM MAb_{AF488} and 350 nM MAb_{AF647} was consequently used throughout all FCS and FCCS measurements. Measurements were performed with unstressed (native) protein and samples after thermal stress (see chapter 7.2.2).

The fluorescence microscope was equipped with two laser light sources at 488 and 633 nm. The detector channels Ch1 and Ch2 were adjusted for the detection of the fluorescence signal from Alexa Fluor 488 and 647, respectively. One measurement run consisted of ten sequences of each 10 s acquisition time. Each sample measurement was replicated at least three times (usually five times) to gain statistical significance. Occasionally, large particles (typically observed with the stressed samples) generated a short massive increase ("spike") in the fluorescence count rate. A data set with such a spike is not suitable for autocorrelation analysis and was rejected. Data analysis was performed using an in-house MATLAB program (MathWorks, Natick, Massachusetts, USA) using a one component fit, which allowed corrections for triplet-blinking of the dye. Furthermore, background fluorescence of the solutions and cross-talk was taken into account. The results of the fits of each measurement run were averaged to obtain mean values with standard deviation.

The molecular weight of the aggregated species was estimated from reference measurements of green fluorescent protein (eGFP) with a known molecular mass of 28 kDa in the corresponding buffers. The diffusion time τ_D obtained by autocorrelation analysis was calculated using the following formula

$$M_{MAb} = M_{eGFP}\left(\frac{\tau_{D,MAb}}{\tau_{D,eGFP}}\right)^3 \quad (7\text{-}1)$$

with M the molar mass of the MAb and the reference eGFP.

7.3 Results and discussion

7.3.1 Autocorrelation (AC) analysis for the detection of protein aggregation

Diffusion times (τ_D) of MAb_{AF488} were obtained from AC analysis of the fluorescence signal in Ch1 (Figure 7-1 A). The native, unstressed labeled MAb molecule showed τ_D values of about 220 µs in the saline buffers. In the mannitol containing buffer, a higher τ_D value of 275 µs was observed as the viscosity is slightly higher due to the sugar alcohol (see DLS results in chapter 6). After thermal stress at 76 °C for 1 h, the increased diffusion times indicate the formation of aggregates containing the labeled MAb_{AF488}. At this temperature, the CH2 domain of the MAb but neither the Fab region nor the CH3 domain unfolded as indicated by DSF experiments (Table 6-2). Furthermore, the stress temperature was below $T_{agg,onset}$ where the formation of large aggregates was observed by turbidity measurements (chapter 6). This finding is in agreement with the formation of aggregates of rituximab at 60 °C that is initiated by at least partial unfolding of CH2 as described by Anderson et al.[19]

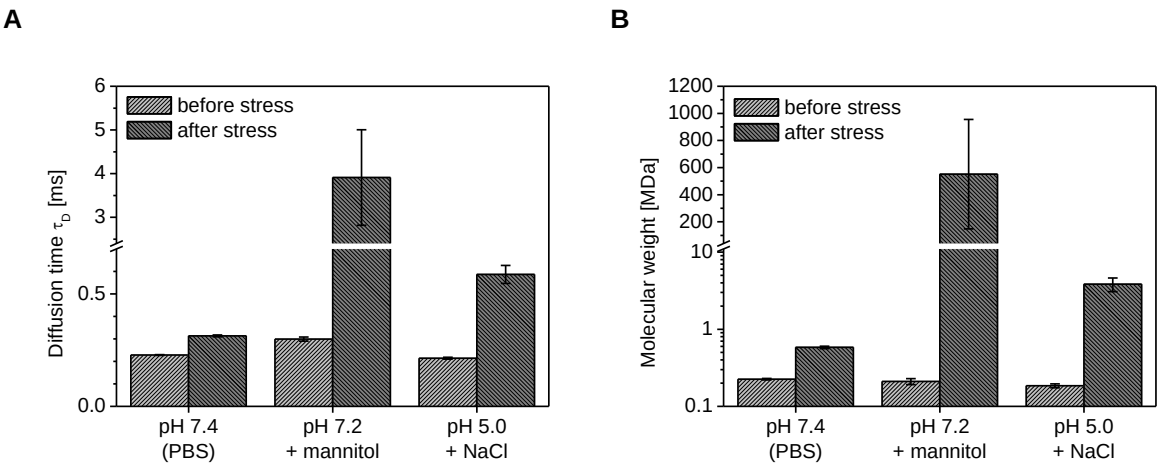

Figure 7-1. Diffusion times obtained by autocorrelation analysis of the samples before and after thermal stress (76 °C, 1 h) (A). The estimated molecular weight of the species obtained from extrapolation of the experimental diffusion time from eGFP (B).

The significantly slower diffusion indicates the formation of large aggregates. To estimate the average molecular weight of the aggregated species, the obtained τ_D

values were extrapolated from τ_D of eGFP with known molecular mass (Figure 7-1 B). In PBS pH 7.4 and pH 7.2 + mannitol, τ_D values of 114 and 152 µs were obtained for eGFP, respectively. eGFP showed a high amount of triplet-blinking at the low pH of 5.0 leading to false τ_D values, and thus a value of 114 µs was assumed for the NaCl containing buffer at pH 5.0. For the unstressed MAb, the estimated molar mass ranged between 185 – 225 kDa, which is a good indicator for the monomer within the precision of this approximation. The smallest aggregates of about 0.6 MDa were detected in physiological PBS, whereas particles in the range of 550 MDa formed in the mannitol containing buffer at pH 7.2. The repulsive positive net charges of the MAb at the low pH of 5.0 were substantially shielded as aggregates of about 4 MDa were observed (compare chapter 6). The approx. 1:200 ratio of labeled molecules suggests that the aggregates consisted predominately of unlabeled MAb.

7.3.2 Cross-correlation (CC) analysis for the detection of protein aggregation and aggregate growth

Additionally, samples containing both MAb_{AF488} and MAb_{AF647} and 2 mg/ml unlabeled MAb were stressed and analyzed. The results from CC analysis are presented in Figure 7-2 A. Before stressing the sample, no significant CC was observed suggesting that MAb_{AF488} and MAb_{AF647} diffuse freely in solution. After thermal stress at 76 °C for 1 h, a significant CC was obtained for all three formulations. Especially for the 10 mM phosphate buffer at pH 7.2 with 280 mM mannitol, a very high amount of about 15.5 % CC was observed. This indicates that significant amounts of both labeled molecules were incorporated in protein aggregates. Furthermore, these results confirm the AC analysis where the longest diffusion time, i.e. the largest aggregates, was observed for the same sample (see Figure 7-1).

Next, samples containing MAb_{AF488} and 2 mg/ml unlabeled MAb were stressed for 1 h at 76 °C. As presented in Figure 7-1 A, aggregates consisting of labeled and predominately unlabeled protein were formed. Subsequently, MAb_{AF647} was spiked into the solution of AF488-carrying MAb aggregates and the CC signal was analyzed after 30 min. A significant CC was observed for all three formulations (Figure 7-2 B). This result suggests that MAb_{AF647} attached or absorbed onto the aggregates which were previously formed by heat stress. Although less likely, a replacement of MAb molecules in the aggregates by new MAb molecules could also explain the increased CC. Interestingly, a different result was obtained when the MAb_{AF647} molecules were

stressed for 30 min at 76 °C. No significant CC was detected in this case (Figure 7-2 B). Thus, already formed MAb aggregates did not interact with other heat stress molecules or aggregates.

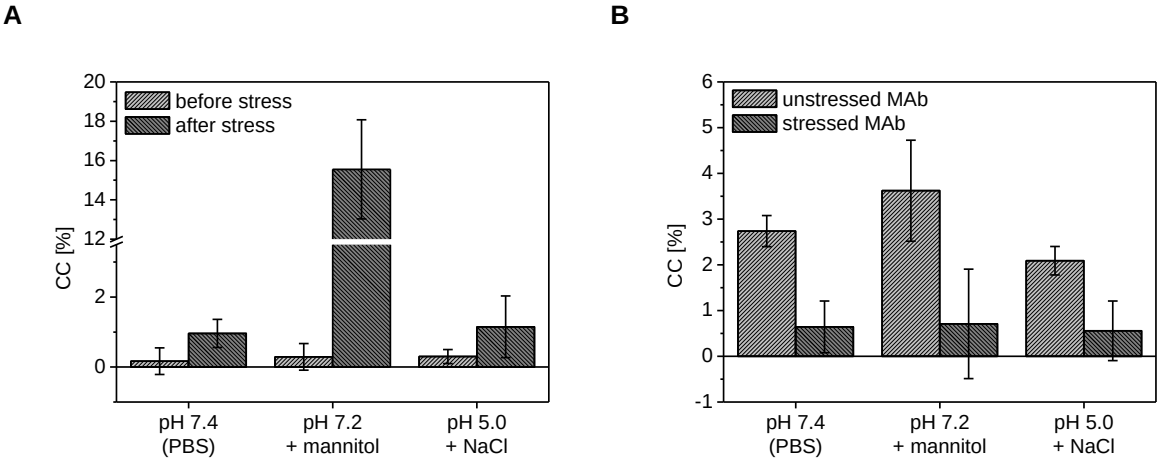

Figure 7-2. Results from cross-correlation (CC) analysis of the samples containing both labeled species before and after thermal stress (76 °C, 1 h) (A). Obtained CC signal when unstressed or stressed (76 °C, 30 min) MAb_{AF647} was added to a stressed sample (76 °C, 1 h) containing MAb_{AF488} (B).

It was reported that heat stress can induce conformational changes to mAb monomers.[20,21] Especially Hawe and coworkers showed that heat stress damaged the mAb structure at similar temperatures, below the critical temperature of aggregation at which the monomers are lost.[21] Thus, one can speculate that structurally perturbed MAbs evaded the interaction with the existing aggregates. This would suggest that structural changes upon heat stress were responsible for the different behavior of stressed and unstressed MAb. Finally, although only up to one dye molecule was conjugated to the MAb ($DOL(MAb_{AF488}) = 1.1$; $DOL(MAb_{AF647}) = 0.4$), and both attached dye moieties are negatively charged,[22-24] an artificial effect induced by the label cannot be ruled out.

7.4 Summary and outlook

The confocal setup of FCS allows the detection of single fluorescently labeled species. By means of AC analysis, the diffusion times of the labeled species can be derived. The application of heat stress to MAb formulations containing a small amount of labeled MAb induced the formation of aggregates, which were detected by an increased diffusion time in FCS. Large aggregates of several MDa were observed.

In addition, FCCS measurements confirmed the aggregate formation, because a significant CC signal was observed when aggregates were formed in the presence of two MAbs carrying two different fluorescent labels. Furthermore, FCCS allowed for the detection of aggregate growth. Significant CC was obtained when MAb monomer was added to preformed MAb aggregates. In contrast, no CC was observed when aggregated and supposedly structurally perturbed MAb was added to already existing MAb aggregates. But further detailed studies appear necessary to substantiate this highly interesting finding. The ability to follow individual entities of both monomeric or aggregated character and the possibility to watch interactions between two species, are a valuable and outstanding chance to gain a comprehensive understanding of the processes involved in aggregation and interaction of proteins.

7.5 Acknowledgements

The FCS/FCCS measurements were performed at the Biotechnology Center of the Technische Universität Dresden, Germany. Dr. Jörg Mütze is gratefully acknowledged for his support on the measurements and data analysis.

7.6 References

1. Arzenšek D, Kuzman D, Podgornik R 2012. Colloidal interactions between monoclonal antibodies in aqueous solutions. J Colloid Interface Sci 384(1):207-216.

2. Saito S, Hasegawa J, Kobayashi N, Kishi N, Uchiyama S, Fukui K 2012. Behavior of Monoclonal Antibodies: Relation Between the Second Virial Coefficient (B 2) at Low Concentrations and Aggregation Propensity and Viscosity at High Concentrations. Pharm Res 29(2):397-410.

3. Lehermayr C, Mahler H-C, Mäder K, Fischer S 2011. Assessment of net charge and protein–protein interactions of different monoclonal antibodies. J Pharm Sci 100(7):2551-2562.

4. Connolly Brian D, Petry C, Yadav S, Demeule B, Ciaccio N, Moore Jamie MR, Shire Steven J, Gokarn Yatin R 2012. Weak Interactions Govern the Viscosity of Concentrated Antibody Solutions: High-Throughput Analysis Using the Diffusion Interaction Parameter. Biophys J 103(1):69-78.

5. Kumar V, Dixit N, Zhou L, Fraunhofer W 2011. Impact of short range hydrophobic interactions and long range electrostatic forces on the aggregation kinetics of a monoclonal antibody and a dual-variable domain immunoglobulin at low and high concentrations. Int J Pharm 421(1):82-93.

6. Chi E, Krishnan S, Randolph T, Carpenter J 2003. Physical Stability of Proteins in Aqueous Solution: Mechanism and Driving Forces in Nonnative Protein Aggregation. Pharm Res 20(9):1325-1336.

7. Chi EY, Weickmann J, Carpenter JF, Manning MC, Randolph TW 2005. Heterogeneous nucleation-controlled particulate formation of recombinant human platelet-activating factor acetylhydrolase in pharmaceutical formulation. J Pharm Sci 94(2):256-274.

8. Tyagi AK, Randolph TW, Dong A, Maloney KM, Hitscherich C, Carpenter JF 2009. IgG particle formation during filling pump operation: A case study of heterogeneous nucleation on stainless steel nanoparticles. J Pharm Sci 98(1):94-104.

9. Kiese S, Pappenberger A, Friess W, Mahler H-C 2010. Equilibrium studies of protein aggregates and homogeneous nucleation in protein formulation. J Pharm Sci 99(2):632-644.

10. Printz M, Kalonia DS, Friess W 2012. Individual second virial coefficient determination of monomer and oligomers in heat-stressed protein samples using size-exclusion chromatography-light scattering. J Pharm Sci 101(1):363-372.

11. Jacobs S, Wu S-J, Feng Y, Bethea D, O'Neil K 2010. Cross-Interaction Chromatography: A Rapid Method to Identify Highly Soluble Monoclonal Antibody Candidates. Pharm Res 27(1):65-71.

12. Madeira A, Vikeved E, Nilsson A, Sjögren B, Andrén PE, Svenningsson P. 2011. Identification of Protein-Protein Interactions by Surface Plasmon Resonance followed by Mass Spectrometry. Current Protocols in Protein Science, ed.: John Wiley & Sons, Inc.

13. Majka J, Speck C. 2007. Analysis of Protein–DNA Interactions Using Surface Plasmon Resonance. In Seitz H, editor Analytics of Protein–DNA Interactions, ed.: Springer Berlin Heidelberg. p 13-36.

14. Becker B, Cooper MA 2011. A survey of the 2006–2009 quartz crystal microbalance biosensor literature. J Mol Recognit 24(5):754-787.

15. Shi X, Wohland T. 2010. Fluorescence Correlation Spectroscopy. In Diaspro A, editor Nanoscopy and Multidimensional Optical Fluorescence Microscopy, ed.: CRC Press.

16. Mütze J, Ohrt T, Schwille P 2011. Fluorescence correlation spectroscopy in vivo. Laser & Photonics Reviews 5(1):52-67.

17. Lakowicz JR. 2006. Principles of Fluorescence Spectroscopy. 3rd ed.: Springer.

18. Dulbecco R, Vogt M 1954. Plaque Formation and Isolation of Pure Lines with Poliomyelitis Viruses. The Journal of Experimental Medicine 99(2):167-182.

19. Andersen CB, Manno M, Rischel C, Thórólfsson M, Martorana V 2010. Aggregation of a multidomain protein: A coagulation mechanism governs aggregation of a model IgG1 antibody under weak thermal stress. Protein Sci 19(2):279-290.

20. Printz M, Friess W 2012. Simultaneous detection and analysis of protein aggregation and protein unfolding by size exclusion chromatography with post column addition of the fluorescent dye BisANS. J Pharm Sci 101(2):826-837.

21. Hawe A, Friess W, Sutter M, Jiskoot W 2008. Online fluorescent dye detection method for the characterization of immunoglobulin G aggregation by size exclusion chromatography and asymmetrical flow field flow fractionation. Anal Biochem 378(2):115-122.

22. Zanetti-Domingues LC, Tynan CJ, Rolfe DJ, Clarke DT, Martin-Fernandez M 2013. Hydrophobic Fluorescent Probes Introduce Artifacts into Single Molecule Tracking Experiments Due to Non-Specific Binding. PLoS ONE 8(9):e74200.

23. Weber PA, Chang H-C, Spaeth KE, Nitsche JM, Nicholson BJ 2004. The Permeability of Gap Junction Channels to Probes of Different Size Is Dependent on Connexin Composition and Permeant-Pore Affinities. Biophys J 87(2):958-973.

24. Sobek J, Aquino C, Schlapbach R. 2011. Analyzing Properties of Fluorescent Dyes Used for Labeling DNA in Microarray Experiments. St. Louis: Sigma-Aldrich. Accessed at: http://www.sigmaaldrich.com/technical-documents/articles/biofiles/analyzing-properties.html.

8 Laser-induced breakdown detection of temperature-ramp generated aggregates of a therapeutic mAb

This chapter is intended for publication. A manuscript is in preparation by Tim Menzen, Wolfgang Friess, and Christoph Haisch.

8.1 Abstract

The detection and characterization of protein aggregation is essential during development and quality control of therapeutic proteins, as aggregates are typically inactive and may trigger anti-drug-antibody formation in patients. Especially large multi-domain molecules, such as the important class of therapeutic monoclonal antibodies (mAbs), can form various aggregates that differ in size and morphology. Although particle analysis advanced over the recent years, new techniques and orthogonal methods are highly valued. To our knowledge, the physical principle of laser-induced breakdown detection (LIBD) was not yet applied to sense aggregates in therapeutic protein formulations. We established a LIBD setup to monitor the temperature-induced aggregation of a mAb. The obtained temperature of aggregation was in good agreement with the results from previously published temperature-ramped turbidity and dynamic light scattering measurements. This study demonstrates the promising applicability of LIBD to investigate aggregates from therapeutic proteins. The technique is also adaptive to online detection and size determination, and offers interesting opportunities for morphologic characterization of protein particles and impurities, which will be part of future studies.

8.2 Introduction

Protein aggregation is a major hurdle for therapeutic proteins as the aggregated species typically lack activity and are potentially more immunogenic than protein monomers in patients.[1] The complex pathways of protein aggregation, especially in case of large multi-domain proteins, such as monoclonal antibodies (mAbs), lead to aggregates of various size and morphology.[2,3] To cover the full size range from several nanometers to micrometers, an arsenal of analytical tools is needed and

employed to investigate aggregates of protein drugs during development and in quality control.[3-5] Not only the size, but also morphology and structure of protein aggregates as well as nonproteinaceous impurities are in the focus of the pharmaceutical scientist and drive the development of new analytical techniques.[6,7] Progress was achieved, especially in the challenging range of micron (1 – 100 µm) and submicron (100 nm – 1 µm) particles, e.g., by micro-flow imaging (MFI) and resonant mass measurement.[8,9] As the obtained size information is always linked to the measurement principle and technique, orthogonal methods are highly valued and also appreciated by the regulatory agencies.[10]

Laser-induced breakdown detection (LIBD) of particles in solution relies on the effect that the energy threshold to induce a plasma breakdown in the focus of an intense pulsed laser is dependent on the dielectric properties (atom number density and refractive index) and is lower for solids than liquids (and gases).[11] The detection and counting of breakdown events induced by micron- and submicron particles by means of acoustic and optical detectors has been exploited mainly in the area of environmental analysis. A minimum detectable diameter of about 19 nm was demonstrated with polystyrene standard particles, while theoretical calculations even suggest a minimum size range of about 1 nm.[12] The probability to induce a breakdown by the laser pulse is increasing with both higher particle concentration and larger particle size,[13] thus complicating size distribution analysis of real-world samples where both parameters are unknown. Although LIBD is not established as routine technique, it was shown to be integrated as mobile, robust field measuring system.[14] To our best knowledge, LIBD has not been used for detection of protein aggregates in protein solutions before.

Consequently, the application of LIBD for the analysis of protein aggregates is highly intriguing. We therefore built a LIBD setup and tried to study the formation of mAb aggregates upon thermal unfolding. Using a temperature-ramped setup to induce aggregation, the breakdown incidence, i.e. the ratio of observed breakdowns to the number of laser pulses within 30 seconds, was monitored. A significant increase in breakdown incidences was observed after protein aggregation demonstrating that LIBD in principle can be used for characterization of protein formulations and the high potential of the method has to be further exploited in future studies.

8.3 Materials and methods

8.3.1 Sample preparation

Stock solutions of an IgG1 monoclonal antibody (“MAb”) in 10 mM sodium phosphate buffer at pH 7.2 or 5.0 with or without 140 mM sodium chloride (NaCl) and 280 mM mannitol were used.[15] Samples of 0.2 mg/ml MAb were prepared by dilution with the corresponding buffer and filtered through a 0.2 µm PVDF membrane syringe filter (Pall Life Sciences, Port Washington, New York, USA) immediately before the experiments.

8.3.2 Temperature-ramped LIBD setup

A schematic illustration of the temperature-ramped LIBD setup is illustrated in Figure 8-1. A pulsed (10 Hz) Surelite Nd:YAG laser (Continuum, San Jose, California, USA) was frequency-doubled to 532 nm. A lens with 20 mm was used to focus the beam into a quartz glass cuvette (Hellma Analytics, Müllheim, Germany). The center of the focus was positioned 1 mm from the cuvette inner wall to reduce loss of laser light in case of turbid solutions. The laser energy was recorded using a beam splitter and laser energy sensor (Ophir Optronics, Jerusalem, Israel). The cuvette was placed in a cell holder that was connected to a Thermo Haake C25P temperature controlled water bath (Thermo Electron, Karlsruhe, Germany). Using a lens of f = 40 mm, the emitted light from a LIBD event passed a long-pass filter and was detected by a photodiode. The electrical signal of the photodiode was amplified and collected using a Tektronix TDS 620A oscilloscope (Tektronix, Wilsonville, Oregon, USA). The oscilloscope also received the trigger signal from the laser source for timing. The LIBD signal was observed after about 300 nanoseconds and the electronic signal was transferred via a GPIB-to-USB converter (National Instruments, Austin, Texas, USA) to a personal computer (PC). The data from the photodiode and the laser energy sensor were recorded and processed using LabVIEW® 2010 (National Instruments Corporation, Austin, Texas, USA). The software logged the laser energy and signal amplitude of the photodiode for every individual pulse.

Before every measurement, the laser was turned on for at least one hour for internal thermal equilibration ensuring laser pulse stability. With a laser pulse energy of 39±4 µJ, the breakdown incidence of highly purified water (MilliQ Plus 185, Merck Millipore, Billerica, Massachusetts, USA) and the filtrated formulation buffers were 0.1

and 0.7 breakdowns/30 s, respectively (5000 laser pulses). The cuvette was filled with 2 ml of the sample and sealed by a rubber stopper equipped with a thermocouple. A linear temperature ramp from 20 °C to 95 °C in 75 min (1 °C/min) was adjusted at the water bath. The temperature in the solution was recorded using a HH147U thermo logger (Omega Engineering, Stamford, Connecticut, USA) connected to the PC.

The signal amplitudes were analyzed in order to identify LIBD events using a threshold value above the background signal amplitude with Origin® 8 SR6 (Originlab, Northampton, Massachusetts, USA). The breakdown incidence was calculated in time bins of 30 s. Using the recorded temperature data over time, the temperature where the breakdown incidence suddenly increased ($T_{agg,LIBD}$), was determined at the intersection of two tangents fitted to the cumulated breakdown incidence at the baseline and the slope.

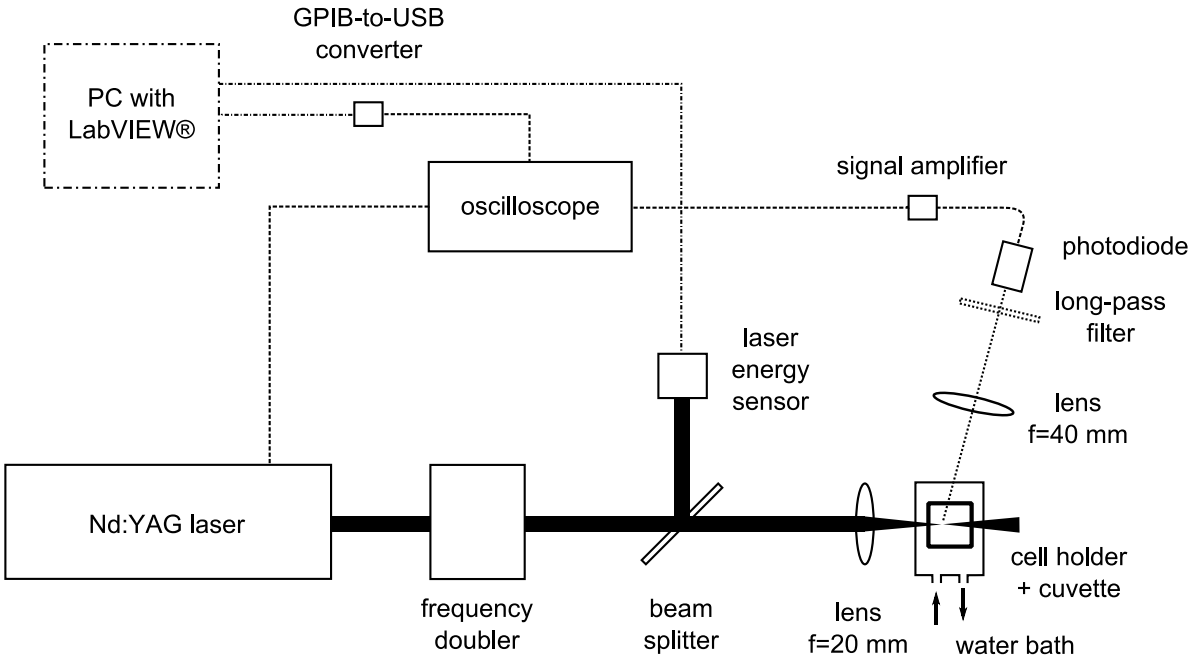

Figure 8-1. Schematic illustration of the temperature-ramped LIBD setup including data acquisition using a LabVIEW® virtual instrument (VI).

8.3.3 Differential scanning calorimetry (DSC)

DSC thermograms from 20 °C to 96 °C at 1 °C/min were obtained from the MAb samples at a concentration of 0.8 mg/ml using a VP-DSC MicroCalorimeter (MicroCal, Northampton, Massachusetts, USA; now Malvern Instruments) as described previously.[16] The apparent melting temperatures (T_m values) of the CH2

and the CH3 domains as well as the Fab part were obtained from the peak maxima of the melting transitions.

8.4 Results

The breakdown incidence represents the number of LIBD events per time bin of 30 s. At the starting temperature of 20 °C, a breakdown incidence of 0 to 5 breakdowns/30 s was observed for all 0.2 mg/ml MAb samples in 10 mM phosphate buffer at pH 7.2 (Figure 8-2). Subsequently, the temperature of the sample was linearly increased with a heating rate of 1 °C/min. The breakdown incidence was constant at the initial level until a sudden onset of breakdown events occurred. This onset was observed for all three MAb formulations at the neutral pH but the $T_{agg,LIBD}$ was slightly lower for the sample without NaCl or with mannitol (Table 8-1). Followed by the strong and sudden onset of breakdown events at a given temperature, the breakdown incidence typically decreased slightly with further increasing temperature.

Table 8-1. Summary of the results from DSC, temperature-ramped turbidity and DLS measurements,* and LIBD measurements of 0.2 mg/ml MAb in 10 mM phosphate buffers at pH 7.2 and 5.0 with or without NaCl and mannitol.

	T_m by DSC [°C]			$T_{agg,onset}$ [°C]	T_{agg} [°C]	$T_{agg\ LIBD}$ [°C]	$T_{Rh\ >\ 10nm}$ [°C]
	CH2	CH3	Fab	Turbidity		LIBD	DLS
pH 7.2	72.1	82.2		77.1±0.1	79.5±0.1	78.2±0.8	65 – 70
+ mannitol	73.0	83.0		78.1	80.5	81.7	65 – 70
+ NaCl	71.4	82.6		78.2	80.5	82.5	65 – 70
pH 5.0	61.0	80.9	87.4	-	-	-	80 – 85
+ mannitol	65.5	83.1	88.6	-	-	-	80 – 85
+ NaCl	63.2	81.8	87.4	82.7	85.2	87.5	70 – 75

*** previously published by Menzen and Friess.[15]**

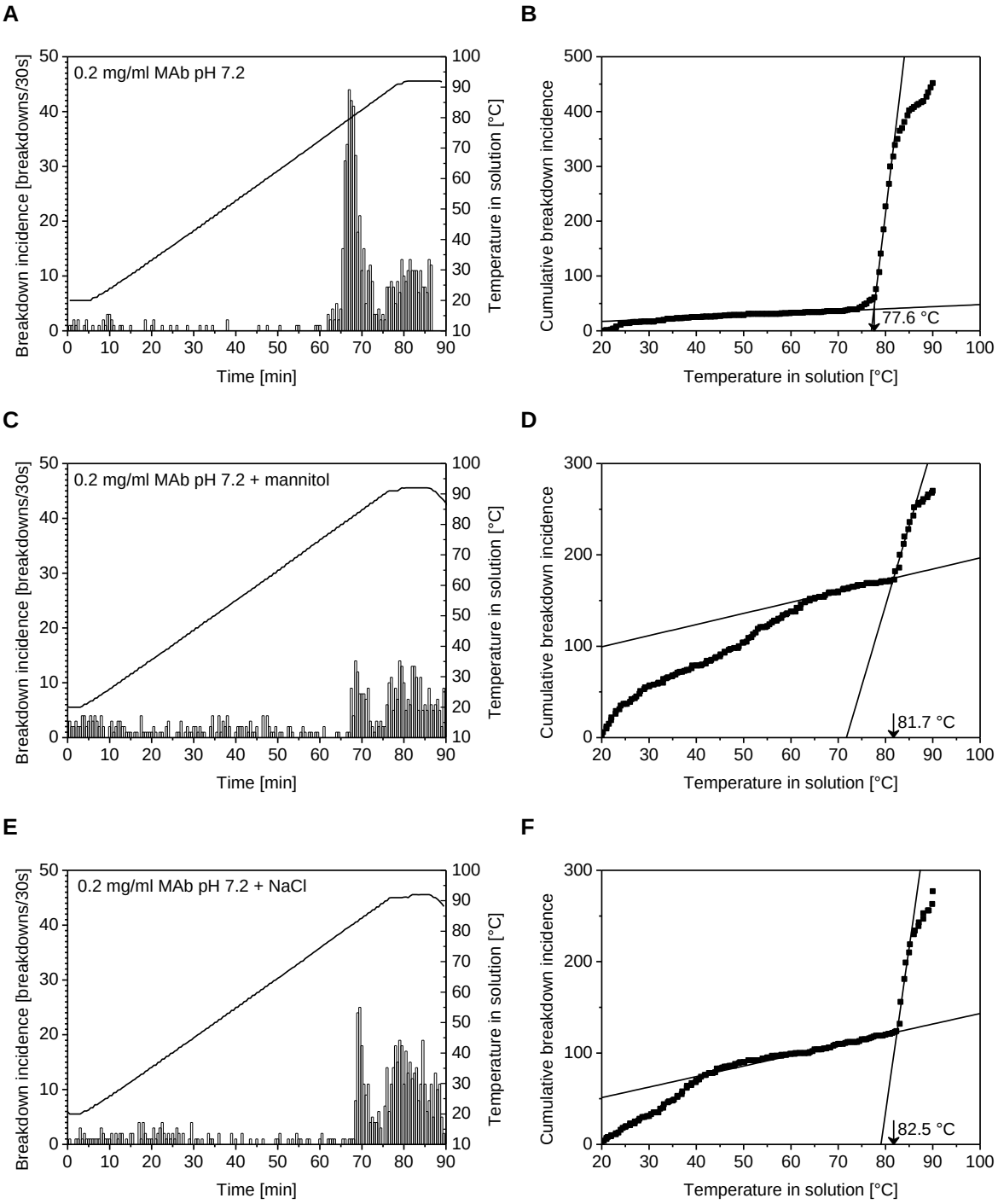

Figure 8-2. Results from experiments with 0.2 mg/ml MAb at pH 7.2 (A + B), with additional 280 mM mannitol (C + D), and with additional 140 mM NaCl (E + F). The LIBD signal was counted in time bins of 30 s while the temperature in solution increased linearly from 20 to 90 °C with a rate of 1 °C/min. The $T_{agg\ LIBD}$ value was analyzed via two intersecting tangents from the accumulated breakdown incidence.

The DSC measurements revealed two melting transitions of the MAb at pH 7.2 (Table 8-1). The first melting transition is caused by the CH2 domain, whereas the larger, second transition at higher temperature reflects simultaneous unfolding of the CH3

domain and the Fab fragment.[15] Aggregation occurred upon heating in all formulations at pH 7.2, and the temperature of aggregation (T_{agg}) and its onset value ($T_{agg,onset}$) from temperature-ramped turbidity measurements were previously reported.[15] In the same study, also the hydrodynamic radius (R_h) was monitored by dynamic light scattering (DLS) upon heating to 85 °C in steps of 5 °C. The temperature range in which R_h exceeded 10 nm, indicating the formation of small aggregates, is provided in Table 8-1.[15]

In case of the 0.2 mg/ml MAb samples at pH 5.0, a sudden breakdown onset was observed only for the formulation containing 140 mM NaCl (Figure 8-3). In contrast, no increase in breakdown incidences and consequently no $T_{agg,LIBD}$ values were determined in case of the other two formulations at the low pH and low ionic strength (Table 8-1).

Similarly, only the NaCl containing sample became turbid upon heating, whereas the MAb solutions remained clear in case of the 10 mM phosphate buffer and with additional mannitol.[15] The formation of small aggregates was detected by DLS. In addition, unfolding of the CH2 and CH3 domain and the Fab fragment was observed as three distinct DSC melting transitions at pH 5.0 (Table 8-1).

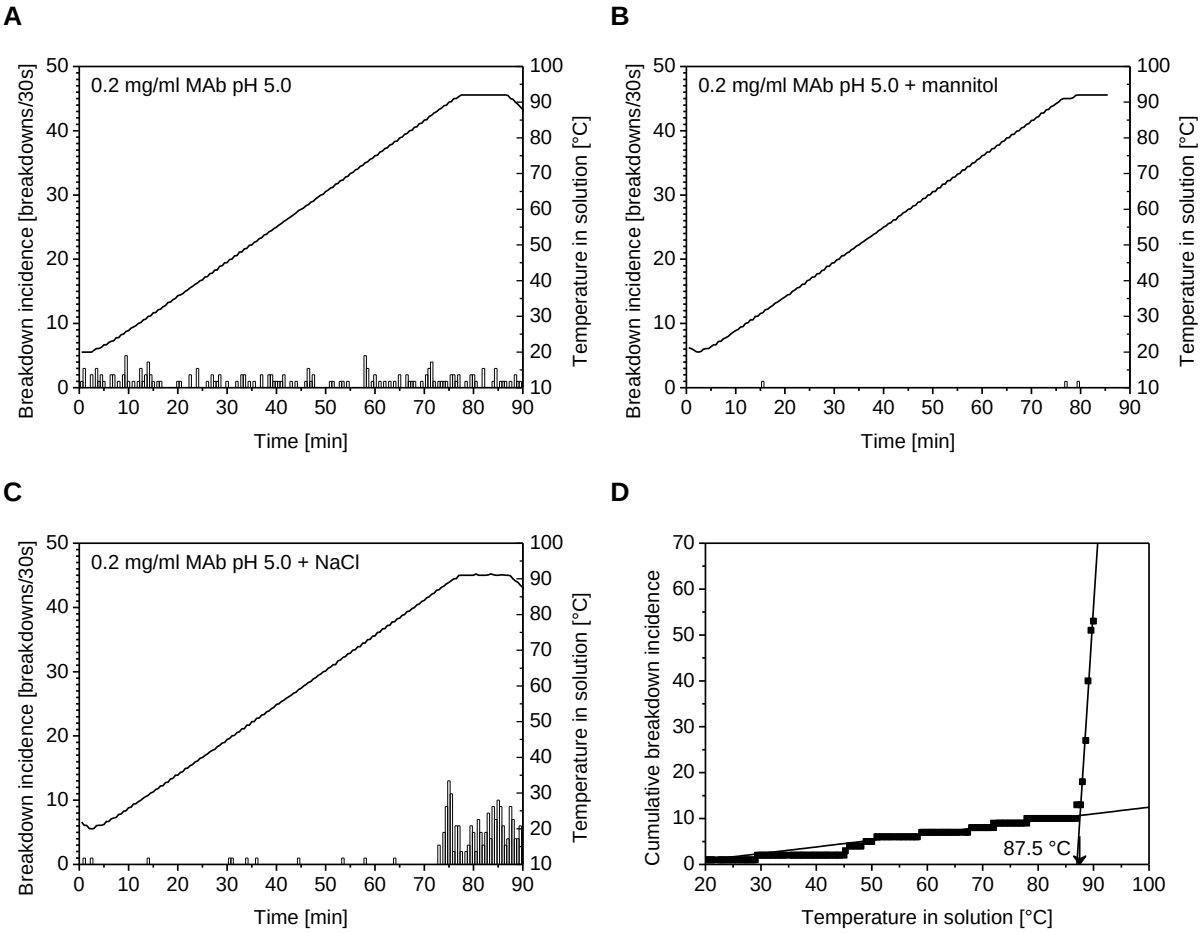

Figure 8-3. Results from experiments with 0.2 mg/ml MAb at pH 5.0 (A), with additional 280 mM mannitol (B), and with additional 140 mM NaCl (C + D). A jump in LIBD incidence was observed only for the NaCl containing sample and its $T_{agg,LIBD}$ value was analyzed via two intersecting tangents from the accumulated breakdown incidence.

8.5 Discussion

At the applied laser energy, the breakdown incidence of the background formulation buffers was below 0.7 breakdowns/30 s. In contrast, the samples at pH 7.2 and 5.0 with NaCl showed a clear sudden onset of breakdown events with rising temperature (Figure 8-2 and Figure 8-3). Breakdown incidences above 10 breakdowns/30 s were detected. This increase is explained by the formation of MAb aggregates, which were induced by thermal unfolding of the protein. Almost identical T_{agg} values were obtained from turbidity measurements (Table 8-1). The same temperature-ramp of 1 °C/min was used during DSC, turbidity, and LIBD measurements. The observed aggregation temperatures from LIBD and turbidity measurements were in the range of the apparent T_m values of the CH3 domain and Fab, which suggests that the process of aggregation is mediated by at least partial unfolding of these regions

(Table 8-1). Although attractive hydrophobic interactions increase upon unfolding due to the exposure of hydrophobic surfaces, the overall positive net charge prevented the MAb from precipitation at the low pH value and at low ionic strength.[15] This electrostatic repulsion is shielded in the presence of 140 mM NaCl, which leads to precipitation of the protein also at pH 5.0, similar to the formulations at pH 7.2.

DLS, although performed with a slower heating rate and in steps of 5 °C, demonstrated an increase in R_h at temperatures below the T_{agg} values identified by the other methods (Table 8-1). This suggests that small MAb oligomers form first. Under conditions that shield repulsive charge interactions, subsequently larger aggregates build up which are detected by an increase in turbidity and LIBD. Consequently, the current LIBD setup allows for the detection of larger protein aggregates, most likely in the low micrometer range. Thus, sedimentation might the reason for the observed reduction in breakdown incidence after the breakdown onset at T_{agg} (Figure 8-2 and Figure 8-3).

Scattered laser light from protein aggregates that are out of the focus may disturb the optical detection of the plasma breakdowns. This interference was suppressed by the confocal breakdown detection geometry and by a long-pass light filter (>600 nm) in front of the photodiode, which blocks the scattered laser light. Furthermore, the focus of the beam was adjusted in close proximity to the inner wall of the cuvette and a low MAb concentration of 0.2 mg/ml was applied to reduce the total amount of protein aggregates in the cell. Thereby, the risk of the laser intensity falling below the breakdown threshold was reduced.

The current method allows reliable detection of the heat-induced protein aggregates in a straight-forward setup. But many more detailed studies have to follow to establish the full strength of LIBD for a comprehensive particle analysis. Since the breakdown incidence depends on both particle size and concentration, it is not possible to determine one of these parameters from a simple counting experiment. One option to obtain the size information is to increase the laser power during the experiment, record the breakdown incidence as a function of the laser energy, and correlate the results to a calibration generated with standard particles.[17,18] Another approach derives the size information from the precise spatial position and dimension of the breakdown within the energy profile of the focused laser beam using a camera.[19-21] In both cases, a rather high number of breakdowns is necessary for statistical analysis,

which requires for a high-repetition laser source, at least in case of low particle concentrations. Furthermore, careful calibration with standard particles is necessary. Moreover, the current sample volume can be easily reduced by glass cuvettes with smaller volume, leading to reduced sample consumption.

The LIBD technique can be combined with symmetrical,[22] and asymmetrical,[23] flow field-flow fractionation for particle separation, revealing improved sensitivity for polystyrene particles below a size of 70 nm compared to static light scattering (SLS). For LIBD, a linear relationship between signal and particle size was observed at low breakdown propensities.[19] The LIBD technique is more sensitive than SLS regarding the detection of small particles.[23,24] Hence, the use of the flow-through cell connected to a size-separation system may enable detailed analysis of small protein aggregates or impurities such as silicone oil droplets, and other foreign particles. Again, a high repetition rate pulsed laser would then be beneficial in order to improve statistics. Thus, the presented setup is a first approach to highlight the promising application of LIBD to investigate foreign (extrinsic), process-related (intrinsic), and proteinaceous (inherent) particles in pharmaceutical protein formulations.

8.6 Summary and outlook

In this study, LIBD was applied for the first time to detect MAb aggregates that were intentially formed by heat stress. Protein aggregation upon heating and the corresponding $T_{agg,LIBD}$ values were determined based on the breakdown incidence. $T_{agg,LIBD}$ was in good agreement with the results from temperature-ramped turbidity measurements. Differences in MAb aggregation corresponded to pH and charge shielding effects by salts as previously described.[15]

The presented temperature-ramped setup induced considerable amounts of protein aggregates in short times from relevant therapeutic formulations, which allowed a comparison with previously published data using orthogonal techniques. Turbidity and DLS measurements suggested that only large particulate MAb aggregates were detected with the current LIBD setup.

In upcoming studies, the power of LIBD for sizing and counting of protein particles has to be investigated. The current setup has potential for further improvement, e.g., by using a smaller volume flow-through cell, a laser featuring a higher pulse repetition

rate, and it can be connected to size-separation techniques. Furthermore, information about particle size could be obtained from spatial and intensity characteristics of the breakdown event using a camera instead of a photodiode.[19-21] LIBD was shown to be applicable over a wide particle size range (nanometer to micrometer), [25] and could be a highly valuable new technique for the challenging analysis of subvisible particles. In future studies, protein particles with well characterized size and morphology, e.g., by means of flow-imaging and resonant mass techniques,[8,9] need to be studied to evaluate potential effects of density, shape, and refractive index of the protein aggregates on the plasma formation. In summary, LIBD is a new and promising, orthogonal approach to investigate protein aggregates or impurities such as silicone oil and nonproteinaceous particles in pharmaceutical samples. It is based on a physical principle different from all other methods utilized in the field of protein formulation development and characterization.

8.7 Acknowledgements

The LIBD experiments were performed in collaboration with Prof. Dr. Christoph Haisch from the Institute of Hydrochemistry of the Technische Universität München, Germany. Prof. Dr. Christoph Haisch and Prof. Dr. Reinhard Niessner, leader of the chair, are gratefully acknowledged for this opportunity.

8.8 References

1. Wang W, Singh SK, Li N, Toler MR, King KR, Nema S 2012. Immunogenicity of protein aggregates—Concerns and realities. Int J Pharm 431(1–2):1-11.

2. Narhi LO, Schmit J, Bechtold-Peters K, Sharma D 2012. Classification of protein aggregates. J Pharm Sci 101(2):493-498.

3. Mahler H-C, Friess W, Grauschopf U, Kiese S 2009. Protein aggregation: Pathways, induction factors and analysis. J Pharm Sci 98(9):2909-2934.

4. Zölls S, Tantipolphan R, Wiggenhorn M, Winter G, Jiskoot W, Friess W, Hawe A 2012. Particles in therapeutic protein formulations, Part 1: Overview of analytical methods. J Pharm Sci 101(3):914-935.

5. den Engelsman J, Garidel P, Smulders R, Koll H, Smith B, Bassarab S, Seidl A, Hainzl O, Jiskoot W 2011. Strategies for the Assessment of Protein Aggregates in Pharmaceutical Biotech Product Development. Pharm Res 28(4):920-933.

6. Carpenter JF, Randolph TW, Jiskoot W, Crommelin DJA, Middaugh CR, Winter G, Fan Y-X, Kirshner S, Verthelyi D, Kozlowski S, Clouse KA, Swann PG, Rosenberg A, Cherney B 2009. Overlooking subvisible particles in therapeutic protein products: Gaps that may compromise product quality. J Pharm Sci 98(4):1201-1205.

7. Carpenter J, Cherney B, Lubinecki A, Ma S, Marszal E, Mire-Sluis A, Nikolai T, Novak J, Ragheb J, Simak J 2010. Meeting report on protein particles and immunogenicity of therapeutic proteins: Filling in the gaps in risk evaluation and mitigation. Biologicals 38(5):602-611.

8. Weinbuch D, Zölls S, Wiggenhorn M, Friess W, Winter G, Jiskoot W, Hawe A 2013. Micro–flow imaging and resonant mass measurement (archimedes) – complementary methods to quantitatively differentiate protein particles and silicone oil droplets. J Pharm Sci 102(7):2152-2165.

9. Zölls S, Weinbuch D, Wiggenhorn M, Winter G, Friess W, Jiskoot W, Hawe A 2013. Flow Imaging Microscopy for Protein Particle Analysis—A Comparative Evaluation of Four Different Analytical Instruments. The AAPS Journal 15(4):1200-1211.

10. Weinberg WC, Ha L, Kirshner SL, Verthelyi DI. 2010. Regulatory Perspective on Aggregates as a Product Quality Attribute. In Wei Wang CJR, editor Aggregation of Therapeutic Proteins, ed., Hoboken, New Jersey: John Wiley & Sons, Inc. p 435-451.

11. Bettis JR 1992. Correlation among the laser-induced breakdown thresholds in solids, liquids, and gases. Appl Opt 31(18):3448-3452.

12. Bundschuh T, Knopp R, Kim JI 2001. Laser-induced breakdown detection (LIBD) of aquatic colloids with different laser systems. Colloids Surf, A 177(1):47-55.

13. Scherbaum FJ, Knopp R, Kim JI 1996. Counting of particles in aqueous solutions by laser-induced photoacoustic breakdown detection. Applied Physics B Laser and Optics 63(3):299-306.

14. Latkoczy C, Kagi R, Fierz M, Ritzmann M, Gunther D, Boller M 2010. Development of a mobile fast-screening laser-induced breakdown detection (LIBD) system for field-based measurements of nanometre sized particles in aqueous solutions. Journal of Environmental Monitoring 12(7):1422-1429.

15. Menzen T, Friess W 2014. Temperature-Ramped Studies on the Aggregation, Unfolding, and Interaction of a Therapeutic Monoclonal Antibody. J Pharm Sci 103(2):445-455.

16. Menzen T, Friess W 2013. High-throughput melting-temperature analysis of a monoclonal antibody by differential scanning fluorimetry in the presence of surfactants. J Pharm Sci 102(2):415-428.

17. Bitea C, Walther C, Kim JI, Geckeis H, Rabung T, Scherbaum FJ, Cacuci DG 2003. Time-resolved observation of ZrO2-colloid agglomeration. Colloids and Surfaces A: Physicochemical and Engineering Aspects 215(1–3):55-66.

18. Bitea C, Müller R, Neck V, Walther C, Kim JI 2003. Study of the generation and stability of thorium(IV) colloids by LIBD combined with ultrafiltration. Colloids and Surfaces A: Physicochemical and Engineering Aspects 217(1–3):63-70.

19. Bundschuh T, Hauser W, Kim JI, Knopp R, Scherbaum FJ 2001. Determination of colloid size by 2-D optical detection of laser induced plasma. Colloids and Surfaces A: Physicochemical and Engineering Aspects 180(3):285-293.

20. Kim JW, Son JA, Yun JI, Jung EC, Park SH, Choi JG 2008. Analysis of laser-induced breakdown images measuring the sizes of mixed aquatic nanoparticles. Chem Phys Lett 462(1–3):75-77.

21. Jung EC, Yun JI, Kim JI, Park YJ, Park KK, Fanghänel T, Kim WH 2006. Size measurement of nanoparticles using the emission intensity distribution of laser-induced plasma. Applied Physics B 85(4):625-629.

22. Thang NM, Knopp R, Geckeis H, Kim JI, Beck HP 1999. Detection of Nanocolloids with Flow-Field Flow Fractionation and Laser-Induced Breakdown Detection. Anal Chem 72(1):1-5.

23. Bouby M, Geckeis H, Manh TN, Yun JI, Dardenne K, Schafer T, Walther C, Kim JI 2004. Laser-induced breakdown detection combined with asymmetrical flow field-flow fractionation: application to iron oxi/hydroxide colloid characterization. J Chromatogr A 18(1):97-104.

24. Bundschuh T, Wagner TU, Köster R 2005. Laser-induced Breakdown Detection (LIBD) for the Highly Sensitive Quantification of Aquatic Colloids. Part I: Principle of LIBD and Mathematical Model. Particle & Particle Systems Characterization 22(3):172-180.

25. Bundschuh T, Wagner TU, Köster R 2005. Laser-induced Breakdown Detection (LIBD) for the Highly Sensitive Quantification of Aquatic Colloids. Part II: Experimental Setup of LIBD and Applications. Particle & Particle Systems Characterization 22(3):181-191.

Summary of the thesis

Protein instabilities are one major obstacle during R&D of therapeutic protein drugs and mAbs in particular. These instabilities arising from the complex protein structure are determined by the chemical nature of the amino acid residues and the physical nature of stabilizing and destabilizing inter- and intramolecular interactions. As a result, proteins are susceptible to chemical degradation and aggregation processes. Both are typically linked to a diminution of the native conformation, a reduced activity or complete loss of function, and unwanted side effects. Monitoring the thermal unfolding is an integral part of assessing the conformational stability of proteins. A high thermal stability reduces the probability of the protein to populate unfolded states at physiological and storage temperatures, and subsequent instability reactions are less likely. Therefore, the T_m value is routinely analyzed and also $T_{m,onset}$ is very interesting as it marks first structural perturbation. Commonly, DSC is applied for thermal analysis but suffers from long analysis times and considerable material consumption. In contrast, DSF is a high-throughput technique for T_m analysis using RT-PCR machines in a multi-well plate format. It utilizes an extrinsic fluorescent dye which monitors protein unfolding by adsorption to hydrophobic structures exposed upon heating. But a DSF method was not yet established in the research group. During DSF method development, sample dilution and effects from the organic solvent were evaluated. The DSF method was applied to mAb concentrations from 40 µg/ml to 175 mg/ml. For data analysis, an Origin® LabTalk script was developed which automatically processes and analyzes the fluorescence raw data and presents T_m and $T_{m,onset}$ values based on first derivative analysis and Boltzmann fitting for individual transitions of multi-domain proteins (OpenTM, see Appendix). A robust DSF method with two RT-PCR machines was established.

The melting profiles of two mAb molecules were comprehensively studied by DSF and DSC. By means of enzymatic cleavage, Fab and Fc fragments were prepared and enabled thorough characterization of the unfolding sequence and thermal sensitivity of the mAbs domains. This fundamental understanding allowed for the specific investigation of intrinsic and extrinsic factors which affect the thermal stability of the mAbs. First, the effect of deglycosylation was studied on the interesting case of

Cetuximab (CX) which carries an additional glycan moiety at the Fab part in comparison to the other mAb. In contrast to the common glycosylation site at Fc that significantly contributes to the thermal stability of the CH2 domain, deglycosylation of the Fab-glycans did not change the T_m values. This effect indicated that these glycans are not involved in conformational stabilization of CX. Next, various buffers, excipients, ionic strength, and pH conditions were investigated as the environment of the protein strongly affects the thermal stability, and thus formulation development is essential for stable and active products. An overall strong effect of the pH value was observed with considerably lower T_m values of the CH2 domain at pH 5.0 compared to pH 7.2, especially in the presence of arginine and histidine. Interestingly, a significant effect of the counterion partner to both basic amino acids was observed. Synergistic stabilizing effects were obtained for arginine and histidine in combination with aspartate and glutamate by reducing the formation of aggregates upon thermal unfolding of the Fab part. Especially DSF was highly valuable for T_m screenings where the high-throughput design was beneficial. A good correlation was found for DSC and DSF with respect to the T_m and $T_{m,onset}$ values although consistently lower values were obtained by DSF. During intensive studies, both methods revealed outstanding benefits but also individual drawbacks which highlight their complementary and orthogonal application (Table I).

Table I. Comparison of DSC and DSF for thermal analysis of proteins.

	DSC	DSF
Unfolding monitored by	Heat capacity (direct)	Fluorescence intensity (indirect)
Benefits	Robust, precise Label-/marker free Provides thermodynamic parameters	High-throughput design Small sample volumes Broader concentration range
Drawbacks	Time and material consuming	Extrinsic fluorescent dye
Limitations	High protein concentrations	Resolution of multiple transitions (Presence of surfactant)

The popular extrinsic dye SYPRO® Orange, which is routinely used for DSF, shows high background fluorescence in the presence of surfactants. Thus, protein formulations containing surfactants, which are typically used as stabilizing agents, are challenging in DSF. A high mAb concentration was necessary to monitor protein unfolding above the background signal of the surfactants with SYPRO® Orange. Furthermore, the molecular rotor dye DCVJ, which is less sensitive towards micelles, was used for the first time for DSF to analyze T_m in the presence of surfactants. The T_m values obtained with both dyes were in excellent agreement. The application of DCVJ allowed T_m analysis at a 10-fold lower mAb concentration. It was shown that careful background subtraction is necessary to obtain good results, especially when $T_{m,onset}$ values are investigated. Automatic background correction by subtraction of a placebo sample is also supported by the OpenTM Origin® LabTalk script. With successful T_m analysis by DSF in the presence of surfactants, a gap for its application to the challenging high-throughput formulation development is closing.

Temperature-ramped studies including DSF, DSC, DLS, and turbidity measurements allowed for interesting insights into the conformational and colloidal stabilities of the mAbs. At pH 5.0, below the pI of the mAb, positive net charges resulted in a strong repulsion of the molecules in solution indicated by large, positive k_D values. In this case, no precipitation was observed upon heating. When 140 mM NaCl was added, the charge shielding effects of the salt reduced the k_D value and aggregation occurred. Similar effects were obtained at pH 7.2 when net charges are neutral. Thus, a high k_D value was indicative for colloidal stability due to repulsive electrostatic interactions. On the other hand, the conformational stability, especially of the sensitive CH2 domain, was significantly reduced at the low pH and by addition of salt. Higher T_m values were found when 280 mM mannitol instead of salt was used to achieve isotonicity. The opposing results underline the indispensability of comprehensive stability studies which include both conformational and colloidal analysis. Based on literature reports, the TIM empiric equation was derived for the transformation of the interaction parameters k_D and A_2 for mAbs for a better estimation of net attraction or repulsion. Moreover, the k_D value was determined upon heating. As long as the monomer was present, a reduction of k_D upon thermal unfolding indicated increasingly attractive interaction due to the exposing hydrophobic structures which lead to aggregation and precipitation of the mAb. While

the isolated Fc fragment behaved similar to the full mAb, the Fab fragment started to aggregate already below its $T_{m,onset}$ value.

Unfortunately, interaction parameters like k_D or A_2 are not transferable to intermolecular interactions between aggregates and monomers which might drive the nucleation of aggregates. An FCS and FCCS approach was chosen to investigate the adsorption of mAb monomers to existing aggregates formed by heat stress. The interesting results suggest that native mAb molecules were adsorbed onto the preformed aggregates while a stressed solution of aggregates and structurally perturbed monomers did not interact. Although detailed studies are necessary, FCCS in particular rendered a powerful technique for the analysis of homogeneous nucleation processes and the observation of interactions between monomeric and aggregated species in solution.

Finally, a LIBD setup was used for the first time to detect protein aggregation. A strong laser was focused into a glass cuvette containing the mAb formulation, and the incidence of breakdown events was monitored upon heating of the cell. Protein aggregation was indicated by a sharp onset of breakdown events at temperatures that were in good agreement with the results from previous temperature-ramped studies. Potential improvements of the setup include a smaller sample volume, connection to size based separation techniques, and advanced breakdown analysis which facilitates particle sizing. Thus, LIBD is a promising orthogonal technique for the investigation of protein aggregates and nonproteinaceous impurities in pharmaceutical samples.

In conclusion, the fundamental understanding of unfolding, aggregation, and interaction processes of mAbs upon heating was deepened. For this purpose, established analytical techniques were challenged, and substantial methodical improvements were achieved. Furthermore, promising results were obtained with novel techniques which expand the current set of protein analytics. Therefore, this work may support scientists working on formulation development of mAbs and encourages the development of more advanced hard- and software to improve rational and successful R&D of therapeutic protein drugs.

Appendix

List of abbreviations

A	Absorption
A_2	Second osmotic virial coefficient, also B_{22}
AC	Autocorrelation
ADC	Antibody-drug conjugate
ANS	1-Anilinonaphthalene-8-sulfonic acid
Asn	Asparagine
AUC	Analytical ultracentrifugation / area under the curve
Bis-ANS	4,4'-Dianilino-1,1'-binaphthyl-5,5'-disulfonic acid
c	Concentration
CC	Cross-correlation
CCD	Charge-coupled device
CCVJ	9-(2-Carboxy-2-cyanovinyl)julolidine
CD	Circular dichroism
CDR	Complementarity-determining region
CHO	Chinese hamster ovary
CMC	Critical micellization concentration
CMT	Critical micellization temperature
Cp	Heat capacity
CV	Column volume
CX	Cetuximab
D	Difusion coefficient
DCVJ	9-(Dicyanovinyl)julolidine
DFFITS	Difference in fits, standardized
DLS	Dynamic light scattering
DMSO	Dimethyl sulfoxide
DNA	Deoxyribonucleic acid
DOE	Design of experiment
DOL	Degree of labeling
DSC	Differential scanning calorimetry, also microcalorimetry (µDSC)
DSF	Differential scanning fluorimetry
DSLS	Differential static light scattering
ε_{280nm}	Extinction coefficient at 280 nm
EDTA	Ethylenediaminetetraacetate
eGFP	Enhanced green fluorescent protein
Em	Emission (wavelength)
Ex	Excitation (wavelength)
f	Focal length
Fab	Fragment, antigen binding
FBDD	Fragment-based drug discovery, also fragment based lead discovery
Fc	Fragment, crystallizable
FCCS	Fluorescence cross-correlation spectroscopy
FCS	Fluorescence correlation spectroscopy
FTIR	Fourier transform infrared spectroscopy

GdnHCl	Guanidinium hydrochloride
GPIB	General purpose interface bus
HIC	Hydrophobic interaction chromatography
His	Histidine
HPLC	High performance liquid chromatography
HP-SEC	High performance size exclusion chromatography
HTS	High-throughput screening
IgG	Immunoglobulin G
IEF	Isoelectric focusing
k_D	Diffusion interaction parameter
LED	Light emitting diode
LIBD	Laser-induced breakdown detection
mAb	Monoclonal antibody
MAb	A therapeutic IgG1 model mAb
MFI	Micro-flow imaging
MWCO	Molecular weight cut-off
MS	Mass spectrometry
NaCl	Sodium chloride
Nd:YAG	Neodymium-doped yttrium aluminium garnet
NHS	N-hydroxysuccinimide
PBS	Phosphate buffered saline
PC	Personal computer
PDB	Protein Data Bank (RCSB PDB)
PES	Polyethersulfone
Phos	Phosphate buffer
pI	Isoelectric point
PMT	Photomultiplier tube
PP	Polypropylene
PS	Polysorbate
PTFE	Polytetrafluoroethylene
PX	Poloxamer
PVDF	Polyvinylidene fluoride
RC	Regenerated cellulose
R&D	Research and development
R_h	Hydrodynamic radius
RT-PCR	Real-time polymerase chain reaction
SEC	Size exclusion chromatography (see also HP-SEC)
SIC	Self-interaction chromatography
SDS	Sodium dodecyl sulfate
SDS-PAGE	Sodium dodecyl sulfate polyacrylamide gel electrophoresis
SLS	Static light scattering
S/N	Signal to noise
T_{agg}	Temperature of aggregation
$T_{agg,onset}$	Onset temperature of aggregation
TICT	Twisted intramolecular charge transfer
TIM	Transformation of the interaction parameters of mAbs
T_m	Protein melting temperature
$T_{m,onset}$	Onset temperature of protein melting / unfolding
USB	Universal serial bus
UV-Vis	Ultraviolet-visible light
VI	Virtual instrument

OpenTM Origin® LabTalk script for the analysis of DSF experiments

```
type "Running openTM version 6.1 R1\nTm analyis script for RT7300 & qTower2 RT-PCR
CSV-files\ndone 2010-2014 by Tim Menzen at the LMU, Munich, Germany";
type "Usage: If necessary create a new workbook and feel free to type in sample
names in 96-well plate scheme (12x8)\nEnter required parameters in the dialog box
(passing arguments via command line is obsolete).";
/*
Recommended sample scheme for 96-well plates and Tm analysis with openTM:
Triplicate sample (S) + one placebo (P) as blank. Start with A1. Fill up column by
column.
  1  2  3  4 ..
A S1 S3 S5 ..
B S1 S3 S5
C S1 S3 S5
D P1 P3 S5
E S2 S4 P5
F S2 S4 ..
G S2 S4
H P2 P4
--> 24 samples per well plate
cave: In case of enabled Background subtraction and Signal averaging, this scheme
is essential.

Tested and supported systems:
- Origin 8 SR6 (!)
- Origin 8.5
- RT7300 (Applied Biosystems)
- qTower 2 & 2.2 (Analytik Jena)

Brief history of the openTM script:
The script was started from the scratch in 2010 with the need to analyze the
protein melting temperature (Tm) from DSF experiments with the RT7300 RT-PCR
machine.
Tm analysis was performed by fitting of the sigmoidal Boltzmann function to the
melting curve.
It was designed to investigate monoclonal antibodies (mAbs) which often show
multiple melting transitions (typically 2-3) due to their distinct domains.
Thus, different procedures were included to define the range of the Boltzmann fit
dependent on the shape of the melting profile.
A robust procedure to calculate the Onset temperature of unfolding was introduced
based on the Boltzmann fit.
Optional Background subtraction of blank samples was included (the script expects
every 4th sample to be a blank starting with A1, B1, C1, etc.).
Next, Tm values were additionally obtained by analysis of the first derivative of
the melting curves. Both values are displayed in the graphs for visual inspection.
Signal averaging was added to generate mean melting curves from the triplicates
(allows easy reporting and manual fitting).
Data import for the qTower 2 RT-PCR was implemented.
Command line usage was replaced by a dialog box for better ease of use and several
smaller fixes and tweaks...

note:
Origin handles CSV files dependent on the regional settings of the operating
system. Thus, dot "." and comma "," mismatches can occur.

why "openTM"?
open = feel free to use the code + TM = melting temperature & Tim Menzen ;-)
```

```
For beginners of LabTalk scripting, the excellent official online wiki is highly
recommended.
*/

// SECTION: SCRIPT INITIALIZATION

// record time point for script runtime
string date1$=%[%[$(@D, D13),>" "], 4:5];
int min1=%(date1$);
string date1$=%[%[$(@D, D13),>" "], 7:8];
int sec1=%(date1$);

// global 96-well plate definition
StringArray AF = {"A","B","C","D","E","F","G","H"};

// grab the open workbook and use it as sample book
SampleBook$="SampleBook";
win -r %H %(SampleBook$); //%H system variable for current active window title
range SampleBookSheet1R=[SampleBook$]1!;
range SampleBookR = [SampleBook$]1!1;


// SUBSECTION: USER INTERFACE

// Check for arguments from User. Arguments are obsolete with version 5.9 due to
getn dialog
int numArgs = macro.narg;
type "$(numArgs) argument(s) has (have) been passed.";
if (numArgs>0) {
	type -n "Command line arguments have been passed. Passing arguments is
obsolete since version 5.9. Ignore arguments?";
}
// initialize variables and open parameter input dialog
int    Device=1, StartCol=1, StopCol = 12, StartFitFilter = 1,    PerformBlankedFit
= 0, StartTemp=20;
double deltaT = 1;
GetN (Device 1=RT7300, 2=qTower) Device
	(Sart with col #) StartCol
	(Stop with col #) StopCol
	(Start Fit with Filter #) StartFitFilter
	(Start temperature / °C) StartTemp
	(Temperature increase / °C) deltaT
	(Background / blanking) PerformBlankedFit
	(Initialize parameters);
// I/O
type "Device %(DeviceName.GetAt(Device)$) has been selected\nStart with column
$(StartCol) and stop with column $(StopCol)\nStart Fit with Filter no.
$(StartFitFilter)\nStart at $(StartTemp) °C with temperature steps of $(deltaT)
°C";
if (PerformBlankedFit==0) {
	type "Perform Fit on all samples (no blanking / background subtraction)";
} else {
	type "Perform Fit for BLANKED samples (subtract placebo spectrum)";
}

// Temperature conversion. cave: temperature ramps different than 1°C/min (i.e. 1
row = 1 °C) are experimental
RowToTemp(x) = StartTemp+x*deltaT-deltaT;
TempToRow(x) = (x+deltaT-StartTemp)/deltaT;
```

```
// SECTION: DATA IMPORT AND PROCESSING

switch (Device) {

case 1:
// SUBSECTION: RT7300

// Device specific script adjustments
StringArray Filter = {"Filter A","Filter B","Filter C","Filter D"};
StringArray WL = {"530nm", "554nm", "578nm", "610nm"};
dataset DetectorLimit = {1100000,2500000,3500000,2900000}; //empiric values
derived from initial fluorescence of tenside solutions
// SampleBook protection (will be overridden otherwise, although firstmode=3
SampleBookR[9]$="RT7300 well plate"; // row 9 not used in 8by12 style 96 well
plates
// open Import dialog
impCSV options.decimal:=0 options.firstmode:=3; // see
http://wiki.originlab.com/~originla/wiki2/index.php?title=X-
Function:Details_of_TreeNodes_in_Import_CSV
string ImpBook$ = %H;
string FileName$=page.longname$;
SampleBookSheet1R.name$=FileName$;//rename SampleBook's worksheet
// create book for processed data
newbook name:="Data RT7300 raw data" result:=ResBook$ sheet:=0;
string tempResBookName$=page.name$;
loop (ii,StartCol,StopCol) {
      loop (jj,0,7) {
            fsample = ($(jj)*12)+$(ii);
            range outputR=[ResBook$]%(AF.GetAt(jj+1)$)$(ii);
            wxt test:=col(2)=$(fsample) iw:=[ImpBook$]1 ow:=outputR sel:=0 c1:=1;
            loop(bb,1,4) {
                  range outputColR=%(outputR)!wcol(bb+2);
                  outputColR[L]$="%(AF.GetAt(bb)$), %(WL.GetAt(bb)$)";
            }
            range outputColR=%(outputR)!col(1);
            outputColR[L]$="Temperature";
            outputColR[C]$="Temperature";
            outputColR[U]$="°C";
            outputColR=RowToTemp(outputColR);
      }
}
// get final temperature from data and input parameter
range DataR = [ResBook$]1!col(1);
double finalTemp = StartTemp+deltaT*(DataR.nrows-1); // 20 + (76-1)*1  = 96
// rename workbook
string ResBook$="Wellplate";
win -r %(tempResBookName$) %(ResBook$);
// I/O
type "Data import from RT7300... done.";
break;


case 2:
// SUBSECTION. qTower

// Device specific script adjustments
StringArray Filter = {"FAM", "SYPRO Orange", "TAMRA", "ROX"}; //edit filter names
dependent on your system
StringArray WL = {"520nm", "580nm", "580nm", "605nm"};
dataset DetectorLimit = {100000,100000,100000,100000}; //empiric values derived
from saturation warning
```

```
// SampleBook protection (will be overridden otherwise, although firstmode=3
SampleBookR[9]$="qTower well plate"; // row 9 not used in 8by12 style 96 well
plates
// open Import dialog
impCSV options.decimal:=2 options.firstmode:=3; // see
http://wiki.originlab.com/~originla/wiki2/index.php?title=X-
Function:Details_of_TreeNodes_in_Import_CSV
string DataSheet$ = wks.name$;
string DataBook$ = %H;
string FileName$=page.longname$;
SampleBookSheet1R.name$=FileName$;//rename SampleBook's worksheet
stringarray WellID;
// log number of samples
range IDrow = [DataBook$]1!col(1);
int nExp = IDrow.nrows;
int nFilters = nExp/96;
range DataR = [DataBook$]1!;
int nSteps = DataR.ncols-1;
double finalTemp = StartTemp+deltaT*(nSteps-1); // 20 + (76-1)*1  = 96
// create intermediate data books
loop (aa,1,nFilters) {
	range DataR = [DataBook$]1!1[1]:end[96];
	wtranspose iw:=DataR ow:=[DataF$(aa)];
	del DataR;
	// add Well ID to longname
	loop (bb,1,96) {
		range SampleR=[DataF$(aa)]1!$(bb);
		SampleR[L]$=SampleR[1]$;
		int CFerror = WellID.add(SampleR[1]$);
	}
	range firstrow=[DataF$(aa)]1![1];
	del firstrow;
	range firstcol = [DataF$(aa)]1!col(1);
	firstcol.type = 1;
}
// create book for processed data
newbook name:="Data qTower raw data" result:=ResBook$ sheet:=0;
string tempResBookName$=page.name$;
loop(i,1,96) {
	newsheet name:=WellID.GetAt(i)$;
	// create x-axis
	range TempR=[ResBook$]$(i)!1;
	TempR = {StartTemp:deltaT:finalTemp};
	TempR[L]$ = "Temperature";
	TempR[U]$ = "°C";
	// set column 2 to well plate position
	range SampleR=[ResBook$]$(i)!2;
	SampleR = {i:0:nSteps};
	// copy data from DataFBooks to WellplateBook
	loop (j,1,nFilters) {
		range DataFromR = [DataF$(j)]1!$(i);
		range DataToR = [ResBook$]$(i)!$(j+2);
		DataToR = DataFromR;
		DataToR[L]$ = Filter.GetAt(j)$;
	}
}
string ResBook$="Wellplate";
win -r %(tempResBookName$) %(ResBook$); //rename
// delete intermediate data books
loop (aa,1,nFilters) {
	range DataFR = [DataF$(aa)];
```

```
	del DataFR;
}
// I/O
type "Data import from qTower... done.";
break;

} // terminate switch


// SECTION: WORKBOOK CREATION

// create new book with well plate sample scheme for the readings
StringArray Plotbookorder = {"JustCurves", "BlankedCurves", "DiffCurves",
"SplinedCurves"};
newbook name:="Graphic results (inserted plot book)" result:=PlotBook$;
wks.autoaddrows=0;
wks.nCols=12;
wks.nRows=8;
wks1.name$=%(Plotbookorder.GetAt(1)$);
loop (aa,2,4) {
	newsheet name:=%(Plotbookorder.GetAt(aa)$);
	wks.autoaddrows=0;
	wks.nCols=12;
	wks.nRows=8;
}
string tempPlotBookName$=page.name$;

// create new book with well plate sample scheme for the processed data (peaks,
etc)
newbook name:="Data process data" result:=PDBook$ sheet:=1;
wks.autoaddrows=0;
wks.nCols=12;
wks.nRows=8;
wks.col1.label$="Sample";
wks.col1.comment$=FileName$;
PDBook$!wks1.name$="Table"; //declare sheet order*/
loop(i,1,Filter.GetSize()) {
	newsheet name:=Filter.GetAt(i)$;// cols:=12 rows:=8; not working since
autoaddrows
}
newsheet name:="DiffData";
string tempPDBookName$=page.name$;

// create new book for S/N data
newbook name:="Results S/N data" result:=SNBook$ sheet:=0;
loop(i,1,Filter.GetSize()) {
	newsheet name:=Filter.GetAt(i)$;
}
string tempSNBookName$=page.name$;

// create new book for signal averaging data
newbook name:="Data averaged signals" result:=AverageBook$ sheet:=0;
string tempAverageBookName$=page.name$;

// create new book with well plate sample scheme for the readings
newbook name:="Graphic average results (inserted averaged plot book)"
result:=AveragedPlotBook$;
wks.autoaddrows=0;
wks.nCols=12;
wks.nRows=2;
wks1.name$=%(Plotbookorder.GetAt(1)$);
```

```
loop (aa,2,4) {
	newsheet name:=%(Plotbookorder.GetAt(aa)$);
	wks.autoaddrows=0;
	wks.nCols=12;
	wks.nRows=2;
}
string tempAveragedPlotBookName$=page.name$;

// I/O
type "Initializing workbooks... done.";


// SECTION: PLOT THE RAW DATA

// global x-axis range calculation
int plotxto = finalTemp+10-MOD(finalTemp,10); // bring up to next 10-digit
loop (ii,StartCol,StopCol) {
	loop (jj,0,7) {
		fsample = ($(jj)*12)+$(ii);
		range outputR=[ResBook$]%(AF.GetAt(jj+1)$)$(ii);

		// PLOT
		plotxy iy:=%(outputR)!(1,3:end) plot:=202
ogl:=[SinglePlot%(AF.GetAt(jj+1)$)$(ii)];
		//change graph style
		yl.text$="Fluorescence intensity [a.u.]";
		layer.x.from=StartTemp; // x-axis start from
		layer.x.to=plotxto; // smart x-scale
		layer.y.label.divideBy=1000;
		layer.y.label.suf$="k";
		//move legend
		legend.y = layer1.y.to - legend.dy / 2;
		legend.x = layer1.x.from + legend.dx / 2;
		//add title label
		label -j 1 -s -sa -n title Position %(AF.GetAt(jj+1)$)$(ii),
%(FileName$)\n%([SampleBook$]1!wcol(ii)[jj+1]$);
		title.fsize=28;
		title.y = layer.y.to + title.dy / 2;
		//change line style
		set %C -z 3; // set symbol size
		// insert graph window into 8by12 worksheet
		insertGraph gname:=SinglePlot%(AF.GetAt(jj+1)$)$(ii)
cell:=[PlotBook$]1!wcol(ii)[jj+1] resizecell:=1;
	}
	// Change sheet style
	range PlotBookCol=[PlotBook$]JustCurves!col($(ii));
	PlotBookCol[L]$="Well plate column #$(ii)";
	PlotBookCol.type=2; //disregard col type
}
PlotBook$="PlotBook";
win -r %(tempPlotBookName$) %(PlotBook$); // rename Books
// I/O
type "%(PlotBook$)... done.";


// SECTION: SIGNAL AVERAGING
// included with 5.1, 20120613

// summary plots (with and without blanking) of all averaged melting curves
StringArray SumPlot = {"SumAvPlot", "SumAvPlotBlanked"};
// determine the number of sample from the arguments
```

```
nSamples = (StopCol-StartCol+1)*2;
// average wells 1-3 & 5-7 of every column (omit blanks)
loop (ii,1,nSamples) {
		// define wells to be averaged
		int AVtoggle = 2-mod(ii,2); // (1..2) toggle
		int AVcounter = round(ii/2,0); // (1,1..2,2..)
		AverageName$ = "%(AF.GetAt(AVtoggle*4-
3)$)$(AVcounter)%(AF.GetAt(AVtoggle*4-2)$)$(AVcounter)%(AF.GetAt(AVtoggle*4-
1)$)$(AVcounter)";
		newsheet book:=%(AverageBook$) name:=AverageName$;
		// prepare X column of averaged data
		range AveragedXR = [%(AverageBook$)]$(ii)!col(1);
		range RawXR = [%(ResBook$)]1!col(1);
		AveragedXR = RawXR;
		AveragedXR[L]$="Temperature";
		AveragedXR[C]$="Temperature";
		AveragedXR[U]$="°C";
		// average the 3 wells over all filters
		loop (gg,StartFitFilter,Filter.GetSize()) {
			// prepare mean values
			range RawWellY1R = [%(ResBook$)]%(AF.GetAt(AVtoggle*4-
3)$)$(AVcounter)!wcol(gg+2); // 1st well.. Filter A starts in col(3)
			range RawWellY2R = [%(ResBook$)]%(AF.GetAt(AVtoggle*4-
2)$)$(AVcounter)!wcol(gg+2); // 2nd well
			range RawWellY3R = [%(ResBook$)]%(AF.GetAt(AVtoggle*4-
1)$)$(AVcounter)!wcol(gg+2); // 3rd well
			range AveragedYR = [%(AverageBook$)]$(ii)!wcol(gg+1); //
destination for averaged signals. Filter A will be in col(2)
			AveragedYR = (RawWellY1R + RawWellY2R + RawWellY3R)/3;
			AveragedYR[C]$="%(Filter.GetAt(gg)$)";
			AveragedYR[U]$="a.u.";
			AveragedYR[L]$="Average of
%(RawWell1R.name$)+%(RawWell2R.name$)+%(RawWell3R.name$)";
			// blank averaged signals
			range RawPlaceboR =
[%(ResBook$)]%(AF.GetAt(AVtoggle*4)$)$(AVcounter)!wcol(gg+2); // Placebo is the
4th well
			range BlankedAveragedYR = [%(AverageBook$)]$(ii)!wcol(gg+5);
// Filter A will be in col(6)
			BlankedAveragedYR = AveragedYR - RawPlaceboR;
			BlankedAveragedYR[C]$="Blanked %(Filter.GetAt(gg)$)";
			BlankedAveragedYR[U]$="a.u.";
			BlankedAveragedYR[L]$="Blanked Average of
%(RawWell1R.name$)+%(RawWell2R.name$)+%(RawWell3R.name$)";
			// for further data processing decide if BLANKED or NON-
BLANKED
			if (PerformBlankedFit==1) {
				InputAveragedYR=BlankedAveragedYR;
			} else {
				InputAveragedYR=AveragedYR;
			}
			// derive (differentiate) (do not smooth the average curves)
			range DerivedBlankedAveragedYR =
[%(AverageBook$)]$(ii)!wcol(gg+9); // Filter A will be in col(10)
			differentiate iy:=InputAveragedYR smooth:=0
oy:=DerivedBlankedAveragedYR;
			DerivedBlankedAveragedYR[C]$="Blanked 1st derivative
%(Filter.GetAt(gg)$)";
			DerivedBlankedAveragedYR[U]$="a.u.";
			DerivedBlankedAveragedYR[L]$="Derived Blanked Average of
%(RawWell1R.name$)+%(RawWell2R.name$)+%(RawWell3R.name$)";
```

```
                    // spline
                    xmaxforspline = RowToTemp(DerivedBlankedAveragedYR.nrows);
                    noip = (xmaxforspline-StartTemp)*10+1;
                    interp1xy iy:=DerivedBlankedAveragedYR method:=spline
npts:=$(noip) xmin:=$(StartTemp) xmax:=$(xmaxforspline) boundary:= notaknot
oy:=[%(AverageBook$)]$(ii)!(14,$(gg+14));
                    range SplinedDerBlaAveXR = [%(AverageBook$)]$(ii)!wcol(14); //
new splined x-axis will be in col(14)
                    SplinedDerBlaAveXR[L]$="Temperature";
                    SplinedDerBlaAveXR[U]$="°C";
                    SplinedDerBlaAveXR[C]$="Blanked+splined 1st derivative";
                    range SplinedDerBlaAveYR = [%(AverageBook$)]$(ii)!wcol(gg+14);
// Filter A will be in col(15)
                    SplinedDerBlaAveYR[C]$="Blanked+splined 1st derivative
%(Filter.GetAt(gg)$)";
                    SplinedDerBlaAveYR[U]$="a.u.";
                    SplinedDerBlaAveYR[L]$="Splined Derived Blanked Average of
%(RawWell1R.name$)+%(RawWell2R.name$)+%(RawWell3R.name$)";
                    // peak find
                    range
SplinedDiffPeakCenters=[%(AverageBook$)]$(ii)!wcol(gg*2+17);
                    range SplinedDiffPeakY=[%(AverageBook$)]$(ii)!wcol(gg*2+18);
                    SplinedDiffPeakCenters[C]$="Temperature";
                    SplinedDiffPeakCenters[U]$="°C";
                    SplinedDiffPeakCenters[L]$="Peaks %(Filter.GetAt(gg)$)";
                    pkFind -se iy:=SplinedDerBlaAveYR method:=first dir:=both
ocenter:=SplinedDiffPeakCenters; // -se to ignore "Keine Peaks gefunden.."
                    NoFoundPeaks=SplinedDiffPeakCenters.nrows;
                    if (0 != xf_get_last_error_code()) {
                          strError$ = "pkFind failed: " +
xf_get_last_error_message()$;
                          type strError$;
                          SplinedDiffPeakCenters[1]=StartTemp;
                          SplinedDiffPeakY[1]=0; // set first row = 0
                          SplinedDiffPeakY[C]$="no peak found";
                          type
"[%(SplineBook$)]%(AF.GetAt(jj+1)$)$(ii)!col($(gg*2+4)) skipping peakfind";
                    } else {
                          SplinedDiffPeakY[C]$="Peaks %(Filter.GetAt(gg)$)";
                          SplinedDiffPeakY[U]$="a.u.";
                          SplinedDiffPeakY[L]$="";
                          loop (uu,1,$(NoFoundPeaks)) {
                                SplinedDiffPeakY[uu] =
SplinedDerBlaAveYR[$(SplinedDiffPeakCenters[uu])];

      SplinedDiffPeakCenters[uu]=SplinedDerBlaAveXR[SplinedDiffPeakCenters[uu]];
                          }
                    }
                    SplinedDiffPeakCenters.type=4; //set as X
             }
             // sort graphs in new 12by2 order
             int helpx = round(ii/2,0)+StartCol-1;
             int helpy = -1*mod(ii,2)+2; //awesome!
             // change graph layouts
             loop (kk,1,4) { //loop through plot book
             // splined graphs have different x-axis scaling
             if (kk==4) {
                    colx = 14;
                    colystart = 15;
                    colystop = 18;
                    plottype = 200;
```

```
                    // plot peak dots
                    loop (yy,1,4) {
                          plotxy
iy:=[%(AverageBook$)]$(ii)!($(yy*2+17):$(yy*2+18)) plot:=201 color:=6
ogl:=[Av%(Plotbookorder.GetAt(kk)$)%(AverageName$)];
                    }
                    loop (xx,1,4) {
                          range
graphPeak=[Av%(Plotbookorder.GetAt(kk)$)%(AverageName$)]1!$(xx);
                          win -o Av%(Plotbookorder.GetAt(kk)$)%(AverageName$) {
                                layer -ilx graphPeak;
                          }
                    }
             } else {
                    colx = 1;
                    colystart = kk*4-2;
                    colystop = kk*4+1;
                    plottype = 202;
             }
             // PLOT
             plotxy iy:=[%(AverageBook$)]$(ii)!($(colx),$(colystart):$(colystop))
plot:=plottype ogl:=[Av%(Plotbookorder.GetAt(kk)$)%(AverageName$)];
             //change Graph style
             yl.text$="Mean fluorescence intensity (n=3) [a.u.]";
             layer.x.from=StartTemp; // x-axis start from
             layer.x.to=plotxto; // smart x-scale
             layer.y.label.divideBy=1000;
             layer.y.label.suf$="k";
             //move legend
             legend.y = layer1.y.to - legend.dy / 2;
             legend.x = layer1.x.from + legend.dx / 2;
             //add title label
             label -j 1 -s -sa -n title Position %(AverageName$),
%(FileName$);//\n%([SampleBook$]1!wcol(ii)[jj+1]$);
             title.fsize=28;
             title.y = layer.y.to + title.dy / 2;
             //change line style
             set %C -z 3; // set symbol size
             //insert plots
             range AveragedPlotsR = [AveragedPlotBook$]$(kk)!wcol(helpx)[helpy];
             insertGraph gname:=Av%(Plotbookorder.GetAt(kk)$)%(AverageName$)
cell:=AveragedPlotsR resizecell:=1;
       }
             // SUMMARY PLOT
             filterno = 3; // 1=A, 2=B, 3=C, 4=D
             coly=5+filterno;
             plotxy iy:=[%(AverageBook$)]$(ii)!(1,$(coly)) plot:=plottype
color:=$(ii) ogl:=[%(SumPlot.GetAt(2)$)];
             coly=1+filterno;
             plotxy iy:=[%(AverageBook$)]$(ii)!(1,$(coly)) plot:=plottype
color:=$(ii) ogl:=[%(SumPlot.GetAt(1)$)];
}
// rename Books
AveragedPlotBook$="AveragePltBk";
win -r %(tempAveragedPlotBookName$) %(AveragedPlotBook$);
AverageBook$="AverageBook";
win -r %(tempAverageBookName$) %(AverageBook$);
// change summary plot style
loop (ll, 1, 2) {
       win -o %(SumPlot.GetAt(ll)$) {
             //change graph style
```

```
            yl.text$="Mean fluorescence intensity (n=3) [a.u.]";
            layer.x.from=StartTemp; // x-axis start from
            layer.x.to=plotxto; // smart x-scale
            layer.y.label.divideBy=1000;
            layer.y.label.suf$="k";
            //move legend
            legend.y = layer1.y.to - legend.dy / 2;
            legend.x = layer1.x.from + legend.dx / 2;
            // Update legend of summary plot
            legend.fsize=12;
            legendupdate mode:=custom custom:="@WS";
      }
}
// I/O
type "%(AverageBook$)... done.";
type "%(AveragedPlotBook$)... done.";


// SECTION: BLANKS SUBTRACTION
// Blank samples are in wells 4 & 8 of every column

// create new workbook and start subtraction
newbook name:="Data blanked data" result:=BlankedBook$ sheet:=0;
string tempBlankedBookName$=page.name$;
int BlankDist=4; //every 4th sample is a blank
loop(ii,StartCol,StopCol) {
      loop(jj,0,7) {
            fsample = ($(jj)*12)+$(ii);
            range BlankedR=[BlankedBook$]%(AF.GetAt(jj+1)$)$(ii)!1;
            range SampleR=[ResBook$]%(AF.GetAt(jj+1)$)$(ii)!1;
            BlankedR=SampleR; //fill in the temperature
            BlankedR.name$="Temp";
            BlankedR[L]$="Temperature";
            BlankedR[U]$="°C";
            int fblank=fsample+BlankDist;
            loop(kk,StartFitFilter,Filter.GetSize()) {//loop over all 4 filters
                  range SampleR=[ResBook$]%(AF.GetAt(jj+1)$)$(ii)!$(kk+2);
                  range
BlankR=[ResBook$]%(AF.GetAt(jj+BlankDist)$)$(ii)!$(kk+2);
                  range BlankedR=[BlankedBook$]%(AF.GetAt(jj+1)$)$(ii)!$(kk+2);
//vorher kk+1 aber da gleicher style notwendig für PerformBlankedFit
                  BlankedR=SampleR-BlankR;
                  BlankedR[L]$="%(AF.GetAt(jj+1)$)$(ii)-
%(AF.GetAt(jj+BlankDist)$)$(ii)=";
                  BlankedR[C]$="Blanked Filter %(AF.GetAt(kk)$)";
            }
            // PLOT
            plotxy iy:=[BlankedBook$]%(AF.GetAt(jj+1)$)$(ii)!(1,3:end) plot:=202
ogl:=[SingleBlankedPlot%(AF.GetAt(jj+1)$)$(ii)]; //vorher (1,2:end) aber da
gleicher style notwendig für PerformBlankedFit
            //change Graph style
            yl.text$="Fluorescence intensity [a.u.]";
            layer.y.label.divideBy=1000;
            layer.y.label.suf$="k";
            //move legend
            legend.y = layer1.y.to - legend.dy / 2;
            legend.x = layer1.x.from + legend.dx / 2;
            layer.x.from=StartTemp; // x-axis start from
            layer.x.to=plotxto; // smart x-scale
            //add title label
```

```
            label -j 1 -s -sa -n title Position %(AF.GetAt(jj+1)$)$(ii),
%(FileName$)\n%([SampleBook$]1!wcol(ii)[jj+1]$);
            title.fsize=28;
            title.y = layer.y.to + title.dy / 2;
            //change line style
            set %C -z 3; // set symbol size
            // insert graphs
            insertGraph gname:=SingleBlankedPlot%(AF.GetAt(jj+1)$)$(ii)
cell:=[PlotBook$]BlankedCurves!wcol(ii)[jj+1] resizecell:=1;
            // adjust BlankDist
            if (BlankDist==1) {
                  BlankDist=4;
            } else {
                  BlankDist-=1;
            }
      }
}
// rename Books
string BlankedBook$="BlankedWell";
win -r %(tempBlankedBookName$) %(BlankedBook$);
// I/O
type "%(BlankedBook$)... done.";


// SECTION: DATA PROCESSING

// Decide if BLANKED or NON-BLANKED samples are to be analyzed
if (PerformBlankedFit==1) {
      ResBook$=%(BlankedBook$);
      type "Using %(BlankedBook$) for fitting!";
}

// Find min, max, peaks, S/N values
loop (ii,StartCol,StopCol) {
      loop (jj,0,7) {
            fsample = ($(jj)*12)+$(ii);
            range outputR=[ResBook$]%(AF.GetAt(jj+1)$)$(ii);
            loop(hh,StartFitFilter,Filter.GetSize()) {
                  range InputR=%(outputR)!wcol(hh+2);//filter A starts in col 3
                  int minPeakHeight = round(max(InputR)/100); // 40: empirical
value.
                  dataset PeakD=peaks(InputR, 4, minPeakHeight);//tweak value
between 4 and 10000
                  loop (ee,1,2) {
                        range DataR=[PDBook$]%(Filter.GetAt(hh)$)!wcol(ee+1);
                        DataR[fsample]=RowToTemp(PeakD[ee]);
                        DataR[L]$="Peak $(ee)";
                  }
                  range TableR=[PDBook$]%(Filter.GetAt(hh)$)!col(1);
                  TableR[fsample]$="%(AF.GetAt(jj+1)$)$(ii)";
                  //table peaks
                  range TableR=[PDBook$]"Table"!wcol(hh+1);//col 1 samples
                  TableR[C]$=Filter.GetAt(hh)$;
                  TableR[U]$="°C";
                  TableR[L]$="Peaks";
                  TableR[fsample]=RowToTemp(PeakD[1]);
                  //table min-max
                  range TableMinR=[PDBook$]"Table"!wcol(hh+5);//col 5 sample,
peaks
                  TableMinR[C]$=Filter.GetAt(hh)$;
                  TableMinR[U]$="°C";
```

```
                    TableMinR[L]$="Min";
                    range TableMaxR=[PDBook$]"Table"!wcol(hh+9);//col 9 sample,
peaks, min
                    TableMaxR[C]$=Filter.GetAt(hh)$;
                    TableMaxR[U]$="°C";
                    TableMaxR[L]$="Max";
                    // find MINUMUM and MAXIMUM
                    mi = min(InputR); // important: variable has to be at least
double (no int), because qTower produces rational numbers
                    mx = max(InputR);
                    for (int gg=1; gg<=InputR.GetSize(); gg++) {
                          if (mi==InputR[gg]) {
                                TableMinR[fsample]=RowToTemp(gg);
                          }
                          if (mx==InputR[gg]) {
                                TableMaxR[fsample]=RowToTemp(gg);
                          }
                    }
                    // S/N Ratio
                    range PDPeak1R=[PDBook$]%(Filter.GetAt(hh)$)!wcol(2);
                    range PDPeak2R=[PDBook$]%(Filter.GetAt(hh)$)!wcol(3);
                    range SNPeakR=[SNBook$]%(Filter.GetAt(hh)$)!col(2);
                    SNPeakR[L]$="Peak";
                    SNPeakR[U]$="°C";
                    range PDFilterC_yR=%(OutputR)!wcol(5); // Filter C in col 5
                    range SNPeak_yR=[SNBook$]%(Filter.GetAt(hh)$)!col(3);
                    SNPeak_yR[L]$="Peak_y=S";
                    SNPeak_yR[U]$="a.u.";
                    range PDMinR=[PDBook$]"Table"!col(8); // Min Filter C
                    range SNMinR=[SNBook$]%(Filter.GetAt(hh)$)!col(4);
                    SNMinR[L]$="Min";
                    SNMinR[U]$="°C";
                    range SNMin_yR=[SNBook$]%(Filter.GetAt(hh)$)!col(5);
                    SNMin_yR[L]$="Min_y=N";
                    SNMin_yR[U]$="a.u.";
                    range SNInit_yR=[SNBook$]%(Filter.GetAt(hh)$)!col(6);
                    SNInit_yR[L]$="Init_y=N";
                    SNInit_yR[U]$="a.u.";

                    // get peak
                    if (PDPeak1R[fsample]>PDPeak2R[fsample]) {
                          SNPeakR[fsample]=PDPeak1R[fsample];
                    } else {
                          SNPeakR[fsample]=PDPeak2R[fsample];
                    }
                    // get min
                    SNMinR[fsample]=PDMinR[fsample];

                    // set S and N values (e.g., corresponding fluorescence
intensities)
                    SNPeak_yR[fsample]=PDFilterC_yR[TempToRow(SNPeakR[fsample])];
                    SNMin_yR[fsample]=PDFilterC_yR[TempToRow(SNMinR[fsample])];
                    SNInit_yR[fsample]=InputR[1];
                    range PHR=[SNBook$]%(Filter.GetAt(hh)$)!col(7); // peak height
                    PHR[L]$="Peak Height";
                    PHR[U]$="a.u.";
                    PHR[fsample]=SNPeak_yR[fsample]-SNMin_yR[fsample];
                    range IHR=[SNBook$]%(Filter.GetAt(hh)$)!col(8); // peak height
                    IHR[L]$="Init Height";
                    IHR[U]$="a.u.";
                    IHR[fsample]=SNInit_yR[fsample]-SNMin_yR[fsample];
```

```
                    range SNRR=[SNBook$]%(Filter.GetAt(hh)$)!col(9);
                    SNRR[L]$="S/N Ratio";
                    SNRR[fsample]=SNPeak_yR[fsample]/SNMin_yR[fsample];
                    range WPRR=[SNBook$]%(Filter.GetAt(hh)$)!col(10);
                    WPRR[L]$="Weighted Peak Ratio";

      WPRR[fsample]=(SNPeak_yR[fsample]+SNMin_yR[fsample])/SNMin_yR[fsample];
                    range AGGCR=[SNBook$]%(Filter.GetAt(hh)$)!col(11);
                    AGGCR[L]$="Agg. content";
                    AGGCR[U]$="%";
                    AGGCR[fsample]=(SNInit_yR[fsample]-
SNMin_yR[fsample])/(SNPeak_yR[fsample]-SNMin_yR[fsample])*100;
                    range TableR=[SNBook$]%(Filter.GetAt(hh)$)!col(1);
                    TableR[fsample]$="%(AF.GetAt(jj+1)$)$(ii)";
             }
             range TableR=[PDBook$]"Table"!col(1);
             TableR[fsample]$="%(AF.GetAt(jj+1)$)$(ii)";
      }
}
// rename books
PDBook$="ProcessData";
win -r %(tempPDBookName$) %(PDBook$);
SNBook$="SNData";
win -r %(tempSNBookName$) %(SNBook$);
// I/O
type "%(PDBook$), %(SNBook$)... done.";


// SECTION: DIFFERENTIATION

// derive the fluorescence melting curves to find the Tm values
loop(gg,StartFitFilter,Filter.GetSize()) {
      loop(ii,StartCol,StopCol) {
             loop(jj,0,7) {
                    fsample = ($(jj)*12)+$(ii);
                    range InputR=[ResBook$]%(AF.GetAt(jj+1)$)$(ii)!;
                    range DataR=%(InputR)wcol(gg+2);
                    differentiate iy:=DataR smooth:=1 poly:=1 npts:=5;
                    // find peaks in differentiation
                    int diffcol=InputR.ncols;
                    range DiffR=%(InputR)wcol(diffcol);

/*                  // new style (experimental)
                    range AllDiffPeakCenters = [DiffTmBook$]$(gg)!wcol(fsample);
                    AllDiffPeakCenters[U]$="°C";
                    AllDiffPeakCenters[C]$=%(AF.GetAt(jj+1)$)$(ii);
                    //AllDiffPeakCenters[L]$="Peak Center";
                    pkFind -se iy:=DiffR method:=max dir:=both
ocenter:=AllDiffPeakCenters;
                    if( 0 != xf_get_last_error_code() ){
                           strError$ = "XFunction Failed: " +
xf_get_last_error_message()$;
                           type strError$;
                           AllDiffPeakCenters=0;
                           type "if loop: diffcol=$(diffcol); %(DiffR)";
                    } else {
                    AllDiffPeakCenters = RowToTemp(AllDiffPeakCenters);
                    type "else loop: diffcol=$(diffcol); %(DiffR)";
                    }
*/
                    // old fashion
```

```
                    int minDiffHeight = round(max(DiffR)/5); // 40: empirical
value.
                    dataset PeakD=peaks(DiffR,5,minDiffHeight); //
                    if (PeakD.getSize()<2) {
                           minDiffHeight = round(minDiffHeight/5);
                           PeakD=peaks(DiffR,10,minDiffHeight);
                    }
                    if (PeakD.getSize()<2) {
                           minDiffHeight = round(minDiffHeight/2);
                           PeakD=peaks(DiffR,10,minDiffHeight);
                    }
                    if ($(PeakD[3])>$(PeakD[2])) {
                           range
BetweenPeaksR=%(InputR)wcol(diffcol)[$(PeakD[2]):$(PeakD[3])];
                           mi=min(BetweenPeaksR);
                    } else {
                           range
BetweenPeaksR=%(InputR)wcol(diffcol)[$(PeakD[1]):$(PeakD[2])];
                           mi=min(BetweenPeaksR);
                    }

                    // find minimum between both peaks -> most negative value =
descending slope
                    range
InputDiffR=[ResBook$]%(AF.GetAt(jj+1)$)$(ii)!wcol(diffcol);
                    for (int ff=1; ff<=InputDiffR.GetSize(); ff++) {
                           if (mi==InputDiffR[ff]) {
                                  mii=ff;
                           }
                    }
                    DiffR=abs(DiffR); //work with absolute values (necessary for
further analysis)
                    range
BetweenMinandPeak2R=%(InputR)wcol(diffcol)[$(mii):$(PeakD[2])];
                    double miatmeltcurve=min(BetweenMinandPeak2R);
                    if ($(miatmeltcurve)=="--") { //fit will break if
miatmeltcurve is empty
                           miatmeltcurve=RowToTemp($(PeakD[2]));
                    }
                    range
InputDiffR=[ResBook$]%(AF.GetAt(jj+1)$)$(ii)!wcol(diffcol);
                    for (int ff=1; ff<=InputDiffR.GetSize(); ff++) {
                           if (miatmeltcurve==InputDiffR[ff]) {
                                  miatmeltcurve=RowToTemp(ff);
                           }
                    }

                    // empirical evaluation for find the local minimum in front of
peak by subtracting an empirical temperature value (-> 4p)
                    if ($(PeakD[3])>$(PeakD[2])) {
                           int ULpeak3 = $(PeakD[3])-2;
                           range localMinDiffR=%(InputR)wcol(diffcol)[$(ULpeak3-
15):$(ULpeak3)]; // 15
                           localmin=min(localMinDiffR);
                    } else {
                           if ($(PeakD[2])>$(PeakD[1])) {
                                  int ULpeak2 = $(PeakD[2])-2;
                                  range
localMinDiffR=%(InputR)wcol(diffcol)[$(ULpeak2-15):$(ULpeak2)]; // 15
                                  localmin=min(localMinDiffR);
                           } else {
```

```
                                int ULpeak1 = $(PeakD[1])-2;
                                range
localMinDiffR=%(InputR)wcol(diffcol)[$(ULpeak1-15):$(ULpeak1)];
                                localmin=min(localMinDiffR);
                        }
                  }
                  range
InputDiffR=[ResBook$]%(AF.GetAt(jj+1)$)$(ii)!wcol(diffcol);
                  for (int ff=1; ff<=InputDiffR.GetSize(); ff++) {
                        if (localmin==InputDiffR[ff]) {
                              localmin=RowToTemp(ff);
                        }
                  }
                  // reporting
                  loop(hh,1,5) {
                        int DiffDataCol = (gg-1)*5+hh+1;
                        range TableR=[PDBook$]"DiffData"!col(DiffDataCol);//col
1 samples
                        if (hh<4) {
                              TableR[C]$=Filter.GetAt(gg)$;
                              TableR[U]$="°C";
                              TableR[L]$="Peak $(hh)";
                              TableR[fsample]=RowToTemp(PeakD[hh]);
                        } else {
                              if (hh==4) {
                              TableR[C]$=Filter.GetAt(gg)$;
                              TableR[U]$="°C";
                              TableR[L]$="Min tween 1&2";
                              TableR[fsample]=miatmeltcurve;
                              } else {
                                    TableR[C]$=Filter.GetAt(gg)$;
                                    TableR[U]$="°C";
                                    TableR[L]$="local Min";
                                    TableR[fsample]=localmin;
                              }
                        }
                  }
                  // create the plots
                  if (gg==4) {
                        //fill first column
                        range TableR=[PDBook$]"DiffData"!col(1);
                        TableR[fsample]$="%(AF.GetAt(jj+1)$)$(ii)";
                        // PLOT
                        plotxy iy:=[ResBook$]%(AF.GetAt(jj+1)$)$(ii)!(1,7:end)
plot:=202 ogl:=[DiffPlot%(AF.GetAt(jj+1)$)$(ii)];
                        //change Graph style
                        yl.text$="Fluorescence intensity [a.u.]";
                        layer.y.label.divideBy=1000;
                        layer.y.label.suf$="k";
                        //move legend
                        legend.y = layer1.y.to - legend.dy / 2;
                        legend.x = layer1.x.from + legend.dx / 2;
                        layer.x.from=StartTemp; // x-axis start from
                        layer.x.to=plotxto; // smart x-scale
                        //add title label
                        label -j 1 -s -sa -n title Position
%(AF.GetAt(jj+1)$)$(ii), %(FileName$)\n%([SampleBook$]1!wcol(ii)[jj+1]$);
                        title.fsize=28;
                        title.y = layer.y.to + title.dy / 2;
                        //change line style
                        set %C -z 3; // set symbol size
```

```
                        //insert graphs
                        insertGraph gname:=DiffPlot%(AF.GetAt(jj+1)$)$(ii)
cell:=[PlotBook$]DiffCurves!wcol(ii)[jj+1] resizecell:=1;
                  }
            }
      }
}
//DiffTmBook$="DiffTmBook";
//win -r %(tempDiffTmBookName$) %(DiffTmBook$); // rename
// I/O
type "Differentiation... done.";



// SECTION: SPLINING

// create new book with interpolated data
newbook name:="Data splined derived data" result:=SplineBook$ sheet:=0;
string tempSplineBookName$=page.name$;
loop(gg,StartFitFilter,Filter.GetSize()) {
      loop(ii,StartCol,StopCol) {
            loop(jj,0,7) {
                  fsample = ($(jj)*12)+$(ii);
                  range InputR=[ResBook$]%(AF.GetAt(jj+1)$)$(ii)!;
                  // interpolate - splining
                  range DiffDataR=%(InputR)wcol(gg+6);
                  xmaxforspline = RowToTemp(DiffDataR.nrows);
                  noip = (xmaxforspline-StartTemp)*100+1;
                  interp1xy iy:=%(InputR)(1,$(gg+6)) method:=spline
npts:=$(noip) xmin:=$(StartTemp) xmax:=$(xmaxforspline) boundary:= notaknot
oy:=[SplineBook$]%(AF.GetAt(jj+1)$)$(ii)!(1,$(gg+1));
                  range
SplinedCol1R=[SplineBook$]%(AF.GetAt(jj+1)$)$(ii)!col(1);
                  SplinedCol1R[U]$="°C";
                  SplinedCol1R[C]$="Temperature";
                  range
SplinedDataR=[SplineBook$]%(AF.GetAt(jj+1)$)$(ii)!wcol(gg+1);
                  SplinedDataR[C]$="Splined %(Filter.GetAt(gg)$)";
                  range
SplinedDiffPeakCenters=[SplineBook$]%(AF.GetAt(jj+1)$)$(ii)!wcol(gg*2+4);
                  range
SplinedDiffPeakY=[SplineBook$]%(AF.GetAt(jj+1)$)$(ii)!wcol(gg*2+5);// 1 col vor
Peak Center
                  SplinedDiffPeakCenters[C]$="Temperature";
                  SplinedDiffPeakCenters[U]$="°C";
                  SplinedDiffPeakCenters[L]$=%(AF.GetAt(jj+1)$)$(ii);
                  pkFind -se iy:=SplinedDataR method:=first dir:=both
ocenter:=SplinedDiffPeakCenters; // -se to ignore "Keine Peaks gefunden.."
                  NoFoundPeaks=SplinedDiffPeakCenters.nrows;
                  if (0 != xf_get_last_error_code()) {
                        strError$ = "pkFind failed: " +
xf_get_last_error_message()$;
                        type strError$;
                        SplinedDiffPeakCenters[1]=StartTemp;
                        SplinedDiffPeakY[1]=0; // set first row = 0
                        SplinedDiffPeakY[C]$="no peak found";
                        type
"[%(SplineBook$)]%(AF.GetAt(jj+1)$)$(ii)!col($(gg*2+4)) skipping peakfind";
                  } else {
                        SplinedDiffPeakY[C]$="Peaks %(Filter.GetAt(gg)$)";
                        SplinedDiffPeakY[U]$="a.u.";
```

```
                        SplinedDiffPeakY[L]$="first derivated fluorescence
intensity";
                        loop (uu,1,$(NoFoundPeaks)) {
                              SplinedDiffPeakY[uu] =
SplinedDataR[$(SplinedDiffPeakCenters[uu])];

      SplinedDiffPeakCenters[uu]=SplinedCol1R[SplinedDiffPeakCenters[uu]];
                        }
                  }
                  SplinedDiffPeakCenters.type=4; //set as X
            }
      }
}
SplineBook$="SplineBook";
win -r %(tempSplineBookName$) %(SplineBook$); //rename
// I/O
type "Splining... done.";



// SUBSECTION: PLOT SPLINED DIFF DATA

loop(ii,StartCol,StopCol) {
      loop(jj,0,7) {
            loop(gg,1,4) {
                  plotxy
iy:=[SplineBook$]%(AF.GetAt(jj+1)$)$(ii)!($(gg*2+4):$(gg*2+5)) plot:=201 color:=6
ogl:=[SplinedDiffPlot%(AF.GetAt(jj+1)$)$(ii)];
            }
            loop (xx,1,4) {
                  range
graphPeak=[SplinedDiffPlot%(AF.GetAt(jj+1)$)$(ii)]1!$(xx);
                  win -o SplinedDiffPlot%(AF.GetAt(jj+1)$)$(ii) {
                        layer -ilx graphPeak;
                  }
            }
            // PLOT
            plotxy iy:=[SplineBook$]%(AF.GetAt(jj+1)$)$(ii)!(1,2:5) plot:=200
ogl:=[SplinedDiffPlot%(AF.GetAt(jj+1)$)$(ii)];
            win -o SplinedDiffPlot%(AF.GetAt(jj+1)$)$(ii) {
                  //change Graph style
                  xb.text$="Temperature [%(?X,@LU)]";
                  layer.y.label.divideBy=1000;
                  layer.y.label.suf$="k";
                  //move legend
                  legend.y = layer1.y.to - legend.dy / 2;
                  legend.x = layer1.x.from + legend.dx / 2;
                  layer.x.from=StartTemp; // x-axis start from
                  layer.x.to=plotxto; // smart x-scale
                  //add title label
                  label -j 1 -s -sa -n title Position %(AF.GetAt(jj+1)$)$(ii),
%(FileName$)\n%([SampleBook$]1!wcol(ii)[jj+1]$);
                  title.fsize=28;
                  title.y = layer.y.to + title.dy / 2;
            }
            insertGraph gname:=SplinedDiffPlot%(AF.GetAt(jj+1)$)$(ii)
cell:=[PlotBook$]SplinedCurves!wcol(ii)[jj+1] resizecell:=1;
      }
}
// I/O
type "Plotting splined differentiation plots ... done.";
```

```
// SECTION: BOLTZMANN FIT --> Tm and Ton

// create new books for the results of the 4 different fit processes (1-4p)
StringArray MainSA = {"1p","2p","3p","4p"};
newbook name:="Results Tm from Boltzmann Fit" result:=FitBook$ sheet:=0;
string tempFitBookName$=page.name$;
newbook name:="Results Tmonset (Onset temperature)" result:=TonBook$ sheet:=0;
string tempTonBookName$=page.name$;
loop(aa,1,4) {
	type "... fitting with %(MainSA.GetAt(aa)$) ";
	// create new sheets in FitBook
	newsheet book:=FitBook$ name:="%(MainSA.GetAt(aa)$)FitTable";//add a new
sheet for table like fit results
	loop (hh,1,4) {
		newsheet book:=FitBook$ name:="%(MainSA.GetAt(aa)$)Tmelt$(hh)";//add
a new sheet for wellplate style x0
		range DataR=[FitBook$]%(MainSA.GetAT(aa)$)Tmelt$(hh)!;
		DataR.autoaddrows=0;
		DataR.nCols=12;
		DataR.nRows=8;
	}
	// create new sheets in TonBook
	newsheet book:=TonBook$ name:="%(MainSA.GetAt(aa)$)TonTable";//add a new
sheet for table like TON results
	loop (hh,1,4) {
		newsheet book:=TonBook$ name:="%(MainSA.GetAt(aa)$)Ton$(hh)";//add a
new sheet for wellplate style x0
		range DataR=[TonBook$]%(MainSA.GetAT(aa)$)Ton$(hh)!;
		DataR.autoaddrows=0;
		DataR.nCols=12;
		DataR.nRows=8;
	}
	//create new sheets in PlotBook
	loop(i,StartFitFilter,Filter.GetSize()) {
		newsheet book:=PlotBook$ name:="%(MainSA.GetAt(aa)$)FitCurves$(i)";
		range DataR=[PlotBook$]%(MainSA.GetAT(aa)$)FitCurves$(i)!;
		DataR.autoaddrows=0;
		DataR.nCols=12;
		DataR.nRows=8;
	}
	//range notation stay constant and can therefore easily been done before the
for-loop
	range rFitSample=[FitBook$]"%(MainSA.GetAt(aa)$)FitTable"!col(1);
	rFitSample[L]$="Sample";
	rFitSample[C]$=FileName$;
	range rTonSample=[TonBook$]"%(MainSA.GetAt(aa)$)TonTable"!col(1);
	rTonSample[L]$="Sample";
	rTonSample[C]$=FileName$;
	// start fitting across all filters...
	loop(gg,StartFitFilter,Filter.GetSize()) {
		range rFitA1 = [FitBook$]"%(MainSA.GetAt(aa)$)FitTable"!wcol(gg*4-2);
// formula StartFitFilter*4-4+2
		rFitA1[L]$="A1 %(Filter.GetAt(gg)$)";
		rFitA1[C]$="Boltzmann for %(Filter.GetAt(gg)$)";
		rFitA1.width=10;
		range rFitA2 = [FitBook$]"%(MainSA.GetAt(aa)$)FitTable"!wcol(gg*4-1);
		rFitA2[L]$="A2 %(Filter.GetAt(gg)$)";
		rFitA2[C]$="Boltzmann for %(Filter.GetAt(gg)$)";
```

```
            rFitA2.width=10;
            range rFitx0 = [FitBook$]"%(MainSA.GetAt(aa)$)FitTable"!wcol(gg*4);
            rFitx0[L]$="x0 %(Filter.GetAt(gg)$)";
            rFitx0[C]$="Boltzmann for %(Filter.GetAt(gg)$)";
            rFitx0.width=10;
            range rFitdx = [FitBook$]"%(MainSA.GetAt(aa)$)FitTable"!wcol(gg*4+1);
            rFitdx[L]$="dx %(Filter.GetAt(gg)$)";
            rFitdx[C]$="Boltzmann for %(Filter.GetAt(gg)$)";
            rFitdx.width=10;
            range rTon = [TonBook$]"%(MainSA.GetAt(aa)$)TonTable"!wcol(gg+1);
            rTon[L]$="Tonset %(Filter.GetAt(gg)$)";
            rTon[U]$="°C";
            rTon[C]$="Lower interception";
            rTon.width=10;
            range PDPeak1R=[PDBook$]%(Filter.GetAt(gg)$)!col(2);
            range PDPeak2R=[PDBook$]%(Filter.GetAt(gg)$)!col(3);
            range DiffPeakR=[PDBook$]"DiffData"!wcol(gg*5);// 5th,starts col 5
            range DiffLocalMinR=[PDBook$]"DiffData"!wcol(gg*5+1);// 5th, col 6
            range TableMinR=[PDBook$]"Table"!wcol(gg+5);//col 6=min Filter A
            loop(ii,StartCol,StopCol) {
                  range
DataR=[FitBook$]"%(MainSA.GetAt(aa)$)Tmelt$(gg)"!col($(ii));
                  DataR[L]$="Col #$(ii)";
                  DataR[U]$="°C";
                  DataR[C]$="%(Filter.GetAt(gg)$)";
                  DataR.type=2;
                  range
DataTonR=[TonBook$]"%(MainSA.GetAt(aa)$)Ton$(gg)"!col($(ii));
                  DataTonR[L]$="Col #$(ii)";
                  DataTonR[U]$="°C";
                  DataTonR[C]$="Tonset %(Filter.GetAt(gg)$)";
                  DataTonR.type=2;
                  loop(jj,0,7) {
                        fsample = ($(jj)*12)+$(ii);
                        range outputR=[ResBook$]%(AF.GetAt(jj+1)$)$(ii);
                        //fill col 1 with Sample Name
                        rFitSample[fsample]$="%(AF.GetAt(jj+1)$)$(ii)";
                        rTonSample[fsample]$="%(AF.GetAt(jj+1)$)$(ii)";
                        // INITIATE FIT RANGE
                        range AddFitCol=%(OutputR)!;
                        AddFitCol.Addcol();
                        int FitColN=AddFitCol.nCols;
                        range NewFitCol=%(OutputR)!wcol(FitColN);
                        NewFitCol.width=10;
                        NewFitCol[L]$="%(Filter.GetAt(gg)$) FitY";
                        NewFitCol[C]$="Boltzmann for %(Filter.GetAt(gg)$)";
                        //get Max bzw. Peaks
                        RowUpper%(MainSA.GetAt(aa)$)=58; //educated guess if
peakfind failed
                        RowLower%(MainSA.GetAt(aa)$)=30;
//                        type "DEBUG: %(MainSA.GetAt(aa)$), %(Filter.GetAt(gg)$):
No Peak found. Using $(RowUpper%(MainSA.GetAt(aa)$)) and
$(RowLower%(MainSA.GetAt(aa)$)) as Upper and Lower value, respectively";
                        if (PDPeak1R[fsample]$!="--" && PDPeak2R[fsample]$!="--
") {
                              RowUpper1p=TempToRow(PDPeak2R[fsample]);
                              RowUpper2p=TempToRow(PDPeak1R[fsample]);
                              RowUpper3p=TempToRow(PDPeak2R[fsample]);
                              RowUpper4p=TempToRow(PDPeak2R[fsample]);
                              RowLower1p=TempToRow(TableMinR[fsample]);
                              RowLower2p=TempToRow(TableMinR[fsample]);
```

```
                                RowLower3p=TempToRow(DiffPeakR[fsample]);//v.28:
PDPeak1R -> DiffPeakR
                                RowLower4p=TempToRow(DiffLocalMinR[fsample]);
//                              type "DEBUG: %(MainSA.GetAt(aa)$),
%(Filter.GetAt(gg)$): TWO Peaks found. Using $(RowUpper%(MainSA.GetAt(aa)$)) and
$(RowLower%(MainSA.GetAt(aa)$)) as Upper and Lower value, respectively";
                            }
                            if (PDPeak1R[fsample]$!="--" && PDPeak2R[fsample]$=="--
") {
                                RowUpper1p=TempToRow(PDPeak1R[fsample]);
                                RowUpper2p=TempToRow(DiffPeakR[fsample]);
                                RowUpper3p=TempToRow(PDPeak1R[fsample]);
                                RowUpper4p=TempToRow(PDPeak1R[fsample]);
                                RowLower1p=TempToRow(TableMinR[fsample]);
                                RowLower2p=TempToRow(TableMinR[fsample]);
                                RowLower3p=TempToRow(DiffPeakR[fsample]);
                                RowLower4p=TempToRow(DiffLocalMinR[fsample]);
//                              type "DEBUG: %(MainSA.GetAt(aa)$),
%(Filter.GetAt(gg)$): ONE Peak found. Using $(RowUpper%(MainSA.GetAt(aa)$)) and
$(RowLower%(MainSA.GetAt(aa)$)) as Upper and Lower value, respectively";
                            }
                            if
(RowUpper%(MainSA.GetAt(aa)$)>RowLower%(MainSA.GetAt(aa)$)) {
                                RowUpper=RowUpper%(MainSA.GetAt(aa)$);
                                RowLower=RowLower%(MainSA.GetAt(aa)$);
//                              type "DEBUG: %(MainSA.GetAt(aa)$),
%(Filter.GetAt(gg)$): Right slope: Peak=$(RowUpper). Min=$(RowLower)";
                            } else {
                                RowLower=RowUpper%(MainSA.GetAt(aa)$);
                                RowUpper=RowLower%(MainSA.GetAt(aa)$);
//                              type "DEBUG: %(MainSA.GetAt(aa)$),
%(Filter.GetAt(gg)$): Left slope: Peak=$(RowUpper). Min=$(RowLower)";
                            }
                            range
FitY=%(OutputR)!wcol(gg+2)[$(RowLower):$(RowUpper)];
                            range FitX=%(OutputR)!1;
                            // FIT!
                            nlbegin iy:=FitY func:=Boltzmann nltree:=tt;
                            nlfit;
                            NewFitCol=fit(FitX);
                            rFitA1[$(fsample)] = $(tt.A1);
                            rFitA2[$(fsample)] = $(tt.A2);
                            rFitx0[$(fsample)] = $(tt.x0);
                            rFitdx[$(fsample)] = $(tt.dx);
                            nlend;
                            // report data
                            DataR[jj+1]=$(tt.x0);
                            // PLOT
                            plotxy iy:=%(OutputR)!(1,$(gg+2)) plot:=202
ogl:=[%(MainSA.GetAt(aa)$)SingleFITPlot%(AF.GetAt(jj+1)$)$(ii)-$(gg)];
                            plotxy iy:=%(OutputR)!(1,$(FitColN)) plot:=200
ogl:=[%(MainSA.GetAt(aa)$)SingleFITPlot%(AF.GetAt(jj+1)$)$(ii)-$(gg)]
color:=color(red);
                            //change Graph style
                            yl.text$="Fluorescence intensity [a.u.]";
                            layer.y.label.divideBy=1000;
                            layer.y.label.suf$="k";
                            //move legend
                            legend.y = layer1.y.to - legend.dy / 2;
                            legend.x = layer1.x.from + legend.dx / 2;
                            layer.x.from=StartTemp; // x-axis start from
```

```
                            layer.x.to=plotxto; // smart x-scale
                            //add title label
                            label -j 1 -s -sa -n title Position
%(AF.GetAt(jj+1)$)$(ii), %(FileName$)\n%([SampleBook$]1!wcol(ii)[jj+1]$);
                            title.fsize=28;
                            title.y = layer.y.to + title.dy / 2;
                            //add upper arrow
                            int xUpA=RowToTemp(RowUpper);// x value as Temp
                            range yUpAR=%(OutputR)!wcol(gg+2);
                            int yUpA=yUpAR[RowUpper];
                            int y2UpA=(((layer.y.to-layer.y.from)/10)+yUpA);// y+20%
                            draw -n "Lup%(AF.GetAt(jj+1)$)$(ii)" -l
{xUpA,yUpA,xUpA,y2UpA};
                            Lup%(AF.GetAt(jj+1)$)$(ii).arrowbeginwidth=15;
                            Lup%(AF.GetAt(jj+1)$)$(ii).arrowbeginshape=4;
                            Lup%(AF.GetAt(jj+1)$)$(ii).color=4;
                            //add label to arrow
                            string labeltext$="$(xUpA)°C";
                            label -s -a 0 0 -n Tup%(AF.GetAt(jj+1)$)$(ii)
%(labeltext$);
                            Tup%(AF.GetAt(jj+1)$)$(ii).x=$(xUpA);

       Tup%(AF.GetAt(jj+1)$)$(ii).y=$(y2UpA)+Tup%(AF.GetAt(jj+1)$)$(ii).dy/2;
                            Tup%(AF.GetAt(jj+1)$)$(ii).color=4;
                            //add lower arrow
                            int xLowA=RowToTemp(RowLower);// x value as Temp
                            range yLowAR=%(OutputR)!wcol(gg+2);
                            int yLowA=yLowAR[RowLower];
                            int y2LowA=(((layer.y.to-layer.y.from)/10)+yLowA);//
y+20%
                            draw -n "Llow%(AF.GetAt(jj+1)$)$(ii)" -l
{xLowA,yLowA,xLowA,y2LowA};
                            Llow%(AF.GetAt(jj+1)$)$(ii).arrowbeginwidth=15;
                            Llow%(AF.GetAt(jj+1)$)$(ii).arrowbeginshape=4;
                            Llow%(AF.GetAt(jj+1)$)$(ii).color=4;
                            //add label to arrow
                            string labeltext$="$(xLowA)°C";
                            label -s -a 0 0 -n Tlow%(AF.GetAt(jj+1)$)$(ii)
%(labeltext$);
                            Tlow%(AF.GetAt(jj+1)$)$(ii).x=$(xLowA);

       Tlow%(AF.GetAt(jj+1)$)$(ii).y=$(y2LowA)+Tlow%(AF.GetAt(jj+1)$)$(ii).dy/2;
                            Tlow%(AF.GetAt(jj+1)$)$(ii).color=4;
                            //draw X at x0
                            double xCross=tt.x0;// x value as Temp
                            double yCross=(tt.A1-tt.A2)/2+tt.A2; //Ladies and
Gentlemen, let's keep it simple ;-)
                            //double yCross=tt.A2+(tt.A1-tt.A2)/(1 +
exp(0/tt.dx));//Ladies and Gentlemen, the Boltzmann function
                            int dyCross=((layer.y.to-layer.y.from)/10);// +%
                            draw -n "hCross%(AF.GetAt(jj+1)$)$(ii)" -l {xCross-
5,yCross,xCross+5,yCross};
                            draw -n "vCross%(AF.GetAt(jj+1)$)$(ii)" -l
{xCross,yCross-dyCross,xCross,yCross+dyCross};
                            hCross%(AF.GetAt(jj+1)$)$(ii).color=4;
                            vCross%(AF.GetAt(jj+1)$)$(ii).color=4;
                            //add label to cross
                            string labeltext$="$(tt.x0)°C";
                            label -s -a 0 0 -n TInfl%(AF.GetAt(jj+1)$)$(ii)
%(labeltext$);
```

```
      TInfl%(AF.GetAt(jj+1)$)$(ii).x=$(xCross)+TInfl%(AF.GetAt(jj+1)$)$(ii).dx/2+2
;
                           TInfl%(AF.GetAt(jj+1)$)$(ii).y=$(yCross)-
TInfl%(AF.GetAt(jj+1)$)$(ii).dy/2;
                           TInfl%(AF.GetAt(jj+1)$)$(ii).color=4;

                           // Calculate ONSET TEMPERATURE
                           double slope=(tt.A2-tt.A1)/(4*tt.dx); // slope at Tm
                           double y_x0=(tt.A1-tt.A2)/2+tt.A2;
                           double intercept=y_x0-(slope*tt.x0); //y-intercept
                           double ton=-intercept/slope; //y-axis intersection
                           double ton2=(tt.A1-intercept)/slope; // (I) Tonset.
Horizontal tangent intersection. dT = Distance between Onset temperature (I) and
the corresponding melting temperature
                           double ton3=ton2-(tt.x0-ton2);  // (II) Tonset. 2x dT
                           //reporting
                           DataTonR[jj+1]=ton3;
                           rTon[$(fsample)]=ton3;
                           if (ton<0) { ton=0; } //bugfix
                           //h-line at A1 and
                           draw -n "hTon%(AF.GetAt(jj+1)$)$(ii)" -d 2 -l
{StartTemp,tt.A1,ton2,tt.A1};
                           draw -n "sTon%(AF.GetAt(jj+1)$)$(ii)" -d 2 -l
{ton2,tt.A1,tt.x0,y_x0};
                           hTon%(AF.GetAt(jj+1)$)$(ii).color=6;
                           sTon%(AF.GetAt(jj+1)$)$(ii).color=6;
                           //add onset arrow 2
                           int yton2A=tt.A1; //label needs an integer as input-
variable ...
                           draw -n "Lton2%(AF.GetAt(jj+1)$)$(ii)" -l
{ton2,yton2A,ton2+8,yton2A};
                           Lton2%(AF.GetAt(jj+1)$)$(ii).arrowbeginwidth=15;
                           Lton2%(AF.GetAt(jj+1)$)$(ii).arrowbeginshape=4;
                           Lton2%(AF.GetAt(jj+1)$)$(ii).color=6; //6 = pink
                           //add label to new lines
                           string labeltext$="$(ton2)°C (I)";
                           label -s -a 10 10 -n Tton2%(AF.GetAt(jj+1)$)$(ii)
%(labeltext$);
                           Tton2%(AF.GetAt(jj+1)$)$(ii).color=6;

      Tton2%(AF.GetAt(jj+1)$)$(ii).x=ton2+Tton2%(AF.GetAt(jj+1)$)$(ii).dx/2+9;

      Tton2%(AF.GetAt(jj+1)$)$(ii).y=yton2A;//+(Tton2%(AF.GetAt(jj+1)$)$(ii).dy/2)
;
                           //add onset arrow 3
                           int yton3A=tt.A1; //label needs an integer as input-
variable ...
                           int y2ton3A=yton3A-((layer.y.to-layer.y.from)/10);
                           draw -n "Lton3%(AF.GetAt(jj+1)$)$(ii)" -l
{ton3,yton3A,ton3,y2ton3A};
                           Lton3%(AF.GetAt(jj+1)$)$(ii).arrowbeginwidth=15;
                           Lton3%(AF.GetAt(jj+1)$)$(ii).arrowbeginshape=4;
                           Lton3%(AF.GetAt(jj+1)$)$(ii).color=6; //6 = pink
                           //add label to new lines
                           string labeltext$="$(ton3)°C (II)";
                           label -s -a 10 10 -n Tton3%(AF.GetAt(jj+1)$)$(ii)
%(labeltext$);
                           Tton3%(AF.GetAt(jj+1)$)$(ii).color=6;

      Tton3%(AF.GetAt(jj+1)$)$(ii).x=ton3+(Tton3%(AF.GetAt(jj+1)$)$(ii).dx/2)+1;
```

```
                        Tton3%(AF.GetAt(jj+1)$)$(ii).y=y2ton3A;
                        //finally, insert graphs
                        insertGraph
gname:=%(MainSA.GetAt(aa)$)SingleFITPlot%(AF.GetAt(jj+1)$)$(ii)-$(gg)
cell:=[PlotBook$]%(MainSA.GetAt(aa)$)FitCurves$(gg)!wcol(ii)[jj+1] resizecell:=1;
                  }
                  //change sheet style
                  range
PlotBookCol=[PlotBook$]%(MainSA.GetAt(aa)$)FitCurves$(gg)!col($(ii));
                  PlotBookCol[L]$="Well plate col. #$(ii)"; //longname
                  PlotBookCol[C]$="%(Filter.GetAt(gg)$)";
                  PlotBookCol.type=2; //disregard col type
            }
      }
}
// rename books
FitBook$="FitBook";
win -r %(tempFitBookName$) %(FitBook$);
TonBook$="TonBook";
win -r %(tempTonBookName$) %(TonBook$);
// I/O
type "Fitting... done.\n%(FitBook$), TonBook... done.";



// SUBSECTION: GENERATE FINAL PLOTS (merge results)

loop (aa,1,3) {
      loop(gg,StartFitFilter,Filter.GetSize()) {
            loop(ii,StartCol,StopCol) {
                  loop(jj,0,7) {
                        fsample = ($(jj)*12)+$(ii);
                        // show signal strength (experimental)
                        range dataR =
[ResBook$]%(AF.GetAt(jj+1)$)$(ii)!wcol(gg+2);
                        absSignalstrength =
round(max(dataR)/DetectorLimit[$(gg)]*100,1);
                        relSignalstrength = round((max(dataR)-
min(dataR))/DetectorLimit[$(gg)]*100,1);
                        string labeltext$ = "signal
strength\nabs=$(absSignalstrength)%\nrel=$(relSignalstrength)%";
                        win -o
%(MainSA.GetAt(aa)$)SingleFITPlot%(AF.GetAt(jj+1)$)$(ii)-$(gg) {
                              label -p 100 100 -s -sa -n
TSS%(AF.GetAt(jj+1)$)$(ii) %(labeltext$);
                              TSS%(AF.GetAt(jj+1)$)$(ii).fsize=16;
                        }
                        //add first derivative maxima, e.g., inflections
                        range
SplinedDiffPeakCenters=[SplineBook$]%(AF.GetAt(jj+1)$)$(ii)!wcol(gg*2+4);
                        range
Readings=[ResBook$]%(AF.GetAt(jj+1)$)$(ii)!wcol(gg+2);
                        loop (vv,1,SplinedDiffPeakCenters.nrows) {
                              win -o
%(MainSA.GetAt(aa)$)SingleFITPlot%(AF.GetAt(jj+1)$)$(ii)-$(gg) {
                                    int xfdi = SplinedDiffPeakCenters[vv];
                                    int x2fdi = layer.x.to;
                                    int roundedTemp=Round(xfdi,0);
                                    int yfdi =
Readings[TempToRow($(roundedTemp))]; //optimize with interpolation (Iu-Il)*R+Il
```

```
                                        draw -n Lfdi%(AF.GetAt(jj+1)$)$(ii)$(vv) -l
{xfdi,yfdi,x2fdi,yfdi};

      Lfdi%(AF.GetAt(jj+1)$)$(ii)$(vv).arrowbeginwidth=15;

      Lfdi%(AF.GetAt(jj+1)$)$(ii)$(vv).arrowbeginshape=4;
                                        Lfdi%(AF.GetAt(jj+1)$)$(ii)$(vv).color=15;
                                        //add label to new lines
                                        string
labeltext$="$(SplinedDiffPeakCenters[vv])°C";
                                        label -s -a 10 10 -n
Tfdi%(AF.GetAt(jj+1)$)$(ii)$(vv) %(labeltext$);
                                        Tfdi%(AF.GetAt(jj+1)$)$(ii)$(vv).color=15;

      Tfdi%(AF.GetAt(jj+1)$)$(ii)$(vv).x=x2fdi+(Tfdi%(AF.GetAt(jj+1)$)$(ii)$(vv).d
x/2)+1;
                                        Tfdi%(AF.GetAt(jj+1)$)$(ii)$(vv).y=yfdi;
                                  }
                            }
                      }
                }
      }
}
// I/O
type "Merging ... done.";


// SECTION: TERMINATION

//report script runtime
string date2$=%[%[$(@D, D13),>" "], 4:5];
int min2=%(date2$);
string date2$=%[%[$(@D, D13),>" "], 7:8];
int sec2=%(date2$);
if (sec1>=sec2) {
      min=min2-min1-1;
      secnd=60+sec2-sec1;
} else {
      min=min2-min1;
      secnd=sec2-sec1;
}
type "Script finished after $(min)min$(secnd)sec.";
```